ANNUAL REPORTS ON
NMR SPECTROSCOPY

Edited by

G. A. WEBB

Department of Chemistry, University of Surrey, Guildford, Surrey, England

VOLUME 26

ACADEMIC PRESS

Harcourt Brace & Company, Publishers

London • San Diego • New York
Boston • Sydney • Tokyo • Toronto

ACADEMIC PRESS LIMITED
24–28 Oval Road,
LONDON NW1 7DX

U.S. Edition Published by

ACADEMIC PRESS INC.
San Diego, CA 92101

This book is printed on acid free paper

A catalogue record for this book is available from the British Library

ISBN 0-12-505326-6
ISSN 0066-4103

Phototypesetting by Alden Multimedia, Northampton
Printed and bound in Great Britain by
Hartnolls Limited, Bodmin, Cornwall

List of Contributors

J.L. Allis, *Oxford Magnet Technology, Wharf Road, Eynsham, Oxford OX8 1BP, UK.*

I. Ando, *Department of Polymer Chemistry, Tokyo Institute of Technology, Ookayama, Meguro-ku, Tokyo 152, Japan.*

S. Ando, *NTT Interdisciplinary Research Laboratories, Midori-Cho, 3-Chome, Musashino-Shi, Tokyo 180, Japan.*

P.S. Belton, *AFRC Institute of Food Research, Norwich Laboratory, Norwich Research Park, Colney, Norwich NR4 7UA, UK.*

I.J. Colquhoun, *AFRC Institute of Food Research, Norwich Laboratory, Norwich Research Park, Colney, Norwich NR4 7UA, UK.*

K. Hatada, *Department of Chemistry, Osaka University, Toyonaka, Osaka 560, Japan.*

B.P. Hills, *AFRC Institute of Food Research, Norwich Laboratory, Norwich Research Park, Colney, Norwich NR4 7UA, UK.*

T. Kitayama, *Department of Chemistry, Osaka University, Toyonaka, Osaka 560, Japan.*

S. Kuroki, *Department of Polymer Chemistry, Tokyo Institute of Technology, Ookayama, Meguro-ku, Tokyo 152, Japan.*

A. Lyčka, *Research Institute of Organic Syntheses, 532 18 Pardubice-Rybitví, Czech Republic.*

A. Shoji, *Department of Biological Sciences, Gunma University, Tenjin-cho, Kiryu-shi, Gunma 376, Japan.*

K. Ute, *Department of Chemistry, Osaka University, Toyonaka, Osaka 560, Japan*

G.A. Webb, *Department of Chemistry, University of Surrey, Guildford, Surrey, UK.*

Preface

The plangent call of NMR as a problem-solving technique is well-known in all areas of molecular science. Thus, at first sight, the collection of topics presented in each volume of *Annual Reports on NMR Spectroscopy* may appear to be a somewhat desultory one. However, taken together, the various volumes of this series seek to provide a fairly comprehensive coverage of advances both in the technique of NMR and in its many applications.

Volume 26 of *Annual Reports on NMR Spectroscopy* serves to evince the fecundity of NMR in five distinct areas of scientific interest. These include food science, structural studies of peptides and polypeptides in the solid state by ^{15}N NMR, high-resolution NMR as applied to polymer chemistry, the uses of cation NMR, in particular ^{87}Rb, in studies on living systems, and finally, azo dyestuffs as studied by multinuclear NMR.

It is a great pleasure for me to be able to express my gratitude to all of the contributors to this volume for the careful preparation and timely submission of their manuscripts. I would also like to thank the staff at Academic Press (London) for their very helpful cooperation in the production of this series of reports.

University of Surrey
Guildford

G.A. WEBB

Applications of NMR to Food Science

P.S. BELTON, I.J. COLQUHOUN and B.P. HILLS

AFRC Institute of Food Research, Norwich Laboratory, Norwich Research Park, Colney, Norwich NR4 7UA, UK

1. INTRODUCTION

It has long been recognized that NMR can be of use to the food scientist and food processor. One of the earliest references to the use of NMR in foods concerns moisture measurement and is dated 1957.[1] However, it is only within the last 10 to 12 years that there has been consistent and widespread growth of the use of NMR. This is probably the result of three separate trends. The first is the increasing sophistication and relative ease of use of NMR instrumentation. This has meant that, for example, multinuclear and solid-state methods have become

ANNUAL REPORTS ON NMR SPECTROSCOPY
VOLUME 26 ISBN 0-12-505326-6

much easier to apply. The second trend is the increasing need of the food industry to understand and innovate in its products and process. Finally, there is the pressure for new methods to enforce legislation and control quality.

The nature of foods has led to the choice of NMR as an investigative method in the same way that nature of biological systems has led biological research to increasingly embrace the technique. The requirement in both cases is to have a non-invasive technique which can extract useful information from a chemically complex and highly heterogeneous system. In foods the requirement for non-invasiveness stems not from any ethical consideration but from the need to preserve and examine the food structure. In this report we attempt to review the main areas of activity during the last decade and indicate where future developments are likely to occur. Table 1 lists major reviews in the relevant areas since 1980. The format of the table is similar to that which will be followed in this review; material is divided up according to the nature of the application rather than the NMR technique involved. The exception is NMR imaging; this technique has only recently found applications in food science and is still very much in its infancy.

It is noticeable from Table 1 that most of the references come from the last half of the period covered. This is partly due to the recent publication of two books[32,33] dealing with NMR applications in food and agriculture, but also reflects the increasing pace of the subject. The time now, therefore, seems ripe for a general review of the area and this is the purpose of this report. We do not aim to cover every reference but have attempted to give a comprehensive indication of the scope and potential of NMR in food and science.

2. WATER

2.1. Introduction

Water is probably the most important component of foods, profoundly affecting food texture and quality, its microbiological safety as well as its nutritional status and digestibility.[34] The growth of pathogenic microorganisms in food materials is determined by the local availability of water to the bacterial cells.[35] A long established general indicator of this "water availability" is the water activity as measured by equilibrium vapour pressures.[34,35] More recently, attempts have been made to use NMR water relaxation times as a measure of "water availability". Based on a theory of Kumosinski and Pessen[36,37] several papers have appeared purporting to relate water proton, deuterium and oxygen-17 relaxation times to solute and water activity in casein,[37–41] lysozyme,[41] β-lactoglobulin,[37,40] corn zein,[41] starch[42] and wheat flour.[43] The translational mobility of water in foods may be measured directly by the pulsed-field gradient spin-echo method. In the first section we review the literature on relaxation and examine whether there is a meaningful correlation

Table 1. Reviews of NMR applications to food science since 1980.

	Subject	Date	Reference
1	Water		
	General review of NMR theory and applications	1990	2
	Comprehensive review of the food literature	1990	3
	Review of literature	1987	4
	Measurement of non freezing water by NMR	1984	5
	Review of literature	1981	6
2	Imaging		
	General review	1990	7
3	Proteins		
	Wheat proteins	1991	8
	Structure and environment of α-lactalbumin	1990	9
	Food proteins and related systems	1990	10
	Cereal proteins	1990	11
	Food proteins	1989	12
4	Polysaccharides		
	The structure and behaviour of starch	1990	13
	Sodium binding to polysacharides	1989	14
	General review of carbohydrate NMR	1986	15
	Disaccharides and trisaccharides	1980	16
5	Analytical methods		
	Site-specific isotope fractionation	1991	17
	Site-specific isotope fractionation in wines	1988	18,19
	Isotope ratio determination by NMR	1986	20
	Wide-line NMR	1990	21
	Wide-line methods for the analysis of fats and oils	1986	22
	High-resolution methods for the characterization of lipids	1986	23
	Fat content of meat products	1985	24
	Analysis of fat and moisture	1984	25
	General review of NMR applications	1984	26
	Wide-line methods for the analysis of oils and fats	1980	27
6	Other areas		
	General review of applications of NMR	1990	28
	General applications to fats and oils	1988	29
	General review of potential of NMR	1984	30
	Post-mortem changes in meat	1980	31

between "water activity" and NMR water relaxation times apart from the trivial observation that both depend on solute concentration. In the second section results on diffusion are reviewed.

2.2. Water relaxation

The theoretical basis for the interpretation of water proton, deuterium and oxygen-17 relaxation in the dilute regime where water activities are close to

unity is now fairly well established.[2,44,45] It is generally appreciated that water proton transverse relaxation in dilute solutions of proteins and carbohydrates is dominated by proton exchange with solute protons[44–50] and, in the case of longitudinal and rotating frame water proton relaxation in gels, by a combination of proton exchange and secular dipolar cross-relaxation.[51,52] Theories for these phenomena have been presented and shown to account quantitatively for water proton relaxation both for polysaccharides and proteins. The shortening of the transverse water proton relaxation times when globular protein solutions are irreversibly thermally denatured reported by Lambelet *et al.*[53] is probably explained by an increase in the intrinsic relaxation rate (and perhaps population) of the exchangeable protein protons rather than by changes in the amount or nature of "bound" water. Chemical exchange with the solute can also contribute to the deuterium water relaxation[50] and for this reason oxygen-17 water relaxation is the only technique which reports primarily on the behaviour of the water. A seminal paper on oxygen-17 water relaxation in dilute protein solutions was published in 1981 by Halle and co-workers.[54] The results were analysed using a model in which water molecules are in fast diffusive exchange between the bulk phase and water interacting with the surface of the protein, the so-called "bound" water. The bound water was shown to reorient anisotropically at the interface such that the major part of the quadrupolar interaction is rapidly averaged with a correlation time, τ_f, while the residual quadrupolar interaction is averaged by slower motions characterized by a correlation time τ_s. Various theoretical models for τ_s have since been presented.[55,56]

Although water relaxation in the dilute regime is now set on a firm theoretical basis, this is not the case in the more concentrated, water-poor regime appropriate to most foods. In the following we will therefore focus mainly on the concentration dependence of the water relaxation, especially the oxygen-17 data, beginning with simple sugar solutions.

2.2.1. Simple sugar solutions

A non-linear, monotonic increase of the oxygen-17 water relaxation rate in sucrose solutions with increasing sucrose concentration has been reported by Richardson *et al.*[57] as well as by Mora-Gutierrez and Baianu[58] and qualitatively explained in terms of water–sucrose and sucrose–sucrose hydrogen bonding. More recently, a quantitative theory has been presented which provides a reasonable fit to the data on sucrose and α1–4-linked glucans (G_N, $N = 1-7$) up to saturation at room temperature.[59] This theory clearly shows how the non-linear concentration dependence arises, primarily, because of the increasing slow bound water correlation time, τ_s, due to increasing solution viscosity, and not directly because of changes in the equilibrium water or solute activity. A similar theory has been shown to account for the concentration dependence of deuterium water relaxation in glucose solutions up to

saturation.[50] In this case additional terms describing the deuterium exchange between water and sugar deuteroxyl groups need to be included. This exchange was shown to give rise to a significant transverse relaxation dispersion when the pulse spacing in the Carr–Purcell–Meiboom–Gill (CPMG) sequence is varied. Far from being a complication to be avoided, quantitative analysis of this deuterium exchange dispersion was shown to yield the concentration dependence of the mean lifetime of the deuteron on the sugar. At neutral pD values this increased dramatically above concentrations corresponding to two water molecules per hydroxyl group, which suggests that each sugar hydroxyl group preferentially hydrogen bonds two water molecules.[50] A similar conclusion had been reached from earlier studies of the sugar hydroxyl proton chemical shift.[60,61]

Large dispersions have also been observed and analysed in the water proton transverse relaxation of dilute sugar solutions.[50] However, as yet, there has been no quantitative theory of the concentration dependence of the water proton relaxation in sugar solutions. Before this can be done it is necessary to separate the proton signals from the water and non-exchanging sugar protons which makes the relaxation biexponential. This important point has been overlooked in some reports. The theory for the proton relaxation is complicated by terms describing intermolecular dipole–dipole interactions between water and sugar protons. Secular dipolar cross-relaxation may also need to be included in the analysis of longitudinal and rotating frame relaxation at high sugar concentrations. There are, as yet, no extensions of these results into the glassy states of sugars.

2.2.2. Protein and polysaccharide solutions

Sorption isotherms of food proteins have been intensively studied for many years;[62] nevertheless, the underlying mechanisms of water sorption still remain to be clarified. For this reason much effort has focused on water relaxation in well-characterized globular protein systems such as lysozyme. Figures 1–3 show the dependence of the oxygen-17 water relaxation for lysozyme solutions over a wide concentration range adapted from three separate papers.[41,63,64] The overall dependence is roughly sigmoidal, the relaxation rate almost levelling out at the highest concentrations of protein (Fig. 3). Up to about 10% w/w lysozyme the transverse relaxation rate increases linearly with concentration and can be interpreted with the two-site fast exchange model, provided the bound water is assumed to re-orient anisotropically with concentration-independent fast (τ_f) and slow (τ_s) correlation times.[54] At higher concentrations the relaxation rate increases non-linearly. Myer-Betts and Baianu[41] interpreted this non-linearity with a theory proposed earlier by Kumosinki and Pessen[36–39] to explain a similar non-linearity in the deuterium water relaxation of milk caseins. According to these authors the fraction of bound water should be replaced by an activity term "$n_H a_p$", where a_p is the protein activity expressed as a virial expansion in the protein concentration and n_H is the hydration

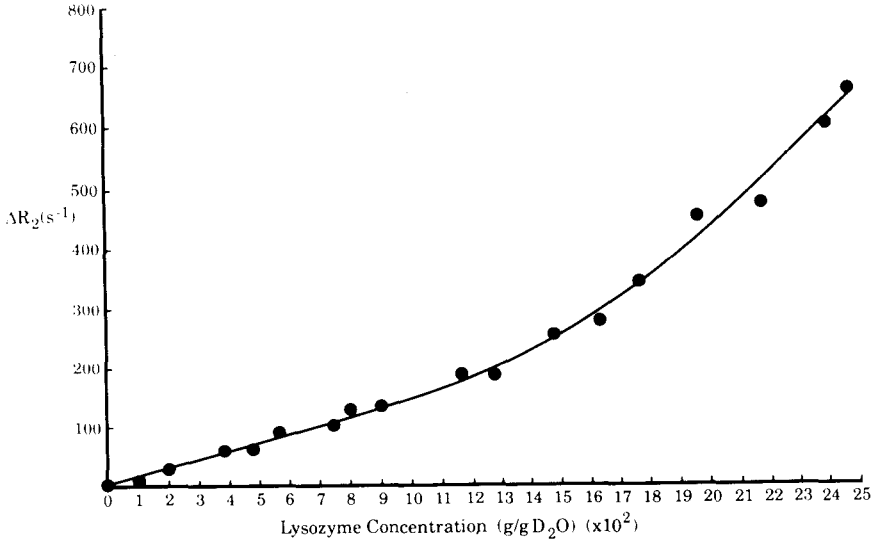

Fig. 1. Dependence of the oxygen-17 (27.13-MHz) excess transverse relaxation rate on lysozyme concentration in D_2O in the presence of 0.1 M NaCl at 21°C and pD = 4.5. $\Delta R_2 = R_{observed} - 196.6\,s^{-1}$. (Replotted from Ref. 63.)

(g H_2O/g dry protein). There appears to be no satisfactory theoretical justification for replacing a proton fraction by a thermodynamic activity term, especially when the virial coefficients are determined by fitting the relaxation data. The fitting procedure also assumes that the bound water correlation times are concentration independent which is certainly not the case with sugar solutions[50,59] and unlikely to be true with protein solutions, except in the linear concentration regime. These defects in the Kumosinski–Pessen "activity" theory probably explain in part why the water activity curve for lysozyme calculated from the NMR relaxation data[40] deviates substantially from the water sorption isotherm data.[41]

Another problem is the use of the relationship $a_w = 1 - \bar{V}_w a_p$. Here $\bar{V}_w$ is the degree of hydration, a_p is the NMR-derived protein activity and a_w the water activity. This underived expression is analogous to a stoichiometric population expression but is inappropriate for activities whose relationships are determined by the Gibbs–Duhem equation. Despite these shortcomings the Kumosinski–Pessen theory has been extensively used in the food literature.[37,38,40–43]

Following the analysis of oxygen-17 relaxation in sugar solutions[59] a more probable explanation, at least of the initial part of the non-linearity in Figs 1 and 2, is the lengthening of the slow bound water correlation time, τ_s, with increasing protein concentration. Assuming τ_s is determined by re-orientation of the protein molecules[50] we can write $\tau_s \propto D_p^{-1}$, where D_p is the rotational diffusion coefficient of the protein (assumed to be spherical). Data on the

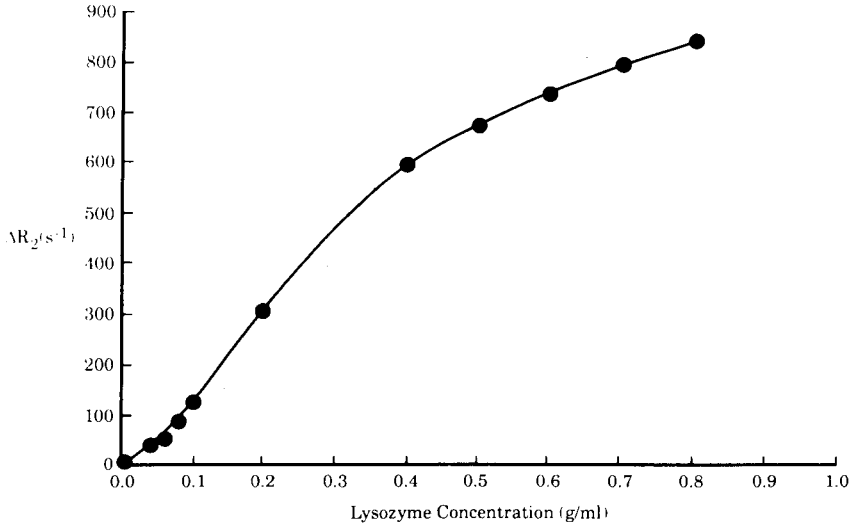

Fig. 2. Dependence of the oxygen-17 (34-MHz) excess transverse relaxation rate on lysozyme concentration in D_2O at pH 7.0 $\Delta R_2 = R_{\text{observed}} - 196.6\,\text{s}^{-1}$. (Replotted from Ref. 41.)

concentration dependence of D_p is available from light scattering,[65,67] fluorescence depolarization or electron spin resonance (ESR).[66] Alternatively various theoretical expressions for D_p can be formulated. Consideration of the factors such as viscosity, ionic environment and charge which will affect protein motion suggest that an equation such as the Gordon equation[67] contains the essential elements. The Gordon equation may be written,

$$D_p = \left\{\frac{q_0^2 D_p^0 D_s^0}{q_p^2 D_p^0 + q_s^2 D_s^0}\right\}\left(\frac{h_0}{h}\right)\left\{1 + \frac{\text{dln}\gamma^{\pm}}{\text{dln}c_p}\right\} \tag{1}$$

where

$$q_p^2 = (4\pi/\epsilon kT)Z_p^2 C_p \tag{2}$$

$$q_s^2 = (4\pi/\epsilon kT)Z_s^2 C_s \tag{3}$$

$$q_0^2 = q_p^2 + q_s^2 \tag{4}$$

Here C_p is the concentration of protein molecules of charge Z_p and C_s is the concentration of counterions of charge Z_s ($Z_pC_p + Z_sC_s = 0$); ϵ is the dielectric constant and h the shear viscosity of the solution at concentration C_p; h_0 is the pure solvent viscosity; D_p^0 and D_s^0 are the diffusion coefficients of the protein and counterion at infinite dilution while $\gamma^{\pm}$ is the mean ionic activity coefficient. Both $\gamma^{\pm}$ and the relative visocity (h_0/h) depend on protein concentration

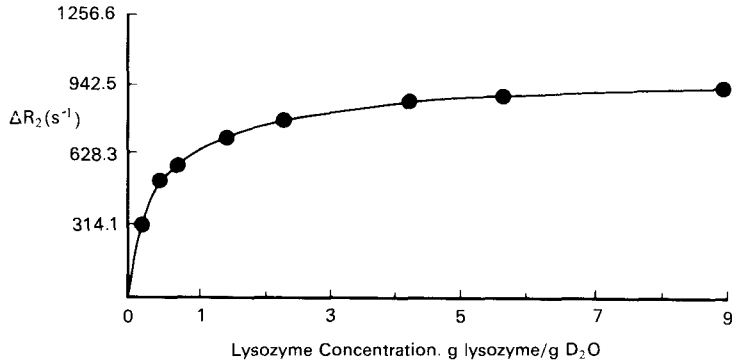

Fig. 3. Dependence of the oxygen-17 (34-MHz) excess transverse relaxation rate on lysozyme concentration in D_2O. $\Delta R_2 = R_{observed} - 196.6\,s^{-1}$. (Replotted from Ref. 64.)

C_p. The concentration dependence of the shear viscosity can often be written, empirically, in the form[34]

$$\log\left(\frac{h}{h_0}\right) = Ac_p/(1 - Bc_p) \tag{5}$$

where A and B are constants. Equation (1) predicts that the oxygen-17 water relaxation rate will depend on the ionic strength and the charge on the protein (through the factors q_p^2 and q_s^2), effects that have been observed in solutions of lysozyme[68] and muscle proteins.[68]

To what extent expressions for τ_s or D_p such as equation (1) succeed in reproducing the observed concentration dependence remains to be investigated. At high concentrations other factors such as protein aggregation (oligomer formation) would need to be explicitly treated. Eventually aggregation would be expected to be so extensive that the protein re-orientational correlation time, τ_p, becomes essentially infinite. At such concentrations τ_s is necessarily determined by some other type of motion such as diffusion over the protein surfaces.[55,56] This might explain the levelling-off apparent in Fig. 2 at concentrations approaching 75%. At concentrations exceeding that found in crystalline lysozyme (*ca.* 75%) the material is best considered not as a solution but as a partially saturated porous powder having various amounts of adsorbed water. Such materials are considered in the following subsection.

Clearly much work remains to be done before the data in Figs 1–3 can be interpreted quantitatively. Of course, it is always possible to fit any curve such as that in Fig. 3 with a series of straight-line segments and assign these to various populations of water. This has been the practice of a number of authors,[64,69,70] but it is an entirely empirical exercise and even the choice of the number of straight-line segments appears arbitrary. For example Lioutas and co-workers[69] analysed their water proton relaxation data on lysozyme using five lines and claimed to have identified "5 populations of water". On

the other hand Fullerton *et al.* used only three water populations to explain their water proton T_1 lysozyme data.[70] Using the intercepts and slopes of these straight lines to calculate intrinsic relaxation rates of the various water "populations"[64,70] is another dubious exercise since it assumes these are constants, independent of concentration. This is unlikely to be the case since correlation times generally depend on concentration.

Piculell and Halle[71] have reported a detailed comparison of deuterium and oxygen-17 water relaxation in dilute lysozyme solutions, and showed that the deuterium relaxation has an additional contribution from exchangeable deuterons on the protein. A three-site model similar to that used to explain deuterium water relaxation in sugar solutions[50] gave good agreement with experiment. Other authors have reported the non-linear concentration dependence of deuterium water relaxation in lysozyme solutions.[63,69] Unfortunately, the concentration dependence of the transverse relaxation dispersion expected for deuterium as a function of CPMG pulse spacing has not yet been investigated. This would give valuable information on the deuterium (and proton) exchange kinetics as already demonstrated for sugar solutions.[50] Table 2 includes a number of other representative papers dealing with water relaxation in protein and polysaccharide solutions published in the last decade.

Table 2. NMR studies of water relaxation in proteins and polysaccharide solutions.

Nucleus	System	Relaxation mode	Reference
^{1}H	Agarose gels	T_2	73
^{1}H	Carrageenan gels	T_2	49, 72
^{1}H	Gelatin gels and sols	T_2, T_1, $T_{1\rho}$	51, 74
^{1}H	Fibrinogen and fibrin gels	T_1, T_2	76, 77
^{1}H	Lysozyme	T_1, T_2	41, 44, 75, 69, 70
^{2}H	Lysozyme	T_1, T_2	63, 64, 71
^{17}O	Lysozyme	T_1, T_2	41, 54, 63, 64, 68, 71
^{1}H	Bovine serum albumin	T_2, T_1	46, 47, 70, 79
^{2}H	Bovine serum albumin	T_1, T_2	78
^{1}H	Corn zeins	T_2	41, 68, 80
^{2}H	β-Lactoglobulin A	T_1, T_2	37, 40
^{2}H	Caseins	T_1, T_2	39, 40, 82, 83, 88, 92
^{1}H, ^{17}O	Myofibrillar proteins	T_2	68, 81
^{1}H	Egg albumen gelation	T_1	86

2.2.3. *Starch suspensions and other heterogeneous polysaccharide and protein systems*

The previous subsections have considered homogeneous solutions and gels. We now address water relaxation in heterogeneous particulate suspensions, pastes and powders. We focus on the starch–water system since starch is widely used as a thickener, texturizer and emulsification aid in the food industry.

Richardson and co-workers[87,88] have reported oxygen-17 and deuterium water transverse relaxation rates in corn starch suspensions over a wide

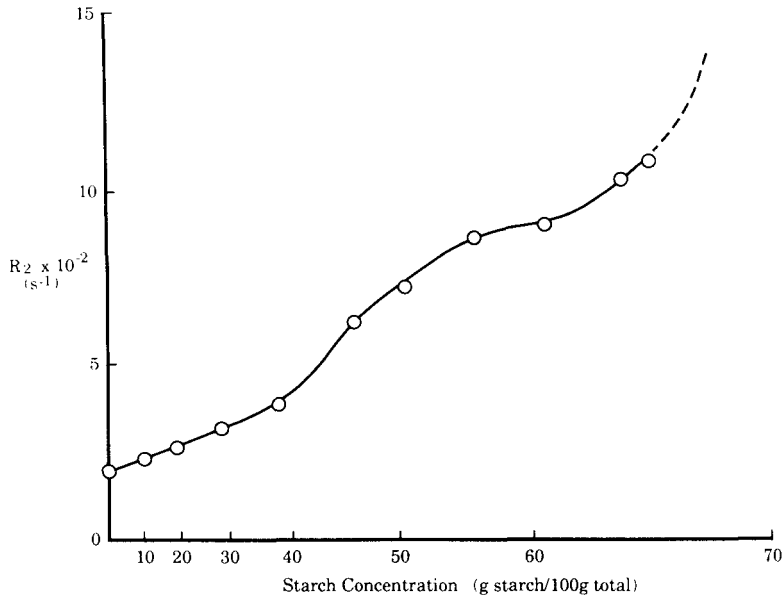

Fig. 4. Variation of the oxygen-17 (33.9-MHz) transverse relaxation rate on corn starch concentration. (Replotted from Ref. 87.)

concentration range (10–96% solids). Their data for oxygen-17 relaxation is replotted in Fig. 4. It is tempting to associate the various regions in this figure with various "states" or populations of water, as has been the tendency in the NMR food literature. But before attempting to do this it is essential to take account of changing morphological factors; an aspect that has been given only scant attention in the past. The observation of single exponential oxygen-17 relaxation[87] suggests that diffusive exchange of water between the bulk and water inside the starch granules is fast compared to the difference in their intrinsic relaxation rates.[89] This is consistent with the small size of the unheated corn starch granules (5–26 μm). As the suspension is concentrated, the relaxation is observed to increase first linearly, then non-linearly, eventually levelling off between 55 and 60% w/w starch. This behaviour is reminiscent of lysozyme solutions and probably finds a similar explanation in terms of the concentration dependence of the bound water slow correlation time, τ_s. However, unlike lysozyme solutions the starch data show a second monotonic increase above 60% starch. The monotonic increase in relaxation rate with concentrations above 70% starch has been reported by Richardson and co-workers[88] but cannot be plotted on the scale in Fig. 4. Given present information we can only speculate about the origin of this second increase. One possibility is that it is associated with the morphological changes accompanying the transition from a water-saturated paste at *ca.* 60% starch to an increasingly unsaturated microporous powder.

Let us assume that at *ca.* 60% by weight starch the system is still saturated with water but contains randomly packed granules. The monotonic increase in relaxation rate between 60 and 70% starch could then arise because bulk water is being replaced by air in progressively smaller pores in the capillary porous starch matrix. According to capillary theory the largest pores would be emptied first and these would be associated, through a surface relaxation mechanism, with the longest relaxation times. This monotonic increase in relaxation rate would be expected to continue through the second falling rate drying period until all bulk intergranular "capillary" water is removed. Assuming the packed, saturated condition occurs at *ca.* 60% starch and the system has a porosity, ϕ, typical of impenetrable, randomly packed polydisperse spheres ($\phi \sim 0.3-0.4$), it is easy to show that all the bulk intergranular capillary water would be removed at *ca.* 70% by weight starch. Between 70 and 90% the system then behaves as a partly dry granular powder containing various amounts of adsorbed water. Indeed, the sorption equilibrium moisture content of corn starch at 100% relative humidity is reported to be at *ca.* 74% w/w starch,[90] which is also the composition of the non-freezing component in frozen corn starch.[90] Monolayer coverage is thought to occur around 92% by weight starch.[88]

Clearly, more experimental and theoretical work is needed to check the validity of this morphological interpretation. It would be especially interesting to use capillary theory to try to relate the relaxation behaviour to pore size distribution in the unsaturated regime between 55 and 70% by weight starch. If this morphological explanation is correct it should be sufficient to include only two "states" of water, viz. bulk water and "bound" water (i.e. water that is anisotropically re-orienting at the starch–water interface), to describe the relaxation over the whole concentration range. The dynamic state of the "bound" water can be studied directly in the most concentrated regime (70–95%) corresponding to starch powder since there is then no bulk water phase. Such a study has recently been reported[91] using proton NMR and has demonstrated the surprising mobility of the "bound" water. Three distinct bound water correlation times were extracted from the relaxation data. These corresponded to the mean lifetime of a water molecule at a particular site on the starch powder (*ca.* 10^{-7} s at room temperature) and the fast (τ_f) and slow (τ_s) bound water correlation times (*ca.* 10^{-9}s and $\geq 6 \times 10^{-5}$ s respectively).

Heating corn starch suspensions to temperatures exceeding *ca.* 60°C results in swelling of the granules and partial release of the amylose fraction, resulting eventually in gelation.[92] Not surprisingly, this results in irreversible changes in the oxygen-17, deuterium and proton water relaxation rates.[93] Table 3 lists a number of other representative water relaxation studies on food materials consisting of particulate suspensions, pastes or powders.

Table 3. Water relaxation studies in suspensions, pastes and powders.

Nucleus	System	Relaxation mode	Reference
^{1}H	Lysozyme powders	T_1	94, 97
^{1}H	Polyproline powder	T_1	95
^{1}H	Hydrated collagen	T_1	96
^{1}H	Starch suspensions and powders	T_1, T_2, T_3	91. 98
^{17}O	Starch suspensions and powders	T_2	87, 88
^{2}H	Starch suspensions	T_2	99
^{17}O	Wheat starch–sugar mixtures	T_2	101
^{1}H, ^{2}H, ^{17}O	Wheat flour suspensions	T_2, T_1	43, 100
^{1}H	BSA–lysozyme aggregates	T_2	47
^{1}H, ^{23}Na	β-Lactoglobulin	T_1	102
^{1}H	Milk proteins	T_2	103, 104
^{1}H, ^{2}H	Wheat flour doughs	T_1, T_2	105, 106
^{17}O	The staling of bread	T_2	107

2.2.4. Plant tissue

Morphology is a major factor determining water relaxation in cellular tissue. In parenchyma plant tissue, for example, there is diffusive exchange of water between a number of compartments such as the extracellular region including the cell wall, the cytoplasm including water inside the various cell organelles, and the vacuoles. The mean lifetime of water molecules in each of these compartments depends on geometric factors, the magnitude of the tonoplast and plasmalemma membrane permeability barriers and the size of the water self-diffusion coefficient in each compartment. Since the various cell compartments are associated with different water relaxation times, predicting the relaxation behaviour of the whole tissue requires development of numerical multicompartment diffusion–relaxation theories beginning with simple model systems.

A packed suspension of Sephadex beads is one of the simplest two-compartment systems displaying the phenomenon of coupled diffusion and relaxation. The dependence of the multiple exponential water proton transverse relaxation on Sephadex bead size, cross-linking density and CPMG pulse spacing has been successfully interpreted using a Monte-Carlo computer simulation.[108] In this system the water relaxation inside the Sephadex beads was shown to be dominated by proton exchange.[48] In later work a similar theory was shown to account semi-quantitatively for the water proton transverse relaxation behaviour in the parenchyma tissue of courgette, onion and apple[109] as well as magnetic resonance imaging (MRI) image contrast in courgettes.[110] Most recently the theory has been extended to pulsed-gradient spin-echo measurements of water diffusivity in plant tissue.[111] Since plant cell morphology is best studied with microscopic methods, the most useful information emerging from these NMR measurements are the magnitudes of the tonoplast and plasmalemma water permeability coefficients. Other NMR methods for measuring these membrane permeabilities have been reviewed recently.[112] The

Table 4. Water relaxation studies in plant tissue.

Nucleus	Plant tissue	Relaxation mode	Reference
^{1}H	Maize root	T_1	113
^{1}H	Winter wheat cells	T_2	114
^{1}H	Elodea leaf	T_2	115
^{1}H	Courgette, onion, apple	T_2	109
^{1}H	Plant cell walls	T_1, T_2, T_{1d}	116
^{1}H	Maize seeds	T_1	117
^{1}H	Various seeds	T_2	118
^{1}H	Intact and neoplastic plant tissue	T_2	119
—	Review	—	120

dependence of these membrane permeabilities on parameters such as temperature and cell age is a topic of current interest in plant physiology. Table 4 lists a number of other representative references on water relaxation in plant tissue.

2.2.5. *Muscle tissue*

The effects of diffusive exchange of water between the extracellular, the sarcoplasmic reticulum and the myofibril compartments on muscle water relaxation have yet to be analysed with realistic models of the cell morphology. The oxygen-17 longitudinal relaxation of water in muscle is reported to be multiple exponential,[121,122] which suggests slow or intermediate diffusive exchange between two or more cell compartments. The effects of varying spectrometer frequency on the oxygen-17 relaxation has yet to be investigated. This could give valuable information about the bound water correlation times in the various compartments. The deuterium[123] and proton[124] transverse water relaxation is also multiple exponential, but with these nuclei chemical exchange between water and exchangeable groups on the myosin and myofibril proteins is expected to contribute significantly to the intrinsic relaxation in the myofibril compartment.[123] This might explain the observed pH (or pD) dependence[123] and the dependence on the CPMG pulse spacing.[124] Secular dipolar cross-relaxation with muscle proteins is expected to contribute to the longitudinal and rotating frame water proton relaxation but not, of course, to the deuterium or oxygen-17 relaxation. The effects induced by post-mortem changes[125,126] and membrane disruption by glycerination[123] have been reported but remain to be interpreted with a diffusion–relaxation model. Table 5 lists a number of other references dealing with water relaxation in muscle.

2.2.6. *Future directions for water relaxation in foods*

NMR remains one of the most powerful techniques for studying the dynamic state of water in foods. Nevertheless, a cursory examination of Tables 2–5 shows that with a few exceptions the application of NMR relaxation methods

Table 5. Water relaxation in muscle tissue.

Nucleus	Muscle type	Relaxation mode	Reference
^1H, ^2H, ^{17}O	Albino mouse	T_1, T_2	123, 127, 128
^1H, ^2H, ^{17}O	Frog sartorius and gastrocnemius	T_1, T_2	121, 122, 124, 126 129
^1H	Barnacle muscle	T_1, $T_{1\rho}$, T_2	130
^1H	Rat and beef muscle	T_1	125
^1H	Pig muscle	T_2	131

to any given food material has tended to be rather piecemeal. To gain maximum information, data from all three nuclei – protons, deuterium and oxygen-17 – need to be systematically compared. Proton studies require comparison of the free induction decay (FID) or spectrum, the transverse, longitudinal and rotating frame relaxation behaviour. Valuable information can often be obtained from the dispersion behaviour found by varying the pulse spacing in the CPMG sequence; the spectrometer frequency with longitudinal relaxation and the radiofrequency field strength in the rotating frame. There remains a need for more systematic measurements of proton secular dipolar cross-relaxation rates by using isotopic dilution in water-rich systems[51] and selective excitation methods in the more concentrated regime.[94–96] The Goldman–Shen pulse sequence can also be used to measure cross-relaxation rates.[91] Bound water correlation times can be derived, at least in principle, from the oxygen-17 or deuterium T_1/T_2 ratios and from the dependence of T_1 or T_2 on spectrometer frequency. This remains to be done as a function of solute concentration to discover the concentration dependence of τ_s and τ_f. With deuterium, account must also be taken of exchange with the solute.

Much work remains to be done on the theoretical side to interpret the non-linear concentration dependence such as that displayed in Figs 1–4. At present there appears to be no rigorous theoretical justification for relating relaxation times directly to water activity, apart from the trivial observation that both depend on concentration. Nor is there any sound basis for postulating more than two dynamic states of water, viz. water in the bulk phase and water interacting with protein or polysaccharide interfaces, the so-called "bound" water. The non-linearities in concentration plots such as those in Figs 1–4 probably find their explanation in the concentration dependence of the bound water correlation times or order parameters and in changing water distribution ("morphology") induced by changing degrees of saturation, rather than in the existence of other dynamic states of the water. The rigorous interpretation of water relaxation in multicompartment systems such as plant tissue and muscle requires development of more sophisticated computer models capable of solving the diffusion–relaxation equations with boundary conditions appropriate to the observed system morphology.[48,108] It is inappropriate to apply equations describing chemical exchange between different sites to multicompartment

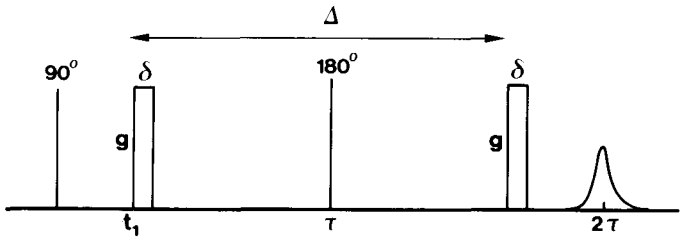

Fig. 5. The standard Stejskal–Tanner pulsed-gradient spin-echo pulse sequence.

food systems since those equations fail to treat the diffusive exchange process explicitly. These issues become paramount in the interpretation of diffusion measurements using pulsed-field gradient spin-echo experiments. This aspect is reviewed in the next section.

2.3. Pulsed gradient spin-echo (PGSE) studies of water in foods

The principles of self-diffusion measurements by pulsed gradient spin echo techniques have been reviewed recently.[132–134] Figure 5 shows the simple PGSE pulse sequence first proposal by Stejskal and Tanner[135] in 1965. The observed echo amplitude, $S(q, \Delta, \tau)$, is a function of the three independent variables: q, the wave vector corresponding to the pulsed gradient area, $q = (2\pi)^{-1}\gamma g\delta$; Δ, the diffusion time (pulsed gradient separation); and τ, the 90°–180° pulse spacing. The functional form of $S(q, \Delta, \tau)$ for water in a food material depends on both the microstructure of the food and on the microdynamics of the water transport. Maximum information is obtained by systematic variation of the wave vector (q) and the timescale (Δ, τ) over the whole of the experimentally accessible $q-\Delta-\tau$ space and by developing realistic (numerical) models to predict the functional form of $S(q, \Delta, \tau)$. Failure to do either of these results in loss of information and possibly incorrect deductions about the nature of the system.

The theoretical form of $S(q, \Delta, \tau)$ is particularly simple for water diffusion in spatially uniform solutions or gels. For these

$$S(q, \Delta, \tau) = S(0) \exp\left[-2\tau/T_2 - q^2 D(\Delta - \tfrac{1}{3}\delta)\right] \tag{6}$$

Here T_2 is the transverse relaxation time and D is the effective water-diffusion coefficient. In protein or polysaccharide solutions or gels there is fast exchange between water molecules in the bulk with those interacting with the macromolecule surface. There is also fast proton exchange between water and macromolecule protons. Both effects imply that $D = f_w D_w + f_s D_s$, where f_w and f_s are the water proton fractions in the bulk phase and surface respectively ($f_s + f_w = 1$) and D_s is the macromolecule diffusion coefficient. Since $D_s \ll D_w$, the second term is negligible so that $D = (1 - f_s)D_w$. This predicts

a linear decrease in D with increasing macromolecule concentration, which is observed in the dilute regime[136] but not at high concentrations.[137] D_w differs from the self-diffusion coefficient of pure water because the macromolecules physically obstruct the translation of the water molecules. For dilute solutions this obstruction effect can be estimated using a theory first developed by Wang[138] who used it to deduce the hydration and shape of ovalbumin molecules.

The form of $S(q, \Delta, \tau)$ for restricted diffusion in spherical droplets is also relatively simple and this has permitted routine and accurate determination of droplet size distributions in water-in-oil emulsions.[139] However, in most heterogeneous food materials water diffusion is restricted by the presence of solid inclusions, fat or oil droplets, cell wall or lipid membrane barriers. Simple analytical expressions for $S(q, \Delta, \tau)$ no longer exist and the relationship between microstructure and $S(q, \Delta, \tau)$ is far from straightforward. Much work remains to be done both theoretically and experimentally to explore this relationship. The difficult nature of this problem probably accounts for the relatively few reports of PGSE measurements of water in complex food materials since its inception in 1965. However, this situation may well change with the reformulation of the PGSE experiment as "q-space microscopy" by Callaghan *et al.*[134,140–142] This is based on the analogy between the PGSE experiment in porous materials at long Δ with diffraction theory. The approach has succeeded in relating echo amplitude to microstructure in randomly packed arrays of polystyrene spheres.[134,141] This novel approach has the potential of resolving microstructure at submicrometre distances.

Most recently these ideas have been combined with a numerical cell model to relate $S(q, \Delta, \tau)$ to cell structure in plant parenchyma tissue.[143] Using PGSE data for apple tissue a value for the plasmalemma membrane permeability was estimated. The application of this numerical cell model to mammalian tissue might enable quantitative interpretation of diffusion weighted contrast in clinical MRI. Table 6 lists a number of other applications of the PGSE method to food-related materials, although few of these studies have attempted to explore systematically the whole of the three-dimensional $q-\Delta-\tau$ space.

Table 6. PGSE studies of water diffusion in food-related materials.

System	Reference
Native potato starch grains	99
Parenchyma apple tissue	143
Wheat starch pastes	144
Endosperm of wheat grains	145
Fat and water diffusion in cheese	146
Frog muscle cells	147

3. MAGNETIC RESONANCE IMAGING OF FOODS

3.1. Introduction

The principles of magnetic resonance imaging (MRI) have been covered in a number of textbooks[131,148–151] and reviews.[152–154] In clinical applications MRI is invaluable in providing high-resolution images revealing anatomical features in a non-invasive way. However, this is not usually the case with food imaging since high-resolution "anatomical" or structural information is most simply obtained by visual or microscopic examination after physically slicing the food sample. There are, of course, advantages in being able to examine foods non-invasively with MRI, but the unique value of food imaging lies in the information not readily obtainable by any other physical technique. This information is contained in the spatial dependence of the NMR parameters determining image contrast. Depending on the imaging protocol these include the spin number density (ρ), the longitudinal, transverse and rotating frame relaxation times, the chemical shift, the self-diffusion coefficient and velocity flow rates.

The first stage in food imaging is therefore to process image contrast to obtain quantitative spatial "maps" of one (or more) of the above mentioned NMR parameters in one, two or three dimensions. The changes in these parameter maps during food processing or storage are themselves of great practical importance but perhaps the most challenging and least understood aspect of food imaging is relating the parameter maps to other, more fundamental, physiochemical properties of the food material. These include chemical composition, microstructure, permeability, porosity, temperature, pH, magnetic susceptibility, etc. This interpretational aspect of food imaging necessarily draws heavily on the study of NMR parameters gained using conventional (i.e. non-imaging) NMR spectroscopy. It is interesting to note that since most food materials display a hierarchy of spatial heterogeneity ranging from the macroscopic to the molecular the interpretation of parameter maps may well depend on the spatial resolution used to acquire the image. This can range from several millimetres in wide-bore magnets to only a few micrometres in specially designed microimaging instruments.[134,155,156,157] A number of papers have analysed the factors limiting spatial resolution, chief of which is loss of signal intensity.[134,158] However, in many food samples diffusion of water between voxels can be an important limiting factor.[159] This possibility has recently been explored using a numerical simulation.[160] Distortions arising from susceptibility gradients can also limit resolution.[161]

As the following applications section illustrates, food imaging is still in its infancy. So far most work has merely explored the feasibility of using imaging methods to investigate topics of interest in food science such as drying or crystallization. Relatively few papers have progressed to the stage of reporting quantitative changes in parameter maps. Even fewer papers have attempted

to interpret changes in these maps in terms of the underlying physiochemical properties of the food material. In the following, therefore, we only attempt to discuss the applications in a general way on the basis of the measured NMR parameters.

3.2. Applications of food imaging

3.2.1. Changes in spin number density

Here the transport and redistribution of water or lipid during food processing or storage is of prime concern. Relevant processes include drying, rehydration, heating, frying, microwaving, extrusion, curing, mixing, drainage and syneresis. To obtain spin density maps it is important to correct the measured signal intensity for attenuation due to transverse and longitudinal relaxation unless long recycle times ($TR > 5T_1$) and short echo times ($TE \ll T_2$) are used. Part a in Table 7 lists some representative references. Much work remains to be done in interpreting the observed water (or oil) redistribution using theories for fluid transport based on diffusion, capillary and gravity flow or percolation.

3.2.2. Changes in longitudinal and/or transverse relaxation times

Here mass transport is of minor importance compared to the changes in relaxation times induced by phase changes such as crystallization of water or lipid, phase separation, gelation and/or macromolecule aggregation and denaturation. Since relaxation times are sensitive to temperature, relaxation time maps might also be used to follow temperature changes and heat transport.

It is important to note that the transverse relaxation rate can depend on both the 90°–180° pulse spacing and the spectrometer frequency. This is true, for example, if there is diffusion through internal magnetic field gradients created by susceptibility changes at phase boundaries.[48,175] Proton exchange between water and dissolved macromolecules,[46,47,49] sugars[50] or amino acids[177] can also give rise to a dependence on pulse spacing and spectrometer frequency. This has recently been shown to be the case with several types of plant tissue.[109] Indeed, with courgettes image contrast can be controlled merely by inserting a train of 180° refocusing pulses between the excitation pulse and image acquisition.[178] These extra pulses have the effect of changing the dephasing effect of susceptibility gradients and proton exchange in the plant tissue. It remains to be seen whether similar mechanisms affect image contrast in mammalian tissue.

Low concentrations of paramagnetic ions dramatically shorten water proton relaxation times so the transport of these ions in, for example, plant tissue can be monitored.[153,179] Fat and water also have different proton relaxation times allowing fat and water distributions in meat[180,181] and fish[173] to be measured

Table 7. Imaging studies of food.

System	References
(a) Proton spin density changes	
Water distribution in stems of transpiring plants	162
Water distribution in plant root systems	163
Water distribution during drying of food gels	164
Water distribution during drying of glass bead suspensions	165
Water distribution during the drying of apple tissue	166
Water distribution during ripening of tomatoes	167
Water distribution during drying of an ear of corn	168
Water drainage in foams	169–172
Fat and water distribution in biscuits during baking	173
Water distribution during the germination of maize seed	174
(b) Relaxation time changes	
Relaxation contrast in courgettes	178
Crystallization of trimyristin–water emulsions	173
Freezing peach halves	173
Syneresis of cheese curds	173
Transport of paramagnetic ions in plant systems	153,163,179
Fat and water distributions in meat	180,181
Fat and water distribution in fish	173
Oil content in French salad dressing	182
Oil/water volume fractions in emulsions	183
(c) Imaging the internal quality of fruit and vegetables	
Bruising in apples, onions and peaches	184
Deterioration of apples in storage	185
Oxygen-dependent core breakdown in Bartlette pears	186
Watercore distribution in apples	187

separately. Other representative applications of relaxation contrast imaging are listed in part b of Table 7. Part c in Table 7 lists a number of miscellaneous reports where imaging has been used to monitor the quality of fruits.

3.2.3. Imaging based on parameters other than spin number density and relaxation times

Imaging protocols based on parameters other than spin number density and relaxation times are still in the developmental stage and there are, as yet, few applications to real food materials. A number of articles have discussed the principles of diffusion and/or flow-weighted imaging[134,188,189] and there are numerous clinical applications.[148,190–192] As discussed in the section dealing with the pulsed gradient spin-echo method, the effects of restricted diffusion become paramount when considering the application of diffusion-weighted imaging to spatially heterogeneous food materials. The potential of diffusion- and velocity-weighted microimaging has been illustrated beautifully by Jenner *et al.*, who studied the circulation of water within a wheat grain.[193] The long

time transport of water in food materials can, in principle, be determined by imaging the transport of D_2O either using the loss of water proton signal as H_2O is replaced by D_2O or directly using deuterium imaging. Both methods have been used to study water flow in plant materials.[153,194] When the NMR parameter maps change very rapidly during, e.g. food processing, it may be necessary to use rapid imaging techniques such as echo planar imaging[176] or snapshot flash imaging,[206] although we are unaware of any such applications to date.

The principles of chemical shift imaging have been reviewed.[148,174] In clinical practice chemical shift imaging can be used to resolve fat and water signals. With heterogeneous food materials problems can arise from broadening due to a wide distribution of relaxation times and strong internal susceptibility gradients. Methods have been proposed to alleviate these problems[195,196] and have been used successfully to image oil and water distribution in sandstone.[196]

Multinuclear imaging techniques are being actively developed in a number of laboratories but there are as yet few reported applications to foods. Papers discussing the principles of imaging with deuterium,[194] fluorine,[197] carbon-13[198] and sodium[148,199] have appeared.

4. PROTEINS

4.1. Introduction

Compared to polysaccharides and lipids, food proteins have had relatively little attention. There has been some work on casein (see Section 7) and some spectra reported on a variety of other proteins,[10,12] but apart from α-lactalbumin[9] and wheat proteins[8,11] there has been little systematic work. This is probably because food proteins of interest are often seed storage proteins; typically these are very high molecular weight and relatively heterogeneous, and good quality spectra are therefore hard to obtain. Recent results by Fisher and co-workers have shown well-resolved and sensitive spectra of soy proteins; however, ^1H solution-state spectra tend to be fairly broad.[200] ^{13}C solution-state spectra can be quite well-resolved, but in general shifts are close to those for amino acids and peptides and thus give little useful information. Solid-state high-resolution ^{13}C spectra of proteins are in general disappointing, and food proteins are no exception. Those reported tend to have fairly broad and unexciting spectra; this situation does change if lipid is present, when sharply resolved peaks are resolved under correct conditions.[201] Probably the most informative approach is to try to obtain dynamic information about the system and from this infer details of structure.[202,203] Where smaller molecules are involved much information is available.[9]

Since NMR food proteins has been fairly comprehensively reviewed in the recent past[8–12] this section will limit itself to an overview to indicate the types of information available; it will restrict itself to wheat proteins and α-lactalbumin.

4.2. Wheat proteins

High-resolution ^{13}C solid-state studies of wheat gluten have been reviewed extensively[8,10–12] and a fairly detailed account of early work has been given.[11] Initially spectral interpretation was considerably confused by observation of signals originating from lipid as well as from the protein. Eventually it was found that careful adjustment of acquisition conditions discriminate the two spectra very well,[8] the lipid appearing at very long contact times or under single-pulse excitation conditions (Fig. 6). These results indicated that the lipid was considerably more mobile than the protein. This is the only positive result from these studies. To date, neither solution-state nor solid-state ^{13}C spectra have been able to shed any light on the problem of the origin of gluten quality.[8,11]

Proton relaxation time experiments have shown a diversity of behaviour and environments in gluten. Transverse relaxation widely shows gluten behaviour which can be satisfactorily described by three significant components:[11] a fast relaxing component, showing Gaussian behaviour; an intermediate exponential component; and a slowly relaxing multi-exponential component. The slowest component can be assigned to lipid.[11] The intermediate component, representing between 5 and 15% of the magnetization depends on the origin of the gluten. Pasta- and bread-making glutens extracted in the laboratory show relaxation times that fall into two distinct but close groups. Glutens obtained from commercial extraction plants form a separate, more slowly relaxing group. Lipid-extracted proteins of any origin show the fastest relaxation rates and the lowest intensity of magnetization. It was concluded that the intermediate component represented a fraction of the protein that was mobilized by lipid. The implication of this is that the lipid is intimately involved with the protein on a molecular scale. This view is supported by the earliest NMR work reported.[204] An alternative view[205] based on ^{31}P NMR and electron microscopy holds that the lipid is present in small vesicles and that gluten may be regarded as a micro-emulsion system. These apparently conflicting views are yet to be resolved. T_1 measurements on dry gluten show double exponential behaviour;[202] the components are not sensitive to gluten type or lipid content, but when disulphide bonds are cut, single-exponential relaxation is observed. Based on an argument about spin diffusion it is concluded that the double exponential behaviour resulted from restricted motion about disulphide linkages in a region which had dimensions of the order of 10 nm.[202]

When deuterated water is added to gluten, the protein transverse relaxation signal may be analysed into fast and slow decaying components. The ratio of these changes with temperature until, at 90°C, about 90% of the signal arises from the fast "mobile"[203] component. Upon cooling no hysteresis is observed, although irreversible hardening of the gluten has occurred. It is concluded that the failure to observe hysteresis is because the heat setting phenomenon is due to the formation of permanent disulphide bonds.[203] This may be the

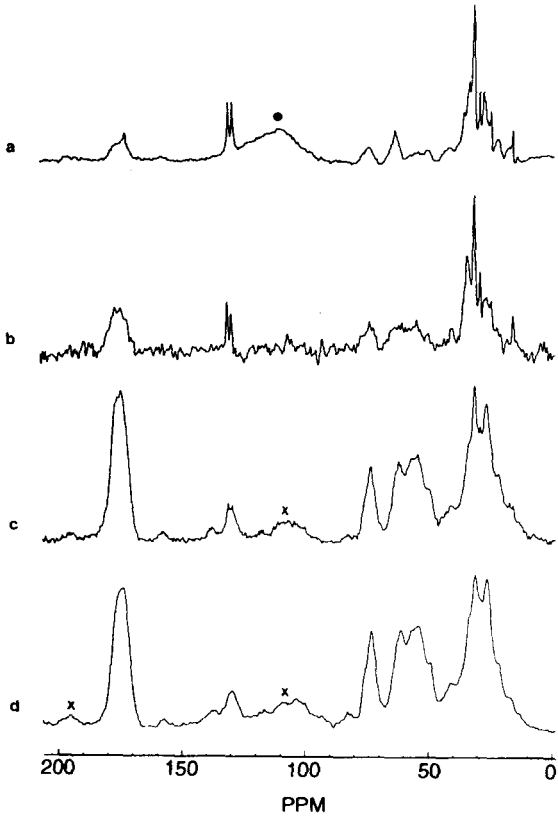

Fig. 6. Solid-state ^{13}C CP/MAS spectra of whole gluten. (a) Single-pulse excitation spectrum. (b, c, d) Cross-polarization spectra with contact times of 20, 5 and 1 ms respectively. (Reproduced from Ref. 201 with permission of John Wiley and Sons.)

case but it may also be that the changes observed result from the behaviour of a small subgroup of proteins. An analogy is the "setting" of water by agar: 1% of agar can turn liquid water into a free-standing gel. If a small percentage of proteins were behaving in an analogous way it may not be possible to detect them by relaxation time measurements.

4.3. α-Lactalbumin

α-Lactalbumin is a milk protein involved in lactose biosynthesis. NMR studies of this compound have been reviewed recently[9] and the interested reader is referred to that reference for further details. A brief survey based on Ref. 9 is given here in order to illustrate further the range of methods available to tackle the problem of structure and function in proteins.

It was not realized, at first, that α-lactalbumin is a calcium-binding protein, and failure to control calcium levels in experimental media made many early results dubious. Direct ^{43}Ca NMR studies have shown that the bound calcium has a chemical shift of −5 ppm, similar to calcium in other calcium-binding proteins. However, the quadrupolar coupling constant obtained indicated a rather more symmetric environment than in comparable systems. In proton relaxation enhancement studies using the binding of Mn^{2+} it was deduced that the binding site was sheltered from direct contact with the solution. Solution-state proton NMR spectra show a range of chemical shift changes on calcium binding. As yet a complete assignment of the spectra has not been made; nevertheless, the chemical shift changes do indicate significant conformational changes on calcium binding.

Photo-CIDNIP is a technique whereby a photo-excited dye reacts reversibly with aromatic amino acids to form radical pairs. Intersystem crossing and interaction with nuclear spins result in changes in nuclear spin population levels which can be observed. The CIDNIP spectrum thus represents signals from nuclei close to the dye. CIDNIP signals were observed from three of the four tyrosines in the system (the fourth was assumed buried) and from tryptophan 104. Signals from tryptophan 60 were the result of cross-relaxation, indicating that it was close to tryptophan 104 but that it was not at the surface. These results, together with nuclear Overhauser effect data, suggest the existence of a hydrophobic box containing aromatic residues. By attaching spin labels to a specific amino acid residue and then examining the effects of the dipolar interaction of the unpaired electron with nuclear spins, it is possible to obtain estimates for the distances from the site of attachment to the spins. In this way a topological map may be constructed giving an insight into the local conformation and its changes on calcium binding.

Whilst there is still much work to be done on α-lactalbumin it is clear that there are a wide range of NMR-based methods which have been used to great effect and which could prove effective on other food proteins provided that they are small enough to give useful high-resolution solution-state spectra. As noted previously, this is a problem with seed storage proteins; however, the synthesis or isolation of smaller peptides representing structural interest may be a useful way of tackling this problem.

5. POLYSACCHARIDES

5.1. Introduction

The interest of the food scientist in polysaccharides includes major dietary components (starch, plant cell wall polysaccharides) and minor but important functional ingredients such as gelling, thickening and stabilizing agents. High resolution NMR is established as one of the most powerful techniques for

structural analysis of carbohydrates in solution[207,208] and the development of cross-polarization magic-angle spinning (CP/MAS) and related techniques has led to studies of polysaccharides in the solid state, in gels, and in heterogeneous samples. In this section we outline some basic features of NMR spectroscopy of carbohydrates and mention recent technical developments. The following sections deal with applications of NMR to food-related polysaccharides in the solution and solid states.

The solvent of choice for most solution-state work is D_2O, so that only resonances of non-exchangeable protons are observed. Occasional use has been made of non-aqueous solvents to solubilize water-insoluble polymers or to study the chemical shifts of hydroxyl protons.[209] The main problem in ^1H NMR spectroscopy of carbohydrates is that the majority of resonances (H-2 to H-6) fall in a limited part of the spectral range, from 3.5 to 4.5 ppm. In structural work, the starting point for interpretation is invariably the less crowded region (4.5–5.5 ppm) containing mainly doublet resonances of anomeric protons. Integration in this region gives the relative numbers of different types of sugar unit, and anomeric configurations are determined from chemical shifts and coupling constants. Tables of chemical shifts and coupling constants for commonly occurring monosaccharides have been published.[210]

Line-broadening can seriously affect resolution in the ^1H spectra of polysaccharides so samples are examined at high temperatures (70°C or above) to increase molecular mobility. ^1H and ^{13}C resonances have similar linewidths, but there is much better dispersion of ^{13}C chemical shifts, and in proton-decoupled spectra single lines are obtained rather than multiplets. For these reasons, ^{13}C NMR has become a standard method for characterization of polysaccharides and useful compilations of ^{13}C chemical shifts for model compounds (mono- and oligosaccharides, homopolymers) have appeared.[211,212] The ^{13}C chemical shifts can be divided into ranges for non-anomeric (60–85 ppm) and anomeric (90–110 ppm) carbons, and the latter region can be subdivided into signals from C-1 at a reducing terminus (90–98 ppm) and C-1 involved in a glycosidic linkage (98–110 ppm). A non-anomeric carbon which is involved in a glycosidic linkage also exhibits a substantial downfield shift (5–10 ppm) relative to the unsubstituted carbon. Resonances of neighbouring carbons are usually shifted upfield, but by smaller amounts. These glycosylation shifts depend upon the type of linkage and on the configuration and conformation of the sugars. An attempt has been made[213] to correlate anomeric and aglyconic ^{13}C glycosylation shifts with conformation using the torsion angle ψ (C_1–O_1–C'_n–H'_n, where n indicates linkage position). Values of ψ were obtained from minimum energy conformations calculated using the hard spheres *exo*-anomeric (HSEA) method. ^1H and ^{13}C glycosylation shifts have been studied systematically for disaccharides with $(1 \rightarrow 6)$,[214] $(1 \rightarrow 2)$ and $(1 \rightarrow 3)$[215] and $(1 \rightarrow 4)$[216] linkages. Glycosylation shifts from these and similar studies form the database of computer programs for the automated determina-

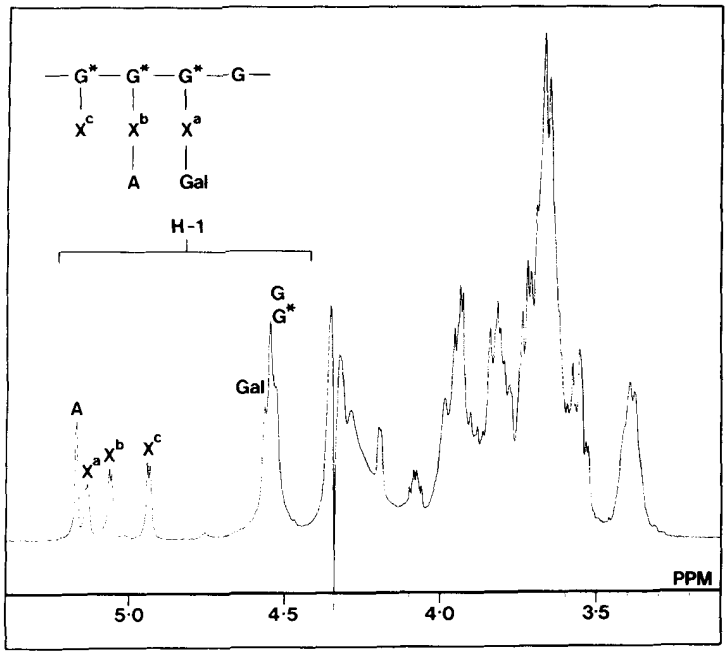

Fig. 7. 400-MHz ^{1}H NMR spectrum (70°C) of potato xyloglucan. G = (1 → 4)β-Glc*p*, G*= (1 → 4, 6)β-Glc*p*, X = (1 → 2) and *t*-α-Xyl*p*, A = *t*-α-Ara*f*, Gal = *t*-β-Gal*p*. The displayed structure is only intended to represent the different sugar residues and does not indicate a repeating unit.

tion of polysaccharide structure based on ^{13}C spectral data[217,218] or a combination of ^{1}H and ^{13}C chemical shift and coupling constant data.[219] One program is being extended[219] to deal with banded structures as well as linear polysaccharides.

Complete assignment of the ^{1}H spectra of complex carbohydrates has become possible with the development of 2D NMR techniques[220,221] such as the COSY, RELAY and HOHAHA experiments. There are a number of examples of the application of these techniques to cellulose[222] and starch[223,224] oligomers. Double-quantum filtered phase-sensitive COSY experiments with adequate digital resolution provide information on the pattern of coupling constants and the chemical shifts within a sugar ring. This is often sufficient to identify the type of sugar residue and the anomeric configuration. Following assignment of the ^{1}H spectrum, subsequent assignment of the ^{13}C spectrum is straightforward if a ^{1}H–^{13}C shift correlation experiment is performed. Alternatively, the excellent dispersion in the ^{13}C dimension may be used to resolve ambiguities in the interpretation of the ^{1}H spectrum. Such experiments are not restricted to oligosaccharides. Figure 7 shows the heavily overlapped ^{1}H spectrum of a xyloglucan polysaccharide isolated from potato cell walls, whilst Fig. 8 illustrates the resolution which can be achieved by 2D heteronuclear shift

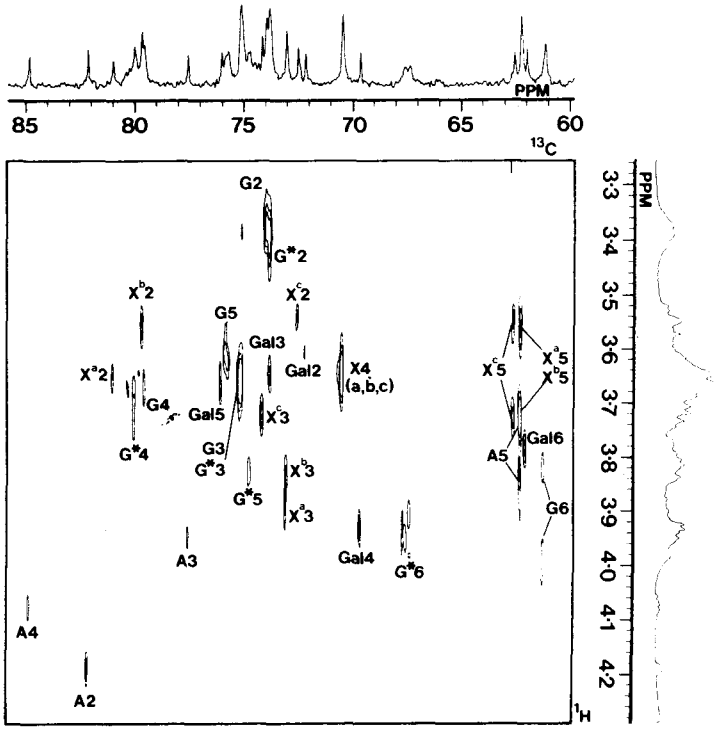

Fig. 8. 2D $^{13}C/^{1}H$ shift correlation spectrum of the xyloglucan polysaccharide shown in Fig. 7. The anomeric region is not shown. A partial assignment of the ^{1}H spectrum was first made from COSY, RELAY and NOESY experiments and was completed using the spectrum shown above. (I.J. Colquhoun, P. Ryden and R.R. Selvendran, unpublished.)

correlation methods for this type of molecule. The introduction of inverse (^{1}H) detection methods[225] now allows heteronuclear correlation spectra to be obtained from much smaller amounts of sample.

The COSY experiment cannot be used directly to determine the sequence of sugars in an oligosaccharide or polysaccharide because the coupling constant between anomeric and aglyconic protons is close to zero. However, indirect evidence for the location of glycosylation sites may be obtained by comparing ^{1}H chemical shifts in the polysaccharide with those of the component monosaccharides. More direct methods have relied on the detection of the NOE between anomeric and aglyconic protons in NOESY[226] and ROESY[227,228] experiments, on the detection of ^{1}H–^{13}C scalar coupling across the glycosidic linkage with the HMBC method,[225,229] or on ^{13}C glycosylation shifts.[217,219]

Although primary structures may be established by qualitative observation of the NOE, the determination of the three-dimensional structure of carbohydrates in solution requires a quantitative treatment of the NOE.[230] In carbo-

hydrates it is rarely possible to measure more than two inter-residue proton–proton distances between any pair of linked residues. NMR data alone cannot define a unique conformation and therefore information from NOE measurements is combined with some form of potential energy calculation. HSEA calculations[231] have been used most widely to exclude sterically unacceptable conformations and restrict the range of allowable glycosidic torsion angles. Recent work has focused on the development of more sophisticated theoretical methods and on problems posed by internal molecular motions.[232,233] The correlation of solid-state NMR data with polysaccharide conformation is dealt with in Section 5.3.

5.2. Polysaccharides in solution

Block structure is an important factor controlling the gelling properties of many polysaccharides. NMR can provide a rapid measurement of overall composition but may also be sensitive to fine details of the polysaccharide sequence, as the following examples show. The degree of esterification (d.e.) of pectins can be determined from the intensity of the galacturonic acid H-5 resonances, since these show a marked downfield shift on esterification. A sequence-dependent splitting of the H-1 and H-5 signals for free (G) and esterified (E) galacturonic acid allowed determination of the frequency of the diads GG, EG(GE), EE and G-centred triads in pectins of different d.e.[234] ^{13}C NMR spectra of the carbonyl region have been used to determine the fraction of different E-centred triads in pectins.[235] In both cases de-esterification by alkali gave a random distribution of ester groups. In galactomannans (e.g. guar, locust bean gum), some mannose residues of the backbone are substituted at C-6 by single galactose residues. The C-4 resonance of mannose is sensitive to sequence and three signals are obtained corresponding to M*M*, M*M plus MM*, MM diads where M* and M are substituted and unsubstituted mannose residues.[236] At a higher magnetic field, splitting of the C-6 resonance of M* permitted determination of the frequency of M*-centred triads.[237] Alginates are linear polysaccharides made up of blocks of guluronic (G) and mannuronic (M) acid residues. Splittings in the C-1, C-6, C-4 (M) and C-5 (M) regions of the 50-MHz ^{13}C spectra enabled the diad and triad frequencies to be obtained and gave an indication of average block lengths.[238] Splittings of the H-5 (G) resonance were observed in 400-MHz ^{1}H spectra, and the chemical shifts were interpreted in terms of the conformation of GM and GG units.[239] The conformation of polyguluronic acid has also been studied by ^{1}H and ^{13}C relaxation time measurements.[240]

Structural features of starch polysaccharides have been quantified from characteristic signals in high-temperature ^{1}H and ^{13}C spectra.[241] The H-1 resonances of $(1 \rightarrow 4)$- and $(1 \rightarrow 6)$-linked glucose units occur at 5.4 and 5.0 ppm respectively. Integration of these signals gave the ratio of $\alpha(1 \rightarrow 4)$ to $\alpha(1 \rightarrow 6)$

linkages in amylopectins. In degraded starches the ratio of non-reducing to reducing units could be determined since H-1 signals of the reducing-end units were well-resolved from those of mid-chain residues. Average side-chain lengths have been determined from ^{13}C spectra of pectic polysaccharides. In onion pectin signals of the terminal non-reducing units of the $\beta(1 \rightarrow 4)$-linked galactan side-chains were resolved from signals of mid-chain residues. An average degree of polymerization (d.p.) of 9 was determined for the side-chains which are attached to the galacturonic acid backbone.[242] The galacturonic acid content of pectic polysaccharides may be underestimated from ^{13}C NMR spectra,[242–244] although there are exceptions.[245] It has been suggested that loss of the uronic acid signal may be attributed to restricted motion of the backbone[243,244] or to interaction with traces of metal ions. Addition of a chelating agent can overcome the latter problem.[234] Detailed ^{1}H and ^{13}C NMR studies have been made of oligo- and polygalacturonic acids[246,247] and 2D NMR was used to identify oligosaccharides containing rhammose, galacturonic acid and galactose produced by enzymic degradation of the hairy regions of apple pectin.[228]

Arabinoxylans have a backbone of $\beta(1 \rightarrow 4)$-linked xylose residues, which can be substituted at O-3 or O-2 and O-3 by α-L-arabinose units. They are minor but important constituents of wheat flour, affecting loaf volume and crumb texture of bread. The degree of substitution and the ratio of mono- to disubstituted xylose residues have been determined from characteristic signals in the anomeric region of the ^{1}H spectrum. The structures of arabinoxylans extracted from flour, dough and bread were investigated in this way.[248] The functional properties of arabinoxylans are related to a gelation process which involves formation of ferulic acid cross-links. Enzymic degradation of arabinoxylans has released oligosaccharides in which phenolics such as ferulic acid are ester-linked to arabinose units. Trisaccharides of this type containing one Ara*f* and two Xyl*p* units have been characterized by 2D NMR.[249]

NMR studies of the gelling polysaccharides agarose, κ- and ι-carrageenan have been reviewed,[250] and the ^{13}C spectra of oligomers of κ- and ι-carrageenan have been assigned.[251,252] The effects of sulphate substitution on ^{1}H and ^{13}C chemical shifts in galactose and anhydrogalactose residues are now well-established from the above and from work on model compounds.[253–255] NMR has been used to study the composition of crude carrageenans (containing a mixture of polysaccharides) and to relate structure to gel properties.[256] Helix–coil transitions of non-gelling κ- and ι-carrageenan "segments" have been investigated by variable-temperature ^{13}C NMR.[257,258] Cooling solutions of κ-carrageenan (in the K^{+} form)[257] or ι-carrageenan (in 0.1 M NaCl)[258] from 80 to 15°C led to complete loss of ^{13}C signals. At intermediate temperatures there was gradual loss of intensity from the high-resolution spectrum, but line-broadening or chemical shift changes to the remaining signals were not observed. This behaviour was taken to support a two-state model in which polymer chains existed either as rigid double helices

or in the random coil form. By contrast, oligomers (d.p. 6–10) of ι-carrageenan in 1 M aqueous salt solution gave broadened and shifted signals at low temperatures as well as signals in the expected positions for the random coil.[259] The broadened signals apparently arise from oligomers which have undergone a transition and in which a range of linkage conformations have been "frozen out". NMR of all the alkali metal ions has been used to study ion binding in κ- and ι-carrageenan gels. There is evidence (from intensity loss, pronounced line-broadening and chemical shift changes) for selective ion-binding of K^+, Rb^+ and Cs^+ in gels of κ-carrageenan,[260,261] and of weaker binding of K^+ and Rb^+ to ι-carrageenan.[262,263] In the case of ι-carrageenan, ^{87}Rb NMR studies of "pure" ι- and mixed ι-/κ-carrageenan gels have suggested that the observed effects are due to the presence of small amounts of κ-carrageenan in the "pure" ι-samples.[264]

NMR has been used for the characterization of bacterial polysaccharides such as xanthan and gellan gum which are approved or proposed for food use. The acetate and pyruvate content of xanthan can be measured from integration of the methyl signals in the high-temperature ^1H spectrum.[265] Disappearance of these signals as the temperature is reduced provides a means of monitoring the transition from coil to helix.[266] Preliminary studies of the high-resolution ^{13}C spectrum of xanthan have appeared. Samples were first sonicated[267] or partially depolymerized with cellulase[265] to reduce the linewidths. More detailed ^1H and ^{13}C 2D NMR studies have been made of xanthan oligosaccharides representing the pentasaccharide repeating unit. Assignments were obtained for oligomers with acetate and pyruvate present and with one or both substituents removed.[268] NMR was used to determine the anomeric configuration of the sugar units in the repeating unit of gellan gum.[269] Subsequent 2D NMR studies of oligosaccharides released by treatment of gellan with anhydrous HF revealed the presence of L-glycerate as a substituent. The locations of the glycerate and of a second substituent, acetate, were determined.[270]

5.3. Solids, gels and heterogeneous systems

Development of the solid-state NMR techniques of cross-polarization magic-angle spinning (CP/MAS) and dipolar decoupling has stimulated many studies of polysaccharides, especially of cellulose[271] and starch,[13] which have been reviewed. The work on starch provides an excellent example of the information obtainable from solid-state NMR. Native starch granules have crystalline and non-crystalline regions. The crystalline regions are made up of an ordered arrangement of polymer chains in the form of double helices, whereas the amorphous regions contain single chains. The two polymorphs of starch, A (from cereals) and B (from tubers), have different packing arrangements of the double helices. CP/MAS spectra of various native starches have clearly distinguishable crystalline and amorphous components.[272] The relative contribu-

tion of the two components was estimated by adding spectra of model compounds in the proportions required to simulate the observed spectrum.

A- and B-type crystalline starches were distinguished by the multiplicity of the C-1 resonance,[272,273] a 1 : 1 : 1 triplet for A and a 1 : 1 doublet for the B form. The same multiplicities have been observed in well-resolved spectra from highly crystalline A- and B-amyloses of low d.p.[274,275] The asymmetric unit is a maltotriose unit for A-starch and a maltose unit for the B-form,[276] in agreement with the observed multiplicities for the C-1 signal. However, at present, it is not possible to say whether these splittings are mainly due to different glycosidic torsion angles within the asymmetric unit[273] or to molecular packing effects.[272] CP/MAS spectra of A- and B-amyloses are dependent upon water content. Dehydration resulted in marked increases in linewidth and changes of chemical shift as the crystal structure was disrupted by loss of water.[274,275] Monodisperse amyloses (d.p. 40, 110 and 250) precipitated from dilute aqueous solution all give the B-type spectrum.[280] The resolution deteriorated as the d.p. was increased, but there was no evidence for presence of amorphous material. This suggests that the amylose chains exist entirely as aggregated double helices but become less perfectly packed as d.p. increases.

CP/MAS spectra have been recorded for a variety of crystalline V-amyloses,[274,277,278] in which the polysaccharide chains are single helices. V-Amyloses gave spectra with broader lines, were less sensitive to dehydration and showed marked chemical shift changes in comparison with the crystalline A- and B-polymorphs. There are similarities between the spectra of V-amyloses and amorphous starches, particularly in the chemical shift (83 ppm) of the C-4 resonance. However, the C-1 resonance of V-amylose is a single line at 103 ppm, whilst in amorphous starch the C-1 signal extends from 93 to 106 ppm with a peak at 103 ppm, and a weighted average value of 101.5 ppm (very similar to the solution-state value). There have been several attempts to correlate the C-1 chemical shift in $\alpha(1 \rightarrow 4)$-linked glucans with glycosidic torsion angles using data from X-ray diffraction studies and CP/MAS experiments on model compounds such as cyclodextrins.[277–279] Two correlations were found between C-1 chemical shift and angle $|\psi|$ or parameter $(|\phi| + |\psi|)$ where ϕ is the angle H-1–C-1–O-1–C-4′ and ψ is H-4′–C-4′–O-1–C-1.[278] A theoretical ϕ, ψ energy map for $\alpha(1 \rightarrow 4)$-linked glucose residues showed a sharp distinction between "allowed" and "disallowed" conformations. Assigning equal weight to all allowed conformations and using the correlation of chemical shift with $|\phi| + |\psi|$, the lineshape of the C-1 resonance in amorphous starch was well-simulated.[278]

The experiments described above were carried out on true solids, but solid-state techniques are also applicable to gels. Contrasting spectra of 10% amylose gels have been provided by single-pulse magic-angle spinning (SP/MAS) and CP/MAS experiments.[280] At room temperature, the SP/MAS experiment

gave a "solution-state" type spectrum of amylose with narrow lines. The signals arose from the single amylose chains which link the junction zones of the gel network. These chains retain a degree of mobility (and hence have short ^{13}C T_1 values), but the motion is anisotropic since MAS is necessary to remove chemical shift anisotropy effects. The room temperature CP/MAS spectrum of the same gel was identical to that obtained for B-type crystalline samples. Here the signals arose from the rigid double helical segments which make up the junction zones. Resonances from both mobile and rigid segments were observed in a CP/MAS spectrum of the frozen gel, although the spectrum of the single chain segments was now broadened and was essentially identical to that of amorphous amylose. At the lower temperature the local conformations are evidently not motionally averaged in the single chains, giving rise to the broad C-1 resonance. The proportion of amylose in the junction zones (70–80% for the samples studied) was estimated by spectral simulation.[280]

^{13}C CP/MAS and SP/MAS spectra have been obtained for galactomannans and glucomannans as powders, hydrates or gels. Comparison of CP and SP experiments on galactomannan gels did not reveal any chemical shift changes (unlike amylose), suggesting that the conformations of mobile and rigid segments are similar. However, minor intensity changes suggested that the degree of substitution of the mannan backbone might differ in the two regions.[281] CP/MAS experiments have been performed on purified carrageenans and agaroses and on the seaweeds which are the source of these materials.[282] Although lines were broad, characterization of the intact algae was possible and various substituents were identified.

High-power ^1H NMR measurements on solutions,[283] gels[280] and plant cell wall materials[116,284] have been used to probe the conformational mobility of polysaccharide chains through measurement of T_2 and other relaxation parameters. The ^1H T_2 can vary from $\sim 10\,\mu s$ for rigid chains to $\sim 100\,ms$ for more flexible segments. Resolution of the signal into different T_2 components allows an estimate to be made of the proportion of polysaccharide in mobile and rigid domains. In studies[116] of bean cell walls hydrated in D_2O it proved possible to divide the polysaccharides into an immobile fraction (75%) consisting of cellulose and associated hemicellulose and a more mobile fraction (25%) made up of pectins and additional hemicellulose. Mobilities were obtained from solid echo experiments, used to measure the proton interpair second moment. T_1 and T_1 (dipolar) relaxation results were combined to estimate the relative size of the cellulose microfibrils and the surrounding hemicellulose layer. ^{13}C CP/MAS experiments have also been used to investigate plant cell wall structure and degradation.[285] Despite considerable technical problems posed by CP/MAS experiments on highly hydrated systems, solid-state NMR clearly holds considerable promise for the study of polysaccharides in gels, cell walls and related environments.

6. ANALYTICAL METHODS

6.1. Introduction

The high cost of NMR spectrometers and the relatively low sensitivity in comparison with competing methods has prevented the adoption of the technique as a routine analytical tool in the food industry. Exceptions to this general statement are provided by the low resolution "bench top" NMR spectrometers which have found widespread use in the edible oils and fats industry. Applications of this technique are dealt with in Section 6.2. Analytical applications of high-resolution NMR to lipids, sugars and miscellaneous compounds are summarized in Section 6.3. For the most part these methods are not in routine use, but remain demonstrations of possibilities. One high-resolution NMR technique which has been highly developed in recent years is site-specific natural isotope fractionation (SNIF) NMR (Section 6.4), which makes use of natural abundance deuterium spectra to investigate the origin and quality of food products. In this case the costs of the sophisticated equipment required can be justified by the unique nature of the information provided.

6.2. Low-resolution NMR

The earliest applications of NMR to analytical problems in the food industry employed CW techniques. Commercial pulsed NMR instruments were introduced at a later stage, but pulsed NMR is now the more widely used of the two methods. Practical aspects of low-resolution pulsed NMR techniques have been reviewed[21,286] and the manufacturers' (Bruker, Oxford) application notes also provide valuable information on specific procedures.

Low-resolution NMR techniques can be divided into three categories: ratio measurements, absolute measurements and analysis of the relaxation decay curve. Ratio measurements (measurement of the FID amplitude at two times following a 90° pulse) are used to determine the solid fat content (SFC) of semi-solid fats. Weighing of the sample is not required. Absolute measurements rely on a measurement of the FID amplitude at a single time following the pulse. The main applications are to determination of the oil content of seeds and moisture content of foods. In this case a calibration must be obtained using an independent method and the sample has to be weighed. The third technique requires analysis of the relaxation decay curve and is used when two species are present (e.g. oil and water) with fairly similar values of T_1 or T_2. Analysis of the decay curves is then readily carried out by transfer of the relaxation data to a PC and treatment with appropriate software to obtain the relaxation times and proportions of the components of interest. NMR is ideally suited to quality control applications where large numbers of similar samples have to be examined. Measuring times are very short (a few seconds), little sample preparation is

required and the technique is non-invasive. Operation is highly automated with both the pulse sequence and the calculation routine contained on an EPROM which can be changed according to application.

Hardware requirements are somewhat different for ratio and absolute measurements. For measurement of solid fat content, short 90° pulses (1–2 μs) and short dead-times (< 10 μs) are the priorities. For absolute measurements good rf homogeneity over the sample volume is required and larger rf coils are designed to achieve this. Typical operating frequencies are 10 or 20 MHz and the sample tubes have diameters from 10 mm to 40 mm. The larger tubes are used with lower-frequency spectrometers (10 MHz) because it is difficult to make permanent magnets with the necessary field stability and homogeneity if the air gap is large.

Measurements of the solid fat content are made by taking the amplitude of the FID at two times (typically 10 and 70 μs) following the 90° pulse. The first amplitude is proportional to the total number of protons (solid plus liquid phase) whereas the second amplitude depends only on the number of liquid-phase protons. The rapid decay of the solid-phase signal requires that a correction factor is determined to allow for the decay of the signal during the spectrometer dead-time. The correction factor is determined using calibration standards of known composition. Details of calibration methods, tempering procedures for fats and a comparison of NMR with other methods can be found in a review.[22] Other publications in this area are listed in Table 8.

The analysis of oil seeds represents one of the major applications of pulsed NMR. This uses the absolute method, relying on measurement of the FID signal at a single time after the pulse when the signal is proportional to the liquid content of the sample. Problems arise in taking the measurement at a single time (e.g. 70 μs) since any moisture present will affect the amplitude. One solution is to dry the sample completely but if moisture is present at a low level (< 15%) this is unnecessary.[286] At low moisture levels the T_2 of water (~ 1 ms) is much shorter than that of the oil (~100 ms) and a Hahn spin-echo technique can be used to obtain a signal which depends only on the oil content. In practice, the echo amplitude is measured 7 ms after the initial 90° pulse. A calibration is necessary using seeds of known oil content or oil which has been extracted from the seeds. The difference between the FID amplitude at 70 μs and the echo amplitude at 7 ms is proportional to the moisture content. In oil seeds with higher water contents or products such as marzipan the T_2 of water is much closer to that of oil. A CPMG experiment must then be carried out and the resulting T_2 relaxation curve analysed to give the proportions of the two components. Even for this procedure the time for experiment and calculation (about 1 min) compares very favourably with alternative procedures such as oven-drying. Other applications of spin-echo and CPMG techniques to analysis are given in Table 8.

The possibilities of using high- and low-resolution NMR for on-line sensing

Table 8. Analytical applications of low-resolution NMR.

Product	Property	Method	References
Milk fat	Solid fat content	FID	287
Cocoa butter	Solid fat content	FID	288
Milk fat			
Cocoa butter	Solid fat content	T_2	289
Edible oils			
Margarine	Solid fat content	FID	290
Model fats	Solid fat content	FID	291
Chocolate	Fat	FID	292
Chocolate	Fat	SE	293
Cocoa butter	Melting curve	FID	294
Oil seeds	Oil	T_2	295
Oil seeds	Oil/moisture	T_2	296
Olive husk	Oil/moisture	FID/SE	297
Yeasts	Moisture	FID	298
Cereal grains	Moisture	SE	299
Sucrose solutions	Moisture	SE	300
Molasses			
Emulsions	Oil/water	T_1	301
Meat	Quality parameters	T_1, T_2	302
Meat	Fat	T_1	24
Meat	Protein	T_2	303
Various	Protein	T_2	304
Maize oil	Unsaturation	T_1	305

SE indicates use of a Hahn spin-echo; T_2 measurement is by the CPMG sequence.

and process control have been investigated. A system incorporating a simple NMR spectrometer has been described for the measurement and on-line control of the moisture content of wheat, using the amplitude of the FID 8 μs and 64 μs after the 90° pulse. The initial value is proportional to the total amount of wheat in the active volume of the NMR coil, and the second amplitude depends only on the moisture content. The method was combined with a measurement of the Hahn echo amplitude (4 ms after the 90° pulse) to determine oil and water content of ground corn samples containing 8–20% moisture and 3–15% oil.[306,307] A high-resolution NMR spectrometer has been modified to make analytical measurements on samples in continuous flow, and the principles of NMR for flowing systems have been reviewed. The amounts of water and fat in a fine meat paste were determined from the intensity ratio of the H_2O and CH_2 resonances as the paste was pumped through the spectrometer.[308] Earlier off-line experiments had illustrated the possibility of using simple high-resolution NMR equipment to measure the fat content of meat.[309] Low-resolution NMR methods have been devised to determine the alcohol content of wines and spirits[310] and to monitor changes of alcohol and sugar concentrations in fermentation processes.[311]

6.3. High-resolution NMR

High-resolution applications of NMR in food science have been reviewed.[26] Since the appearance of this review in 1984, the use of 2D NMR techniques has become commonplace, greatly increasing the power of NMR as a method for structural analysis of complex natural products, including many minor food components. In this section, however, attention will be given to quantitative rather than structural applications of high-resolution NMR.

^{1}H and ^{13}C NMR are established methods for the characterization of lipids.[23] Experimental requirements for the quantitative determination of the fatty acid composition of triglycerides by ^{13}C NMR are well-understood.[312] As an example, palm oil is composed of triglycerides, mainly of palmitic, P (16 : 0), oleic, O (18 : 1[*cis*]-9), and linoleic, L (18 : 2, [*cis*, *cis*]-9,12) acids. The mole fractions of P, O and L are readily calculated from integration of ^{13}C resonances assigned to the saturated carbons C_3, $[O_{8,11} + L_{8,14}]$ and L_{11}. The integrals are proportional to the total number of chains (saturated and unsaturated), to the number of unsaturated chains, and to the number of linoleic acid chains, respectively. Alternatively the O : L ratio may be obtained from integration of the olefinic carbon resonances, $O_{9,10}$, $L_{9,10,12,13}$, in the 127–130 ppm region of the spectrum.[313] The method can also be applied to triglycerides containing less common fatty acids. For example, the composition of seed oils containing various isomeric conjugated trienoic acids has been determined.[314] The positional distribution of O, L and linolenic, Ln (18 : 3, [*cis*, *cis*, *cis*]-9,12,15) acid chains may be determined from the high-field ^{13}C spectra of triglycerides.[315,316] The olefinic resonances, $O_{9,10}$, $L_{9,10}$ and $Ln_{9,10}$ are sensitive to the position of attachment (1,3- or 2-) of the unsaturated chains to the glycerol group. Similar information is obtainable from the carbonyl resonances,[317] but the spectrum in this region also indicates the distribution of saturated chains between 1,3- and 2-positions. However, different saturated chains (palmitic, stearic) are not distinguished.

The possibility of using standard high-resolution ^{13}C NMR techniques to determine the oil composition of single intact soyabean seeds was demonstrated in 1974.[318] At this time it was not possible to quantify the different types of unsaturated fatty acid from ^{1}H NMR spectra of intact seeds because internal variations in magnetic susceptibility caused unacceptable line-broadening. Improved resolution in both ^{1}H and ^{13}C spectra of oil seeds has been achieved through application of the MAS technique.[316,319] Quantitative measurements of the oil composition of sunflower seeds have been obtained using ^{1}H and ^{13}C (gated decoupling) MAS. Rape seeds have low oil content (about 2 mg oil/seed compared with 20 mg oil/seed for sunflower seeds) and a complex unsaturated fatty acid profile. Sensitivity has been improved by use of the distortionless enhancement by polarization transfer (DEPT) technique in combination with MAS and this has permitted determination of the relative amounts of O. L, Ln and total eicosenoic (20 : 1, [*cis*]-11) plus erucic

(22 : 1, [*cis*]-13) fatty acids in rape seeds.[316] ^{13}C NMR of lipids extracted from rice endosperm, aleurone cells plus grain coat, and embryo has been used to determine the amount of lipid associated with each component and the ratio of saturates to unsaturates.[320] High-field ^{31}P NMR has been used for the quantitative analysis of phospholipid mixtures.[321,322] Special precautions are required to obtain narrow linewidths and reproducible chemical shifts because the dispersion of chemical shifts for the different phospholipids is small (~ 2 ppm). If these precautions are followed, good resolution may be obtained. For example, 11 phospholipids were identified and quantified in an extraction mixture from soyabean.[322]

^{31}P NMR methods have been devised for the analysis of phytate (*myo*-inositol hexaphosphate) in cereals and other foods.[323,324] Measurement of phytate levels has been of interest to nutritionists because the availability of some essential metals is reduced by formation of metal–phytate complexes. NMR is probably not suitable as a routine method of phytate analysis but it has the advantage that the hexaphosphate is distinguished from lower inositol phosphates which may be present. ^{31}P NMR has been used to follow the step-wise enzymic hydrolysis of inositol hexaphosphate to lower phosphates and eventually to inorganic phosphate. The hydrolysis of phytate in soluble extracts of whole-grain wheat flour and in bread dough during fermentation has been studied by NMR. The conventional ferric ion precipitation method for determination of phytate gave consistently higher results than ^{31}P NMR because the chemical method was not specific for hexaphosphate.[325] ^{31}P NMR was used to show that there is comparable phytase activity in oats and in whole-grain wheat flour. However, no breakdown of phytate was observed in oats that had received heat treatment, presumably because this treatment inactivates phytase.[326]

A method for the determination by ^{13}C NMR of sugars (glucose, fructose, sucrose, maltose) present in extracts from tropical root crops has been described.[327] The peak heights of characteristic signals in the sugar mixture were determined relative to an internal standard, present at a fixed concentration in all solutions. Sugar solutions of known concentration, also containing internal standard, were used for calibrations.[327] ^{13}C NMR has been used for the analysis of minor disaccharides present in honey. Sample preparation included reduction of the sugars with sodium borohydride and use of DMSO as a solvent with addition of a relaxation agent.[328] Numerous monosaccharides, disaccharides, sugar alcohols and sugar acids have been identified and determined by ^{13}C NMR spectroscopy of wine. Compounds with concentration greater than 1 g/litre are determined directly by examination of the natural wine, but concentrates are used for lower concentrations. 1,3-Propanediol is added as an internal standard.[329] In comparison with ^{13}C NMR, high-resolution ^{1}H NMR of aqueous systems has received relatively little attention as a multicomponent analytical technique in food science. This is partly because of the increased complexity of the spectra and reduced spectral dispersion and

partly because there is a need to suppress the massive water signal. Efficient methods for the suppression of the water signal are now available and have been applied to samples such as milk, fruit juices and coffee.[330,331] However, only the major solute signals (sucrose, fructose, citrate, caffeine, etc.) were identified in these studies and little quantitative work has been done. In view of the great progress made with high-field ^{1}H NMR of aqueous systems in biomedical research, it seems likely that this will be an area for future expansion in food science.

6.4. Site-specific natural isotope fractionation NMR

The percentage of heavy isotope occurring for a given element (hydrogen, carbon, oxygen) in natural products is not a fixed qantity, but depends on the history of the sample. Various geographical, climatic and biochemical factors determine the isotope ratios. The variation arises from differences in isotopic composition of the starting materials (e.g. the rainwater at different latitudes) and from fractionation effects which occur in the course of bioconversions. A well-known example is provided by the difference in $^{13}C/^{12}C$ ratios found in organic material from "C_3-" and "C_4-plants".[20] The measurement of isotope ratios by mass spectrometry is a widely used method for assessment of the authenticity of food products.[20] However, an overall or average isotope ratio is determined and information on the intramolecular distribution of the heavy isotopes is lost. An important advance came with the introduction and development, mainly by the Nantes group, of the SNIF (site specific natural isotope fractionation) NMR technique. Quantitative natural abundance ^{2}H NMR is used to measure the deuterium to hydrogen isotope ratios $(D/H)_i$ at specific sites, i, in the molecule. The introduction of these new parameters has greatly extended the scope and discriminatory power of isotope ratio methods in food science. A comprehensive review has appeared[17] covering fundamental aspects, experimental details and quality assessment applications.

The site-specific isotope ratio, $(D/H)_i$, is related to the overall isotope ratio for the molecule, $\overline{(D/H)}$, by equations (7) and (8):

$$(D/H)_i = \frac{f_i}{F_i}\overline{(D/H)} \tag{7}$$

$$\overline{(D/H)} = \sum_i F_i (D/H)_i \tag{8}$$

where f_i and F_i represent actual and statistical mole fractions of monodeuterated isotopomer i. f_i values are measured from the ^{2}H NMR spectrum, and can be used to obtain relative values of the isotope ratios. Absolute values of $(D/H)_i$ can be obtained from the NMR spectrum with use of a suitable reference (see below).

SNIF-NMR was originally developed to detect addition of exogenous sugars during the wine-making process. Analysis and characterization of wines[18] and other alcoholic drinks[332,333] has remained one of the main applications and this area will be used to illustrate the main principles of the technique. Samples from alcoholic drinks are examined as distillates containing $\sim 95\%$ ethanol. Collection and analysis of the NMR data have been highly automated.[18] The proton-decoupled ^2H NMR spectrum of an ethanolic distillate consists (in the slow exchange limit) of four resonances, one from each of the monodeuterated isotopomers, CH_2DCH_2OH (I), CH_3CHDOH (II), CH_3CH_2OD (III) and one from HDO. In the fast exchange limit the signals for (III) and HDO collapse to a single resonance. Following equation (8), the overall isotope ratio is given by

$$\overline{(D/H)} = \tfrac{1}{2}(D/H)_I + \tfrac{1}{3}(D/H)_{II} + \tfrac{1}{6}(D/H)_{III} \tag{9}$$

The parameter R, obtainable directly from the NMR spectrum has been defined[332] as

$$R = 3\frac{S_{II}}{S_I} = 2\frac{(D/H)_{II}}{(D/H)_I} \tag{10}$$

where S_{II} and S_I are the signal intensities (peak areas or heights) associated with the methylene and methyl resonances respectively. A value of 2 is expected for R in the event of a purely statistical distribution of deuterium, but values of ~ 2.2–2.7 are found in alcohols from different sources,[332] indicating the occurrence of strong site-specific fractionation effects. The isotope ratios for the hydroxyl site $(D/H)_{III}$ and the water $(D/H)_W^Q$ are not independent but are related via the equilibrium constant, K_e (= 1.03) for the reaction:

$$C_2H_5OH + HOD \rightleftharpoons C_2H_5OD + HOH$$

$$(D/H)_{III} = K_e(D/H)_W^Q \tag{11}$$

$(D/H)_W^Q$ can be obtained by NMR, but is normally measured by mass spectroscopy (MS) of the water remaining after distillation.[18]

Absolute values of $(D/H)_i$ may be obtained if the NMR signal intensities of the ethanol or other test material are measured relative to that of a working standard (WS), with a known isotope ratio, $(D/H)^{WS}$. The working standard may be an external reference (in a coaxial tube) or an internal reference added to the test solution. The merits of different referencing procedures have been discussed.[334] For measurements on ethanol, tetramethylurea (TMU) is used as an internal reference. $(D/H)^{WS}$ is determined by MS with respect to an internationally agreed water standard, a value of 135 ppm being used currently for TMU.[19] The isotope ratio for site i of a compound A may then be calculated from

$$(D/H)_i^A = \frac{P^{WS}}{P_i^A} \cdot \frac{m^{WS}}{m^A} \cdot \frac{M^A}{M^{WS}} \cdot T_i^A \cdot (D/H)^{WS} \tag{12}$$

where P^{WS}, P_i^A are the stoichiometric number of protons in WS and site i of A, m^{WS} and m^A are the masses of WS and A in the sample, M^{WS} and M^A are the molecular weights, and T_i^A is the ratio of the NMR signal intensities (S_i^A/S^{WS}). An intramolecular referencing procedure has also been used in studies of glucose.[335] Conversion of glucose to glucose pentaacetate, using acetic anhydride of known (D/H) ratio, provides an in-built reference and gives better dispersion of ^2H signals from individual glucose sites.

The parameter R has been used[332] to distinguish ethanols produced by fermentation of sugars from C_4 plants (sugar cane, corn have $R \sim 2.23$) and C_3 plants (wheat, barley, apple and grape have $R \sim 2.50$; sugar beet and potato, $R \sim 2.72$). Most of the variation was accounted for by differences in the $(D/H)_I$ ratio rather than $(D/H)_{II}$. This suggests a connection between the deuterium content of the methyl group in ethanol and the non-exchangeable sites of the sugars. The spread of values found within a given class (for sugar beet ethanols, $R = 2.72 \pm 0.05$) is attributed to climatic factors. The results have been applied[333] to studies of the origin of raw materials used in the manufacture of commercial spirits (whisky, vodka, gin, rum and fruit brandies).

The characterization of wines requires a more detailed analysis of the data than that indicated above. Fundamental studies[335] have traced the relationship between the deuterium content of the end-products of fermentation (ethanol, water) and the starting materials (glucose, water). Experiments have been carried out in which the (D/H) ratios of the starting materials have been systematically controlled. Values were measured for the starting water, $(D/H)_W^S$ and for the glucose, $(D/H)_G^{NE}$, where NE indicates non-exchangeable sites. The effects of changing sugar concentration, yeast strain and temperature were also investigated. Statistical analysis of the results provided a quantitative relationship between the deuterium content of the starting materials and the end-products.

$$(D/H)_I = 1.1(D/H)_G^{NE} + 0.23(D/H)_W^S - 90 \tag{13a}$$

$$(D/H)_{II} = 0.74(D/H)_W^S + 18 \tag{13b}$$

$$(D/H)_W^Q = 0.04(D/H)_G^{NE} + 0.96(D/H)_W^S + 1.3 \tag{13c}$$

$(D/H)_I$ and $(D/H)_{II}$ are the isotope parameters for the methyl and methylene sites of ethanol and $(D/H)_W^Q$ is the isotope ratio for the water in the final product.

These relationships are independent of the yeast strain and of the fermentation temperature, within normal limits. Typical values of the parameters for natural wines are $(D/H)_I \simeq 102$ ppm, $(D/H)_{II} \simeq 131$ ppm, $(D/H)_W^Q \simeq 160$ ppm, $(D/H)_W^S \simeq 155$ ppm. The deuterium content of methyl and methylene sites is greatly reduced with respect to glucose and starting water, but $(D/H)_I$ is about 5 times more sensitive to the (D/H) ratio of the glucose than to the starting water, whereas $(D/H)_{II}$ depends almost entirely on the starting water.

A dependence of $(D/H)_W^Q$ on initial sugar concentration was also found.[335] This allows the deuterium content of the original must water, $(D/H)_W^S$, to be

determined for natural wines when $(D/H)_W^Q$ and the alcoholic strength have been measured.[19] The isotope parameters for the raw materials (sugars, must water) in wine-making are determined by geographical, climatic and biochemical factors. By showing the connection between the isotope parameters of starting materials and end-products, these experiments[335] confirm that the isotope ratios measured for ethanol and water can be used as "fingerprints" for the characterization of wines.

The ability of the SNIF-NMR technique to distinguish wines of different origins has been tested in an extensive series of experiments and statistical analyses.[19] Parameters R, $(D/H)_I$, $(D/H)_{II}$, $(D/H)_W^Q$ and $(D/H)_W^S$ were obtained for numerous wines from different vine varieties, geographical locations and years of production. On a worldwide scale differences of vine variety are outweighed in importance by geographical (climatic) factors. Discriminant factor analysis, using the four isotope parameters for ethanol and water, clearly distinguished wines (different varieties and vintages) from three groups of countries which could be classified on the basis of temperature and rainfall figures. Narrower discrimination is also possible. Using the same isotope parameters, wines from three French regions (within 2° of latitude of each other) could be distinguished when samples of a single vintage were taken, and even better discrimination was achieved if samples were further restricted to a particular variety.[19] SNIF-NMR is now the most efficient technique available for detection of chaptalization (enrichment with exogenous sugars) and watering of wines.[18] Detailed investigations of barley fermentation have been carried out in connection with characterization of beers.[336]

Many applications of SNIF-NMR to the determination of the origin and quality of non-alcoholic products have been demonstrated.[17] These include studies of the origin (natural or synthetic) of aromas and flavours such as vanillin[337,338] and anethole,[339] of vinegars[340] and of possible adulteration of fruit juices and jams. The technique is expected to assume increasing importance in response to the demands of consumers and regulatory authorities for guarantees of food quality.

7. OTHER SYSTEMS

7.1. Introduction

The chemistry and physical properties of meat and dairy products have not yet been subjected to the thorough examination by NMR that some other products and substances have been. Nevertheless there is sufficient in the literature to indicate that such a thorough examination would be well worthwhile. The publications available make use, to a large extent, of ^{31}P NMR, and exemplify the power of NMR to concentrate on a particular group of chemicals in a particular physical state. Both milk and meat contain solid-like and liquid-like phases and

a huge variety of chemicals. By choosing experimental conditions such that mobile or immobile nuclei are observed and by choosing nuclei present only in limited numbers of chemical species it is possible to filter the information obtained such that useful deductions can be drawn.

7.2. Dairy products

Work in this area has concentrated either on whole milks or on milk extracts, although NMR as an analytical method has been applied to the whole range of dairy products. The earliest work concerned itself with ^{31}P resonance of caseins.[341–343] The general features of the spectra are that multiple resonances are observed which are strongly pH dependent. The spectrum of whole casein can largely be accounted for as a composite of the spectra of α- and β-caseins with possibly some contribution from κ-casein.[343] Analysis of the pH dependence of the spectra of β-casein showed that cooperative ionization of the phosphate groups was involved,[342] a view supported by the analysis of the effects of manganese binding.[343]

Whole casein micelles have been examined in suspension in milk salt solutions[344,345] and in whole milk.[346] The proton spectra of the micelles showed a very well-resolved component,[344] which would be unexpected if all of the protein were in a compact mass. The explanation lies in the "hairy" nature of the micelle in which the C-terminal fragment of κ-casein extends out into the solution from the micelle surface. This idea was supported by the observation that the addition of ethanol to the solution broadens the lines: consistent with a collapse of the hairs on changing the solvent. When chymosin is added the lines become sharper, consistent with the removal of the hairs and subsequent aggregation of the micelles. It is suggested that the mechanism of coagulation during digestion is due to the removal of these stearically stabilizing hairs. In whole cows' milk[346] the signal from casein in the ^{31}P spectrum appears as a broad low-intensity resonance. On addition of EDTA this sharpens into three clearly distinguishable peaks, provided the milk pH is above 6.6; below this value only one broad peak is observed.

Since milk is the vehicle by which the infant mammal obtains its calcium and phosphorus requirements for growth, the fluid must contain large quantities of both elements. Both solid and solution phases coexist, but the solid phase is maintained in a colloidal state by interaction with protein and the nature of the solid state is of considerable interest.[347] In the ^{31}P solution-state spectrum of whole cow's milk the inorganic phosphate time is broad; on adding EDTA this narrows and increases in intensity. This is consistent with the dissolution of the solid phase and reduction of the interaction of the phosphate with either the solid phase and/or the protein.[346] The temperature dependence of ^{31}P signal intensity has been measured in simulated milk ultrafiltrate solution (SMUF), a colloidal calcium phosphate-free milk (CCP-free) and a casein micelle suspension (CMS).[345]

In SMUF, inorganic phosphate signal intensity decreased with increasing temperature, consistent with observations of precipitation at high temperature. This effect was much less marked in CCP-free and no change with temperature was observed in CMS. This conflicts with the known increase in insoluble phosphate when milk is heated. To explain this the authors propose that fast exchange of phosphate between solid and solution phases contributes to the signal. That exchange occurs is likely[346] but it does not appear that all the solid phase contributes to the liquid-phase signal (see above), so that the mechanism by which the signal remains constant cannot be by simple addition of signals from both phases. If, on the other hand, there was slow exchange or some line-narrowing of the broad signals this might increase the visible phosphate signal, whilst precipitation was decreasing it. It would be surprising, however, if the two proccesses exactly compensated, resulting in the constant intensity observed. Using ^{43}Ca NMR it is possible to follow the fate of soluble calcium.[345] In SMUF there is irreversible loss of signal on heating, consistent with the ^{31}P results. In CCP-free there was less than SMUF but in CMS the signal loss was as high as in SMUF. The explanation is that casein in CCP-free inhibits calcium precipitation, whilst in CMS all the Ca binding sites on the protein are saturated and thus precipitation can proceed. Apparently, therefore, the compensation mechanisms proposed for phosphate do not apply to calcium. Linewidth results showed increasing widths with temperature in CCP-free and CMS but decreasing widths with SMUF. These increases in width were explained by exchange effects.

It is clear from the foregoing that the solution-state spectra of the mineral components of milk still require considerable work before they are understood. This is also true of the solid-state spectra of the mineral phase. In principle, solid-state ^{31}P method should enable distinction between the various chemical species that have been proposed to form the milk solid phase.[348] Solid-state high-resolution spectra were obtained under a variety of conditions and compared with the spectra of standards. The chemical shifts of the calcium phosphate species do not vary much, but their chemical shift anisotropy patterns, reflected in the spinning sidebands, are very sensitive to chemical type. The problem is to obtain samples which are representative of the mineral phase and are not significantly contaminated with phosphorus from the protein. This cannot be achieved completely,[348] but spectra can be interpreted in terms of a signal arising from an organic and inorganic part. When this is done deuteration and non-quaternary suppression experiments indicate that the inorganic phosphate is not protonated and is thus consistent with a model in which the calcium phosphate in micelles most closely resembles calcium hydroxy apatite.[349]

There are numerous other compounds in milk. In skimmed cow's milk the only other detectable species is glyceryl phosphoryl choline;[346] however, in milk from other species remarkable variations in spectra and hence phosphorous compounds may be observed[350] (Fig. 9). When cow's milk is concen-

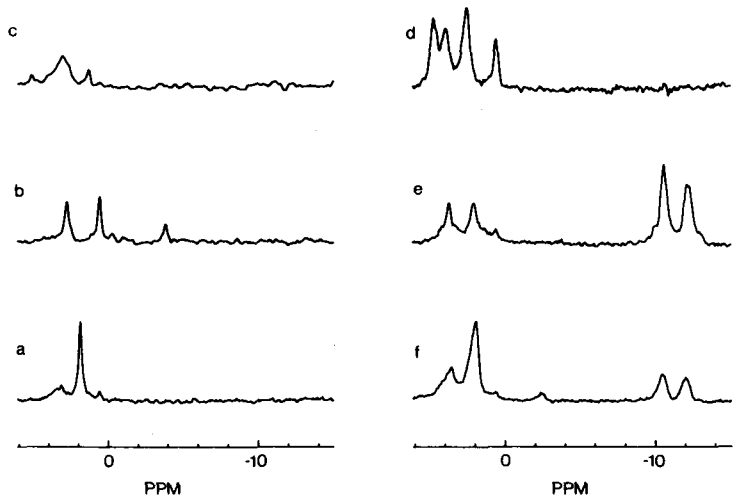

Fig. 9. ^{31}P NMR spectra of various milks. (a) Cow; (b) baboon; (c) human; (d) rabbit; (e) sheep; (f) goat. Chemical shifts are referenced to 85% H_3PO_4. (Reproduced from Ref. 350 with permission.)

trated a much wider variety of species, about 20, become apparent.[351] There is clearly considerable potential for using NMR as a test for authentification of milk samples and it may be expected that proton NMR will be of great interest too. However, to date only one preliminary investigation in this area has been published.[330]

7.3. Meat

Considering the widespread use of NMR to monitor metabolism in living muscle it is surprising that relatively little use has been made of the method in meat science. Those papers that have been produced, however, indicate that much information of value may be obtained. There has yet to be, though, a long-term and systematic study of the applications of NMR to meat science.

The problem of post-mortem changes in muscle is one that is of considerable interest as these are related to final meat quality. In an early review Gadian[352] pointed out the potential of NMR to tackle this problem. Vogel and co-workers[353] were the first to use ^{31}P NMR to observe post-mortem metabolism in real meat systems. They examined the changes in metabolite level as a function of time post-mortem and compared the electrically stimulated and non-stimulated bovine muscle. In the stimulated muscle ATP and phosphocreatine disappeared faster than in the unstimulated case. Inorganic phosphate was higher in the stimulated case, as a result of ATP and phosphocreatine breakdown. pH differences, measured by inorganic phosphate chemical shift, were

small. This result was contrary to results reported using electrochemical measurement of pH, and there were discrepancies when both methods were used on the same samples. The origins of these differences are not clear but may indicate an invasive effect of the electrochemical method.

^{13}C and ^{1}H NMR present difficulties because of the low signal from ^{13}C and the problem of water suppression in the ^{1}H spectrum. Despite these difficulties useful spectra can be obtained.[354] The proton spectra show some 40 distinguishable resonances, most of which can be assigned. Of special interest is the post-mortem build up of lactate and the changes in pH, monitored by observation of the carnosine C_4–H peak. It was also possible to monitor the conversion of phosphocreatine to creatine. In the ^{13}C spectra 37 resonances were observed and it was also possible to measure pH and lactate production. An additional feature was that signals from glycogen were also visible so that the glycogen to lactate conversion processs could be observed directly.

Polyphosphates are often added to meat to improve water-holding capacity and cohesion in comminuted products. The chemistry of polyphosphate in meat is an ideal problem to tackle by ^{31}P NMR. The earliest work in this area was reported by Douglas and co-workers.[355,356] They observed the effect of storage on polyphosphate in frozen chicken. The results were somewhat variable, probably indicating the variability in the injection method rather than some intrinsic problem with the spectroscopy. Results in comminuted chicken muscle were more reproducible.[357] When sodium tripolyphosphate was mixed with comminuted muscle, half-lives for the disappearance of tripolyphosphate were between 20 and 40 minutes. In the presence of 3% NaCl half-lives were less than 10 min. The first stage of the tripolyphosphate breakdown was to produce pyrophosphate. When tripolyphosphate with no sodium chloride was added the half-life of pyrophosphate was similar to the tripolyphosphate half-life, indicating that breakdown of the trimer was the rate-determining step. When sodium chloride was present as well, pyrophosphate half-lives decreased by a factor of about two, indicating some inhibition of enzyme activity. When pyrophosphate was added to muscle on its own, hydrolysis was very rapid in fresh muscle but tended to become slower as the muscle aged post-mortem.

In the treatment of comminuted meats it is often held that sodium chloride and tripolyphosphates have a synergistic effect. One way of investigating the behaviour of sodium chloride is to observe directly ^{35}Cl resonance.[358] When a muscle was soaked in sodium chloride solution and the muscle packed into an NMR tube, a single chloride resonance was seen. However, when care was taken to align the muscle so that the axis of the fibres was perpendicular to the magnetic field, triplet structure was observed. Such a structure is typical of a single-crystal pattern for a spin-$\frac{3}{2}$ nucleus. It indicated that highly anisotropic motion is taking place, with motion along the muscle fibres much less hindered than motion perpendicular to the fibres. When sodium tripolyphosphate was added to the muscle, the triplet structure collapsed to a singlet. This was interpreted as representing a loss of protein structure within the

muscle. The observation was thus consistent with the accepted view that the role of polyphosphate was to solubilize myosin, which increased the water-binding capacity of the muscle and the self-binding ability of the comminuted product. The results clearly demonstrated that chloride did not have the same effect as polyphosphate so that the reported synergy was not simply an additive effect. It was concluded that the probable role of chloride was to bind to the protein, increasing the net negative charge and enhancing repulsive electrostatic interactions. The repulsive forces increase inter-protein distance, causing swelling and hence increased water holding.

REFERENCES

1. T.F. Conway, R.F. Cohee and R.J. Smith, *Manufacturing Confectioner*, 1957, **37**, 27.
2. P.S. Belton, *Comments Agric. Food Chem.*, 1990, **2**, 179.
3. S.J.R. Schmidt, in *NMR Applications to Biopolymers* (ed. J.W. Finlay, S.J. Schmidt and A. Serianni), p. 415. Plenum, New York, 1990.
4. S.J. Richardson and M.P. Steinberg, in *Water Activity: Theory and Applications* (ed. L.B. Rockland and L.R. Beuchat), p. 235. Marcel Dekker, New York, 1987.
5. N. Nagashima and E. Suzuki, *Appl. Spectrosc. News*, 1984, **20**, 1.
6. N. Nagashima and E. Suzuki, in *Water Activity: Influences on Food Quality* (ed. L.B. Rockland and G.F. Stewart), p. 247. Academic, New York, 1981.
7. M.J. McCarthy and R.J. Kauten, *Trends Food Sci. Technol.*, 1990, 134.
8. J.C. Autran, in *Modern Methods of Plant Analysis* (ed. H.F. Linksens and J.F. Jackson), 1992, New series, Vol. **14**, 109.
9. L.J. Berliner, R. Kaptein, K. Koga and G. Musci, in *NMR Applications to Biopolymers* (ed. J.W. Finlay, S.J. Schmidt and A. Serianni), p. 231. Plenum, New York, 1990.
10. I.C. Baianu, T.F. Kumonsinki, P.J. Bachtel, P.A. Myeres-Betts, P. Yahuba and A. Mora, in *NMR Applications to Biopolymers* (ed. J.W. Finlay, S.J. Schmidt and A. Serianni), p. 361. Plenum, New York, 1990.
11. A.S. Tatham, P.R. Shewry and P.S. Belton, in *Advances in Cereal Science and Technology*, Vol. X (ed. Y. Pomeranz), p. 1. American Association of Cereal Chemists, St. Paul, USA, 1990.
12. I.C. Baianu, in *Nuclear Magnetic Resonance in Agriculture* (ed. P.E. Pfeffer and W.V. Gerasimowicz), p. 167. CRC Press, Boca Raton, USA, 1989.
13. J.M.V. Blanshard, E.M. Jarozkiewicz and M.J. Gidley, in *NMR Applications to Biopolymers* (ed. J.W. Finlay, S.J. Schmidt and A. Serianni), p. 155. Plenum, New York, 1990.
14. S.J. Schmidt and N. Ayya, in *Frontiers in Carbohydrate Research – 1, Food Applications* (ed. R.P. Millane, J.N. BeMiller and R. Chandrasehan), p. 200. Elsevier Applied Science, London, 1989.
15. E.B. Rathbone, in *Analysis of Food Carbohydrate* (ed. G.G. Birch), p. 149. Elsevier Applied Science, London, 1985.
16. B. Coxon, in *Developments in Food Carbohydrates*, Vol. 2 (ed. C.K. Lee), p. 351. Applied Science, London, 1980.
17. M.L. Martin and G.J. Martin, in *NMR Basic Principles and Progress*, Vol. 23 (ed. P. Diehl, E. Fluck, M. Günther, R. Kosfeld and J. Seelig). Springer Verlag, Berlin, 1991.
18. G.J. Martin and M.L. Martin, in *Wine Analysis* (ed. H.F. Linskeps and J.F. Jackson), p. 258. Springer Verlag, Berlin, 1988.
19. G.J. Martin, C. Guillou, M.L. Martin, M.T. Cabanis, Y. Tep and J. Aerny, *J. Agric. Food Chem.*, 1988, **36**, 316.
20. H.L. Schmidt, *Z. Anal. Chem.*, 1986, **324**, 760.

21. P.J. Barker, in *Rapid Methods for Analysis of Food and Food Material* (ed. W. Baltes), p. 267. Technomic, Lancaster, PA, USA, 1990.
22. D. Waddington, in *Analysis of Fats and Oils* (ed. R.J. Hamilton and J.B. Rossell), p. 341. Elsevier Applied Science, London, 1986.
23. M. Pollard, in *Analysis of Fats and Oils* (ed. R.J. Hamilton and J.B. Rossell), p. 401. Elsevier Applied Science, London, 1986.
24. J.P. Renou, J. Kopp and C. Valin, *J. Food Technol.*, 1985, **20**, 23.
25. D.H. Kropf, *J. Food Qual.*, 1984, **6**, 199.
26. I. Horman, in *Analysis of Foods and Beverages: Modern Techniques* (ed. G. Charalambous), p. 205. Academic, London, 1984.
27. D. Waddington, in *Fats and Oils: Chemistry and Technology* (ed. R.J. Hamilton and A. Bhati), p. 25. Applied Science, London, 1980.
28. P.S. Belton and I.J. Colquhoun, *Spectrosc. Int.*, 1990, **2**, 22.
29. T.M. Eads and W.R. Croasmun, *J. Am. Oil Chem. Soc.*, 1988, **65**, 78.
30. P.S. Belton, in *Biophysical Methods in Food Research* (ed. H.W-S. Chan), p. 103. Blackwell Scientific, Oxford, 1984.
31. D.G. Gadian, in *Developments in Meat Science*, Vol. 1 (ed. R. Lawrie), p. 89. Applied Science, London, 1980.
32. J.W. Finlay, S.J. Schmidt and A. Serianni (Eds), *NMR Applications to Biopolymers*. Plenum, New York, 1990.
33. P.E. Pfeffer and W.V. Gerasimowicz (Eds), *Nuclear Magnetic Resonance in Agriculture*. CRC Press, Boca Raton, USA, 1989.
34. J.A. Troller, in *Water and Food Quality* (ed. T.M. Hardman), p. 1. Elsevier Applied Science, New York, 1989.
35. L.M. Lenovich, in *Water Activity: Theory and Applications to Food* (ed. L.B. Rockland and L.R. Beuchat), p. 119. Marcel Dekker, New York, 1987.
36. T.F. Kumosinski and H. Pessen, *Arch. Biochem. Biophys.*, 1982, **218**, 286.
37. T.F. Kumosinksi and H. Pessen, in *Nuclear Magnetic Resonance in Agriculture* (ed. P.E. Pfeffer and W.V. Gerasimowicz), p. 219. CRC Press, Boca Raton, USA, 1989.
38. H. Pessen and T.F. Kumosinski, *Methods Enzymol.*, 1985, **117**, 219.
39. T.F. Kumosinski, H. Pessen, S.J. Prestrelski and H.M. Farrell Jr., *Arch Biochem. Biophys.*, 1987, **257**, 259.
40. T.F. Kumosinski, H. Pessen and H.M. Farrell, Jr., *J. Ind. Microbiol.*, 1988, **3**, 147.
41. P.A. Myers-Betts and I.C. Baianu, *J. Agric. Food Chem.*, 1990, **38**, 1171.
42. S.J. Richardson, I.C. Baianu and M.P. Steinberg, *Starch*, 1987, **39**, 79.
43. S.J. Richardson, I.C. Baianu and M.P. Steinberg, *J. Agric. Food Chem.*, 1986, **34**, 17.
44. B.P. Hills, S.F. Takacs and P.S. Belton, *Food Chem.*, 1990, **37**, 95.
45. B.P. Hills, *Spectrosc. Int. J.*, 1990, **8**, 149.
46. B.P. Hills, S.F. Takacs and P.S. Belton, *Mol. Phys.*, 1989, **67**, 903.
47. B.P. Hills, S.F. Takacs and P.S. Belton, *Mol. Phys.*, 1989, **67**, 919.
48. B.P. Hills, K.M. Wright and P.S. Belton, *Mol. Phys.*, 1989, **67**, 1309.
49. B.P. Hills, C. Cano and P.S. Belton, *Macromolecules*, 1991, **24**, 2944.
50. B.P. Hills, *Mol. Phys.*, 1991, **72**, 1099.
51. B.P. Hills, *Mol. Phys.*, 1992, **76**, 489.
52. B.P. Hills, *Mol. Phys.*, 1992, **76**, 509.
53. P. Lambelet, R. Berrocol and F. Ducret, *J. Dairy Res.*, 1989, **56**, 211.
54. B. Halle, T. Andersson, S. Forsen and B. Lindman, *J. Am. Chem. Soc.*, 1981, **103**, 500.
55. B. Halle, *Mol. Phys.*, 1987, **61**, 963.
56. B. Halle, *J. Chem. Phys.*, 1991, **94**, 3150.
57. S.J. Richardson, I.C. Baianu and M.P. Steinberg, *J. Food Science*, 1987. **52**, 806.
58. A. Mora-Gutierrez and I.C. Baianu, *J. Agric. Food Chem.*, 1989, **37**, 1459.
59. P.S. Belton, S.G. Ring, R.L. Botham and B.P. Hills, *Mol. Phys.*, 1991, **72**, 1123.

60. J.M. Harvey, M.C.R. Symons and R.J. Naftalin, *Nature*, 1976, **261**, 435.
61. J.M. Harvey and M.C.R. Symons, *J. Soln. Chem.*, 1978, **7**, 571.
62. R.L. D'Arcy and I.C. Watt, in *Water Activity: Influences on Food Quality* (ed. L.B. Rockland and G.F. Stewart), p. 111. Academic Press, New York, 1981.
63. L.T. Kakalis and I.C. Baianu, *Arch. Biochem. Biophys.*, 1988, **267**, 829.
64. T.S. Lioutas, I.C. Baianu and M.P. Steinberg, *Arch. Biochem. Biophys.*, 1986, **247**, 68.
65. G.D.J. Phillies, G.B. Benedek and N.A. Mazur, *J. Chem. Phys.*, 1976, **65**, 1883.
66. D.D. Thomas, L.R. Dalton and J.S. Hyde, *J. Chem. Phys.*, 1976, **65**, 3006.
67. H.J.V. Tyrrell and K.R. Harris, *Diffusion in Liquids*, p. 262. Butterworths, London, 1984.
68. I.C. Baianu, T.F. Kumosinski, P.J. Bechtel, P.A. Myers-Betts, P. Yakubu and A. Mora, in *NMR Applications to Biopolymers* (ed. J.W. Finlay, S.J. Schmidt and A. Serianni), p. 361. Plenum, New York, 1990.
69. T.S. Lioutas, I.C. Baianu and M.P. Steinberg, *J. Agric. Food Chem.*, 1987, **35**, 133.
70. G.D. Fullerton, M.F. Finnie, K.E. Hunter, V.A. Ord and I.L. Cameron, *Magn. Reson. Imaging*, 1987, **5**, 353.
71. L. Piculell and B. Halle. *J. Chem. Soc. Faraday Trans. I*, 1986, **82**, 401.
72. G.P. Lewis, W. Derbyshire, S. Ablett, P.J. Lillford and I.T. Norton, *Carbohydr. Res.*, 1987, **160**, 397.
73. P.S. Belton, B.P. Hills and E.R. Raimbaud, *Mol. Phys.*, 1988, **63**, 825.
74. G.E. Santyr, R.M. Henkelman and M.J. Bronskill, *J. Magn. Reson.*, 1988, **79**, 28.
75. M. Rydzy and W. Skrzynkis, *Biochim. Biophys. Acta*, 1982, **705**, 33.
76. S. Conti, *Mol. Phys.*, 1986, **59**, 449.
77. S. Conti, *Mol. Phys.*, 1986, **59**, 483.
78. J. Gallier, P. Rivet and J. de Certaines, *Biochim. Biophys. Acta*, 1987, **915**, 1.
79. J. Grad and R.G. Bryant, *J. Magn. Reson.*, 1990, **90**, 1.
80. P.A. Myers-Betts and I.C. Baianu, *J. Agric. Food Chem.*, 1990, **38**, 477.
81. T.S. Lioutas, I.C. Baianu, P.J. Bechtel and M.P. Steinberg, *J. Agric. Food. Chem.*, 1988, **36**, 437.
82. S.P.F.M. Reofs, H. van As and T. van Vliet, *J. Food Sci.*, 1989, **54**, 704.
83. H. Pessen, T.F. Kumosinski and H.M. Farrell Jr., in *NMR Applications to Biopolymers* (ed. J.W. Finlay, S.J. Schmidt and A. Serianni), p. 175. Plenum, New York, 1990.
84. A.G. Curme, S.J. Schmidt and M.P. Steinberg, *J. Food Sci.*, 1990, **55**, 430.
85. S.P.F.M. Roefs, H. van As and T. van Vliet, *J. Food Sci.*, 1989, **54**, 704.
86. S.M. Goldsmith and R.T. Toledo. *J. Food Sci.*, 1985, **50**, 59.
87. S.J. Richardson, I.C. Baianu and M.P. Steinberg, *Starch*, 1987, **39**, 79.
88. S.J. Richardson, I.C. Baianu and M.P. Steinberg, *Starch*, 1987, **39**, 198.
89. P.S. Belton and B.P. Hills, *Mol. Phys.*, 1987, **61**, 999.
90. H.K. Leung and M.P. Steinberg, *J. Food Sci.*, 1979, **44**, 1212.
91. S.F. Tanner, B.P. Hills and R. Parker, *J. Chem. Soc. Faraday Trans.*, 1991, **87**, 2613.
92. M.J. Miles, V.J. Morris, P.D. Orford and S.G. Ring, *Carbohydr. Res.*, 1985, **135**, 271.
93. P. Chinachoti, V.A. White, L. Lo and T. Stengle, *Cereal Chem.*, 1991. **68**, 238.
94. W.M. Shirley and R.G. Bryant, *J. Am. Chem. Soc.*, 1982, **104**, 2910.
95. J.A. Stanley and H. Peemoeller, *J. Magn. Reson.*, 1991, **91**, 209.
96. H.T. Edzes and E.T. Samulski, *J. Magn. Reson.*, 1978, **31**, 207.
97. H. Peemoeller, D.W. Kydon, A.R. Sharp and L.J. Schreiner, *Can. J. Phys.*, 1984, **62**, 1002.
98. P.T. Callaghan, K.W. Jolley, J. Lelievre and R.B.K. Wong, *J. Colloid Interface Sci.*, 1983, **92**, 332.
99. H.T. Lechert, in *Water Activity: Influence on Food Quality* (ed. L.B. Rockland and G. Stewart), p. 223. Academic Press, New York, 1981.
100. D.A. d'Avignon, C.-C. Hung, M.T.L. Pagel, B. Hart, G.L. Bretthorst and J.H. Ackerman, in *NMR Applications to Biopolymers* (ed. J.W. Finlay, S.J. Schmidt and A. Serianni), p. 391. Plenum, New York, 1990.

101. D. Sobczynska, C. Setser, H. Lim, L. Hansen and J. Paulstelis, in *NMR Applications to Biopolymers* (ed. J.W. Finlay, S.J. Schmidt and A. Serianni), p. 461. Plenum, New York, 1990.
102. J. Fanni, D. Canet, K. Elbayed and J. Hardy, *J. Food Sci.*, 1989, **54**, 909.
103. E. Brosio, G. Altobelli and A. di Nola, *J. Food Technol.*, 1984, **19**, 103.
104. E. Brosio, G. Altobelli, Y. Yun-Shin and A. di Nola, *J. Food Technol.*, 1983, **18**, 219.
105. H.K. Leung, J.A. Magnuson and B.L. Bruinsma, *J. Food Sci.*, 1983, **48**, 95.
106. H.K. Leung, J.A. Magnuson and B.L. Bruinsma, *J. Food Sci.*, 1979, **44**, 1408.
107. M.-S. Kim-Shin, F. Mari, P.A. Rao, T.R. Stengle and P. Chinachoti, *J. Agric. Food Chem.*, 1991, **39**, 1915.
108. B.P. Hills, K.M. Wright and P.S. Belton, *Mol. Phys.*, 1989, **67**, 193.
109. B.P. Hills and S.L. Duce, *Magn. Reson. Imaging*, 1990, **8**, 321.
110. S.L. Duce, T.A. Carpenter, L.D. Hall and B.P. Hills, *Magn. Reson. Imaging*, 1992, **10**, 289.
111. B.P. Hills and J.E.M. Snaar, *Mol. Phys.*, 1992, **76**, 979.
112. B.P. Hills and P.S. Belton, *Ann. Reports NMR Spectrosc.*, 1989, **21**, 99.
113. G. Bacic and S. Ratkovic, *Biophys. J.*, 1984, **45**, 767.
114. P.M. Chen, L.V. Gusta and D.G. Stout, *Plant Physiol.*, 1978, **61**, 878.
115. D.G. Stout, R.M. Cotts and P.L. Steponkus, *Can. J. Bot.*, 1977, **55**, 1623.
116. A.L. Mackay, J.C. Wallace, K. Sasaki and I.E.P. Taylor, *Biochemistry*, 1988, **27**, 1467.
117. S. Ratkovic, *Seed Sci. Technol.*, 1987, **15**, 147.
118. S.I. Aksenov, N.A. Askochenskaya and E.A. Golovina, *Fiziol. Rast.*, 1977, **24**, 1251.
119. C.J. Lewa and M. Lewa, *J. Magn. Reson.*, 1990, **89**, 219.
120. P.S. Belton and R.G. Ratcliffe, *Prog. NMR Spectrosc.*, 1985, **17**, 241.
121. M.M. Civan and M. Shporer, *Biochim. Biophys. Acta*, 1974, **343**, 399.
122. M.M. Civan, A.M. Achlama and M. Shporer, *Biophys. J.*, 1978, **21**, 127.
123. B.M. Fung and P.S. Puon, *Biophys. J.*, 1981, **33**, 27.
124. P.S. Belton, R.R. Jackson and K.J. Packer, *Biochim. Biophys. Acta*, 1972, **286**, 16.
125. R.W. Currie, R. Jordan and F.H. Wolfe, *J. Food Sci.*, 1981, **46**, 822.
126. D.C. Chang, C.F. Hazelwood and D.E. Woessner, *Biochim. Biophys. Acta*, 1976, **437**, 253.
127. B.M. Fung and T.W. McGaughy, *Biophys. J.*, 1979, **28**, 293.
128. B.M. Fung, D.L. Durham and D.A. Wassil, *Biochim. Biophys. Acta*, 1975, **399**, 191.
129. M.C. Neville and S. White, *J. Physiol.*, 1979, **288**, 71.
130. E.E. Burnell, M.E. Clark and N.R. Chapman, in *Magnetic Resonance in Colloid and Interface Science* (ed. J.P. Fraissard and H.A. Resing), p. 661. D. Reidel, London, 1980.
131. J.P. Renou, J. Kopp, P. Gatellier, G. Monin and G. Kosak-Reiss, *Meat Sci.*, 1989, **26**, 101.
132. P. Stilbs, *Prog. NMR Spectrosc.*, 1987, **19**, 1.
133. J. Kärger, H. Pfeifer and W. Henk, *Adv. Magn. Reson.*, 1988, **12**, 1.
134. P.T. Callaghan, *Principles of Nuclear Magnetic Resonance Microscopy*. Oxford University Press, Oxford, 1991.
135. E.O. Stejskal and J.E. Tanner, *J. Chem. Phys.*, 1965, **42**, 288.
136. W. Brown and P. Stilbs, *Chem. Scripta*, 1982, **19**, 161.
137. R. Lamanna and S. Cannistraro, *Chem. Phys. Lett.*, 1989, **164**, 653.
138. J.H. Wang, *J. Am. Chem. Soc.*, 1954, **76**, 4755.
139. J.C. Van den Enden, D. Waddington, H. Van Aalst, C.G. Van Kralingen and K.J. Packer, *J. Colloid Interface Sci.*, 1990, **140**, 105.
140. P.T. Callaghan, D. MacGowan, K.J. Packer and F.O. Zelaya, *J. Magn. Reson.*, 1990, **90**, 177.
141. P.T. Callaghan, A. Coy, D. MacGowan, K.J. Packer and F.O. Zelaya, *Nature*, 1991, **351**, 467.
142. R.M. Cotts, *Nature*, 1991, **351**, 443.
143. B.P. Hills and J.E.M. Snaar, *Mol. Phys.*, 1992, **76**, 979.
144. P.T. Callaghan, K.W. Jolley, J. Lelievre and R.B.K. Wong, *J. Colloid Interface Sci.*, 1983, **92**, 332.
145. P.T. Callaghan, K.W. Jolley and J. Lelievre, *Biophys. J.*, 1979, **28**, 133.

146. P.T. Callaghan, K.W. Jolley and R.S. Humphrey, *J. Colloid Interface Sci.*, 1983, **93**, 521.
147. K. Yoshizaki, Y. Seo, H. Nishikawa and T. Morimoto, *Biophys. J.*, 1982, **38**, 209.
148. D.D. Stark and W.G. Bradley, *Magnetic Resonance Imaging*. The C.V. Mosby Co., Washington, 1988.
149. P. Mansfield and P.G. Morris, *NMR Imaging in Biomedicine* (Supplement 2 to *Advances in Magnetic Resonance*, ed. J.S. Waugh). Academic Press, New York, 1982.
150. P.G. Morris, *Nuclear Magnetic Resonance Imaging in Medicine and Biology*. Oxford University Press, Oxford, 1986.
151. M.A. Foster, N.J.F. Dodd, F.D. Rolls and R.R. Price, *Nuclear Magnetic Resonance Imaging*. W.B. Saunders, Philadelphia, 1983.
152. R.R. Ernst, *Quart. Rev. Biophys.*, 1987, **19**, 183.
153. G. Gassner, in *Nuclear Magnetic Resonance in Agriculture* (ed. P.E. Pfeffer and W.V. Gerasimowicz), p. 405. CRC Press, Boca Raton, USA, 1989.
154. J.M. Pope and V. Sarafis, *Chem. Australia*, 1990, **57**, 221.
155. C.D. Eccles and P.T. Callaghan, *J. Magn. Reson.*, 1986, **68**, 393.
156. J.B. Aguayo, S.T. Blackband, J. Schoeniger, M.A. Mattingly and M. Hinterman, *Nature*, 1986, **322**, 190.
157. G.P. Cofer, J.M. Brown and G.A. Johnson, *J. Magn. Reson.*, 1989, **83**, 608.
158. P.T. Callaghan and C.D. Eccles, *J. Magn. Reson.*, 1987, **71**, 426.
159. P.T. Callaghan and C.D. Eccles, *J. Magn. Reson.*, 1988, **78**, 1.
160. B.P. Hills, K.M. Wright and P.S. Belton, *Magn. Reson. Imaging*, 1990, **8**, 755.
161. P.T. Callaghan, *J. Magn. Reson.*, 1990, **87**, 304.
162. G.A. Johnson, J.M. Brown and P.J. Kramer, *Proc. Natl. Acad. Sci. USA* 1987, **84**, 2752.
163. P.A. Bottomley, H.H. Rogers and T.H. Foster, *Proc. Natl. Acad. Sci. USA*, 1986, **83**, 87.
164. G.W. Schrader and J.B. Litchfield, American Society of Agricultural Engineers paper no. 91-6055, 1991.
165. J.E. Maneval, M.J. McCarthy and S. Whitaker, *Mater. Res. Soc. Symp. Proc.*, 1990, **195**, 531.
166. E. Perez, R. Kavten and M.J. McCarthy, in *Drying '89* (ed. A.S. Mujumdo). Hemisphere, New York, 1989.
167. H. Ishida, T. Kobayashi, M. Koizumi and H. Kano, *Agric. Biol. Chem.*, 1989, **53**, 2363.
168. H. Song and J.B. Litchfield, *Cereal Chem.*, 1990, **67**, 580.
169. J.E. German and M.J. McCarthy, *J. Agric. Food Chem.*, 1989, **37**, 1321.
170. J.R. Heil, K.L. McCarthy, B.J. German, M.J. McCarthy and H. Patino, *Am. Soc. Brew. Chem.*, 1990, **48**, 119.
171. M.J. McCarthy, *Am. Inst. Chem. Engrs J.*, 1990, **36**, 287.
172. M.J. McCarthy and J.R. Heil, *Am. Inst. Chem. Engrs J. Symp. Ser.*, 1990, **88**, 100.
173. M.J. McCarthy and R.J. Kauten, *Trends Food Sci. Technol.*, 1990, 134.
174. Z.H. Cho and H.W. Park, *Adv. Magn. Reson. Imaging*, 1989, **1**, 1.
175. R.J. Kurland and F.Q.H. Ngo, *Magn. Reson. Med.*, 1986, **3**, 425.
176. M.K. Stehling, R. Turner and P. Mansfield, *Nature*, 1991, 43.
177. D. Crucker, J. Steibel, Y. Mauss, B. Dumitresco, J.P. Armspach and J. Chambron, *Mol. Phys.*, 1990, **70**, 903.
178. S.L. Duce, T.A. Carpenter, L.D. Hall and B.P. Hills, *Magn. Reson. Imaging*, 1992, **10**, 289.
179. A. Connelly, J.A.B. Lohman, B.C. Loughman, H. Quiquampoix and R.G. Ratcliffe, *J. Exp. Bot.*, 1987, **38**, 1713.
180. M.F. Fuller, M.A. Foster and J.M.S. Hutchinson, *Magn. Reson. Imaging*, 1984, **2**, 187.
181. E. Groeneveld, E. Kallweit, M. Henning and A. Pfau, in *In vivo Measurement of Body Composition in Meat Animals* (ed. D. Lister), p. 84. Elsevier, London, 1984.
182. J.R. Heil, W.E. Perkins and M.J. McCarthy, *J. Food Sci.*, 1990, **55**, 763.
183. R.J. Kauten, J.E. Maneval and M.J. McCarthy, *J. Food Sci.*, 1991, **56**, 355.
184. P. Chen, M.J. McCarthy and R. Kauten, *Trans. American Society of Agricultural Engineers*, 1989, **32**, 1747.

185. S.L. Duce, T.A. Carpenter and L.D. Hall, in *31st Experimental NMR Spectroscopy Conference Proceedings* (ed. E.O. Stejskal), p. 193. Asilonar, California, 1990.
186. C.Y. Wang and P.C. Wang, *Hortic. Sci.*, 1989, **24**, 106.
187. S.Y. Wang, P.C. Wang and M. Faust, *Sci. Hortic.*, 1988, **35**, 227.
188. P.T. Callaghan and Y. Xia, *J. Magn. Reson.*, 1991, **91**, 326.
189. J. Stepisnik, *Prog. NMR Spectrosc.*, 1985, **17**, 187.
190. D. LeBihan, R. Turner and J.R. Macfall, *Magn. Reson. Med.*, 1989, **10**, 324.
191. I.R. Young, G.A. Coutts, D.J. Bryant and G.M. Bydder, *Magn. Reson. Med.*, 1989, **10**, 349.
192. D. LeBihan, E. Breton, D. Lallemand, M.-L. Aubin, J. Vignaud and M. Laval-Jeantet, *Radiology*, 1988, **168**, 497.
193. C.F. Jenner, Y. Xia, C.D. Eccles and P.T. Callaghan, *Nature*, 1988, **336**, 399.
194. J. Link and J. Seelig, *J. Magn. Reson.*, 1990, **89**, 310.
195. P. Bornert and W. Dreher, *J. Magn. Reson.*, 1990, **87**, 220.
196. M.A. Horsfield, C. Hall and L.D. Hall, *J. Magn. Reson.*, 1990, **87**, 319.
197. P. Börnert, W. Dreher and W. Schneider, *NMR Biomed.*, 1989, **2**, 278.
198. L.D. Hall, A.G. Webb and S.C.R. Williams, *J. Magn. Reson.*, 1989, **81**, 565.
199. J.B. Ra, S.K. Hilal and C.H. Oh, *Magn. Reson. Med.*, 1986, **3**, 296.
200. M.S. Fisher, W.E. Marshall and H.F. Marshall, in *NMR Aplications to Biopolymers* (ed. J.W. Finlay, S.J. Schmidt and A. Serianni), p. 199. Plenum, New York, 1990.
201. P.S. Belton, S.L. Duce, I.J. Colquhoun and A.S. Tatham, *Magn. Reson. Chem.*, 1988, **26**, 245.
202. P.S. Belton, S.L. Duce and A.S. Tatham, *J. Cereal Sci.*, 1988, **7**, 113.
203. S. Ablett, D.J. Barnes, A.P. Davies, S.J. Ingram and D.W. Patient, *J. Cereal Sci.*, 1988, **8**, 11.
204. M.P. Wehrli and Y. Pomeranz, *Cereal Chem.*, 1970, **47**, 160.
205. D. Marion, C. LeRoux, S. Akoka, C. Tellier and D. Gallant, *J. Cereal Sci.*, 1987, **5**, 101.
206. A. Haase, *Magn. Reson. Med.*, 1990, **13**, 77.
207. A.D. Perlin and B. Casu, in *The Polysaccharides* Vol. 1 (ed. G.O. Aspinall), p. 133. Academic Press, New York, 1982.
208. B. Casu, in *Polysaccharides – Topics in Structure and Morphology* (ed. E.D.T. Atkins), p. 1. Macmillan, Basingstoke, 1985.
209. R. Nardin and M. Vincendon, *Makromol. Chem.*, 1988, **189**, 153.
210. K. Bock, and H. Thogersen, *Ann. Reports NMR Spectrosc.*, 1982, **13**, 1.
211. K. Bock, C. Pedersen and H. Pedersen, *Adv. Carbohydr. Chem. Biochem.*, 1984, **42**, 193.
212. J.H. Bradbury and G.A. Jenkins, *Carbohydr. Res.*, 1984, **126**, 125.
213. K. Bock, A. Brignole and B.W. Sigurskjold, *J. Chem. Soc. Perkins Trans. II*, 1986, 1711.
214. M. Forsgren, P.-E. Jansson and L. Kenne, *J. Chem. Soc. Perkins Trans. I*, 1985, 2383.
215. P.-E. Jansson, L. Kenne and E. Scweda, *J. Chem. Soc. Perkins Trans. I*, 1988, 2729.
216. I. Backman, B. Erbing, P.-E. Jansson and L. Kenne, *J. Chem. Soc. Perkins Trans. I*, 1988, 889.
217. P.-E. Jansson, L. Kenne and G. Widmalm, *Carbohydr. Res.*, 1987, **168**, 67.
218. N.K. Kochetkov, *Chem. Soc. Rev.*, 1990, **19**, 1.
219. P.-E. Jansson, L. Kenne and G. Widmalm, *Carbohydr. Res.*, 1989, **188**, 169.
220. S.W. Homans, R.A. Dwek and T.W. Rademacher, *Biochemistry*, 1987, **26**, 6571.
221. C.A. Bush, *Bull, Magn. Reson.*, 1988, **10**, 73.
222. M. Ikura and K. Hikichi, *Carbohydr. Res.*, 1987, **163**, 1.
223. K. Bock, *Pure Appl. Chem.*, 1987, **59**, 1447.
224. D.D. McIntyre and H.J. Vogel, *Starch*, 1990, **42**, 287.
225. L. Lerner and A. Bax, *Carbohydr. Res.*, 1987, **166**, 35.
226. T.A.W. Koerner, J.H. Prestegard, P.C. Demou and R.K. Yu, *Biochemistry*, 1983, **22**, 2687.
227. J. Breg, D. Romijn, J.F.G. Vliegenthart, G. Strecker and J. Montreuil, *Carbohydr. Res.*, 1988, **183**, 19.
228. I.J. Colquhoun, G.A. de Ruiter, H.A. Schols and A.G.J. Voragen, *Carbohydr. Res.*, 1990, **206**, 131.
229. H. van Halbeek, *UCLA Symp. Mol. Cell Biol., New Series*, 1990, **109**, 195.

230. P. Cagas and C.A. Bush, *Biopolymers*, 1990, **30**, 1123.
231. K. Bock, *Pure Appl. Chem.*, 1983, **55**, 605.
232. S.W. Homans, *Prog. NMR Spectrosc.*, 1990, **22**, 55.
233. J.P. Carver, *Curr. Opinion Struct Biol.*, 1991, **1**, 716.
234. H. Grasdalen, O.E. Bakoy and B. Larsen, *Carbohydr. Res.*, 198, **184**, 183.
235. E. Westerlund, P. Aman, R.E. Andersson and R. Andersson, *Carbohydr. Polym.*, 1991, **14**, 179.
236. H. Grasdalen and T.J. Painter, *Carbohydr. Res.*, 1980, **81**. 59.
237. A.E. Manzi, A.S. Cerezo and J.N. Shoolery, *Carbohydr. Res.*, 1986, **148**, 189.
238. H. Grasdalen, B. Larsen and O. Smidsrod, *Carbohydr. Res.*, 1981, **89**, 179.
239. H. Grasdalen, *Carbohydr. Res.*, 1983, **118**, 255.
240. W. Mackie, S. Pérez, R. Rizzo, F. Taravel and M. Vignon, *Int. J. Biol. Macromol.*, 1983, **5**, 329.
241. M.J. Gidley, *Carbohydr. Res.*, 1985, **139**, 85.
242. P. Ryden, I.J. Colquhoun and R.R. Selvendran, *Carbohydr. Res.*, 1989, **185**, 233.
243. R. Pressey and D.S. Himmelsbach, *Carbohydr. Res.*, 1984, **127**, 356.
244. M.H.J. Keenan, P.S. Belton, J.A. Matthew and S.J. Howson, *Carbohydr. Res.*, 1985, **138**, 168.
245. G.B. Seymour, I.J. Colquhoun, M.S. DuPont, K.R. Parsley and R.R. Selvendran, *Phytochemistry*, 1990, **29**, 725.
246. S.B. Tjan, A.G.J. Voragen and W. Pilnik, *Carbohydr. Res.*, 1974, **34**, 15.
247. M. Rinaudo, G. Ravanat and M. Vincendon, *Makromol. Chem.*, 1980, **181**, 1059.
248. E. Westerlund, R. Andersson, P. Aman and O. Theander, *J. Cereal Sci.*, 1990, **12**, 33.
249. I. Mueller-Harvey, R.D. Hartley, P.J. Harris and E.H. Curzon, *Carbohydr. Res.*, 1986, **148**, 71.
250. A.I. Usov, *Bot. Mar.*, 1984, **27**, 189.
251. C. Rochas, M. Rinaudo and M. Vincendon, *Int. J. Biol. Macromol.*, 1983, **5**, 111.
252. C.W. Greer, C. Rochas and W. Yaphe, *Bot. Mar.*, 1985, **28**, 9.
253. R.R. Contreras, J.P. Kamerling, J. Breg and J.F.G. Vliegenthart, *Carbohydr. Res.*, 1988, **179**, 411.
254. A. Rashid, W. Mackie, I.J. Colquhoun and D. Lambla, *Can. J. Chem.*, 1990, **68**, 1122.
255. E. Parra, H.-N. Caro, J. Jiménez-Berbero, M. Martín-Lomas and M. Bernabé, *Carbohydr. Res.*, 1990, **208**, 83.
256. C. Rochas, M. Rinaudo and S. Landry, *Carbohydr. Polymers*, 1989, **10**, 115.
257. C. Rochas, M. Rinaudo and M. Vincendon, *Biopolymers*, 1980, **19**, 2165.
258. T.A. Bryce, A.A. McKinnon, E.R. Morris, D.A. Rees and D. Thom, *Faraday Discuss. Chem. Soc.*, 1974, **57**, 221.
259. O. Smidsrød, I.-L. Andresen, H. Grasdalen, B. Larsen and T. Painter, *Carbohydr. Res.*, 1980, **80**, C 11.
260. H. Grasdalen and O. Smidsrød, *Macromolecules*, 1981, **14**, 229.
261. P.S. Belton, V.J. Morris and S.F. Tanner, *Int. J. Biol. Macromol.*, 1985, **7**, 53.
262. P.S. Belton, G.R. Chilvers, V.J. Morris and S.F. Tanner, *Int. J. Biol. Macromol.*, 1984, **6**, 303.
263. P.S. Belton, V.J. Morris and V.J. Tanner, *Macromolecules*, 1986, **19**, 1618.
264. L. Piculell, S. Nilsson and P. Ström, *Carbohydr. Res.*, 1989, **188**, 121.
265. M. Rinaudo, M. Milas, F. Lambert and M. Vincendon, *Macromolecules*, 1983, **16**, 618.
266. E.R. Morris, D.A. Rees, G. Young, M.D. Walkinshaw and A. Darke, *J. Mol. Biol.*, 1977, **110**, 1.
267. D. Horton, O. Mols, Z. Walaszek and W.C. Wernau, *Carbohydr. Res.*, 1985, **141**, 340.
268. N.W. Cheetham and E.N.M. Mashimba, *Carbohydr. Polymer*, 1992, **17**, 127.
269. P.E. Jansson, B. Lindberg and P.A. Sandford, *Carbohydr. Res.*, 1983, **124**, 135.
270. M.-S. Kuo, A.J. Mort and A. Dell, *Carbohydr. Res.*, 1986, **156**, 173.
271. F. Horii, in *Nuclear Magnetic Resonance in Agriculture* (ed. P.E. Pfeffer and W.V. Gerasimowicz), p. 311. CRC Press, Boca Raton, USA, 1989.
272. M.J. Gidley and S.M. Bociek, *J. Am. Chem. Soc.*, 1985, **107**, 7040.
273. R.P. Veregin, C.A. Fyfe, R.H. Marchessault and M.G. Taylor, *Macromolecules*, 1986, **19**, 1030.

274. F. Horii, H. Yamamoto, A. Hirai and R. Kitamaru, *Carbohydr. Res.*, 1987, **160**, 29.
275. S.F. Tanner, S.G. Ring, M.A. Whittam and P.S. Belton, *Int. J. Biol. Macromol.*, 1987, **9**, 219.
276. A. Imberty, A. Buléon, V. Tran and S. Pérez, *Starch*, 1991, **43**, 375.
277. R.P. Veregin, C.A. Fyfe and R.H. Marchessault, *Macromolecules*, 1987, **20**, 3007
278. M.J. Gidley and S.M. Bociek, *J. Am. Chem. Soc.*., 1988, **110**, 3820.
279. R.P. Veregin, C.A. Fyfe, R.H. Marchessault and M.G. Taylor, *Carbohydr. Res.*, 1987, **160**, 41.
280. M.J. Gidley, *Macromolecules*, 1989, **75**, 351.
281. M.J. Gidley, A.J. McArthur and D.R. Underwood, *Food Hydrocolloids*, 1991, **5**, 129.
282. C. Rochas and M. Lahaye, *Carbohydr. Polymers*, 1989, **10**, 189.
283. S. Ablett, A.H. Clarke and D.A. Rees, *Macromolecules*, 1982, **15**, 597.
284. A.C. MacKay, M. Bloom, M. Tepfer and I.E.P. Taylor, *Biopolymers*, 1982, **21**, 1521.
285. P.L. Irwin, in *Nuclear Magnetic Resonance in Agriculture* (ed. P.E Pfeffer and W.V. Gerasimowicz), p. 337. CRC Press, Boca Raton, USA, 1989.
286. P.J. Barker and H.J. Stronks, in *NMR Applications to Biopolymers* (ed. J.W. Finlay, S.J. Schmidt and A. Serianni), p. 481. Plenum, New York, 1990.
287. P. Lambelet, *Lebensm.-Wiss. u.-Technol.*, 1983, **16**, 90.
288. P. Lambelet, *Lebensm.-Wiss. u-Technol.*, 1983, **16**, 200.
289. P. Lambelet, C. Desarzens and A. Raemy, *Lebensm.-Wiss. u-Technol.*, 1986, **19**, 77.
290. D.N. Rutledge, M. El-Khaloui and C.J. Ducauze, *Rev. Fr. Corps Gras,*, 1988, **35**, 157.
291. D.J. McClements and M.J.W. Povey, *Int. J. Food Sci. Technol.*, 1988, **23**, 159.
292. H.K. Leung, G.R. Anderson and P.J. Norr, *J. Food Sci.*, 1985, **50**, 942.
293. C. Desarzens and F. Michel, *Rev. Fr. Corps Gras.*, 1982, **29**, 419.
294. E. Brosio, F. Conti, A. di Nola and S. Sykora, *J. Am. Oil Chem. Soc.*, 1980, **57**, 78.
295. V.T. Srinivasan, B.B. Singh, P.K. Chidambaresweran and V. Sunderam, *J. Am. Oil Chem. Soc.*, 1985, **62**, 1021.
296. P.N. Gambhir and A.K. Agarwala, *J. Am. Oil Chem. Soc.*, 1985, **62**. 103.
297. E. Brosio, F. Conti, A. di Nola, O. Scorano and F. Balestrieri, *J. Food Technol.*, 1981, **16**, 629.
298. D. Le Botlan and M. Nicolaidis, *Sci. des Aliments*, 1989, **9**, 543.
299. B.S. Miller, M.S. Lee, J.W. Hughes and Y. Pomeranz, *Cereal Chem.*, 1980, **57**, 126.
300. D. Le Botlan, M. Guillou-Charpin and C. Tellier, *Sci. des Aliments*, 1988, **8**, 565.
301. E. Brosio, F. Conti, A. di Nola, M. Scalzo and E. Zulli, *J. Am. Oil Chem. Soc.*, 1982, **59**, 59.
302. J.P. Renou, G. Monin and P. Sellier, *Meat Sci.*, 1985, **15**, 225.
303. L.R.H. Tipping, *Meat Sci.*, 1982, **7**, 279.
304. N.D. Shiralkar, H.-P. Harz and H. Weisser, *Lebensm.-Wiss u.-Technol.*, 1983, **16**, 18.
305. E. Brosio, F. Conti, A. di Nola and S. Sykora, *J. Food Technol.*, 1981, **16**, 67.
306. R.M. Pearson, L.R. Ream, C. Job and J. Adams, *Ceral Foods World*, 1987, **32**, 822.
307. R.M. Pearson and J.Q. Adams, in *NMR Applications to Biopolymers* (ed. J.W. Finlay, S.J. Schmidt and A. Serianni), p. 499. Plenum, New York, 1990.
308. C. Tellier, M. Trierweiler, J. Lejot and G.J. Martin, *Analusis*, 1990, **18**, 67.
309. J.P. Renou, A. Briguet, P. Gatellier and J. Kopp, *Int. J. Food Sci Technol.*, 1987, **22**, 169.
310. M. Guillou and C. Tellier, *Anal. Chem.*, 1988, **60**, 2182.
311. C. Tellier, M. Guillou-Charpin, P. Grenier and D. le Botlan, *J. Agric. Food Chem.*, 1989, **37**, 988.
312. J.N. Shoolery, *Prog. Nucl. Magn. Reson. Spectrosc.*, 1977, **11**, 79.
313. S. Ng and W.L. Ng, *J. Am. Oil Chem. Soc.*, 1983, **60**, 1266.
314. A.P. Tulloch, *Lipids*, 1982, **17**, 544.
315. S. Ng, *Lipids*, 1984, **19**, 56.
316. K. Wollenberg, *J. Am. Oil Chem. Soc.*, 1991, **68**, 391.
317. S. Ng, *Lipids*, 1985, **20**, 778.
318. J. Schaefer and E.O. Stejskal, *J. Am. Oil Chem. Soc.*, 1974, **51**, 210.
319. V. Rutar, *J. Agric. Food Chem.*, 1989, **37**, 67.
320. J.H. Bradbury and J.G. Collins, *Cereal Chem.*, 1982, **59**, 159.

321. N. Sotirhos, B. Herslöf and L. Kenne, *J. Lipid Res.*, 1986, **27**, 386.
322. P. Meneses and T. Glonek, *J. Lipid Res.*, 1988, **29**, 679.
323. I.K. O'Neill, M. Sargent and M.C. Trimble, *Anal. Chem.*, 1980, **52**, 1288.
324. E.P. Mazzola, B.Q. Phillippy, B.F. Harland, T.H. Miller, J.M. Potemsa and E.W. Katsimpiris, *J. Agric. Food Chem.*, 1986, **34**, 60.
325. W. Frølich, T. Drakenberg and N.G. Asp, *J. Cereal Sci.*, 1986, **4**, 325.
326. W. Frølich, M. Wahlgren and T. Drakenberg, *J. Cereal Sci.*, 1988, **8**, 47.
327. J. Tamate and J.H. Bradbury, *J. Sci. Food Agric.*, 1985, **36**, 1291.
328. N.H. Low, T. Brisbane, G. Bigam and P. Sporns, *J. Agric. Food Chem.*, 1988, **36**, 953.
329. A. Rapp, A. Markowetz, M. Spraul and E. Humpfer, *Z. Lebensm. Unters. Forsch.*, 1989, **188**, 138.
330. T.M. Eads and R.G. Bryant, *J. Agric. Food Chem.*, 1986, **34**, 834.
331. D.L. Rabenstein and S. Fan, *Anal. Chem.*, 1986, **58**, 3178.
332. G.J. Martin, M.L. Martin, F. Mabon and M.J. Michon, *Anal. Chem.*, 1982, **54**, 2382.
333. G.J. Martin, M.L. Martin, F. Mabon and M.J. Michon, *J. Agric. Food Chem.*, 1983, **31**, 311.
334. G.J. Martin, X.Y. Sun, C. Guillou and M.L. Martin, *Tetrahedron*, 1985, **41**, 3285.
335. G.J. Martin, B.L. Zhang, N. Naulet and M.L. Martin, *J. Am. Chem. Soc.*, 1986, **108**, 5116.
336. J.-M. Franconi, N. Naulet and G.J. Martin, *J. Cereal Sci.*, 1989, **10**, 69.
337. C. Maubert, C. Guerin, F. Mabon and G.J. Martin, *Analusis*, 1988, **16**, 434.
338. B. Toulemonde, I. Horman, H. Egli and M. Derbesy, *Helv. Chim. Acta*, 1983, **66**, 2342.
339. G.J. Martin, M.L. Martin and F. Mabon, *J. Am. Chem. Soc.*, 1982, **104**, 2656.
340. C. Vallet, M. Arendt and G.J. Martin, *Biotechnol. Techn.*, 1988, **2**, 83.
341. C. Mo, J.A. Magnuson, J.B. Wilson, N.S. Magnuson and R.J. Kundland, *Biochemistry*, 1969, **8**, 2074.
342. R.S. Humphrey and K.W. Jolley, *Biochim. Biophys. Acta*, 1982, **708**, 294.
343. R.W. Sleigh, A.G. Mackinlay and J.W. Pope, *Biochim. Biophys. Acta*, 1983, **742**, 175.
344. M.C.A. Griffin and G.C.K. Roberts, *Biochem. J.*, 1985, **228**, 273.
345. N.M. Wahlgren, P. Dejmek and T. Drakenberg, *J. Dairy Res.*, 1990, **57**, 355.
346. P.S. Belton, R.L.J. Lyster and C.P. Richards, *J. Dairy Res.*, 1985, **52**, 47.
347. D.G. Schmidt, in *Developments in Dairy Chemistry*, Vol. 1 (ed. P.F. Fox), p. 61. Applied Science, London, 1982.
348. I.J. Cox, PhD thesis, University of East Anglia, 1984.
349. R.L.J. Lyster, *Biochem. Soc. Trans.*, 1976, **4**, 735.
350. P.S. Belton and R.L.J. Lyster, *J. Dairy Res.*, 1991, **58**, 443.
351. M. Wahlgren, T. Drakenberg, H.J. Vogel and P. Dejmek, *J. Dairy Res.*, 1986, **53**, 539.
352. D.G. Gadian, in *Developments in Meat Science*, Vol. 1 (ed. R. Lawrie), p. 89. Applied Science, London, 1980.
353. H.J. Vogel, P. Lundberg, S. Fabiasson, H. Ruderus and E. Tornberg, *Meat Sci.*, 1985, **13**, 1.
354. P. Lundberg, H.J. Vogel and H. Ruderus, *Meat Sci.*, 1986, **18**, 133.
355. M. Douglas, M.P. McDonald, I.K. O'Neill, R.C. Osner and C.P. Richards, *J. Food Technol.*, 1979, **14**, 193.
356. I.K. O'Neill and C.P. Richards, *Chem. Ind.*, 1978, 65.
357. P.S. Belton, K.J. Packer and T.E. Southon, *J. Sci. Food Agric.*, 1987, **40**, 283.
358. P.S. Belton, K.J. Packer and T.E. Southon, *J. Sci. Food Agric.*, 1987, **41**, 267.

Structural Studies of Peptides and Polypeptides in the Solid State by Nitrogen-15 NMR

A. SHOJI,* S. ANDO,[†,‡] S. KUROKI,[†] I. ANDO[†] and G.A. WEBB[§]

**Department of Biological Sciences, Gunma University, Tenjin-cho, Kiryu-shi, Gunma 376, Japan*
[†]*Department of Polymer Chemistry, Tokyo Institute of Technology, Ookayama, Meguro-ku, Tokyo 152, Japan*
[§]*Department of Chemistry, University of Surrey, Guildford, Surrey, UK*
[‡]Present Address: *NTT Interdisciplinary Research Laboratories, Midori-cho, 3-Chome, Musashino-shi, Tokyo 180, Japan*

1. INTRODUCTION

The investigation of peptides, proteins and other biopolymers in the solid state is being increasingly pursued by means of NMR studies. This important area of scientific investigation regularly merits mention in three chapters of the *Specialist Periodical Reports on NMR*, namely those relating to solid-state NMR, synthetic macromolecules and natural macromolecules. The plethora of references contained in these reports leave little doubt as to the importance of solid-state NMR studies to the various areas of science in which peptides and related species play a key role.

The present review concentrates on the uses of nitrogen NMR studies in the structural investigations of peptides and similar compounds. Many of the molecules of interest are insufficiently soluble to permit solution-state NMR studies and thus solid-state measurements are the method of necessity. An

ANNUAL REPORTS ON NMR SPECTROSCOPY
VOLUME 26 ISBN 0-12-505326-6

additional virtue of solid-state NMR is that it provides the possibility of obtaining special information which the tumbling motion of molecules in a solution would average out. Analysis of orientation-dependent data obtained from solid-state NMR measurements, such as dipolar coupling between nitrogen and neighbouring nuclei and the nitrogen chemical shielding anisotropy (CSA) can provide an insight into molecular structure. Oriented molecules, in general, have NMR spectra which are very sensitive to changes in orientation with respect to the direction of the applied magnetic field. Thus, small changes in molecular orientation normally produce readily observable changes in the NMR signal splitting arising from CSA or dipolar coupling.

In order to be able to interpret such NMR spectra in terms of the molecular orientations it is necessary to have an accurate knowledge of the principal values and orientation of the chemical shielding or dipolar tensors in the molecule of interest. The experimental procedures used to determine these and related data are reviewed in Section 2. The following section, 3, deals with some possible theoretical interpretations of the shielding tensor and its principal components. Sections 4 and 5 cover applications of nitrogen NMR measurements to studies on oligopeptides and synthetic polypeptides respectively. The majority of the reports mentioned deal with ^{15}N NMR investigations. The additional quadrupolar signal-broadening produced by ^{14}N NMR is often counterproductive to the work which forms the main focus of this review.

2. EXPERIMENTAL PROCEDURES

2.1. Static measurements

2.1.1. Single-crystal measurements

The CSA is an unsymmetric nuclear spin interaction represented by a second rank Hermitian tensor. The anisotropy originates from the unsymmetric spatial distribution of electrons surrounding the observed nucleus. However, since the contribution from the antisymmetric parts can be neglected, the symmetric components of the CSA tensor can always be diagonalized. The CSA tensor is, therefore, characterized by the three principal values $(\sigma_{11}, \sigma_{22}, \sigma_{33})$ (σ_{11}, σ_{22} and σ_{33} are defined to be from high to low frequency in this review article) and their principal axis directions, which forms a principal axis system (PAS).[1,2] The observed chemical shieldings (σ_{obs}) of nuclei are displaced according to the orientation of the applied magnetic field with respect to the PAS of the CSA.

The angular dependence of the CSA interaction is given by

$$\sigma_{obs} = \sigma_{11} \cos 2\alpha \sin 2\beta + \sigma_{22} \sin 2\alpha \sin 2\beta + \sigma_{33} \cos 2\beta \qquad (1)$$

where α and β are the Euler angles which express the relative directions of the PAS with respect to the direction of the applied magnetic field. From the

rotation plots of the chemical shielding line positions the principal values and the direction of the chemical shielding tensor can be determind.[1-3]

2.1.2. *Polycrystalline measurements*

Large single crystals of peptides, necessary for single-crystal measurements, are usually not available because they are difficult to grow. For polycrystalline samples, the NMR spectrum becomes the sum of single-crystal spectra for all directions, the so-called "powder pattern".

According to the calculation of Bloembergen and Rowland,[4] the intensity of the NMR signal at the frequency ω is expressed as

$$I(\omega) = \pi^{-1}(\omega - \omega_{11})^{-1/2}(\omega_{33} - \omega_{22})^{-1/2}K(m) \tag{2}$$

for

$$\omega_{33} > \omega > \omega_{22}$$

where

$$m^2 = (\omega_{22} - \omega_{11})(\omega_{33} - \omega)/(\omega_{33} - \omega_{22})(\omega - \omega_{11}) \tag{3}$$

$$I(\omega) = \pi^{-1}(\omega_{33} - \omega)^{-1/2}(\omega_{22} - \omega_{11})^{-1/2}K(m) \tag{4}$$

for

$$\omega_{22} > \omega > \omega_{11}$$

where

$$m^2 = (\omega - \omega_{11})(\omega_{33} - \omega_{22})/(\omega_{33} - \omega)(\omega_{22} - \omega_{11}) \tag{5}$$

and

$$I(\omega) = 0 \quad \text{in case } \omega > \omega_{33} \text{ and } \omega < \omega_{11}$$

where $K(m)$ is the complete elliptic integral of the first kind as

$$K(m) = \int_0^{\pi/2} (1 - m^2 \sin^2 \phi)^{-1/2} \mathrm{d}\phi \tag{6}$$

The principal values of the shielding tensor $(\sigma_{11}, \sigma_{22}, \sigma_{33})$ can be obtained directly from the powder pattern but no information is obtained about the orientation of the shielding tensor. The orientation can be determined from a single-crystal study, theoretical calculation, symmetrical consideration, or from related compounds whose tensor orientations are already determined.

As shown in Fig. 1, a typical ^{15}N powder pattern of a peptide reveals axial symmetry because the electronic structure around the nitrogens of the peptide bonds is nearly symmetrical around the axes of the N–H bonds. In such cases, the orientation of the principal axis is difficult to determine even from a single-crystal study. The directions of the two principal values, σ_{11} and σ_{22}, are determined by using the dipolar interactions between the nitrogen and the adjacent

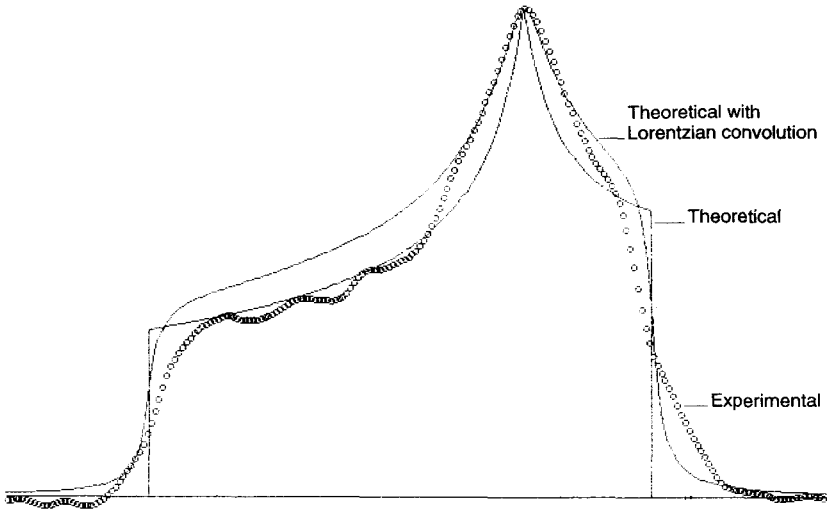

Fig. 1. Schematic representation of experimental powder pattern and theoretical powder pattern and theoretical powder pattern convoluted with the Lorentzian function. The circles indicates the experimental data for glycylglycine·HNO_3. (S. Kuroki and I. Ando, unpublished data.)

carbonyl carbon nucleus. Another problem in this experiment is that the background signal due to unenriched sites often contributes to the skirts of the powder pattern spectrum. Even though the nitrogen of interest is enriched, the two principal values read off from the outer regions, σ_{11} and σ_{33}, are likely to contain some errors.

2.2. Cross-polarization/magic-angle spinning and double cross-polarization NMR measurements

2.2.1. ^{15}N cross-polarization/magic-angle spinning NMR method

Since the ^{15}N nucleus has spin-$\frac{1}{2}$ but low natural abundance (0.365%) and a low magnetogyric ratio ($\gamma = -2.7126 \times 10^7$ rad/s T) and so a rather low NMR sensitivity,[5–7] it is difficult to obtain a solid sample spectrum from a single pulse experiment. Recently, the cross-polarization/magic-angle spinning (CP/MAS) technique[1,2,8] has been applied to solid samples and thus we can obtain high-resolution NMR spectra from solids. The CP experiment involves polarization transfer from ^1H to dilute spin-$\frac{1}{2}$ nuclei such as ^{13}C or ^{15}N. The matching condition can be predicted from the Hartmann–Hahn condition as

$$\gamma_N \sigma B_N = \gamma_H \sigma B_H \tag{7}$$

where σB_N and σB_H are the magnetic fields for the ^{15}N and ^{1}H nuclei, respectively, in the rotating frame. When this matching condition is satisfied, the ^{15}N signal intensity is increased by $\gamma_H/\gamma_N = 9.86$ times. Magic-angle spinning removes the CSA. Since the CSA of a peptide amide nitrogen ^{15}N is about 3–5 kHz, the sample has to be spun at more than 4 kHz.

2.2.2. ^{1}H–^{13}C–^{15}N double CP NMR method

The double CP experiment[9,10] involves the sequential transfer of polarization among three spin-$\frac{1}{2}$ systems. This technique can be used to observe selectively one type of spin (e.g. ^{15}N) which is directly bonded to another nucleus (e.g. ^{13}C). Since both ^{15}N and ^{13}C nuclei are rare spins, ^{13}C–^{15}N bonds are extremely rare occurrences in natural isotopic abundance peptides. The ^{13}C–^{15}N bonds observed in this experiment originate from doubly-labelled compounds. The different kinds of labelled ^{13}C–^{15}N bonds and their concentrations can be detected.

2.2.3. Spinning sideband intensity method

The NMR lineshapes observed in proton-decoupled ^{15}N spectra are dominated by the CSA. In the CP/MAS experiment, high resolution is achieved at the expense of the information contained in the anisotropy. But when the spinning frequency is less than the nuclear shielding anisotropy, the isotropic line in the NMR spectrum is flanked on both sides by sidebands spaced at the spinning frequency. Maricq and Waugh[11,12] have shown that the second and third moments of the NMR spectra can be used to extract the shielding anisotropy from the sideband intensities. Herzfeld and Berger[13] have derived general integral and series expansions for sideband intensities. Principal values of the shielding tensor can be derived from the intensities of a relatively small number of sidebands. An example of this experiment for glycylglycine · HNO_3 is shown in Fig. 2. The sample was spun 1.6 kHz, and three principal values of the components of the shielding tensor are obtained as $\sigma_{11} = 197$ ppm, $\sigma_{22} = 52$ ppm and $\sigma_{33} = 21$ ppm.

2.2.4. Dipolar NMR method

In the simple CP/MAS experiment for ^{15}N and ^{13}C nuclei in a peptide, scalar coupling to ^{1}H is not observed because high-power ^{1}H decoupling is used to remove the ^{1}H–^{15}N or ^{1}H–^{13}C dipolar interactions. However, for the carbons directly bonded to nitrogens, ^{14}N–^{13}C or ^{15}N–^{13}C dipolar interactions are not averaged out by MAS and broadened asymmetric doublets are observed.[14–17] Accord-

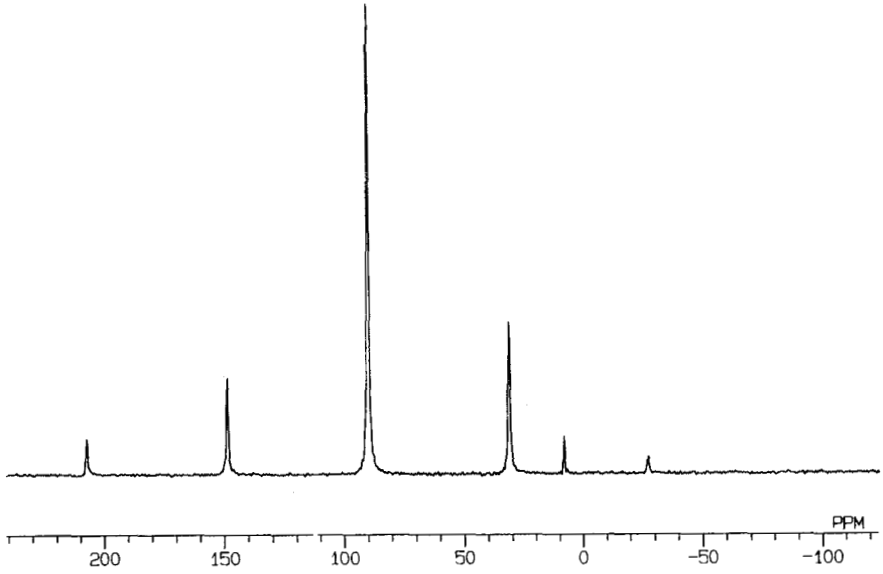

Fig. 2. The 27.3-MHz ^{15}N CP/MAS NMR spectrum of glycylglycine · HNO_3 in the solid state. The magic-angle spinning rate is 1.6 kHz. (S. Kuroki and I. Ando, unpublished data.)

ing to the scheme expressed by Linder *et al.*,[14] the powder pattern spectrum, $S(v)$, of a dipolar-coupled nuclear site can be expressed in the following form:

$$S(v) = \sum_i s(v_i) = \sum_i \int_{\theta=0^\circ}^{180^\circ} \int_{\phi=0^\circ}^{360^\circ} g_i[v, v_i(\theta, \phi, \alpha_D, \beta_D)] \sin\theta \, d\theta \, d\phi \qquad (8)$$

where θ and ϕ are polar angles which describe the orientation of the chemical shielding PAS with respect to the magnetic field fixed in the laboratory frame;

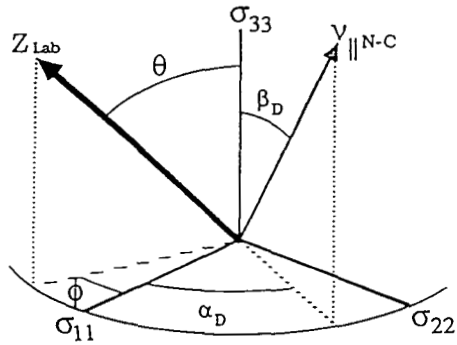

Fig. 3. The orientation of the N–C_1 internuclear vector ($v_{\|N-C}$) with respect to the shielding tensor (σ_{ii}) is given by α_D and β_D. The orientation of the laboratory Z axis (Z_{Lab}) with respect to the shielding tensor is given by θ and ϕ.

α_D and β_D are rotations which transform the dipolar interaction into the PAS of the shielding tensor (Figs 3 and 4), v is the observed frequency, and $v_i(\theta, \phi, \alpha_D, \beta_D)$ is the transition frequency for a particular orientation of the shielding and dipolar tensors.

On the other hand, the dipolar coupled signal of nitrogen is observed when the carbons directly bonded to nitrogen are labelled by ^{13}C or when the hydrogens are not decoupled.[18] The double labelling of the peptide nitrogen and carbon with ^{15}N and ^{13}C is, however, frequently used to extract information about the orientation of the N–C bond because a principal axis of the dipolar tensor always coincides with that of the C–N bond.[19] The dipolar interactions between nitrogen (^{14}N and ^{15}N) and hydrogen have been studied to obtain the bond lengths of N–H bonds.[20,21]

3. THEORETICAL INTERPRETATION OF NITROGEN NMR SHIELDINGS

The general principles involved in calculations of NMR nuclear shieldings from quantum mechanical considerations have been described elsewhere.[22] Only a very brief summary of the available types of shielding calculation likely to be relevant to peptides and polypeptides is given here. Normally, for large molecules semi-empirical molecular orbital (MO) procedures are employed for nuclear shielding calculations. This contrasts with the situation for smaller molecules, containing a maximum of about 11 heavy atoms, for which *ab initio* MO methods can produce very satisfactory estimates of nuclear shielding.[23] Progress in nuclear shielding calculations forms the basis of an annual report.[24] Nuclear shieldings are determined by the molecular environment in which the nucleus finds itself. Thus the effectiveness of a MO calculation of nuclear shielding depends on the success of the procedure used in describing the molecular electronic environment. Commonly used procedures provide estimates of the major shielding contributions, namely the diamagnetic and paramagnetic contributions which usually have opposite signs. For a given

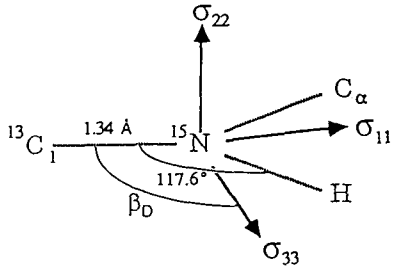

Fig. 4. Orientation of the shielding tensor elements in the molecular frame on alanyl-alanine, σ_{11} lies essentially in the plane of the peptide linkage as do the N–H, N–C_α, and N–C_1 bonds.

type of nucleus, such as nitrogen, in a variety of electronic environments the diamagnetic contribution to the change in shielding is usually about 3% or less of the total change. Consequently, it is the paramagnetic contribution which controls the variation of nuclear shielding with environment. Unfortunately, this is the more difficult of the two types of contributions to calculate reliably.

Both the sum-over-states (SOS) and finite perturbation theory (FPT) have been widely employed to estimate the diamagnetic and paramagnetic shielding contributions for molecules of various sizes. The SOS approach requires an accurate knowledge of the molecular excited states and their excitation energies. This can be difficult to obtain by self-consistent field (SCF) MO methods, in particular by semi-empirical MO procedures. In contrast the FPT approach has the advantage of not requiring explicit wavefunctions for the excited states. The FPT-INDO method has been successfully used in nitrogen shielding calculations on *N*-methylacetamide which has been employed as a model compound in conjunction with nitrogen NMR spectra taken on a variety of solid oligopeptides, (X–Gly–Gly)[25] and (Boc–Gly).[26] The importance of *ab initio* nitrogen shielding calculations, using an individual gauge for localized molecular orbitals (IGLO) and the localized orbital local origins (LORG) methods, has been discussed in a review.[27] In general these procedures can provide satisfactory estimates of nitrogen shielding tensors for small molecules. IGLO calculations have been reported for DNA bases with some success.[28] Similar calculations on some model peptides could be of interest. It should be recognized that the results of MO calculations on monomeric species may not be readily transferable to polymers. This arises from the fact that in small molecules the electrons are confined to a finite region of space whereas this may not be the case for polymers. Consequently calculations of polymer electronic structure require the inclusion of long range and interchain interactions. These can be incorporated into calculations of nuclear shielding by means of the tight-binding (TB) procedure.[29]

Calculations of nuclear shielding normally provide values for each of the nine components of the second-order shielding tensor. Thus theoretical estimates are available for the principal components of the tensor as well as its anisotropy and the isotropic value of the nuclear shielding, the latter of which is usually available from high-resolution CP/MAS NMR measurements. Methods for experimentally determining the principal tensor components, and its anisotropy, are described in the previous section.

4. OLIGOPEPTIDES

4.1. Shielding tensors

In order to establish the orientation of a peptide backbone or side-chain residue from chemical interactions, the orientation of the shielding tensor in the molecular frame needs to be determined.

The ^{15}N shielding tensor of a peptide was first determined for L-histidine hydrochloride monohydrate from a single-crystal study by Harbison *et al.*[30] The principal components of the shielding of the imidazole ring nitrogens are oriented approximately along the molecular symmetry directions differing from them by only 3° and 5°, and the most shielded element, σ_{33}, is perpendicular to the plane of the imidazole ring.

The orientation of the ^{15}N shielding tensor in the amino group was determined for L-asparagine·H_2O from the sideband intensities in the ^{15}N–^{1}H dipolar/chemical shift spectrum by Herzfeld *et al.*[31] In the presence of magic-angle spinning, two-dimensional solid-state NMR spectra of magnetically dilute $I = \frac{1}{2}$ nuclei split into rotational sidebands spaced at the spinning frequency in both dimensions. The dipolar slice, corresponding to particular shift sidebands, is asymmetric and contains information regarding the relative orientations of the shielding and dipolar tensors. The calculated two-dimensional spectra for the six orientations are compared to the observed spectrum, and a good match is only obtained for that in which the quasi-unique component σ_{11} is perpendicular to the H–N–H disector in the H–N–H plane.

It is concluded that σ_{33} lies along the H–N–H bisector, σ_{22} lies perpendicular to the H–N–H plane, and σ_{11} lies in the H–N–H plane, perpendicular to the H–N–H bisector.

Through the observation of proton-decoupled ^{15}N NMR lineshapes of two crystalline phases of Boc-glycylglycyl[^{15}N,^{2}H]glycine benzyl ester, the ^{15}N–^{2}H bond length and the direction of the most deshielded component of the shielding tensor, σ_{11}, have been determined, combined with X-ray diffraction data.[32]

The ^{15}N shielding tensor of the amide group was examined for uniformly ^{15}N-labelled glycylglycine hydrochloride monohydrate, from the dipolar/chemical shift spectra produced by two-dimensional magic-angle NMR methods.[33] It is found that the nearly axially symmetric ^{15}N shielding tensor is tilted 25° away from the N–H bond. The same ^{15}N shielding tensor was determined for [1-^{13}C]glycyl[^{15}N]glycine hydrochloride monohydrate from a single-crystal study.[34] Although one of the components of the ^{15}N tensor is perpendicular to the plane of the peptide bond, the tensor is very close to being axially symmetric. The orientations of σ_{33} and σ_{22} could not be determined. The angle between the N–H bond vector and σ_{11} is 21.3°, which is larger than that of the imidazole nitrogen in histidine.

The ^{15}N–^{1}H dipolar/chemical shift spectra were observed for polycrystalline samples of [^{15}N]acetylvaline, α-[^{15}N]glycyl-[^{15}N]glycine, [^{15}N]glycyl-[^{15}N]glycine·HCl·H_2O, [^{15}N]acetyl-glycine, [π-^{15}N]-1-histidine·HCl·H_2O, and [ϵ-^{15}N]tryptophan[21] (Fig. 5).

The first four ^{15}N–^{1}H systems, all peptide linkages, yield similar results to [1-^{13}C]glycyl[^{15}N]glycine·HCl·H_2O where the σ_{11} principal axis of the shielding tensor is rotated approximately 20° from the unique principal axis

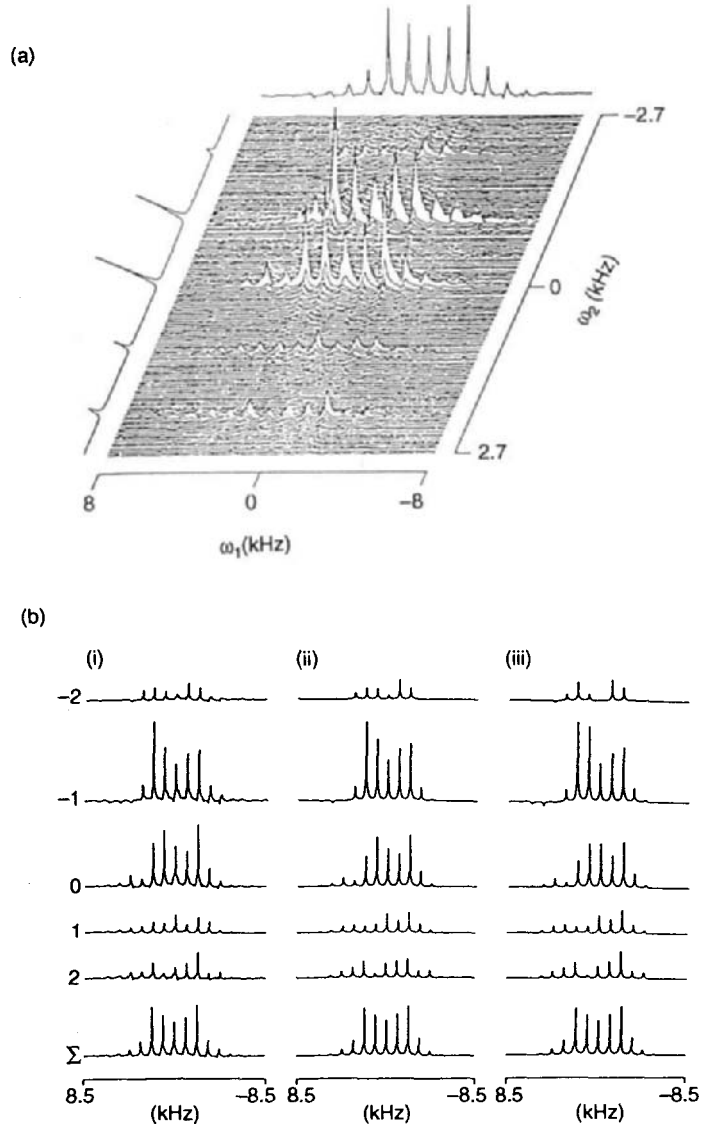

Fig. 5. (a) Two-dimensional ^{15}N–^{1}H dipolar/chemical shift spectrum obtained from [^{15}N]acetylvaline showing the dipolar and chemical shift projections. Linewidths are typically 50–150 Hz for the dipolar and 0.5–1.0 ppm for the chemical shift dimension. $\upsilon_R = 1.07$ kHz. (b) Dipolar cross-sections taken from the 2D spectrum. Each trace runs parallel to ω_1, through a particular rotational sideband in ω_2. (i) Experimental ^{15}N–^{1}H spectra from [^{15}N]acetylvaline, $\upsilon_R = 1.07$ kHz. The two simulations (ii and iii) assume two different orientations of the dipolar and shielding tensors, ($\beta_D = 22°$, $\alpha_D = 0°$) and ($\beta_D = 17°$, $\alpha_D = 0°$), respectively, and illustrate the subtle differences in orientation which can be detected in the spectra.

of the dipolar tensor. However, the location of the other two principal axes cannot be determined accurately because of the almost axial symmetry of the ^{15}N shielding tensor. In addition, the dipolar/chemical shift experiments yield a value of the length of the ^{15}N–^{1}H bond which is accurate to within 0.005 Å and the mutual orientations of the dipolar and shielding tensors accurate to within 3°. A comparison of the bond lengths obtained from NMR experiments with similar data from neutron diffraction experiments shows that the former is uniformly 0.0035 Å longer than the latter.

The dipolar-coupled ^{15}N shielding powder patterns contain enough information to allow the determination of the orientation of the dipolar vector (N–C or H–N bond) in the PAS of the shielding tensor. Hartzell *et al.*[35] have determined the orientation of the ^{15}N shielding tensor relative to the molecular frame for polycrystalline L-[1-^{13}C]alanyl-L-[^{15}N]alanine using a ^{1}H dipole-modulated, ^{13}C dipole-coupled ^{15}N spectrum (Fig. 6). The orientation of the ^{13}C–^{15}N bond to the most shielded component, σ_{33}, is 106°, in which the angle between the N–H bond and σ_{33} is 12°. In addition, the σ_{22} is perpendicular to the peptide plane, and σ_{11} is in the peptide plane perpendicular to σ_{22} and σ_{33}.

The ^{15}N shielding tensors of a homologous series of peptides of the form *N*-acetyl[1-^{13}C]glycyl[^{15}N]X-amide (X = glycine, L-alanine and tyrosine) and the unprotected dipeptide [1-^{13}C]glycyl[^{15}N]glycine hydrochloride have been determined from ^{13}C dipole-coupled ^{15}N powder patterns.[36,37] It is reported that the common shielding tensor orientation places σ_{22} perpendicular to the peptide plane, and σ_{33} at a 99° angle with respect to the C–N bond. The orientations of σ_{11} and σ_{22} were first determined for ^{15}N shielding tensors of amides, there are no significant differences in the molecular orientations of the tensors, although there are large lattice-dependent variations in the ^{15}N shielding tensor principal values.

On the other hand, the orientation of the σ_{33} component of the amide ^{15}N shielding tensor was determined from dipolar-coupled ^{15}N powder patterns by Teng *et al.*[38–40] (Fig. 7). Two doubly-labelled molecules, [1-^{13}C]glycyl$_2$[^{15}N]-alanyl$_3$-gramicidin-A and [1-^{13}C]alanyl$_3$[^{15}N]-D-leucyl$_4$-gramicidin-A, in a liquid environment were used, and the orientations of the ^{13}C–^{15}N bonds to the σ_{33} component are 104° and 105°, in which the angles between the N–H bond and σ_{33} range between 12° and 14°. These results are very close to those reported for alanylalanine by Hartzell *et al.* (12°),[35] but slightly deviate from other data by Oas *et al.* (20° ± 2°),[36] Munowitz *et al.* (25° ± 5°)[33] and Harbison *et al.* (21°).[34] It can be said that the orientation of the shielding tensor relative to the molecular frame is variable and consequently there is a need to determine the tensor orientation for each site of interest.

A rotational-echo, double-resonance (REDOR) ^{15}N–^{13}C NMR experiment has been performed on an alanine co-crystallized from five-component alanines, isotopically enriched in ^{13}C, ^{15}N, or ^{13}C.[41–43] REDOR ^{15}N–^{13}C NMR involves the dephasing of carbon magnetization by ^{15}N 180° pulses synchronized with magic-angle spinning. The C–N dipolar coupling deter-

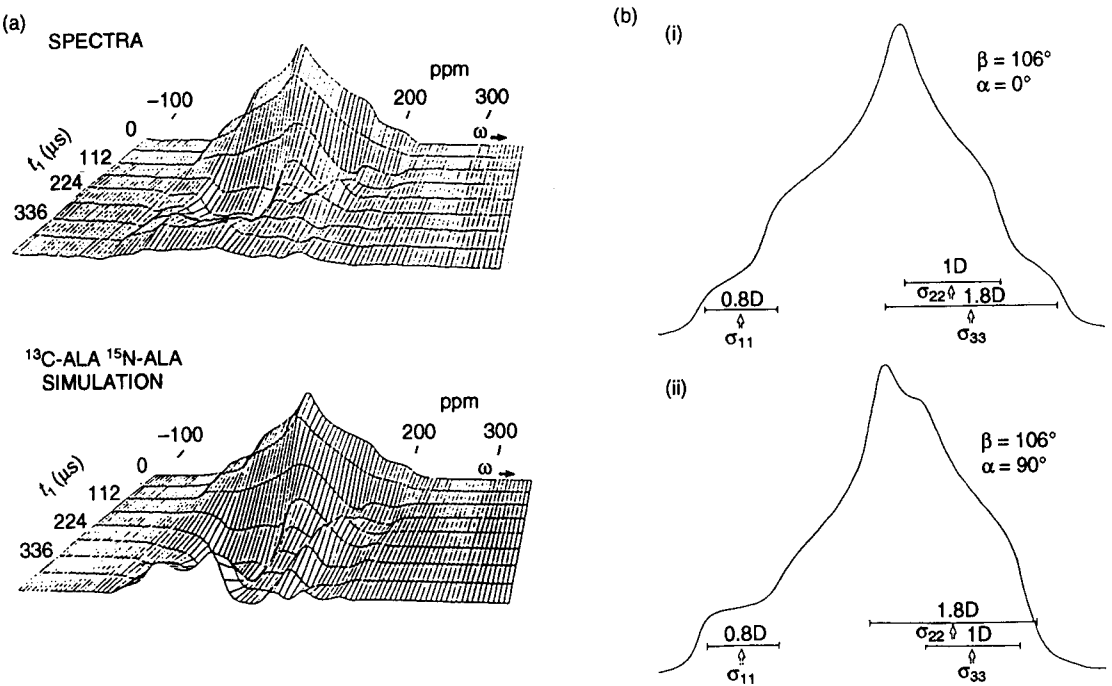

Fig. 6. (a) Transform in t_2 of the ^{1}H dipole-modulated, ^{13}C dipole-coupled, ^{15}N powder FID of [1-^{13}C]alanyl-[^{15}N]alanine. The number of MREV-8 cycles (56 μs) was increased from 0 to 8 during t_1. The frequency axis is reported in ppm relative to liquid NH_3 at −50°C. (b) Unmodulated simulations for two orientations of σ_{33} and σ_{22} relative to the peptide plane. (i) The orientation described by $\beta_{CN} = 106°$, $\alpha_{CN} = 90°$ places σ_{33} perpendicular to the plane and σ_{22} in the plane nearly parallel to the C–N bond. (ii) The orientation described by $\beta_{CN} = 106°$, $\alpha_{CN} = 90°$ places σ_{33} perpendicular to the plane and σ_{22} in the plane nearly parallel to the C–N bond.

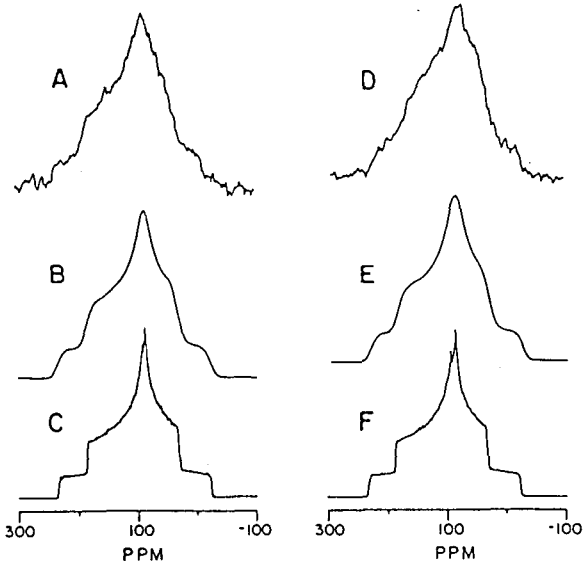

Fig. 7. Experimental (A and D) and theoretical (B < C < E and F) ^{15}N powder pattern spectra of doubly labelled gramicidin A. (A) Spectrum of [1-^{13}C]glycyl$_2$[^{15}N]alanyl$_3$-granicidin A with an observed dipolar splitting, $\Delta\nu_3 = 970$ Hz, indicating a β_D angle of 106°. (B) Broadened (360 Hz of Gaussian broadening) version of theoretical spectrum shown in C. (C) Theoretical spectrum yielding a best fit to the experimental data with $\alpha_D = 0°$ and $\beta_D = 104°$. (D) Spectrum of [1-^{13}C]alanyl$_3$-D-[^{15}N]leucyl$_4$-gramicidin A with an observed dipolar splitting, $\Delta\nu_3 = 1010$ Hz, indicating a β_D angle of 105°. (E) Broadened (360 Hz of Gaussian broadening) version of theoretical spectrum shown in (F). (F) Theoretical spectrum yielding a best fit to the experimental data with $\alpha_D = 0°$ and $\beta_D = 105°$.

mines the extent of dephasing. These experiments on alanine show that it is practical to use REDOR to measure the C–N dipolar coupling of 5 μmol of a ^{13}C–^{15}N-labelled pair having an internuclear separation of the order of 4.5 Å.

4.2. Isotropic chemical shifts

High-resolution ^{15}N CP/MAS NMR spectra of a variety of solid oligopeptides (X-glycylglycine) have been measured by Kuroki *et al.*[25] in order to clarify the relationship between the hydrogen bonding structure and ^{15}N shielding. It is found that there is no relationship between hydrogen bond length ($R_{N\cdots O}$) and Gly NH amide ^{15}N isotropic shielding (Fig. 8), but that the decrease of the N–H bond length (R_{N-H}) leads to a linear increase in ^{15}N isotropic shielding (Fig. 9). The expression for this relationship is

$$\delta_{obs} = 39.32R_{N-H} + 57.73 \text{ (ppm)}$$

In order to investigate the relationship between R_{N-H} and $R_{N\cdots O}$, quantum

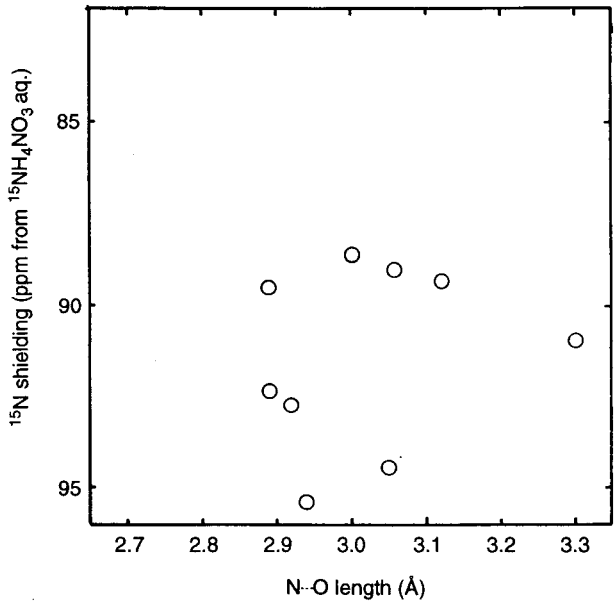

Fig. 8. Plot of the observed ^{15}N shielding of oligopeptides in the crystalline state against the N···O hydrogen bond length.

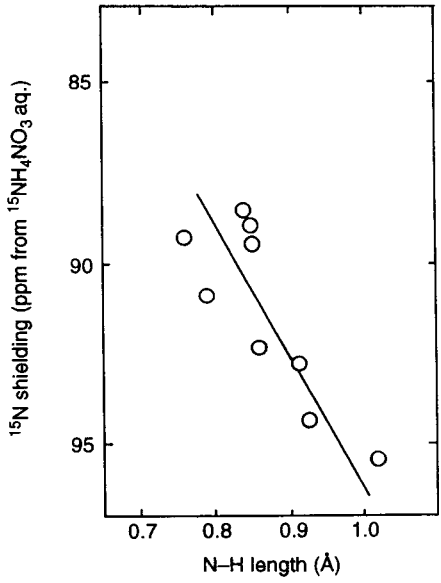

Fig. 9. Plot of the observed ^{15}N shielding of oligopeptides in the crystalline state against the N–H bond length.

chemical calculations were carried out using two hydrogen-bonded *N*-methyl acetamides. It is shown that at the region forming hydrogen bond, an increase of $R_{N\cdots O}$ leads to a decrease in R_{N-H} (Fig. 10). On the other hand, X-ray diffraction studies have shown that the R_{N-H} values decrease with an increase in the $R_{N\cdots O}$ values. Further, it is found that not only the hydrogen bond length but also the hydrogen bond angle ($\angle$N–H$\cdots$O) is related to the ^{15}N shielding. As shown in Section 3, ^{15}N shielding calculations were carried out using a model compound, by the FPT-INDO method; the calculated results reasonably explain the experimental ones in Fig. 11.

The relationship between amide nitrogen isotropic shielding and the principal values (σ_{11}, σ_{22}, and σ_{33}) of the shielding and hydrogen bond length $R_{N\cdots O}$ and hydrogen bond angle $\angle$N–H$\cdots$O has been studied by observing CP/MAS and CP/static ^{15}N NMR spectra of a variety of solid oligopeptides (*tert*-butyloxycarbonylglycyl-X).[25] From the results of the observed ^{15}N shieldings, it was found that the isotropic ^{15}N shieldings (σ_{iso}) of the glycine residues increase with an increase of hydrogen bond length ($R_{N\cdots O}$) between the nitrogen and oxygen atoms in the amide groups (Fig. 12), and that the principal values of σ_{33} decreases linearly with a decrease of $R_{N\cdots O}$ and there is no relationship between the principal values σ_{11}, σ_{22} and $R_{N\cdots O}$ (Fig. 13).

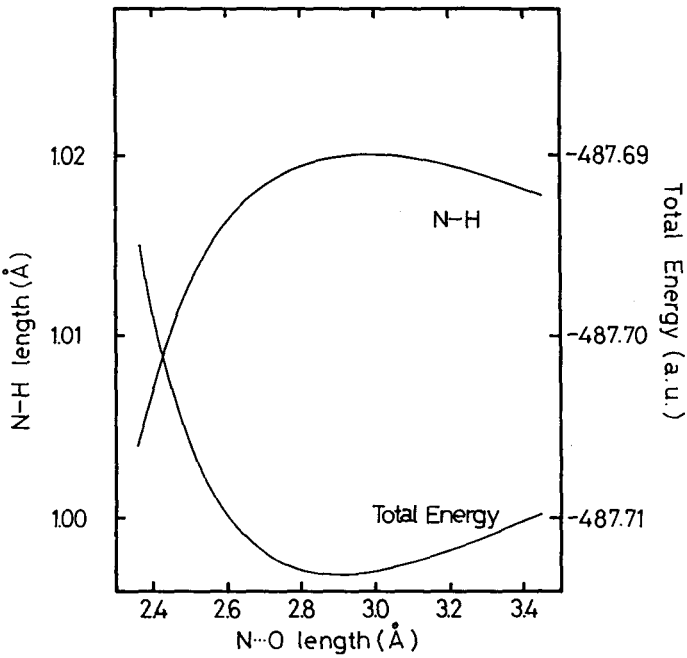

Fig. 10. Plot of the calculated N–H bond length and total energy against the hydrogen bond length (N$\cdots$O) obtained by using the *ab initio* STO-3G MO method.

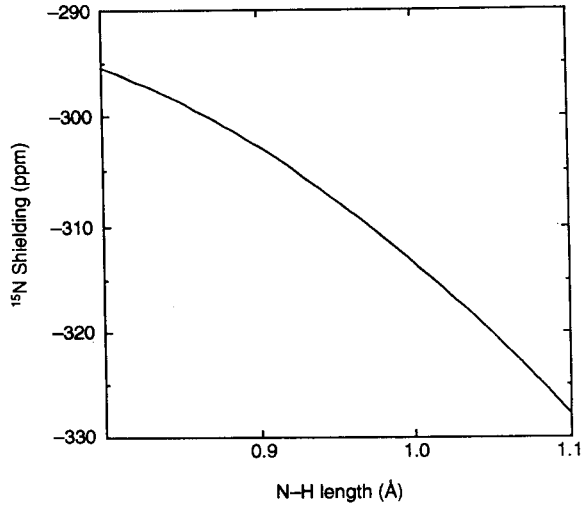

Fig. 11. Plot of the calculated ^{15}N shielding against the N–H bond length obtained from the FPT-INDO method.

As shown in Section 3, quantum chemical calculations of the ^{15}N shielding constant for the model compounds were carried out by the FPT-INDO method, and the relationship between ^{15}N shielding and $R_{N\cdots O}$, $\angle$N–H$\cdots$O was discussed (Figs 14 and 15). These results show that the σ_{11} and σ_{22} components are related not only to the hydrogen bond length ($R_{N\cdots O}$), but also to the hydrogen bond angle ($\angle$N–H$\cdots$O), but σ_{33} is related to the hydrogen bond

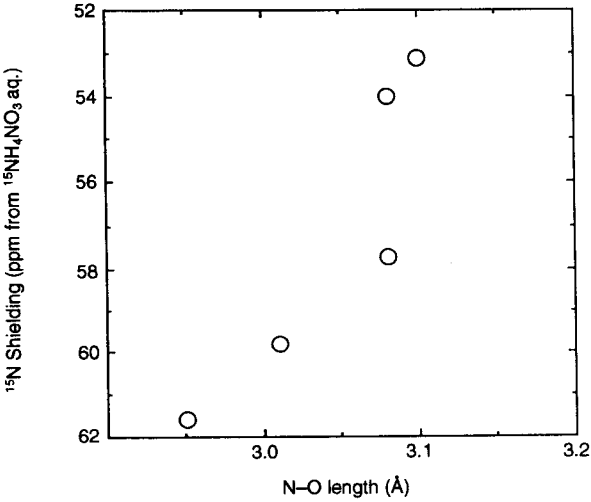

Fig. 12. Plot of the observed ^{15}N shielding in the solid state against the N$\cdots$O length.

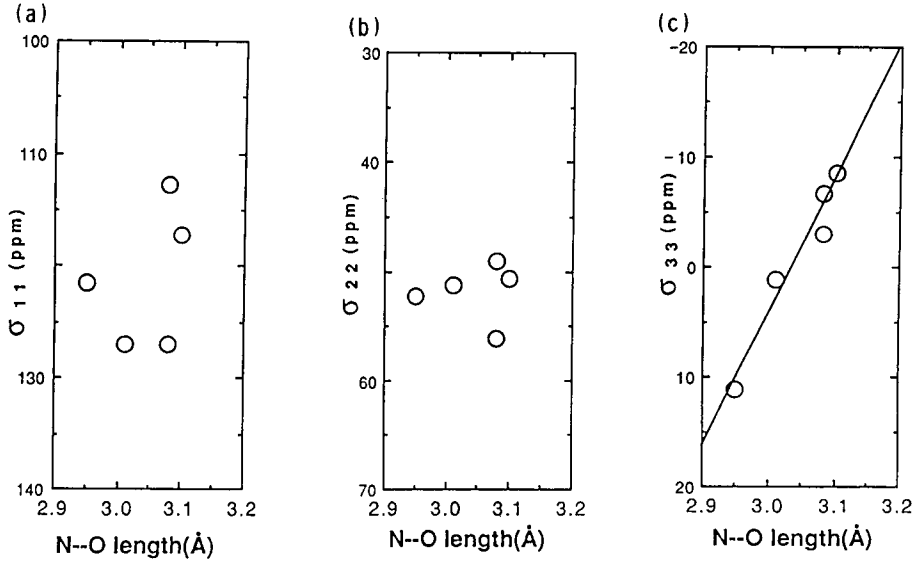

Fig. 13. Plots of the observed principal values of ^{15}N shielding tensors (a) σ_{11}, (b) σ_{22}, and (c) σ_{33} against the N···O bond length.

length ($R_{N\cdots O}$) only. Therefore, it can be said that the ^{15}N isotropic shielding and the three principal values of the shielding of the amide nitrogen provide useful information about the hydrogen bond length and hydrogen bond angle.

5. SYNTHETIC POLYPEPTIDES

High-resolution and solid-state ^{15}N NMR has been increasingly applied to the investigation of polypeptides, proteins and biopolymers.[30,44–59] This is because, especially in polypeptides and proteins, nitrogen is very often functionally important due to its ability to form hydrogen bonds, most of the nitrogen sites are in the amide linkage of the backbone and the structure and dynamics of the backbone strongly reflect the conformation and the flexibility of these macromolecules. Foerster *et al.*[47] have measured the ^{15}N CP/MAS NMR spectra of some synthetic polypeptides in the solid state and found that the isotropic ^{15}N chemical shift depends upon conformational features such as the secondary structure determined by the peptide bonds of the backbone. Shoji *et al.*[57–59] have studied systematically the relation between the ^{15}N chemical shifts and structure such as primary, secondary and higher ordered structures of various kinds of synthetic polypeptides in the solid state. They have demonstrated that the ^{15}N chemical shifts in the peptide backbone of these polypeptides change depending on conformation, nature of amino acid residue, amino acid sequence and manner of hydrogen bonding. It is noteworthy

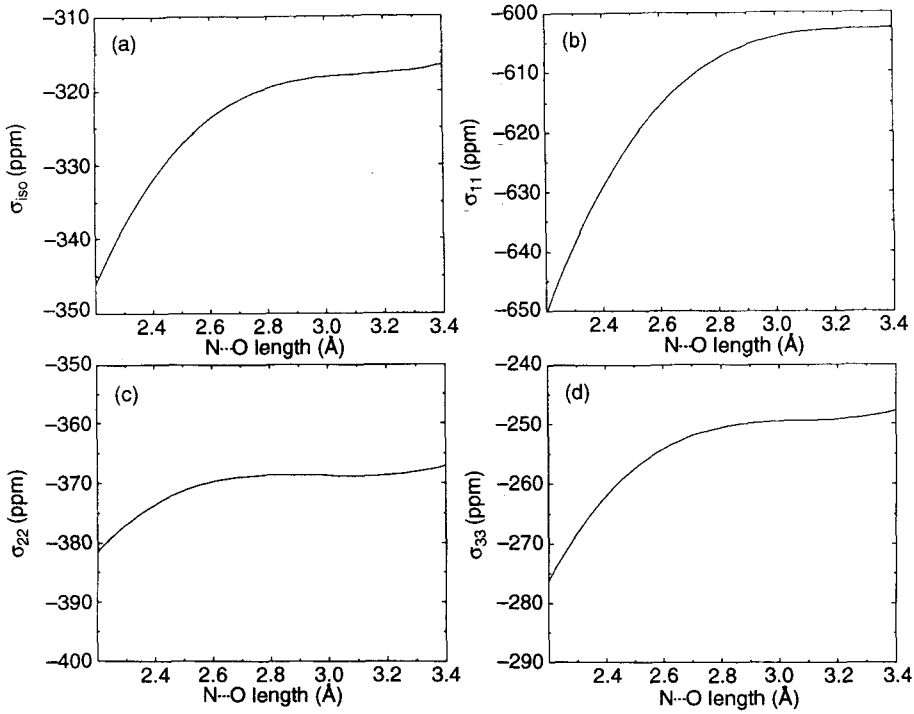

Fig. 14. Variation of the calculated ^{15}N shielding and its tensor components with the N···O hydrogen bond length: (a) σ_{iso}, (b) σ_{11}, (c) σ_{22}, and (d) σ_{33}.

that the ^{15}N shielding tensors are related to the structures of the solid polypeptides. Thus, it is now possible to determine the conformation of polypeptides and some proteins in the solid state by the ^{15}N CP/MAS NMR method. The NMR work is likely to become increasingly important in the study of the structure and dynamics of synthetic polypeptides and natural proteins in the solid state. Accordingly, if the sensitivity problem can be overcome, ^{15}N would be an ideal candidate for investigating polypeptides, proteins and biopolymers.

5.1. Isotropic ^{15}N chemical shifts

5.1.1. Homopolypeptides

Foerster *et al.*[47] measured the first ^{15}N CP/MAS NMR spectra of some ^{15}N-labelled homopolypeptides in the solid state. Figure 16 shows the 30.5-MHz ^{15}N CP/MAS NMR spectra of poly(L-leucine), poly(L-phenylalanine) and poly(glycine). The ^{15}N chemical shifts of solid homopolypeptides[47] are

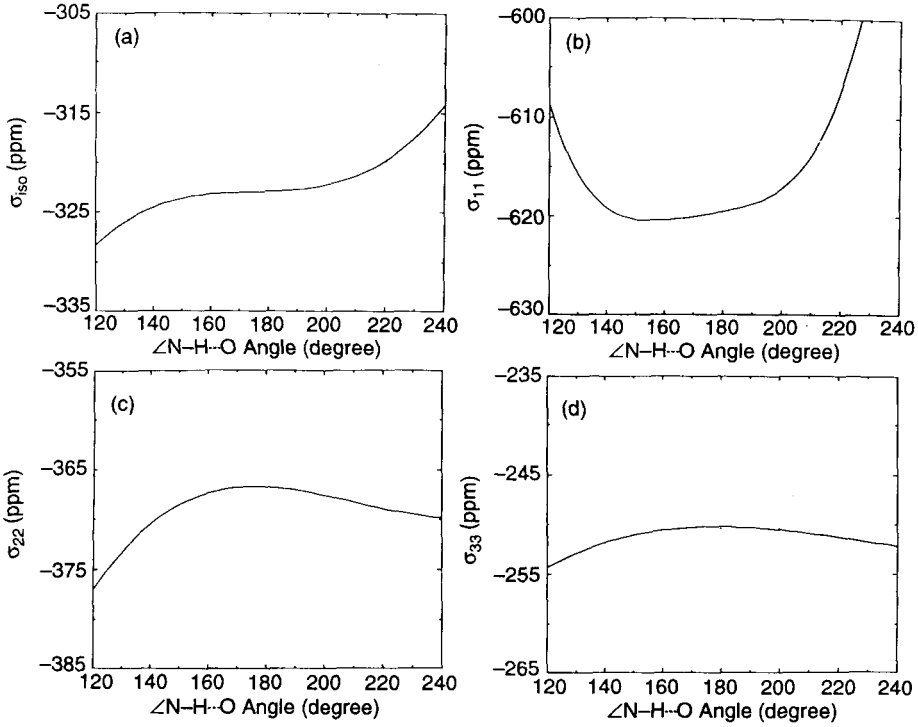

Fig. 15. Variation of the calculated ^{15}N shielding and its tensor components with the hydrogen bond angle (∠N–H···O): (a) σ_{iso}, (b) σ_{11}, (c) σ_{22} and (d) σ_{33}.

summarized in Table 1. Foerster *et al.* suggested that (1) the most interesting observation is the 9–10 ppm low-frequency shift for the right-handed α-helix (α-helix) structures compared to antiparallel β-sheet (β-sheet) structures of poly(L-leucine) and poly(L-phenylalanine), which allows the identification and quantification of the composition of secondary structures of polypeptides; (2) the PGI (β-sheet) and PGII (3_1-helix) forms of poly(glycine) differ by 4.5 ppm in the ^{15}N NMR spectra, whereas the PPI (right-handed 10_3-helix; *cis*-type) and PPII (left-handed 3_1-helix; *trans*-type) of poly(L-proline) do not exhibit any shift differences; (3) all polypeptides having one α-substituent absorb several parts per million to high frequency of poly(glycine) and poly(L-proline) absorbs at the highest frequency; and (4) the shift effects of γ- and δ-carbons are smaller and less systematic in the solid state.

Shoji *et al.*[57] have studied the relation between ^{15}N chemical shift and structural parameters such as primary and secondary structures of various natural abundance homopolypeptides in the solid state. In order to test systematically the power of ^{15}N CP/MAS NMR for the structural analysis of solid polypeptides, they have prepared various kinds of model homopolypeptides:

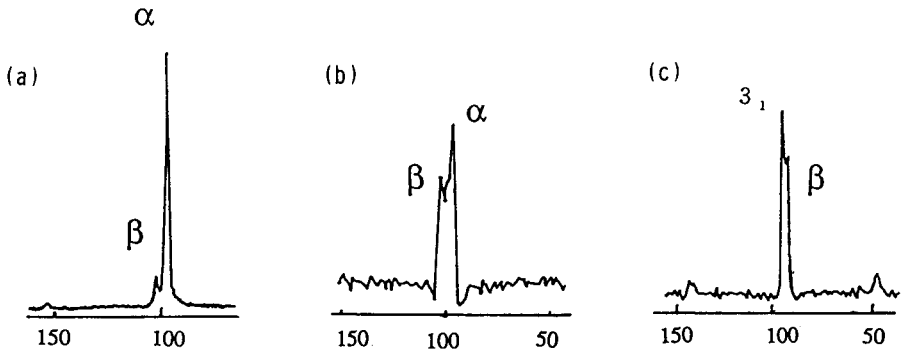

Fig. 16. 30.5-MHz ^{15}N CP/MAS NMR spectra of (a) poly(L-leucine) (d.p. = 50; 10% ^{15}N); (b) poly(L-phenylalanine) (d.p. = 50; 10% ^{15}N; 300 scans); and (c) poly(glycine) (20% ^{15}N; dialyses from LiBr solution; 100 scans).

poly(L-alanine), poly(L-leucine), poly(β-benzyl L-aspartate), poly(γ-benzyl L-glutamate), poly(γ-methyl L-glutamate), poly(L-valine), poly(L-isoleucine), poly(L-glycine) and poly(L-proline), which show characteristic differences in conformation. The 27.4-MHz ^{15}N CP/MAS NMR spectra of natural abundance homopolypeptides, poly(L-alanine) and poly(L-leucine), are shown in Fig. 17. The observed ^{15}N NMR chemical shifts of solid homopolypeptides[57–62]

Table 1. ^{15}N NMR chemical shifts δ (ppm, relative to $^{15}NH_4NO_3$) and linewidths of solid polypeptides.

Polypeptide (d.p.)	Catalyst,[a] solvent, temperature	δ of α-helix structure	δ of sheet structure	Line width (Hz)
Poly(glycine) 50	Benzylamine Acetonitrile/20°C	89.9[b]	85.4	220
Poly(L-alanine) 50	Benzylamine Dioxane/20°C	100.5	—	200
Poly(D,L-alanine) 20	Aniline Dioxane/100°C	—	109.3	300
Poly(L-leucine) 50	Benzylamine Dioxane/20°C	97.9	108.7	150
Poly(D,L-leucine) 50	Benzylamine Dioxane/20°C	98.9	108.5	300
Poly(L-valine) 50	Benzylamine Dioxane/20°C	—	106.9 (105.9)	250
Poly(L-phenylalanine) 50	Isopropylamine Dioxane/20°C	94.7	108.2	—
Poly(γ-methyl-L-glutamate) 50	Benzylamine Dioxane/20°C	97.9	—	200
Poly(L-proline)	Pyridine/20°C	108.8[b]	—	220

[a] Polymerization of amino acid *N*-carboxyanhydrides.
[b] 3_1-Helix.

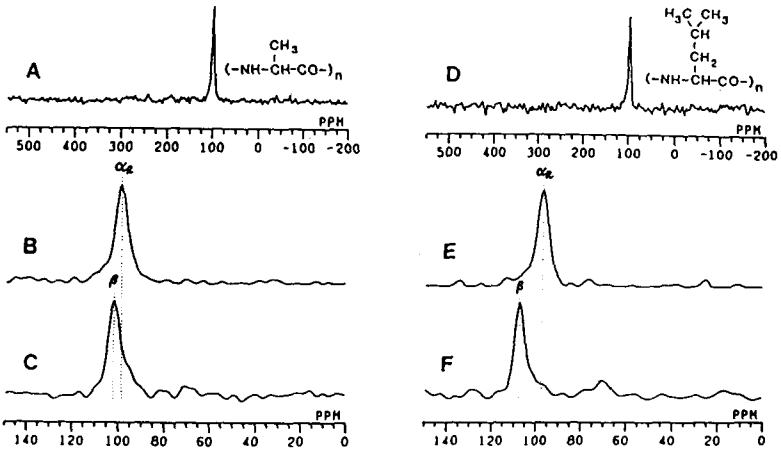

Fig. 17. Natural abundance 27.4-MHz ^{15}N CP/MAS NMR spectra of some poly(L-alanines) and poly(L-leucines) in the solid state. (A and B) PLA1a-50 (α-helix form, 2874 scans); (C) Z-$(Ala)_7$-NHBu (β-sheet form, 1927 scans); (D and E) PLLeu-100 (α-helix, 850 scans); (F) Z-$(Leu)_6$-OEt (β-sheet, 1142 scans).

are summarized in Table 2. It has been confirmed that the isotropic ^{15}N chemical shifts in the peptide backbone of homopolypeptides exhibit a significant conformation-dependent change from the observation and theoretical calculation. It has been found that the σ_{iso} for the α-helix form (97.0–99.2 ppm) appears to low frequency by *ca.* 1.2–10.0 ppm with respect to that for the β-sheet form (99.5–107.0 ppm) of the same homopolypeptides, which obviously depends on the structure of individual amino acid residues. Some ^{15}N chemical shift differences are rather small, but they should be on safe grounds for homopolypeptides. The variations of the σ_{iso} for various kinds of homopolypeptides are *ca.* 2.5 ppm in the α-helix form and *ca.* 7.5 ppm in the β-sheet form. In addition, the σ_{iso} of the β-sheet form of the L-Leu, L-Val, and L-Ile residues, which possess alkyl side-chains, appear to high frequency with respect to that of the L-Ala residue. In contrast, the σ_{iso} value for the β-sheet form of the L-Asp(OBzl), L-Glu(OBzl) and L-Glu(OMe) residues, which possess side-chain esters, is decreased with respect to that of the L-Ala residue. These results indicate that the ^{15}N chemical shift difference between the α-helix and β-sheet forms depends on the side-chain structure of individual amino acid residues.

Another important result is that σ_{iso} gives information about the helix sense (right-handed α-helix or left-handed α-helix) of poly(β-benzyl L-aspartate)[60] (α-helix: 99.2; α_L-helix: 97.0 ppm). In addition, the ^{15}N chemical shift value of PBLAsp-5 (low molecular weight; β-sheet form) is identical with that of PBLAsp-100-III (high molecular weight; β-sheet form), indicating that the ^{15}N chemical shift of a solid polypeptide is independent of the chain length, if no conformational changes occur. Accordingly, the ^{15}N chemical shift depends mainly on the conformation and side-chain structure of individual amino acid

Table 2. Isotropic ^{15}N chemical shifts of some homopolypeptides with various conformations (α-helix, β-sheet, α_L-helix, ω_L-helix, PGI, PGII, PPI and PPII forms) in the solid state (ppm from $^{15}NH_4NO_3$, ±0.5 ppm).

Sample[a]	Conformation[b]	^{15}N δ	Δ δ[c]
PLA1a-50	α-helix	98.6	−3.2
Z-(L-Ala)$_7$-NHBu	β-sheet	101.8	
PLLeu-100	α-helix	97.0	−10.0
Z-(L-Leu)$_6$-OEt	β-sheet	107.0	
PBLAsp-100	α-helix	99.2	−1.2
PBLAsp-100-I	α_L-helix	97.0	
PBLAsp-100-II	ω_L-helix	96.8	
PBLAsp-100-III	β-sheet	100.4	
PBLAsp-5	β-sheet	100.4	
PBLGlu-100	α-helix	97.6	−1.9
Nps-(L-Glu(OBzl))$_6$-NHBu	β-sheet	99.5	
PMLGlu-100	α-helix	97.6	−1.9
Nps-(L-Glu(OMe))$_4$-OH	β-sheet	99.5	
PLVal-100	β-sheet	105.9	
PLIle-100	β-sheet	106.1	
PGly-100	β-sheet (PGI)	83.5	(−5.0)
PGly-100-S	3_1-helix (PGII)	88.5	
PPro-100	10_3-helix (PPI)	107.4	(+2.5)
PPro-100-S	3_1-helix (PPII)	104.9	

[a] Abbreviations: Ala, alanine; Leu, leucine; BLAsp, β-benzyl L-aspartate; BLGlu, γ-benzyl L-glutamate; MLGlu, γ-methyl L-glutamate; Val, valine; Ile, isoleucine; Gly, glycine; Pro, proline; Bu, butyl; Et, ethyl; Bzl, benzyl; Me, methyl; Z, benzyloxycarbonyl; Nps, (*o*-nitrophenyl)sulphenyl.
[b] Abbreviations: PGI, poly(glycine) I form (β-sheet); PGII, poly(glycine) II form (3_1-helix); PPI, poly(L-proline) I form (10_3-helix); PPII, poly(L-proline) II form (3_1-helix).
[c] Differences in the ^{15}N chemical shifts of the α-helix relative to those of the β-sheet form.

residues. Furthermore, Shoji *et al.* have obtained some different results from Forester *et al.*:[47] (1) σ_{iso} of the PGI form of poly(glycine)[61] appears to low frequency by 5 ppm with respect to that of the PGII form, and the PPI and PPII helices of poly(L-proline)[62] differ by 2.5 ppm in the ^{15}N NMR spectra; and (2) the ^{15}N chemical shift of the L-proline residue of $[Pro–Ala–Gly]_n$ (collagen-like triple-helical structure) appears at a higher frequency (108.8 ppm) in comparison with that of poly(L-proline). A diagram of the observed isotropic ^{15}N chemical shift of some homopolypeptides $[X]_n$ with various conformations (α-helix, β-sheet, α_L-helix, ω_L-helix, PGI, PGII, PPI and PPII forms) is shown in Fig. 18.

In order to support the view that ^{15}N chemical shifts are conformation dependent, theoretical calculations of ^{15}N chemical shifts are required, using the electronic states derived by quantum chemical methods. The relative ^{15}N NMR chemical shifts[57] (isotropic magnetic shielding constants) of a dipeptide fragment, *N*-acetyl-L-alanine methylamide (forming hydrogen bonds with two formamide molecules) have been calculated using the FPT-INDO theory,[57,63] as

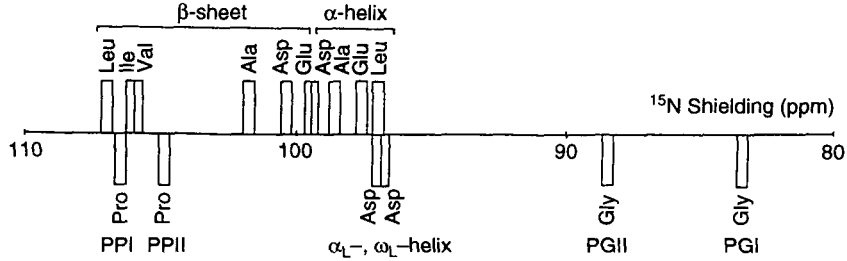

Fig. 18. A diagram of the observed isotropic ^{15}N shielding (σ_{iso}) of some homopolypeptides $[X]_n$ with various conformations (α-helix, β-sheet, α_L-helix, ω_L-helix, PGI, PGII, PPI and PPII forms).

described in Section 3, where the structural data, including the distance between the nitrogen and oxygen atoms, 2.83 and 2.86 Å for the β-sheet and α-helix forms, respectively, were taken from X-ray diffraction studies of poly(L-alanine).[64–66]

Figure 19 shows the observed ^{15}N chemical shift diagram of poly(L-alanine) and the ^{15}N shielding constant (chemical shift) diagram of *N*-acetyl-L-alanine methylamide calculated by the FPT-INDO method. The calculated ^{15}N shieldings for the α-helix and β-sheet forms of poly(L-alanine) are −254.9 and −257.3 ppm, respectively. The calculated ^{15}N chemical shift for the α-helix form appears to low frequency by 2.4 ppm with respect to that of the β-sheet form. This calculated ^{15}N chemical shift displacement is qualitatively in good agreement with the observed one. As a conclusion, the ^{15}N chemical shift of poly(L-alanine) depends on conformation, which can be interpreted mainly in terms of the changes of the electronic structure. Accordingly, ^{15}N chemical shifts determined by the ^{15}N CP/MAS NMR method are very sensitive to the

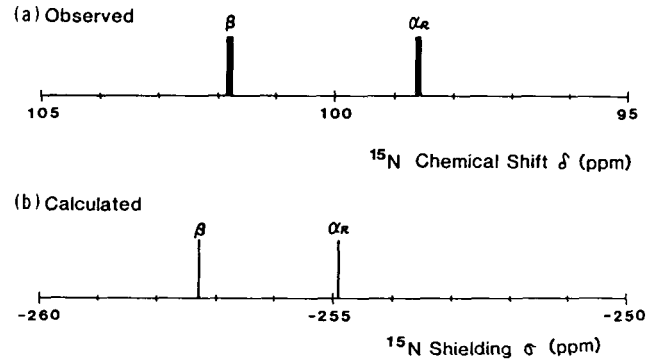

Fig. 19. (a) Observed ^{15}N chemical shift diagram of poly(L-alanine) in the solid state. (b) Calculated ^{15}N shielding diagram of *N*-acetyl-L-alanine methylamide (taking hydrogen bonds with two formamide molecules), as a dipeptide model of poly(L-alanine), by means of the FPT-INDO method.

primary structure such as side-chain effects of a variety of amino acid residues as well as the secondary structure (the main-chain conformation) such as the α-helix and β-sheet forms of homopolypeptides in the solid state.

5.1.2. Copolypeptides

The ^{15}N NMR signals of solid copolypeptides are sensitive to sequence effects; yet they are, in most cases, sensitive to secondary structure. Table 3 shows the ^{15}N chemical shifts of the guest–host copolypeptides in the solid state.[47] It is found that: (1) when a helix-forming amino acid residue such as L-alanine or L-leucine is incorporated into the β-sheet structure of poly(L-valine), the chemical shift has a value typical of the host polypeptide ($\sim$ 108.5 ppm); (2) when the non-helix-forming amino acid residue, L-valine is incorporated into the helices of poly(L-alanine) or poly(L-leucine), it shows the characteristic chemical shift of a helical polypeptide (98.5 $\sim$ 97.5 ppm); (3) glycine incorporated into the α-helix of $[Ala]_n$ does not exhibit any shift difference compared with poly(glycine) in the β-sheet form; (4) when glycine units are incorporated into the β-sheet structures of $[Val]_n$ or $[\beta\text{-Ala}]_n$, they absorb several parts per million to high frequency of the β-sheet of $[Gly]_n$, indicating strong neighbouring sequence effects.

The relation between the isotropic ^{15}N chemical shift and the structural parameters of various kinds of synthetic copolypeptides in the solid state have been studied.[58,59,61,67] For this, a series of ^{15}N-labelled polypeptides were prepared, $[Ala^*, X]_n$, $[Gly^*, X]_n$ and $[Leu^*, X]_n$, consisting of ^{15}N-labelled amino acids (Ala*: L-alanine, Gly*: glycine, Leu*: L-leucine) and other normal amino acids (X; natural abundance of ^{15}N), where the following amino acids were selected for the X residue: (1) L-alanine, D-alanine and L-leucine, which contain

Table 3. ^{15}N NMR chemical shifts δ (ppm, relative to $^{15}NH_4NO_3$) of solid guest–host copolypeptides.

Copolypeptide	Secondary structure	δ of host	δ of guest
Gly* in poly(L-alanine)	α-helix	100.5	85.7
Gly* in poly(γ-methyl-L-glutamate)	α-helix	97.9	87.9
Gly* in poly(L-valine)	β-sheet	105.9	93.4 (90.5–85.1)[a]
Gly* in poly(β-alanine)	β-sheet	99.5	94.4
L-Ala* in poly(L-leucine)	α-helix		99.6
L-Leu* in poly(L-alanine)	α-helix	100.3[a]	97.2
L-Leu* in poly(L-valine)	β-sheet	—	108.5
L-Val* in poly(L-alanine)	α-helix	—	98.5
L-Val* in poly(L-leucine)	α-helix	—	97.5

[a] Poorly resolved shoulders.
* Denotes ^{15}N enrichment.

non-polar hydrocarbon side-chains and stabilize an α-helix; (2) β-benzyl L-aspartate, γ-benzyl L-glutamate, and γ-methyl L-glutamate, which contain polar side-chain esters and stabilize an α-helix; (3) glycine, which is optically inactive and stabilizes a β-sheet; (4) L-valine and L-isoleucine, which contain non-polar hydrocarbon side-chains and stabilize a β-sheet; (5) sarcosine (= *N*-methyl glycine), which destabilizes both an α-helix and a β-sheet.

For the copolypeptides $[Ala^*, X]_n$, the σ_{iso} values of the Ala* residue for the α-helix and β-sheet forms are observed in the range $98.1 \sim 101.5$ and $98.8 \sim 107.0$ ppm, respectively, as shown in Table 4 and Fig. 20. This suggests that σ_{iso} depends not only on the conformation but also on the primary structure or probably on the higher order structure. Thus, the origin of ^{15}N chemical shifts is rather complex as compared with that of ^{13}C chemical shifts,[68] and it may be generally difficult to estimate the conformation of copolypeptides from the σ_{iso} value. However, σ_{iso} for the α-helix form is always displaced to low frequency with respect to the β-sheet form for the same kind of polypeptide. Another important result is that σ_{iso} gives information about the helix sense of polypeptides by the ^{15}N CP/MAS NMR method. It has been already established by the infrared (IR),[74] far-IR[75] and ^{13}C CP/MAS NMR[68–73] methods that the stable conformation of $[Ala^*, D\text{-}Ala]_n$ (A3-1 and A3) is the left-handed α-helix; the Ala* residues (minor component, $5 \sim 20$ mol%) are incorporated into the left-handed α-helix of the major D-Ala residues. The σ_{iso} values (α_L-helix, $96.5 \sim 96.7$ ppm) of the Ala* residues of $[Ala^*, D\text{-}Ala]_n$ (A3-1 and A3) are displaced to low frequency by *ca.* 2 ppm as compared with that of $[L\text{-}Ala]_n$ (α-helix, $98.6 \sim 98.8$ ppm, which is exactly equal to σ_{iso} of $[D\text{-}Ala]_n$). A similar ^{15}N chemical shift displacement was obtained for the homopolypeptide $[L\text{-}Asp(OBzl)]_n$, as described above. Thus, the value of σ_{iso} is sensitive to the helix sense of polypeptides in the solid state.

For the copolypeptides $[Gly^*, X]_n$, the σ_{iso} values of the Gly* residue of the α-helix and β-sheet forms are observed in the ranges $84.2 \sim 85.8$ and $83.5 \sim 87.8$ ppm, respectively, as shown in Table 5 and Fig. 21. This suggests that the value of σ_{iso} of the Gly* residue depends not only on the conformation but also on the primary structure (or probably on the higher ordered structure). It seems that the displacement of σ_{iso} of the Gly* residue is similar to that of $[Ala^*, X]_n$, and is affected by the strong neighbouring amino acid sequence effects. The origin of ^{15}N chemical shifts is rather complex, and thus it is difficult to directly estimate the conformation of copolypeptides from the σ_{iso} value. The σ_{iso} of the Gly* residue in the α-helix is always displaced to low frequency with respect to the β-sheet form. Furthermore, the σ_{iso} value is displaced to low frequency by $10 \sim 20$ ppm with respect to that of homopolypeptides of host amino acid residue $[X]_n$. Thus, it is emphasized that σ_{iso} may be useful for the study on such a conformational change of copolypeptides having identical primary structure and some natural proteins such as collagen fibrils or silk fibroins.

In contrast, for the copolypeptides $[Leu^*, X]_n$ (except for $[Leu^*, Gly]_n$ in the

Table 4. Isotropic ^{15}N shielding (σ_{iso}), ^{15}N principal shielding elements ($\sigma_{11}, \sigma_{22}, \sigma_{33}$), anisotropy ($\Delta\sigma$) and asymmetry parameter (η) of solid polypeptides [Ala*, X]$_n$ containing ^{15}N-labelled L-alanine residue in the α-helix, α_L-helix, and β-sheet forms.

	Sample	Composition[a] (%)			Conformation[b]	^{15}N shielding[c] (ppm)				$\Delta\sigma$[d]	η[e]
		Ala*	Ala	X		σ_{iso}	σ_{11}	σ_{22}	σ_{33}		
A1	[Ala*]$_n$	20	80		α-helix	98.8	204	54.4	38	158	0.16
A2	[Ala*]$_n$-5	20	80		β-sheet	102.2	201	61.7	44	148	0.18
A3-1	[Ala*, D-Ala]$_n$	5	0	95	α_L-helix	96.7	197	57.1	36	151	0.21
A3	[Ala*, D-Ala]$_n$	20	0	80	α_L-helix	96.5	198	55.1	36	153	0.19
A4	[Ala*, Gly]$_n$	20	0	80	β-sheet	98.8	200	59.6	37	152	0.22
A5	[Ala*, Gly]$_n$	20	60	20	α-helix	98.6	202	57.4	36	155	0.21
A6-1	[Ala*, Leu]$_n$	5	0	95	α-helix	98.6	205	56.0	35	160	0.20
A6	[Ala*, Leu]$_n$	20	0	80	α-helix	98.6	204	56.9	35	158	0.21
A6-2	[Ala*, Leu]$_n$	5	45	50	α-helix	98.3	207	54.2	34	163	0.19
A6-3	[Ala*, Leu]$_n$	5	75	20	α-helix	98.1	203	57.1	34	158	0.22
A7-1	[Ala*, Val]$_n$	5	0	95	β-sheet	107.0	210	63.5	47	155	0.16
A7	[Ala*, Val]$_n$	20	0	80	β-sheet[f]	99.7	202	62.4	35	153	0.27
A7-2	[Ala*, Val]$_n$	5	25	70	α-helix[g]	98.6	201	53.1	42	154	0.11
A8	[Ala*, Ile]$_n$	20	0	80	β-sheet	101.0	200	63.0	40	149	0.23
A9-1	[Ala*, Asp(OBzl)]$_n$	5	0	95	α-helix	101.3	210	54.7	39	163	0.14
A9-2	[Ala*, Asp(OBzl)]$_n$	10	0	90	α-helix	101.1	210	56.0	37	164	0.17
A9	[Ala*, Asp(OBzl)]$_n$	20	0	80	α-helix	101.5	208	58.7	38	160	0.19
A10	[Ala*, Glu(OBzl)]$_n$	20	0	80	α-helix	100.4	206	56.7	39	158	0.17
A11	[Ala*, Glu(OMe)]$_n$	20	0	80	α-helix[h]	99.9	205	58.1	37	157	0.20
A12	[Ala*, Sar]$_n$	20	0	80	?	99.0	198	62.2	37	148	0.26

[a] Copolymer composition (%). Abbreviations: Ala*, ^{15}N-labelled L-alanine (99 atom % of ^{15}N purity); Ala, L-alanine (natural abundance of ^{15}N); X, other amino acids (natural abundance of ^{15}N).

[b] Abbreviations: α-helix, right-handed α-helix; α_L-helix, left-handed α-helix; β-sheet, antiparallel β-sheet.

[c] ^{15}N shielding of Ala* of polypeptides: ± 0.5 ppm for σ_{iso} and σ_{22} and ± 2 ppm for σ_{11} and σ_{33}, from $^{15}NH_4NO_3$.

[d] Anisotropy: $\Delta\sigma = \sigma_{11} - (\sigma_{22} + \sigma_{33})/2$.

[e] Asymmetry parameter: $\eta = (\sigma_{22} - \sigma_{33})/(\sigma_{11} - \sigma_{iso})$.

[f] Major conformation of [Ala*, Val]$_n$ (A7) is the β-sheet form containing small amounts (assumed below 10–20%) of the α-helix form.

[g] Major conformation of [Ala*, Val]$_n$ (A7-2) is the α-helix form containing small amounts (assumed below 10%) of the β-sheet form.

[h] Major conformation of [Ala*, Glu(OMe)]$_n$ is the α-helix form containing small amounts (assumed below 20–30%) of the β-sheet form.

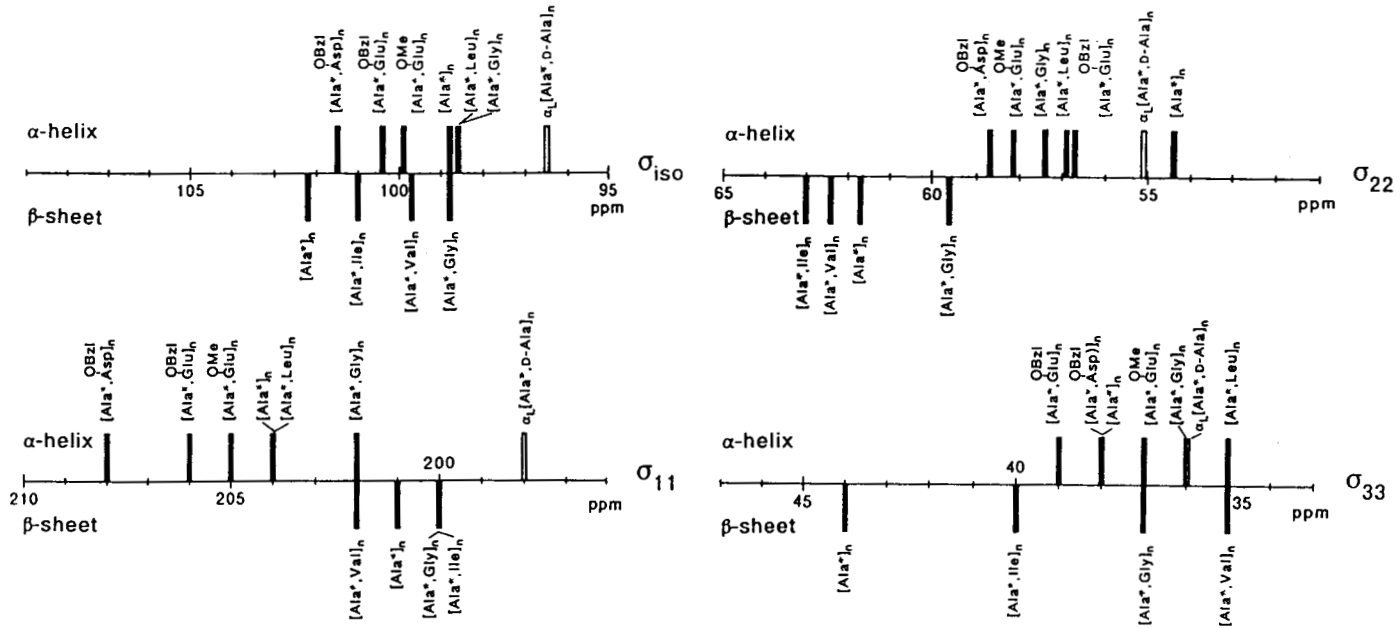

Fig. 20. A diagram of the observed isotropic ^{15}N shielding (σ_{iso}) and the principal shielding elements (σ_{11}, σ_{22} and σ_{33}) of the Ala* residue of some polypeptides $[Ala^*, X]_n$ (Ala* content is nearly 20%) in the solid state.

Table 5. Isotropic ^{15}N shieldings (σ_{iso}), ^{15}N principal shielding elements ($\sigma_{11}, \sigma_{22}, \sigma_{33}$), anisotropy ($\Delta\sigma$) and asymmetry parameter (η) of solid polypeptides [Gly*, X]$_n$ containing ^{15}N-labelled glycine residue.

	Sample	Composition[a] (%)			Conformation[b]	^{15}N shielding[c] (ppm)				$\Delta\sigma$[d]	η[e]
		Gly*	Gly	X		σ_{iso}	σ_{11}	σ_{22}	σ_{33}		
G1	[Gly*]$_n$	20	80		β-sheet	83.5	185	40.7	25	152	0.15
G1-S	[Gly*]$_n$	20	80		3_1-helix	88.5	194	42.1	29	158	0.12
G2	[Gly*, Ala]$_n$	20	0	80	α-helix	84.2	192	36.9	24	162	0.12
G3	[Gly*, Ala]$_n$	20	60	20	β-sheet	83.5	186	45.3	19	154	0.26
G4-1	[Gly*, Leu]$_n$	5	0	95	α-helix	84.5	190	38.7	25	158	0.13
G4-2	[Gly*, Leu]$_n$	5	5	90	α-helix	84.4	190	38.9	24	159	0.14
G4	[Gly*, Leu]$_n$	20	0	80	α-helix	85.3	190	41.0	25	157	0.15
G4-3	[Gly*, Leu]$_n$	5	45	50	α-helix	84.4	186	43.0	24	153	0.19
G4-4	[Gly*, Leu]$_n$	20	60	20	β-sheet	83.7	186	45.5	20	153	0.25
G5	[Gly*, Val]$_n$	20	0	80	β-sheet	85.1	183	53.9	19	147	0.36
G6	[Gly*, Ile]$_n$	20	0	80	β-sheet	87.8	189	47.6	25	153	0.22
G7	[Gly*, Asp(OBzl)]$_n$	20	0	80	α-helix	86.0	188	50.8	19	153	0.31
G8	[Gly*, Glu(OBzl)]$_n$	20	0	80	α-helix	85.8	190	40.5	27	156	0.13

[a] Copolymer composition (%). Abbreviations: Gly*, ^{15}N-labelled glycine (99 atom % of ^{15}N purity); Gly, glycine (natural abundance of ^{15}N); X, other amino acids (natural abundance of ^{15}N).

[b] Abbreviations: α-helix, right-handed α-helix; β-sheet, antiparallel β-sheet; PGI, polyglycine I form; PGII, polyglycine II form.

[c] ^{15}N shielding of Gly* of polypeptides (from $^{15}NH_4NO_3$).

[d] Anisotropy.

[e] Asymmetry parameter.

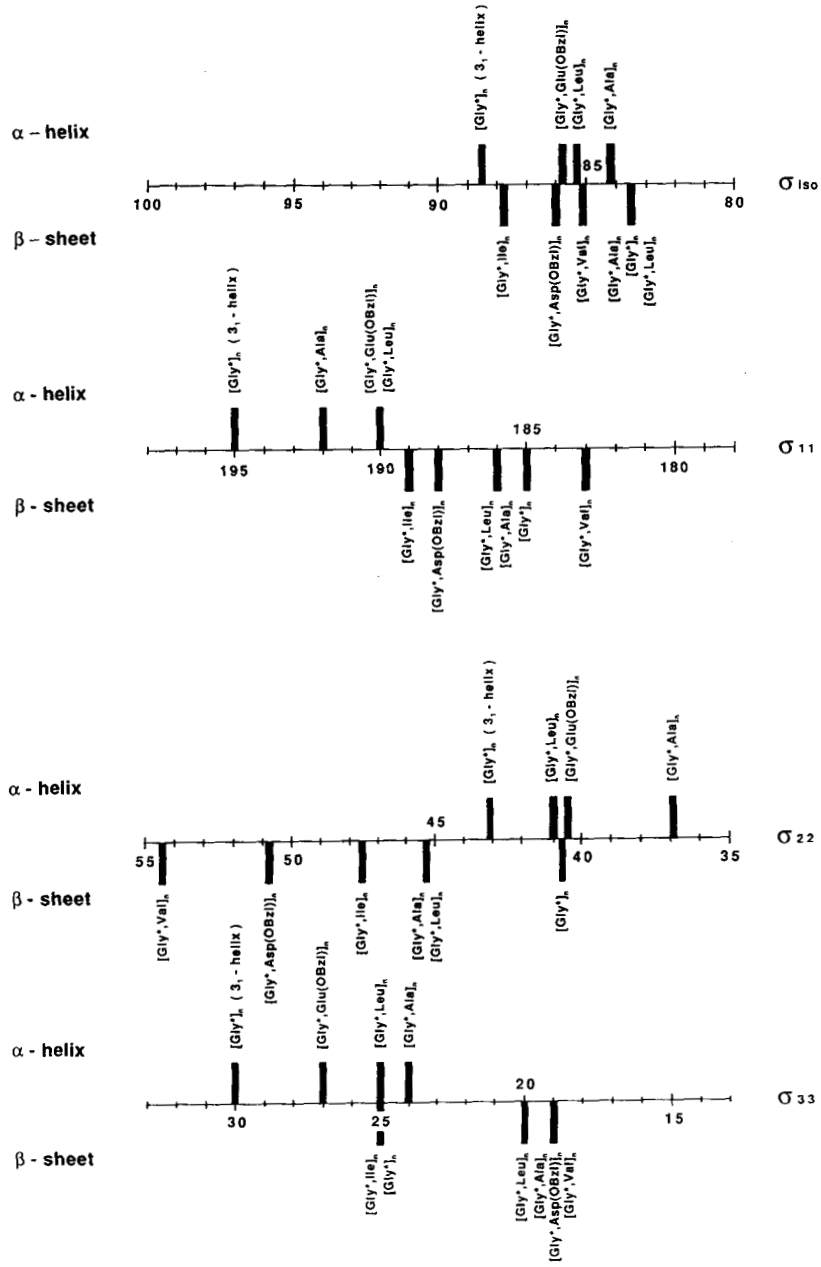

Fig. 21. A diagram of the observed isotropic ^{15}N shielding (σ_{iso}) and the principal shielding elements (σ_{11}, σ_{22} and σ_{33}) of the Gly* residue of some polypeptides $[Gly^*, X]_n$ (Gly* content is nearly 20%) in the solid state.

β-sheet form), the σ_{iso} values of the Leu* residue of the α-helix and β-sheet forms are observed in the ranges 96.2 ~ 97.7 and 105.1 ~ 107.0 ppm, respectively, as shown in Table 6 and Fig. 22. The σ_{iso} values are very similar to those of the homopolypeptide $[Leu^*]_n$ (α-helix: 97.0 and β-sheet: 107.0 ppm). It is noteworthy that the ^{15}N chemical shift difference of the Leu* residue between the α-helix and the β-sheet forms is large (7–11 ppm), but that the ^{15}N chemical shift differences from the neighbouring amino acid sequence effects are small (within 2 ppm). This is quite a different result from those obtained for $[Ala^*, X]_n$ and $[Gly^*, X]_n$. Thus, the origin of ^{15}N chemical shifts of the Leu* residue is rather simple compared with that of the Ala* or Gly* residues. Since the σ_{iso} value of the Leu* residue depends mainly on the conformation, with a very small dependence on the primary structure (or higher ordered structure), it may be very useful for the conformational analysis of copolypeptides in the solid state.

As mentioned above, it has been shown that the origin of the isotropic

Table 6. Isotropic ^{15}N shielding (σ_{iso}) and ^{15}N shielding tensor element (σ_{22}) of solid polypeptides $[Leu^*, X]_n$ containing ^{15}N-labelled L-leucine residue in the α-helix and β-sheet forms.

	Sample	Composition[a] (%)			Conformation	^{15}N shielding[b] (ppm)	
		Leu*	Leu	X		σ_{iso}	σ_{22}
L1	$[Leu^*]_n$	20	80		α-helix	97.0	55.7
L2	$[Leu^*]_n$-5	20	80		β-sheet	107.0	66.9
L3	$[Leu^*, Val]_n$	20	0	80	β-sheet	107.0	65.1
L3-1	$[Leu^*, Val]_n$	20	10	70	β-sheet[c]	107.0 (97.0)	65.3
L3-2	$[Leu^*, Val]_n$	20	30	50	α-helix	97.0	55.3
L3-3	$[Leu^*, Val]_n$	20	50	30	α-helix	96.9	54.0
L3-4	$[Leu^*, Val]_n$	20	60	20	α-helix	96.8	54.0
L4	$[Leu^*, Ala]_n$	20	0	80	α-helix	96.2	55.5
L4-1	$[Leu^*, Ala]_n$	20	30	50	α-helix	96.5	55.5
L4-2	$[Leu^*, Ala]_n$	20	60	20	α-helix	96.8	51.0
L5	$[Leu^*, Gly]_n$	20	0	80	β-sheet	96.9	61.2
L5-1	$[Leu^*, Gly]_n$	20	30	50	α-helix	97.2	55.5
L5-2	$[Leu^*, Gly]_n$	20	60	20	α-helix	96.8	53.2
L6	$[Leu^*, Lys(Z)]_n$	20	0	80	β-sheet[d]	105.1 (97.2)	63.0
L7	$[Leu^*, Ile]_n$	20	0	80	β-sheet	106.7	58.0
L7-1	$[Leu^*, Ile]_n$	20	30	50	α-helix	97.1	56.0
L8	$[Leu^*, Asp(OBzl)]_n$	20	30	50	α-helix	97.7	56.7
L9	$[Leu^*, Glu(OBzl)]_n$	20	30	50	α-helix	97.6	50.1

[a] Copolymer composition (%): Leu*, ^{15}N-labelled L-leucine (99 atom % of ^{15}N purity).
[b] ^{15}N shielding of Leu* of polypeptides (±0.5 ppm, from $^{15}NH_4NO_3$).
[c] Major conformation of $[Leu^*, Val]_n$ (L3-1) is the β-sheet form containing small amounts (assumed below 30–40%) of the α-helix form.
[d] Major conformation of $[Leu^*, Lys(Z)]_n$ (L6) is the β-sheet form containing small amounts (assumed below 25–35%) of the α-helix form.

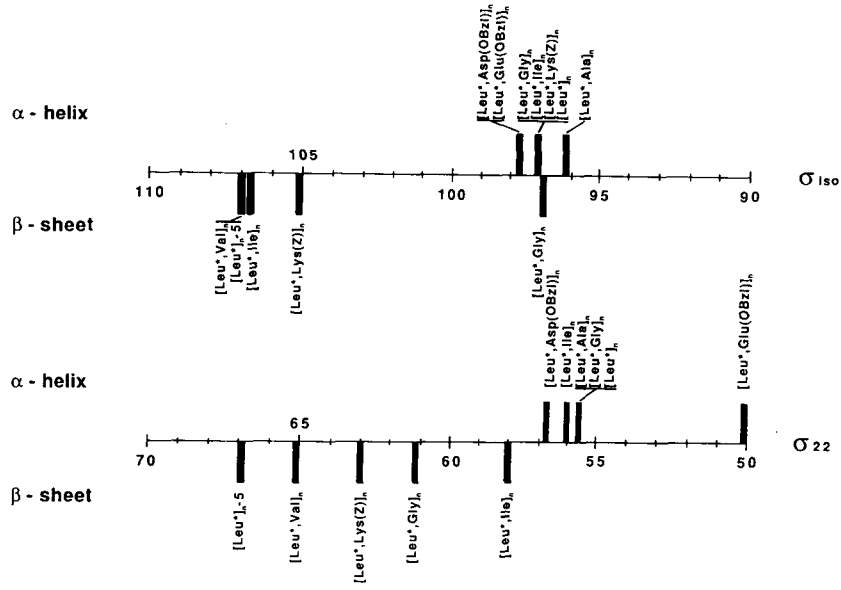

Fig. 22. A diagram of the observed isotropic ^{15}N shielding (σ_{iso}) and the principal shielding element (σ_{22}) of the Leu* residue of some polypeptides [Leu*, X]$_n$ (Leu* content is nearly 20%) in the solid state.

^{15}N chemical shifts of copolypeptides is related to the conformation, the side-chain effects of amino acid residue and neighbouring amino acid sequence effects.[58–62,67] Especially, for the Leu* residue, the σ_{iso} value depends mainly on conformation, and the neighbouring amino acid sequence effects are very small. In contrast, for the Ala* and Gly* residues, the σ_{iso} value depends both on conformation and strong neighbouring amino acid sequence effects.

In α-helical copolypeptides [Leu*, X]$_n$ such as [Leu*, Ala]$_n$, [Leu*, Glu(OBzl)]$_n$, and [Leu*, Asp(OBzl)]$_n$, the σ_{iso} values of the Leu* are displaced to low frequency by $0 \sim 2.5$ ppm with respect to those of the corresponding host homopolypeptide [X]$_n$. In β-sheet copolypeptides such as [Leu*, Val]$_n$ and [Leu*, Ile]$_n$, the σ_{iso} values are displaced to high frequency by $0.6 \sim 1.1$ ppm with respect to those of the corresponding host homopolypeptide. As a result, the σ_{iso} regions of the Leu* for the [Leu*, X]$_n$ with the α-helix ($96 \sim 98$ ppm) and β-sheet forms ($106 \sim 107$ ppm) are distinguishable. That is to say, the σ_{iso} value of the Leu* residues depends mainly upon the conformation of the copolypeptides in the solid state.

In α-helical copolypeptides [Ala*, X]$_n$ such as [Ala*, Leu]$_n$, [Ala*, Asp(OBzl)]$_n$, [Ala*, Glu(OBzl)]$_n$ and [Ala*, Glu(OMe)]$_n$, the σ_{iso} values of the Ala* are displaced conversely to high frequency by $2 \sim 3$ ppm with respect to those of the corresponding host homopolypeptide [X]$_n$ (see Fig. 23). In β-sheet

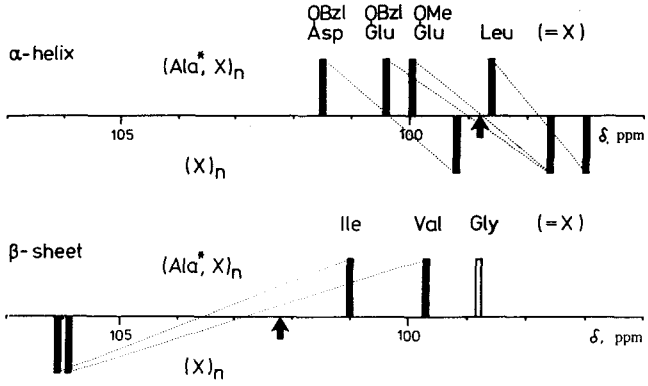

Fig. 23. Correlation of the ^{15}N chemical shifts of Ala* of copolypeptides, $[Ala^*, X]_n$, with those of host homopolypeptides $[X]_n$ in the solid state. The arrow indicates the ^{15}N chemical shift of poly(L-alanine).

copolypeptides such as $[Ala^*, Val]_n$ and $[Ala^*, Ile]_n$, the σ_{iso} values of the Ala* are displaced to low frequency by 5–6 ppm with respect to those of the corresponding host homopolypeptide. For this, the σ_{iso} regions of the Ala* in the copolypeptides with the α-helix (98 ~ 102 ppm) and β-sheet forms (99 ~ 102 ppm) are overlapping.

Furthermore, in α-helical copolypeptides $[Gly^*, X]_n$ such as $[Gly^*, Ala]_n$, $[Gly^*, Leu]_n$, $[Gly^*, Glu(OBzl)]_n$ and $[Gly^*, Asp(OBzl)]_n$, the σ_{iso} values of the Gly* are displaced to low frequency by 12 ~ 15 ppm with respect to those of the corresponding host homopolypeptide $[X]_n$ (see Fig. 24). In β-sheet copolypeptides such as $[Gly^*, Ala]_n$, $[Gly^*, Leu]_n$, $[Gly^*, Val]_n$, $[Gly^*, Ile]_n$, and $[Gly^*, Asp(OBzl)]_n$, the σ_{iso} values of the Gly* are displaced to low frequency

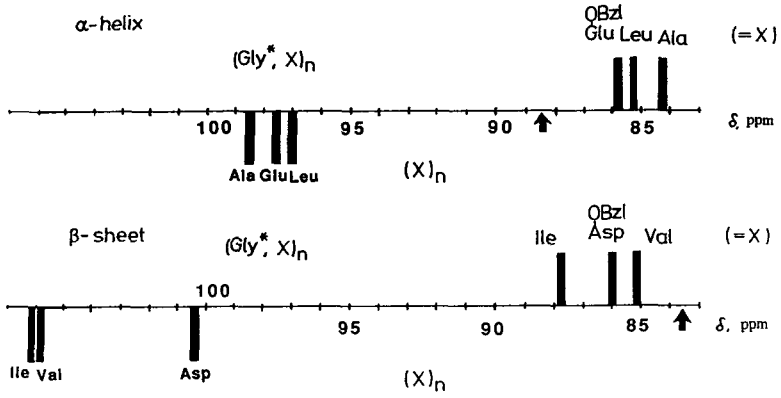

Fig. 24. Correlation of the ^{15}N chemical shifts of Gly* of copolypeptides, $[Gly^*, X]_n$, with those of host homopolypeptides $[X]_n$ in the solid state. The arrow indicates the ^{15}N chemical shift of poly(glycine).

by 14 ~ 22 ppm with respect to that of the corresponding host homopolypeptide. As a result, the σ_{iso} regions of the Gly* in the copolypeptides with the α-helix (84 ~ 86 ppm) and β-sheet forms (83 ~ 88 ppm) are overlapping. It is very interesting that the σ_{iso} values of copolypeptides depend on side-chain effects of amino acid residues. Especially for the Ala* and Gly* residues, the σ_{iso} values depend on strong neighbouring amino acid sequence effects. Although the origin of ^{15}N chemical shifts is rather complex, this point needs further clarification.

The relationship between the σ_{iso} value and the copolymer composition for copolypeptides has been studied. Figures 25 and 26 show the plots of the σ_{iso} data of the Ala* residue in [Ala*, Leu]$_n$ and [Ala*, Val]$_n$, respectively, against the L-alanine content (%). For a series of [Ala*, Leu]$_n$, where Leu has a hydrophobic alkyl side-chain and stabilizes an α-helix conformation, σ_{iso} is found to be almost constant over a wide range of L-alanine contents (5 ~ 80%).

In contrast, for a series of [Ala*, Val]$_n$, where the Val residue has a hydrophobic side-chain and stabilizes a β-sheet form, the stable conformation was found to be the β-sheet form at $\leq$ 20% L-alanine content (A7-1, A7) and α-helix form at $\geq$ 30% L-alanine content (A7-2). In this narrow range of

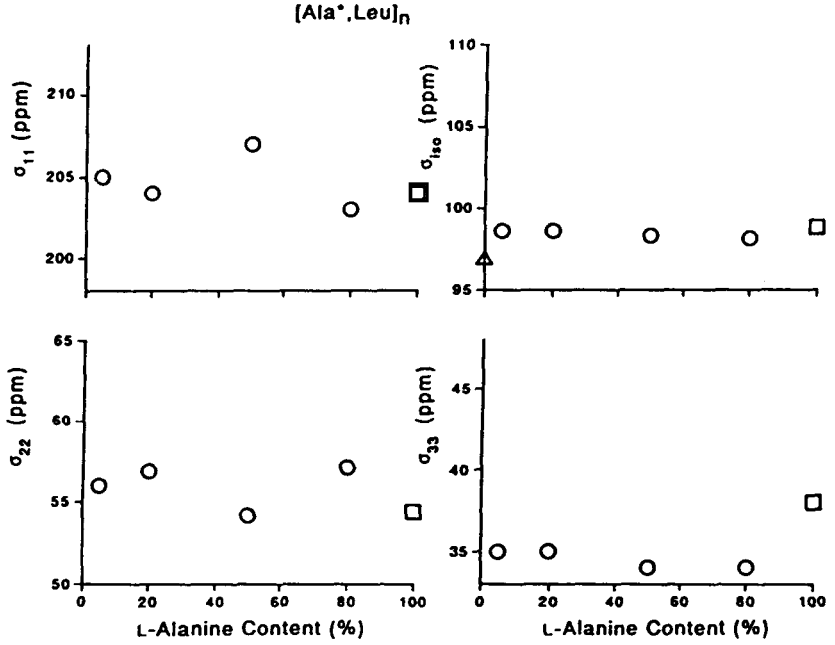

Fig. 25. Plots of the isotropic ^{15}N shielding (σ_{iso}) and the principal shielding elements (σ_{11}, σ_{22} and σ_{33}) of the Ala* residue in [Ala*, Leu]$_n$ against the L-alanine content (%): (○) α-helix form; (□) poly(L-alanine) (α-helix form); (△) poly(L-leucine) (α-helix form).

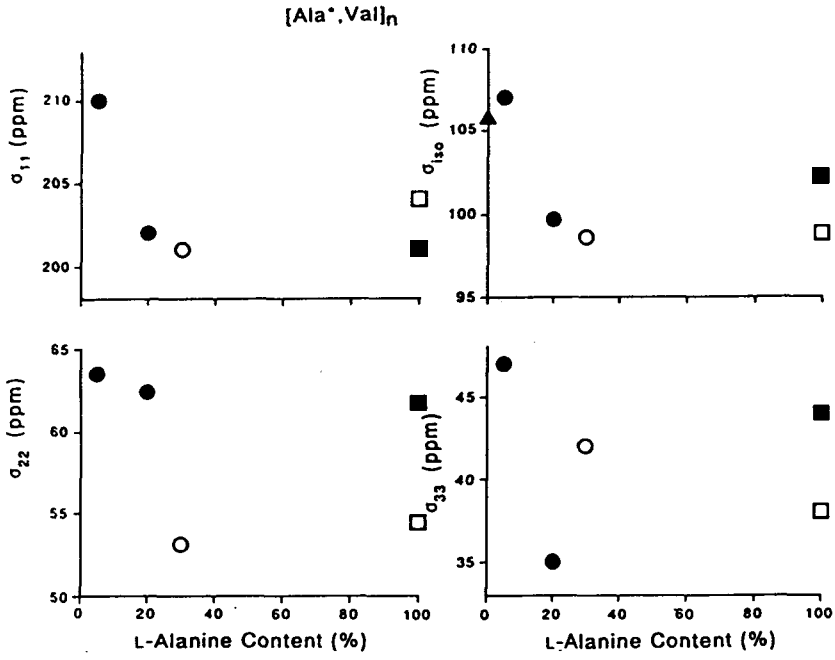

Fig. 26. Plots of the isotropic ^{15}N shielding (σ_{iso}) and the principal shielding elements (σ_{11}, σ_{22} and σ_{33}) of the Ala* residue in [Ala*, Val]$_n$ against the L-alanine content (%): (○) α-helix form; (●) β-sheet form; (□) poly(L-alanine) (α-helix form); (■) poly-(L-alanine) (β-sheet form); (▲) poly(L-valine) (β-sheet form).

L-alanine content (between 20 and 30%), any significant changes in σ_{iso} are not observed. A large chemical shift change was observed for σ_{iso} at $5 \sim 20\%$ L-alanine content. Such chemical shift changes may be mainly due to the side-chain effect of the L-valine residue and the neighbouring amino acid sequence effects, but apparently are not due to the main-chain conformation of copolypeptides.

Figures 27 and 28 show the plots of the σ_{iso} value of the Gly* residue in [Gly*, Ala]$_n$ and [Gly*, Leu]$_n$, respectively, against the glycine content.

For a series of [Gly*, Ala]$_n$ and [Gly*, Leu]$_n$, σ_{iso} is almost constant, indicating that this is independent of the wide range of L-alanine contents ($5 \sim 80\%$). Accordingly, for a series of [Gly*, Ala]$_n$ and [Gly*, Leu]$_n$, the chemical shift displacements in σ_{iso} may be indepenent of the main-chain conformation of copolypeptides. The reason for this is not clarified yet.

Figure 29 shows the plots of σ_{iso} of the Leu* residue in [Leu*, Ala]$_n$, [Leu*, Gly]$_n$ and [Ala*, Val]$_n$, respectively, against the L-leucine content (%). For all of the series of [Leu*, Ala]$_n$, [Leu*, Gly]$_n$, , [Leu*, Val]$_n$, the changes of the values of σ_{iso} are negligibly small against copolymer

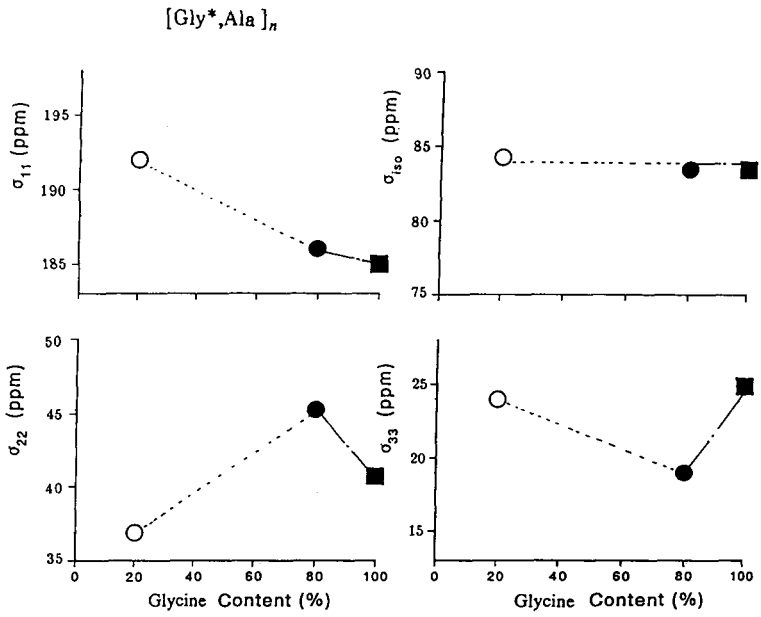

Fig. 27. Plots of the isotropic ^{15}N shielding (σ_{iso}) and the principal shielding elements (σ_{11}, σ_{22} and σ_{33}) of the Gly* residue in [Gly*, Ala]$_n$ against the glycine content (%): (○) α-helix form; (●) β-sheet form; (■) poly(glycine) (β-sheet form).

composition, where no conformational changes occur. In contrast, a large chemical shift displacement (*ca.* 8 ~ 10 ppm) was observed between the α-helix and β-sheet forms, which is ascribed to the main-chain conformation of copolypeptides.

5.2. Principal values of ^{15}N shielding tensors (σ_{11}, σ_{22} and σ_{33})

The development of high-resolution solid-state NMR techniques has made possible the study of shielding tensors. No doubt ^{15}N will receive more attention in the near future for a number of reasons such as the increased availability of high-field spectrometers and the development of polarization transfer techniques for solids. Recently some interesting results on the relation between ^{15}N shielding tensors and structures of solid polypeptides have been reported. Nitrogen NMR could, therefore, be a useful intrinsic probe in ^{15}N NMR studies of polypeptides and proteins in the solid state, particularly in cases where selective ^{15}N labelling is possible.

5.2.1. Homopolypeptides

The principal values of the ^{15}N shielding tensors were obtained by fitting the

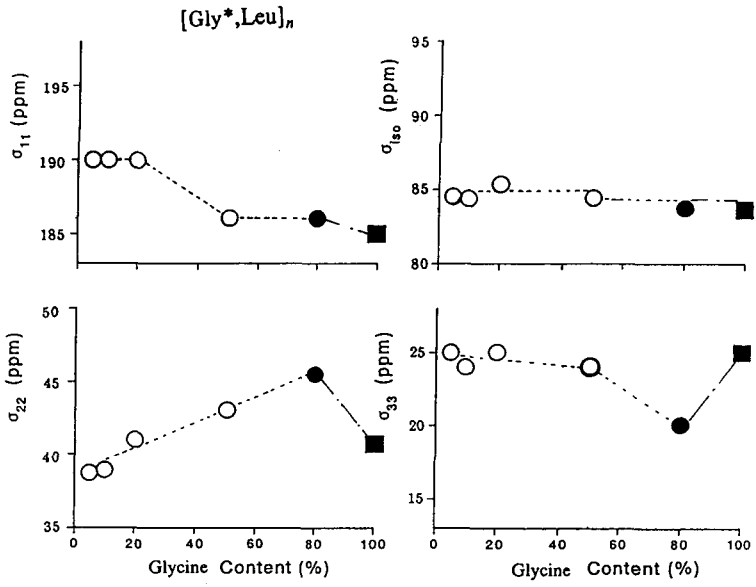

Fig. 28. Plots of the isotropic ^{15}N shielding (σ_{iso}) and the principal shielding elements (σ_{11}, σ_{22} and σ_{33}) of the Gly* residue in [Gly*, Leu]$_n$ against the glycine content (%): (○) α-helix form; (●) β-sheet form; (■) poly(glycine) (β-sheet form).

theoretical powder pattern lineshape[58] which is convoluted with Lorentzian functions to the observed powder patterns (Fig. 30). The σ_{iso} and σ_{22} data can be read directly from the observed CP/MAS and powder pattern (CP-static) spectra, respectively. The error limits of the σ_{11} and σ_{33} values ($\leq \pm 2$ ppm) are larger than those for σ_{iso} and σ_{22} ($\leq \pm 0.5$ ppm).[58,59]

Table 4 summarizes the isotropic ^{15}N shielding (σ_{iso}) and principal values of the ^{15}N shielding tensors of [Ala*]$_n$ and [Ala*, X]$_n$. The σ_{11}, σ_{22}, and σ_{33} data of the α-helical [Ala*]$_n$ are decreased by -3, 7.3, and 6 ppm, respectively, with respect to the β-sheet [Ala*]$_n$ in the solid state. For [Ala*]$_n$, (1) only the σ_{11} value of the α-helix form appears to high frequency with respect to that of the β-sheet form, whereas the other values (σ_{22} and σ_{33}) of the α-helix appear to low frequency with respect to those of the β-sheet and (2) the differences between the σ_{22} (and σ_{33}) values for the α-helix and β-sheet forms are larger than those of σ_{iso}.

On the other hand, the σ_{11}, σ_{22} and σ_{33} values of the α-helical [Leu*]$_n$ are decreased by 5, 11.2 and 2 ppm, respectively, with respect to those of the β-sheet [Leu*]$_n$ in the solid state (Table 6). The displacement of the σ_{11}, σ_{22} and σ_{33} values between the α-helical [Leu*]$_n$ and the β-sheet [Leu*]$_n$ is different from those of the [Ala*]$_n$, the reason for which is unclear at present. For [Leu*]$_n$, (1) all principal values of the nitrogen shielding tensor of α-helical

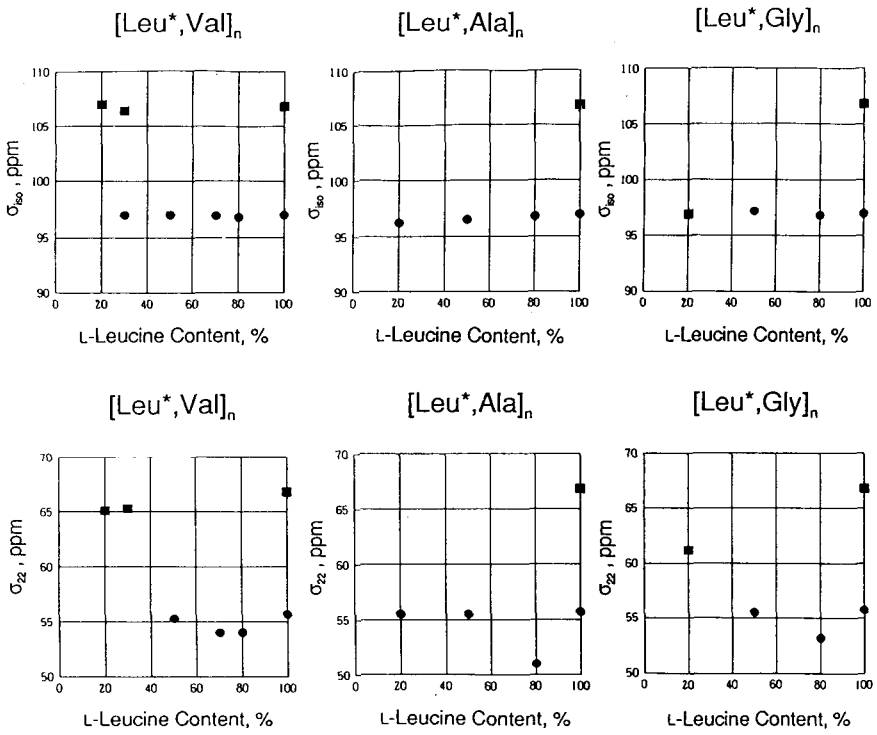

Fig. 29. Plots of the isotropic ^{15}N shielding (σ_{iso}) and the principal shielding element (σ_{22}) of the Leu* residue in [Leu*, Val]$_n$, [Leu*, Ala]$_n$ and [Leu*, Gly]$_n$ against the L-leucine content (%): (●) α-helix form; (■) (β-sheet form).

[Leu*]$_n$ are displaced to low frequency with respect to those of the β-sheet one and (2) the difference between the σ_{22} values of these two forms is quite large with respect to those of the others (σ_{11} and σ_{33}).

Next, the σ_{11}, σ_{22} and σ_{33} values of the PGII form are displaced to high frequency by 9, 1.4 and 4 ppm, respectively, with respect to those of the PGI form (Table 5). For [Gly*]$_n$, (1) all of principal values of the PGII form are displaced to high frequency with respect to those of the β-sheet form and (2) the difference between the σ_{11} values of these two forms is large with respect to those of the others (σ_{22} and σ_{33}).

Why is the displacement of the σ_{11} different for [Ala*]$_n$ and [Leu*]$_n$? The reason for this is not clear at present, but this is a very important question in reaching and understanding of the correlation between structures and the ^{15}N shielding tensor. The ^{15}N shielding tensor may be useful for conformational analysis of solid polypeptides, if the origin of the chemical shift displacements can be elucidated.

According to recent work by Oas *et al.*[36,37] the alignment of the ^{15}N shielding tensors of L-[1-^{13}C]-alanyl-L-[^{15}N]-alanine has been determined from the

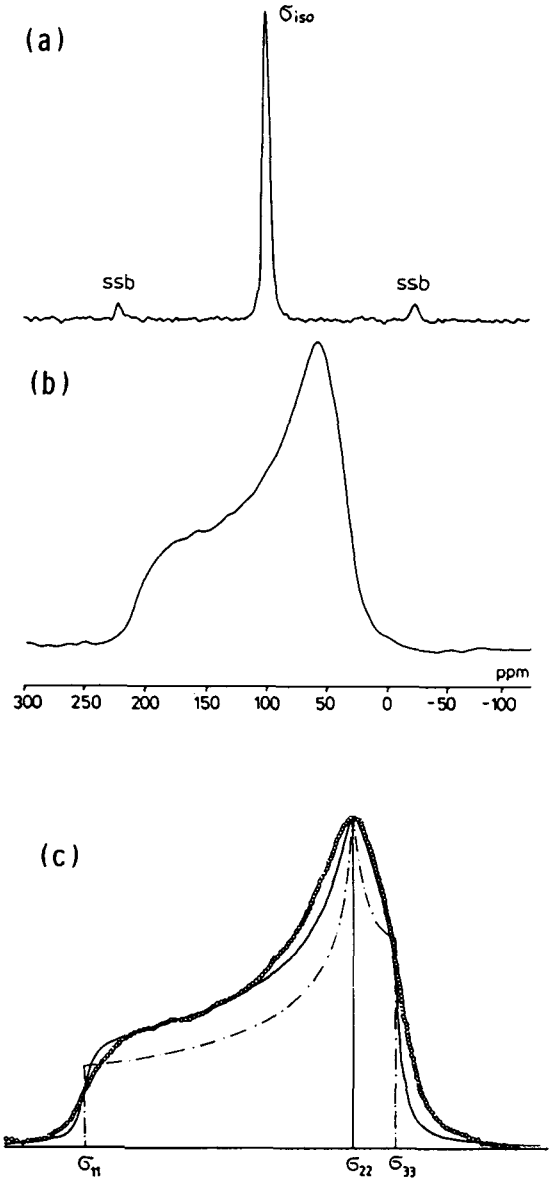

Fig. 30. 27.4-MHz ^{15}N CP/MAS NMR spectra (a), ^{15}N CP-static (powder pattern) NMR spectra (b), and theoretical powder pattern (– · –) (c) (convoluted with the Lorentzian function (——) and experimental points (○)) for $[Ala^*, Leu]_n$ (A-6).

dipole-coupled powder patterns. It was assumed that the orientations of σ_{11} (nearly parallel to the N–H bond) and σ_{33} (parallel to the C′–N bond) lie in the peptide plane but that the orientation of σ_{22} is perpendicular to the peptide bond (Fig. 31). It has been accepted that the alignment of the tensor element σ_{11} is nearly parallel to the hydrogen bonding (N–H $\cdots$ O) direction,[34,36,37] whereas the alignments of σ_{22} and σ_{33} are not always decided. Therefore, σ_{11} may offer certain information about the manner of the hydrogen bonding of polypeptides and proteins.

5.2.2. Copolypeptides

Figure 20 shows the diagram of the observed ^{15}N data of the Ala* residue of some polypeptides [Ala*, X]$_n$ (Ala* content is nearly 20%). The range of σ_{22} values of the α-helical [Ala*, X]$_n$ is displaced to low frequency with respect to those of the β-sheet [Ala*, X]$_n$, whereas the range of σ_{11} values of the α-helix is displaced to high frequency with respect to that of the β-sheet form. The dependence of the displacement of σ_{33} on conformation is ambiguous for [Ala*, X]$_n$. This result is consistent with that of [Ala*]$_n$. Since the alignment of the tensor element σ_{11} is nearly parallel to the hydrogen-bonding (N–H $\cdots$ O) direction,[32,34,36,37] it is anticipated that σ_{11} may offer certain information about the manner of the hydrogen bonding of polypeptides. In addition, the σ_{11} of the Ala* residues of [Ala*, D-Ala]$_n$ (A3, α_L-helix) is significantly decreased by 6 ppm with respect to that of [Ala*]$_n$ (A1, α-helix), whereas the difference between the right-handed and left-handed α-helices is not so large for σ_{22} (0.7 ppm) and σ_{33} (2 ppm). This indicates that σ_{11} is sensitive to the helical sense as well as the manner of the hydrogen bonding.

The displacement of σ_{22} of [Ala*, X]$_n$ is very sensitive to the conformational changes of copolypeptides. The σ_{22} values of the Ala* of the α-helix and β-sheet forms are observed separately in the ranges 54 $\sim$ 59 and 61 $\sim$ 63 ppm, respectively. The variation of the values of σ_{11}, σ_{22} and σ_{33} among the α-helical [Ala*, X]$_n$ is 6, 4.3 and 4 ppm, respectively. The variation of the values of σ_{11}, σ_{22} and σ_{33} among the β-sheet [Ala*, X]$_n$ is 2, 3.4 and 9 ppm. The variation of the σ_{33} data among the β-sheet form is very large with respect to that of the α-helix form. This suggests that σ_{33} may be related to side-chain structures of copolypeptides.

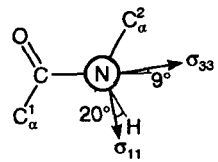

Fig. 31. The orientation of σ_{11}, σ_{22} and σ_{33} of a peptide: the orientation of σ_{11} and σ_{33} in the peptide plane, assuming σ_{22} is perpendicular to the peptide plane and positive above the page. (From Ref. 36.)

Figures 25 and 26 show the plots of σ_{iso}, σ_{11}, σ_{22}, and σ_{33} of various $[Ala^*, Leu]_n$, and $[Ala^*, Val]_n$, respectively, against the L-alanine content. The changes of σ_{iso} and σ_{33} are negligibly small over a wide range of L-alanine content ($5 \sim 80\%$). In contrast, the σ_{11} and σ_{22} data seem to depend slightly on the L-alanine content: σ_{22} value at 50% L-alanine content seems to be displaced to low frequency, whereas the σ_{11} value at 50% L-alanine content seems to be displaced to high frequency with respect to that of other contents. The reason for this is not clarified yet.

For a series of $[Ala^*, Asp(OBzl)]_n$, the value of σ_{22} decreases linearly as the L-alanine content increases ($5 \sim 20\%$ of the L-alanine content). This change of the σ_{22} value may be due mainly to neighbouring amino acid sequence effects, but not to the main-chain conformation of polypeptides. The σ_{iso}, σ_{11} and σ_{33} values, on the other hand, do not change at this L-alanine content ($5 \sim 20\%$).

For a series of $[Ala^*, Val]_n$ compounds, the stable conformation was found to be the β-sheet form at $\leq 20\%$ L-alanine content (A7-1, A7) and the α-helix form at $\geq 30\%$ L-alanine content (A7-2), as shown in Table 4. An interesting result was that, in the narrow range of L-alanine content (between 20 and 30%), the σ_{22} value exhibits a drastic decrease (*ca.* 9 ppm) as the L-alanine content increases. In contrast, no conformational change occurs (β-sheet form) at $5 \sim 20\%$ L-alanine content, whereas very few changes occur in the values of σ_{22}. This supports the view that σ_{22} is governed mainly by the conformation of copolypeptides and is conformation dependent. As described above, it is generally difficult to estimate the main-chain conformation of a variety of copolypeptides on the basis of σ_{iso} data. However, it is now possible to determine the conformation of copolypeptides on the basis of σ_{22} values, if the ^{15}N-labelled copolypeptide (or natural protein) can be provided. Large changes are seen for the σ_{iso}, σ_{11}, and σ_{33} values (other than σ_{22}) at $5 \sim 20\%$ L-alanine content. These changes may be mainly due to the neighbouring amino acid sequence effects (or higher ordered effects) of copolypeptides. For a series of $[Ala^*, D\text{-}Ala]_n$, no displacements of σ_{iso}, σ_{11}, and σ_{33} were detected over $5 \sim 20\%$ L-alanine content. The value of σ_{22} is, however, decreased as the L-alanine content increases. This may be ascribed to neighbouring amino acid sequence effects.

Figure 21 shows the diagram of the observed σ_{iso}, σ_{11}, σ_{22}, and σ_{33} data of the Gly* residue of $[Gly^*, X]_n$ (Gly* content is nearly 20%). The range of the σ_{22} values of the α-helical $[Gly^*, X]_n$ decreases with respect to those of the β-sheet $[Gly^*, X]_n$, whereas the range of the σ_{11} and σ_{33} values of the α-helix increases with respect to that of the β-sheet form. The displacement of σ_{11} and σ_{22} of $[Gly^*, X]_n$ is very sensitive to the conformational changes of copolypeptides. The σ_{11} and σ_{22} data of the Gly* of the α-helix form and those of the β-sheet form are observed separately, and are quite similar to those of the Ala* of $[Ala^*, X]_n$. However, the displacement of the tensor element σ_{33} (parallel to the C′–N bond direction[36,37]) of the α-helix and β-sheet forms is different

from that of the $[Ala^*, X]_n$. This suggests that σ_{33} is related to the side-chain structures of solid polypeptides, although further study is needed to confirm this.

Figures 27 and 28 show the plots of σ_{iso}, σ_{11}, σ_{22}, and σ_{33} values of various $[Gly^*, Ala]_n$ and $[Gly^*, Leu]_n$ against glycine content. It is interesting that the value of σ_{iso} is nearly constant, but the principal shielding tensor components are displaced over a wide range of glycine content ($20 \sim 100\%$). Therefore, these tensor components contain some information about neighbouring amino acid sequence effects as well as conformation. The reason for this is not clear at present.

Figure 22 shows the observed σ_{iso} and σ_{22} data of the Leu* residue of $[Leu^*, X]_n$ (Leu* content is nearly 20%). The range of σ_{22} values of the α-helical $[Leu^*, X]_n$ is smaller than that of the β-sheet $[Leu^*, X]_n$. The σ_{22} values of the Leu* of the α-helix and β-sheet forms are observed separately in the ranges $50 \sim 57$ and $58 \sim 67$ ppm, respectively. Thus, the displacement of σ_{22} of $[Leu^*, X]_n$ is very sensitive to the conformational changes of copolypeptides. The variation of σ_{22} among the α-helical $[Leu^*, X]_n$ is 7 ppm, and that of the β-sheet form is 9 ppm. This result suggests that the σ_{22} value of the Leu* residue may be related to strong neighbouring amino acid sequence effects as well as conformational effects.

Figure 29 shows the plots of σ_{iso} and σ_{22} of various $[Leu^*, Val]_n$, $[Leu^*, Ala]_n$ and $[Leu^*, Gly]_n$ against the L-leucine content. The σ_{iso} value is nearly constant, but the shielding tensor elements are displaced over a wide range of L-leucine content ($20 \sim 100\%$). Therefore, the σ_{22} value contains some information about neighbouring amino acid sequence effects and any higher ordered interactions, as well as conformation-dependent interactions.

In particular, we can now determine the main-chain conformation of various copolypeptides (and some proteins) in the solid state from the σ_{iso} and σ_{22} data by ^{15}N CP/MAS and/or CP-static NMR methods, if the ^{15}N-labelled copolypeptide or ^{15}N-labelled natural protein can be provided. As the relation between the nitrogen shielding and the structures (primary, secondary and higher ordered structures) is clarified in the future, we will be able to get more detailed information on the structure of polypeptides and proteins in the solid state.

Finally, we would like to mention briefly that solid-state ^{15}N NMR has been successfully applied to the structural characterization of natural proteins in addition to solid-state ^{13}C NMR. As there is no space to describe it in detail, we provide some references only.[45,46,54,76–82]

REFERENCES

1. M. Mehring, *Principles of High Resolution NMR in Solids* (2nd edition). Springer-Verlag, Berlin, 1983.

2. P. Granger and R.K. Hains (eds), *Multinuclear Magnetic Resonance in Liquids and Solid-Chemical Applications*. Kluwer Academic Publishers, Dordrecht, 1990.
3. R.G. Griffin, J.D. Ellett, M. Mehring, J.D. Bullitt and J.S. Waugh, *J. Chem. Phys.*, 1972, **57,** 2147.
4. N. Bloembergen and J.A. Rowland, *Acta Met.*, 1953, **1,** 731.
5. M. Witanowoki and G.A. Webb (eds), *Nitrogen NMR*. Plenum, London, 1973.
6. G.C. Levy and R.L. Lichter, *Nitrogen-15 NMR Spectroscopy*. John Wiley & Sons, New York, 1979.
7. G.J. Martin, M.L. Martin and J.P. Govesnard, ^{15}N *NMR Spectroscopy*. Springer-Verlag, Berlin, 1981.
8. B.C. Gerstein and C.R. Dybowski, *Transient Technique in NMR of Solids*. Academic Press, London, 1985.
9. J. Schaefer, R.A. McKay and E.O. Stejskal, *J. Magn. Reson.*, 1979, **34,** 443.
10. J. Schaefer, E.O. Stejskal and R.A. McKay, *ACS Symp. Series*, 1982, **191,** 187.
11. M.M. Maricq and J.S. Waugh, *Chem. Phys. Lett.*, 1977, **47,** 327.
12. M.M. Maricq and J.S. Waugh, *J. Chem. Phys.*, 1979, **70,** 3300.
13. J. Herzfeld and A.E. Berger, *J. Chem. Phys.*, 1980, **73,** 6021.
14. M. Linder, A. Hohener and R.R. Ernst, *J. Chem. Phys.*, 1980, **73,** 4959.
15. M.G. Munowitz, R.G. Bodenhousen and T.H. Huang, *J. Am. Chem. Soc.*, 1981, **103,** 2529.
16. M.G. Munowitz and R.G. Griffin, *J. Chem. Phys.*, 1982, **76,** 2848.
17. J.E. Roberts, S. Vega and R.G. Griffin, *J. Am. Chem. Soc.*, 1984, **106,** 2506.
18. R.A. Haberkorn, R.E. Stark, H. van Willigen and R.G. Griffin, *J. Am. Chem. Soc.*, 1983, **103,** 2534.
19. R.E. Stark, L.W. Jelinski, D.J.Rubin, D.A. Torchia and R.G. Griffin, *J. Magn. Reson.*, 1983, **55,** 266.
20. R.E. Stark, R.A. Haeberkorn and R.G. Griffin, *J. Chem. Phys.*, 1978, **68,** 1996.
21. J.E. Roberts, G.S. Harbison, M.G. Munowitz, J. Herzfeld and R.G. Griffin, *J. Am. Chem. Soc.*, 1987, **109,** 4163.
22. I. Ando and G.A. Webb, *Theory of NMR Parameters*. Academic Press, London, 1983.
23. D.B. Chestnut, in *Annual Reports on NMR Spectroscopy*, Vol. 21 (ed. G.A. Webb), p. 51. Academic Press, London, 1989.
24. *Specialist Periodical Report on NMR*, Vol. 20 (ed. G.A. Webb). Royal Society of Chemistry, London, 1991.
25. S. Kuroki, S. Ando, I. Ando, A. Shoji, T. Ozaki and G.A. Webb, *J. Mol. Struct.*, 1990, **240,** 19.
26. S. Kuroki, S. Ando, I. Ando, A. Shoji and T. Ozaki, *J. Mol. Struct.*, 1991, **245,** 69.
27. M. Witanowski, L. Stefaniak and G.A. Webb, in *Annual Reports on NMR Spectroscopy*, Vol. 24 (ed. G.A. Webb). Academic Press, London, 1991.
28. M. Schindler, *J. Am. Chem. Soc.*, 1988, **110,** 6623.
29. I. Ando, T. Yamanobe, H. Kurosu and G.A. Webb, in *Annual Reports on NMR Spectroscopy*, Vol. 22 (ed. G.A. Webb), p. 206, Academic Press, London, 1990.
30. G. Harbison, J. Herzfeld and R.G. Griffin, *J. Am. Chem. Soc.*, 1987, **109,** 4163.
31. J. Herzfeld, J.E. Roberts and R.G. Griffin, *J. Chem. Phys.*, 1987, **86,** 597.
32. Y. Hiyama, C.H. Niu, J.V. Silverton, A. Bavoso and D.A. Torchia, *J. Am. Chem. Soc.*, 1988, **110,** 2378.
33. M. Munowitz, W.P. Aue and R.G. Griffin, *J. Chem. Phys.*, 1982, **77,** 1686.
34. G.S. Harbison, L.W. Jelinski, R.E. Stark, D.A. Torchia, J. Herzfeld and R.G. Griffin, *J. Magn. Reson.*, 1984, **60,** 79.
35. C.J. Hartzell, T.K. Pratum and G. Drobny, *J. Chem. Phys.*, 1987, **87,** 4324.
36. T.G. Oas, C.J. Hartzell, F.W. Dahlquist and G.P. Drobny, *J. Am. Chem. Soc.*, 1987, **109,** 5962.
37. C.J. Hartzell, M. Whitfield, T.G. Oas and G.P. Drobny, *J. Am. Chem. Soc.*, 1987, **109,** 5966.
38. Q. Teng and T.A. Cross, *J. Magn. Reson.*, 1989, **85,** 439.

39. Q. Teng, L.K. Nicholson and T.A. Cross, *J. Mol. Biol.*, 1991, **218,** 607.
40. L.K. Nicholson, Q. Teng and T.A. Cross, *J. Mol. Biol.*, 1991, **218,** 621.
41. G.R. Marshall, D.D. Beusen, K. Kociolek, A.S. Redlinski, M.T. Leplawy, Y. Pan and J. Schaefer, *J. Am. Chem. Soc.*, 1990, **112,** 963.
42. Y. Pan, T. Gullion and J. Schaefer, *J. Magn. Reson.*, 1990, **90,** 330.
43. Y. Pan and J. Schaefer, *J. Magn. Reson.*, 1990, **90,** 341.
44. G.A. Webb and M. Witanowski, *Proc. Indian Acad. Sci. (Chem. Sci)*, 1985, **94,** 241.
45. T.A. Cross, J.A. Diverdi and S.J. Opella, *J. Am. Chem. Soc.*, 1982, **104,** 1759.
46. T.A. Cross, M.H. Frey and S.J. Opalla, *J. Am. Chem. Soc.*, 1983, **105,** 7471.
47. H.G. Foerster, D. Mueller and H.R. Kricheldorf, *Int. J. Biol. Macromol.*, 1983, **5,** 101.
48. T.H. Huang, W.W. Bachovchin, R.G. Griffin and C.M. Dobson, *Biochemistry*, 1984, **23,** 5933.
49. E.O. Stejskal, J. Schaefer and R.A. McKay, *J. Magn. Reson.*, 1984, **157,** 471.
50. C.N. Matthews, R. Ludicky, J. Schaefer, E.O. Stejskal and R.A. McKay, *Origins Life*, 1984, **14,** 243.
51. T.A. Cross and S.J. Opella, *J. Mol. Biol.*, 1985, **182,** 367.
52. B.S. Choi, J.E. Roberts, J.N.S. Evans and M.F. Roberts, *Biochemistry*, 1986, **25,** 557.
53. J. Schaefer, J.R. Garbow, G.S. Jacob, T.M. Forrest and G.E. Wilson, Jr., *Biochem. Biophys. Res. Commun.*, 1986, **137,** 7361.
54. P.L. Stewart, K.G. Valentine and S.J. Opella, *J. Magn. Reson.*, 1987, **71,** 45.
55. S.O. Smith, S. Farr-Jones, R.G. Griffin and W.W. Bachovchin, *Science*, 1989, **244,** 961.
56. H.J.M. de Groot, S.O. Smith, J. Courtin, E. van den Berg, C. Winkle, J. Lugtenburg, R.G. Griffin and J. Herzfeld, *Biochemistry*, 1990, **29,** 6873.
57. A. Shoji, T. Ozaki, T. Fujito, K. Deguchi and I. Ando, *Macromolecules*, 1987, **20,** 2441.
58. A. Shoji, T. Ozaki, T. Fujito, K. Deguchi, S. Ando and I. Ando, *Macromolecules*, 1989, **22,** 2860.
59. A. Shoji, T. Ozaki, T. Fujito, K. Deguchi, S. Ando and I. Ando, *J. Am. Chem. Soc.*, 1990, **112,** 4693.
60. A. Shoji, T. Ozaki, T. Fujito, K. Deguchi and I. Ando, manuscript in preparation.
61. A. Shoji, T. Ozaki, T. Fujito, K. Deguchi and I. Ando, manuscript in preparation.
62. A. Shoji, T. Ozaki, T. Fujito, K. Deguchi, I. Ando and J. Magoshi, manuscript in preparation.
63. I. Ando, H. Saito, R. Tabeta, A. Shoji and T. Ozaki, *Macromolecules*, 1984, **17,** 457.
64. S. Arnott and A.J. Wonacott, *J. Mol. Biol.*, 1966, **21,** 371.
65. S. Arnott, S.D. Dover and A. Elliott, *J. Mol. Biol.*, 1967, **30,** 201.
66. S. Arnott and S.D. Dover, *J. Mol. Biol.*, 1967, **30,** 209.
67. A. Shoji, H. Katoh, T. Ozaki, S. Kuroki and I. Ando, manuscript in preparation.
68. A. Shoji, T. Ozaki, H. Saito, R. Tabeta and I. Ando, *Macromolecules*, 1984, **17,** 1472.
69. T. Taki, S. Yamashita, M. Satoh, A. Shibata, T. Yamashita, R. Tabeta and H. Saito, *Chem. Lett.*, 1981, 1803.
70. H. Saito, R. Tabeta, A. Shoji, T. Ozaki and I. Ando, *Macromolecules*, 1983, **16,** 1050.
71. H. Saito, R. Tabeta, I. Ando, T. Ozaki and A. Shoji, *Chem. Lett.*, 1983, 1437.
72. H.R. Kricheldorf and D. Mueller, *Macromolecules*, 1983, **16,** 615.
73. H. Saito and I. Ando, in *Annual Reports on NMR Spectroscopy*, Vol. 22 (ed. G.A. Webb), p. 209. Academic Press, London, 1989.
74. T. Miyazawa, *Poly-a-Amino Acids* (ed. G.D. Fasman), Chap. 2 and references therein. Marcel Dekker, New York, 1967.
75. K. Ito, H. Katabuchi and T. Shimanouchi, *Nature, New Biol.*, 1972, **239,** 42, and references therein.
76. C.M. Gall, T.A. Cross, J.A. DiVerdi and S.J. Opella, *Proc. Natl. Acad. Sci. USA*, 1982, **79,** 101.
77. L. Mueller, M.H. Frey, A.L. Rockwell, L.M. Gierasch and S.J. Opella, *Biochemistry*, 1986, **25,** 557.
78. L.K. Nicholson, F. Moll, T.E. Mixon, P.V. LoGrasso, J.C. Lay and T.A. Cross, *Biochemistry*, 1987, **26,** 6621.
79. J.A. Killian, L.K. Nicholson and T.A. Cross, *Biochim. Biophys. Acta*, 1988, **943,** 535.

80. D.M. Schneider, R. Tycko and S.J. Opella, *J. Magn. Reson.*, 1987, **73,** 568.
81. M.J. Bogusky, R.A. Schiksnis, G.C. Leo and S.J. Opella, *J. Magn. Reson.*, 1987, **72,** 186.
82. G.B. Fields, C.G. Fields, J. Petefish, H.E. VanWart and T.A. Cross, *Proc. Natl. Acad. Sci. USA*, 1988, **85,** 1388.

Application of High-Resolution NMR Spectroscopy to Polymer Chemistry

K. HATADA, T. KITAYAMA and K. UTE

Department of Chemistry, Osaka University, Toyonaka, Osaka 560, Japan

ANNUAL REPORTS ON NMR SPECTROSCOPY
VOLUME 26 ISBN 0-12-505326-6

1. INTRODUCTION

Like many scientific fields, polymer chemistry has benefited from the introduction of NMR spectroscopy, and it is now widely used in areas such as tacticity determination, analysis of end-groups and irregular linkages, comonomer sequence determination in copolymers, and chain dynamics studies. This information is of primary importance for polymer characterization, but it also provides profound and stimulating knowledge about the reaction mechanism by which the polymer of interest is formed.

Organic chemists routinely use NMR spectrometers for product analysis to understand what has happened in the reaction flask. This should also be done by polymer chemists, but they have been faced with certain difficulties, mainly because polymers are statistical mixtures of various kinds of chain molecules. Even a single polymer molecule is made up of various constituents, such as the monomeric unit, end-group, irregular enchainment and various sequences of configuration.

Our research group has devoted itself to the investigation of the polymerization mechanism, especially in stereoregular polymerization, and to the control of polymer structure based on an understanding of the polymerization reaction. Well aware of the importance of detailed structural analysis of polymers in these studies, we have realized that NMR spectroscopy is the best tool for this purpose. This has encouraged us for a long time to commit to NMR spectroscopy of polymers. This chapter consists of several topics from our research work selected from the viewpoint described above.

First, we describe the reliability and limits of NMR analysis of polymer fine structure, which should be the basis of further investigations. Some of the quantitative data on polymers such as tacticity and monomer sequence distribution can only be obtained by NMR spectroscopy and thus much higher accuracy and precision are required for these analyses. End-groups and irregular linkages existing in polymer chains in very small amounts have become targets of NMR analysis since the introduction of the superconducting NMR spectrometer. The accuracy and limits of NMR microanalysis are discussed.

Next, NMR studies on end-group analysis for polymers are reviewed. The section includes the deuterated monomer method, in which a totally deuterated monomer is polymerized with an undeuterated initiator and the resultant polymer is analysed by ^{1}H NMR spectroscopy to determine the initiator fragment incorporated into the polymer chain. This method, which was invented by the authors, has brought fruitful results. Other related topics of end-group analysis of vinyl polymers, including labelled initiator methods, are also reviewed.

Tacticity determination of vinyl polymers by NMR has been one of our main concerns in connection with stereoregular polymerization. Major developments in the stereochemical assignment of NMR spectra of vinyl polymers and

oligomers are described in Sections 4 and 5 together with the reliability of tacticity data.

Nuclear magnetic relaxation parameters give important information on molecular motion and have become more and more familiar to and inevitable for NMR users after the introduction of the Fourier transform (FT) method to NMR technology. The relaxation parameters are also of essential importance in adjusting data acquisition conditions in FT-NMR measurements to obtain quantitative data. Section 6 covers the reliability of spin-lattice relaxation time (T_1) and the nuclear Overhauser enhancement (NOE) factor of polymers in solution and the tacticity dependence of ^{1}H- and ^{13}C-T_1 values of vinyl polymers in solution.

Section 7 introduces a recently developed on-line coupled gel permeation chromatography (GPC) and NMR system, in which a 500-MHz ^{1}H NMR spectroscopy is used as a detector for GPC. The system facilitates evaluation of molecular weight dependence of polymer characteristics such as tacticity and comonomer composition and determination of molecular weight without using standard polymer samples.

The relationships between chemical shift of vinyl monomers and their reactivities in the polymerization reaction are discussed in the last section.

2. QUANTITATIVE ANALYSES BY NMR SPECTROSCOPY IN POLYMER CHEMISTRY

2.1. Effects of operating conditions

Quantitative data on polymer structure, such as tacticity, *cis–trans* isomerism and monomer sequences, can be obtained from relative intensities of responsible NMR signals for these structures. Since these quantitative data are not collected by other analytical means, the NMR measurements for the analyses should be performed with much higher accuracy and precision, compared with those for low molecular weight compounds, in which only approximate intensity ratios, such as $CH_3 : CH_2 = 3 : 2$, are required.

We have been concerned with the precision and accuracy of NMR data of polymers since we first started NMR studies on polymers.[1–4] Using continuous-wave (CW) spectrometers, the effects of measurement conditions including temperature, sample concentration and radiofrequency (rf) field strength, were examined using several polymer and copolymer samples.[2] Since our research group have been deeply involved in stereospecific polymerization of methacrylates, one of the main concerns about NMR measurement was the precision of tacticity determination by NMR. The errors in determining the tacticity of poly(methyl methacrylate) (PMMA) and those in the results of polymerization of methyl methacrylate (MMA) by radical and anionic initiators were examined and found to be satisfactorily small.[4] Although there

are no theoretical values for tacticity, the accuracy of the measurement was proved by measuring the tacticity of a mixture of two PMMA samples with different tacticities and comparing it with the values calculated from those of each component polymer and the mixture ratio.[3]

Nowadays almost all the NMR data are acquired by the pulsed Fourier transform (FT) method. In this method, the consideration of spin-lattice relaxation times (T_1) for the signals of interest, that is, proper selection of the observed pulse width (or flip angle) and of pulse repetition time (or pulse interval) is of primary importance for quantitative analysis.[5–8]

The effects of flip angle and pulse repetition time on relative peak intensities were examined for radically prepared PMMA in chloroform-*d* at 55°C using a 500-MHz NMR spectrometer.[9] Figure 1 shows the relative intensities of methylene and methoxy proton signals against that of an α-methyl proton signal measured with various repetition times and flip angles. At a flip angle of 16°, relative intensities of OCH_3 and CH_2 proton signals are close to the theoretical values even at a pulse repetition time of 0.2 s. With a flip angle of 90°, the intensity of OCH_3 ($T_1 = 1.2$ s) is 97% of the theoretical value when

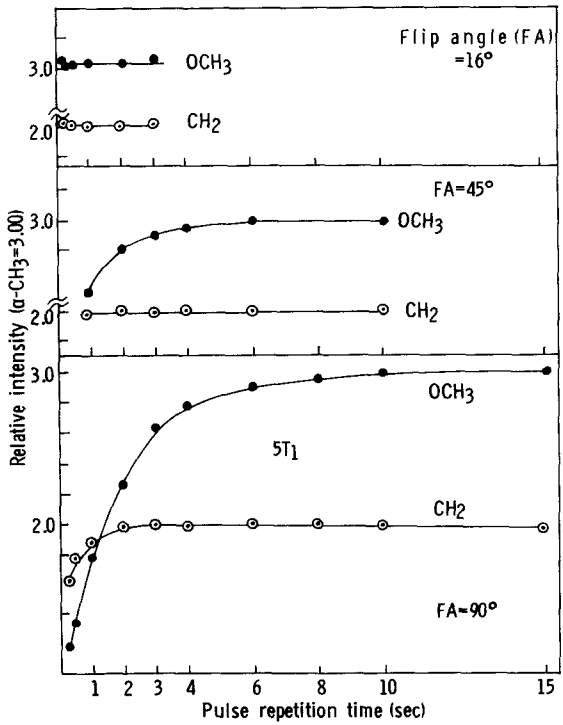

Fig. 1. Relative intensities of OCH_3 and CH_2 proton signals against α-CH_3 signals in PMMA at various pulse repetition times and flip angles.

the pulse repetition time is 6 s (5 times of the T_1) and reaches the theoretical value with a pulse repetition time as long as 10 s. The reliability of the intensity measurement is fairly good, and the standard deviations for five runs are 1–2% (Table 1).

Relative intensities of ^{13}C NMR signals against α-CH_3 carbon signals were also measured under various conditions using the same spectrometer operated at a frequency of 125 MHz.[9] With a flip angle of 45°, relative intensities of C=O, CH_2, OCH_3 and quaternary carbon signals against α-CH_3 carbon signals under complete ^1H decoupling conditions become constant at a pulse repetition time of 5 s, but are less than unity due to the larger NOE value for α-CH_3 carbon than those for other carbons (Table 1). The relative intensities observed with a gated decoupling mode with suppression of NOE are close to the theoretical value of unity with deviations of 2.2–8.7%. The standard deviation for five runs is in the range of 1.5–4.5% (Table 1). It is worth noting that the NOE values for each carbon signal at 25 MHz are close to the theoretical maximum, so that the relative intensities observed under complete decoupling conditions are close to the theoretical value.[10]

Triad tacticities obtained from α-CH_3, quaternary and C=O carbon signals agreed well with one another.[9] However, the *mm* triad fraction determined from the α-CH_3 proton signal deviated from other values because of the overlapping of the α,α'-azobisisobutyronitrile (AIBN) fragment signals. Correction for this contribution makes the *mm* value closer to the average (cf. Section 4.1).

2.2. Reliability of chemical shift and signal intensity

In order to assess the reliability of NMR data, Research Group on NMR, the Society of Polymer Science, Japan (SPSJ), collected ^1H and ^{13}C NMR spectra of two identical samples, a radically prepared PMMA and solanesol (a naturally occurring isoprene oligomer) from a number of NMR spectrometers by "round robin" method.[10]

^1H NMR spectra of the PMMA in $CDCl_3$ were measured on 26 spectrometers, whose resonance frequencies ranged from 90 to 500 MHz. Chemical shift data of OCH_3 protons scatter only within ±0.01 ppm, with a few exceptions. The standard deviation is 0.0038 ppm for 19 data obtained from FT instruments and 0.0169 ppm for 7 data obtained from CW spectrometers. Standard deviations for α-CH_3 and CH_2 proton shifts are less than 0.01 ppm. The chemical shift of water, which was incidentally introduced into sample solutions, scatters from 1.56 to 1.76 ppm. If the temperatures of measurements are almost constant, the water contents in the sample solutions are estimated to be from 0.07 to 0.20%. Relative intensity data, $3(CH_2 + \alpha\text{-}CH_3)/OCH_3$, agreed with the theoretical value of 5. Standard deviations of the intensity measurements are larger for the

Table 1. Mean values of relative intensities of ^{1}H and ^{13}C NMR signals of PMMA in $CDCl_3$ at 55°C for five runs.[a]

^{1}H (α-CH_3 = 3.00)[b]		^{13}C (α-CH_3 = 1.00) COM[c]				^{13}C (α-CH_3 = 1.00) NNE[c]			
OCH_3	CH_2	C=O	CH_2	OCH_3	Quat.	C=O	CH_2	OCH_3	Quat.
3.02	2.00	0.48	0.77	0.79	0.81	0.98	1.02	1.08	1.09
(0.8)	(1.8)	(1.9)	(2.0)	(2.4)	(2.6)	(1.5)	(4.5)	(2.1)	(1.8)

From Ref. 9.

[a]Values in parentheses represent standard deviations (%).

[b]Frequency 500 MHz; pulse width 45°; repetition time 10 s; scan 4–16.

[c]Frequency 125 MHz; pulse width 45°; repetition time 5 s; scan 5000.

COM: complete proton decoupling, NNE: proton decoupling without NOE.

FT method than for the CW method, while those for chemical shifts are larger for the CW method.

The ^{13}C NMR spectra of the same PMMA sample were measured in $CDCl_3$ on 24 instruments, whose resonance frequencies ranged from 15.0 to 125 MHz. All carbons except for OCH_3 are sensitive to the tacticity of the polymer chain. The number of distinguishable peaks depends on magnetic field strength. The standard deviations for chemical shift vary from 0.1 to 0.3 ppm, excluding those for OCH_3 and $CDCl_3$. Precisions of chemical shift for OCH_3 and $CDCl_3$ are better than those for others. Compared with the case of PMMA, solanesol shows higher precision of chemical shift.

Relative peak intensities for C=O, ($OCH_3 + CH_2$) and quaternary carbons against α-CH_3 were obtained with much poorer accuracy than those of ^1H NMR. Only four instruments (22.5 MHz and 25 MHz instruments) out of 24 were found to give data agreeable with theoretical values within $\pm 10\%$ deviation. Relative intensities obtained by 50 MHz or higher frequency instruments generally show large negative deviations. One of the sources of errors in these quantitative measurements is the variation in NOE values with magnetic field strength. The NOE values for each carbon at 22.5 and 25 MHz are close to 2.99. However, the NOE decreases with increasing magnetic field strength, strongly depending on the type of carbon (cf. Section 6.1).[11] The relative peak intensities were corrected by the NOE values and the results are shown in Table 2. Agreement within $\pm 10\%$ relative errors was obtained in the measurements at a field strength of 22.5–67.5 MHz. The corrected values for 90.6- and 100-MHz spectra still showed negative deviations due to saturation of the resonances, since a pulse repetition of about 1 s was used and the ^{13}C-T_1 values increase by a factor of at most 2.5 when the magnetic field is changed from 25 to 100 MHz.[11] As described in the previous section, measurement on a 125-MHz spectrometer at a pulse repetition of 5 s with 45° pulse gives reliable relative intensities within a 10% error, when the spectrum is measured under a gated decoupling with suppression of NOE.

The compositional analysis of a copolymer can be achieved by several methods other than NMR spectroscopy, such as elemental analysis, infrared and ultraviolet spectroscopies, and pyrolysis–gas chromatography. However, NMR spectroscopy has several advantages: it does not need calibration if the operation conditions are properly set, and it can distinguish impurities easily. Quantitative aspects of compositional analysis by ^1H and ^{13}C NMR have been discussed for styrene–MMA copolymer[12] and vinylidene chloride–acrylonitrile copolymer,[13] respectively.

Table 3 shows the results of compositional analysis for radically prepared copolymer of MMA and styrene.[14] ^1H and ^{13}C NMR analyses and elemental analysis gave consistent results as seen in the table, indicating good accuracy for all these analyses.

Table 2. Intensities of ^{13}C NMR signals of PMMA in $CDCl_3$ at 55°C.

Frequency (MHz)	n^a	Signal intensity[b]					
		Observed			Corrected by NOE		
		A	B	C	A	B	C
22.5	3	0.86	1.93	1.00	1.11	2.15	1.07
25	3	0.86	2.00	1.00	1.04	2.07	1.08
50	3	0.54	1.45	0.92	0.87	1.80	1.14
67.5	1	0.55	1.52	0.75	1.01	1.94	0.96
90.6	1	0.43	1.33	0.70	0.62	1.61	0.72
100	1	0.33	1.54	0.67	0.66	2.05	0.84

From Ref. 10.

[a]Number of determinations.

[b]A, B and C denote the relative intensities of C=O/α-CH_3, (OCH_3 + CH_2)/α-CH_3 and Quat.C/α-CH_3.

Table 3. Composition analysis of a copolymer of methyl methacrylate and styrene.

Method		Styrene content (%)
^{1}H NMR (phenyl, aliphatic)		52
^{13}C NMR[a]	(C_x, α-CH_3)	51
	(C_x, C=O)	53
	(CH_2(St), α-CH_3)	52
	(CH_2(St), C=O)	53
Elemental analysis		51

From Ref. 14.
[a]C_x: quarternary carbon in the phenyl group of styrene unit.

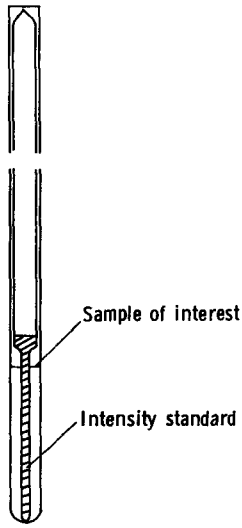

Fig. 2. Assembly of precision coaxial tubing. (From Ref. 19.)

2.3. Absolute and quantitative analysis by coaxial tubing method

In quantitative analysis, in which absolute intensity of signal of interest is required, an external[15] or internal[16,17] standard method can be used. In the external method, there is a possibility of instrumental variation during the interval between recording the spectra of the sample and that of the standard. In the internal method, contamination of the sample by the standard compound cannot be avoided, and it is difficult to mix a reasonable amount of the standard with the sample solution.

We have developed a technique for absolute and quantitative analysis using precision coaxial tubing.[18,19] Figure 2 illustrates the assembly of the coaxial tubing. The hydrogen content of the sample is calculated according

to the following equation:

$$H(\%) = 100F \times R/C \tag{1}$$

where R is the ratio of the signal intensity of the sample of interest placed in the surrounding annulus to that of the intensity standard in the inner cell; C (g/litre) is the concentration of the sample and F (g hydrogen/litre) is the concentration factor of the standard solution in the inner cell. The F value is determined by intensity measurements using the outer cell containing a known amount of hydrogen-containing compound. In this coaxial tubing method, the signal intensity of the standard can be easily adjusted to be close to that of the sample by selecting the appropriate inner cell.

The method was applied for the determination of hydrogen contents for various organic compounds, amount of non-deuterated hydrogen compound in deuterated solvents and composition of multicomponent mixtures such as waste solvents.[19]

Coaxial tubing is also used in the determination of volume magnetic susceptibility (χ_v)[20–23] by NMR spectroscopy. Recently, we found an easier and more accurate method of χ_v determination.[23] The chemical shifts of the sample in the outer cell are observed on a superconducting solenoid spectrometer (500 MHz) (δ_1) and an electromagnetic spectrometer (100 MHz) (δ_2) by referring to the external standard signal from the inner cell. The difference between the chemical shifts, $\delta_1 - \delta_2$, is described as follows:

$$\delta_1 - \delta_2 = K(\chi_s - \chi_r) \tag{2}$$

where χ_s and χ_r represent χ_v values of the sample and the reference sample in the inner cell. Using deuterated acetone as the external reference and several solvents whose χ_v values are known, the plots of $\delta_1 - \delta_2$ and $\chi_s - \chi_r$ gave $K = 6.2629$, which is very close to the theoretically expected value[24] of 2π (6.2832). Accuracy of χ_v determination by this simple method is within $\pm 0.6\%$.

2.4. Microanalysis by NMR spectroscopy

Analysis of end-group or abnormal linkage in polymer chains often gives us important information on the mechanism of polymerization (see Section 3). Although the low concentrations of these groups has often made them difficult to detect, the superconducting NMR spectrometer permits greater sensitivity and thus more detailed analysis of microstructures in polymers.

The coaxial tubing method is applicable to the quantitative analysis of a sample of interest with a wide range of concentrations by selecting an inner cell with appropriate F value, and is useful in microanalysis. Combined with a 500-MHz ^{1}H NMR spectrometer, the method allowed us to make

quantitative determinations of small amounts of impurities in carbon tetrachloride such as benzene, chloroform, dichloromethane, water and tetramethylsilane (TMS).[25] The inner cell contained hexamethyldisiloxane (HMDS) in acetone-d_6 as the intensity standard and the F factor was 1.43×10^{-5} gH/litre. The HMDS signal could not be detected by a 100-MHz ^{1}H NMR spectrometer. With measurement for 30 min, 1 ppm of benzene or dichloromethane could be analysed quantitatively. TMS, which has 12 equivalent hydrogen atoms in a molecule, could be detected at a concentration of 10^{-2} ppm. To examine the lower limit of the analysis, the sample was diluted 20 times with acetone-d_6 and analysed by the same procedure. The results shown in Table 4 indicate that the quantitative determination for 10^{-2} ppm of sample is possible with good accuracy.[25]

In microanalysis by ^{1}H NMR spectroscopy, impurities contained in NMR solvents even at very low levels may give interfering signals. Figure 3 shows the 500-MHz ^{1}H NMR spectrum of a commercial chloroform-d.[25] Along with strong signals due to chloroform and water, signals due to impurities at levels of a few parts per million or less are observed. It is therefore advisable in the microanalysis of polymer samples to take the spectrum of the solvent used and check carefully for impurities in the solvent. Haloalkanes may be contained in the solvent, while acetone and TMS might be contaminants introduced during laboratory use.

Water is often a major impurity in deuterated solvents, especially in polar solvents. For example, commercial acetone-d_6 contains 150–250 ppm of water even immediately after opening the bottle. The water content in acetone-d_6 kept in an NMR sample tube with a plastic cap increases 100 ppm/day in the chemical laboratory. When the sample in the NMR tube is kept in an effectively air-conditioned room (NMR laboratory), the water uptake rate decreases to 40 ppm/day. Sealing with Parafilm is not effective in reducing the rate of water uptake. Sealing with shrinkable tube made of polyethylene effectively decreases the rate to *ca.* 10 ppm/day, even in the chemical laboratory. When the tube with plastic cap is

Table 4. Quantitative determination of C_6H_6, $CHCl_3$ and CH_2Cl_2 in $CCl_4/(CD_3)_2CO$ (1/19 v/v) by precision coaxial tubing method.[a]

Compound	Concentration (ppm g/ml)	
	Taken	Found
C_6H_6	0.052	0.047
$CHCl_3$	1.892	1.792
CH_2Cl_2	0.074	0.077

From Ref. 25.

[a] 45° pulse; pulse repetition 10 s; 8411 scans (23.5 h); inner cell: HMDS/$(CD_3)_2CO$ ($F = 1.43 \times 10^{-5}$ g H/litre).

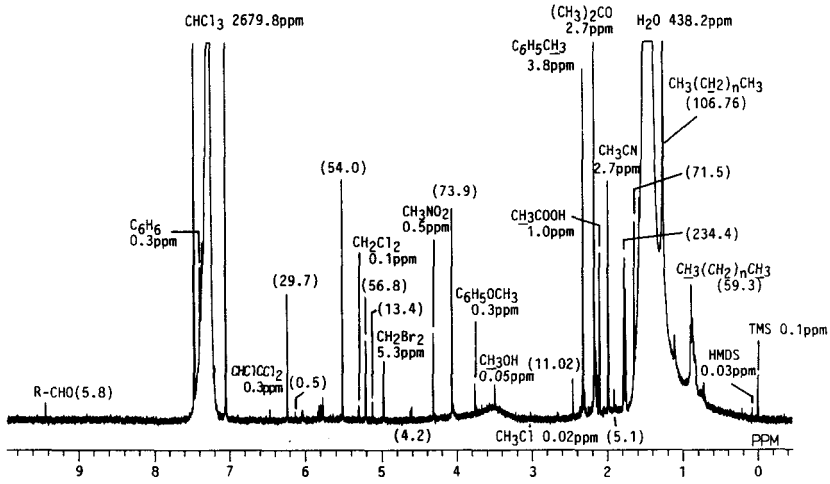

Fig. 3. 500-MHz ^{1}H NMR spectrum of $CDCl_3$ measured at 30°C. Chemical shifts in ppm, impurities in g/ml. Figures in parentheses are the concentrations expressed in 10^{-6} gH/litre. (From Ref. 25.)

stored in a refrigerator, the rate is reduced to 5.4 ppm/day. The content of water does not increase when the solvent is stored in a reagent bottle tightly capped and kept in a refrigerator. The water contents and uptake rates of several NMR solvents are shown in Table 5.[25]

In the course of these experiments, we noticed that some commercial deuterated solvents contained deuterium oxide, which in turn underwent H–D exchange with water introduced during storage to give DHO. Figure 4 gives the ^{1}H and ^{2}H NMR spectra of a commercial acetone-d_6. Exchange between H_2O, D_2O and DHO is slow enough to show each distinguishable signal. The total amount of water exceeded 0.25% even immediately after opening the bottle. The addition of D_2O to deuterated solvents may suppress the apparent water content observed by ^{1}H NMR but may then cause trouble when the sample is sensitive to water or the spectral features, including chemical shifts, are affected by the water content in the sample.

When the structure of an end-group is definitely known as A–$(M)_n$–B (M: monomeric unit), the quantitative determination of the relative intensities of the signals due to the end-groups against that of the signals due to the monomeric units is a simple and straightforward way of determining number average molecular weight ($\bar{M}_n$). Such a well-defined polymer sample can be obtained by living polymerization, in which the polymerization proceeds without transfer or termination reaction and every initiating species produces one polymer chain having one initiator fragment at the chain end. Polymerization of MMA with *t*-C_4H_9MgBr in toluene at low

Table 5. Contamination of deuterated solvents by atmospheric water.

	Acetone-d_6 (99%D)	Chloroform-d (99.8%D)	Nitrobenzene-d_5 (99%D)	Carbon tetrachloride
Original	268.2	104.6	117.6	49.8
NMR tube				
with plastic cap				
in chemical laboratory	110.6	39.3	37.7	2.4
in NMR laboratory	39.8	—	—	—
in refrigerator	5.4	—	—	—
with Parafilm seal				
in chemical laboratory	106.0	—	—	—
with PE seal				
in chemical laboratory	8.8	—	—	—

From Ref. 25.

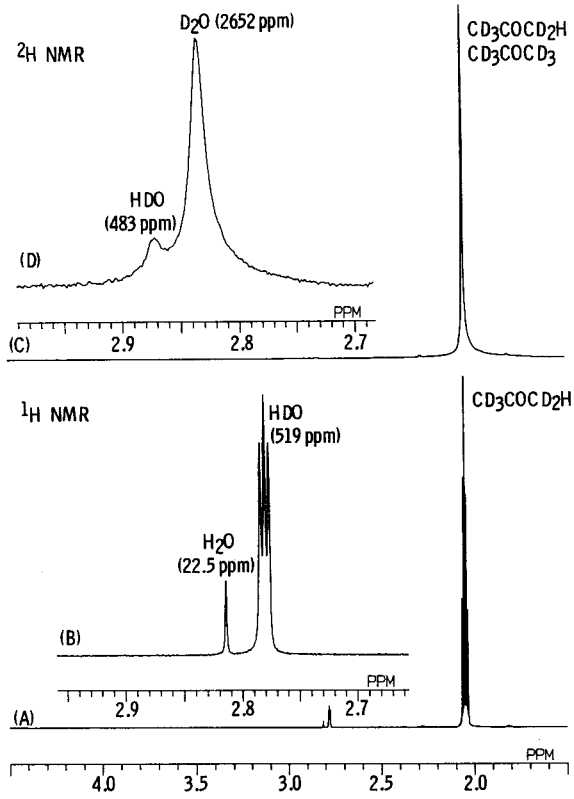

Fig. 4. 270-MHz ^{1}H and 41.34-MHz ^{2}H NMR spectra of acetone-d_6 (99%D) at 30°C. (From Ref. 25.)

temperature proceeds in a living manner to afford highly isotactic PMMA with the structure:[26,27]

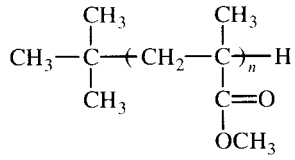

^{1}H NMR spectrum of the PMMA in nitrobenzene-d_5 showed a singlet signal of the t-C_4H_9 protons at 0.82 ppm clearly separated from the α-CH_3 proton signals. The measurement of relative intensity of the t-C_4H_9 signal against that of monomeric unit, for example OCH_3 proton signal at 3.60 ppm, provides the $\bar{M}_n$: $\bar{M}_n = I(OCH_3)/I(t\text{-}C_4H_9) \times 3 \times 100.14 + 58$. The $\bar{M}_n$ values thus

determined by 100-MHz ^{1}H NMR spectroscopy agreed well with those determined by gel permeation chromatography (GPC) and vapour pressure osmometry (VPO).[27] An isotactic PMMA ($\bar{M}_n = 27\,000$) was mixed with radically prepared PMMA to obtain the polymer sample, in which the ratio of $OCH_3/t\text{-}C_4H_9$ corresponds to much higher $\bar{M}_n$. It was found that the intensity ratio corresponding to an $\bar{M}_n$ of 3×10^6 can be determined accurately by 500-MHz ^{1}H NMR spectroscopy (Table 6).[28] $\bar{M}_n$ values of syndiotactic PMMAs prepared with 1,1-diphenylhexyllithium in tetrahydrofuran could also be determined by ^{1}H NMR and agreed with those determined by GPC and/or VPO up to $\bar{M}_n$ 5×10^5.[29]

In an NMR measurement where a weak signal is observed together with extremely strong signals due to monomeric units, the dynamic range of the spectrometer receiver as well as that of the analogue-to-digital converter (ADC) should come into question. Mathematical considerations on this point have been reviewed by Cooper.[30] Levy and his co-workers[31] investigated the accuracy and precision of ^{13}C NMR spectroscopic determination for components in a high dynamic range mixture of low molecular weight compounds with mole ratios from 10 : 1 to 600 : 1.

To test this point experimentally for a polymer sample, nitrobenzene-d_5 solutions of PMMA containing small amounts of nitromethane were prepared and the intensity ratios of the signals due to CH_3NO_2 and OCH_3 (PMMA) were measured on 100-MHz and 500-MHz ^{1}H NMR spectrometers, with 12-bit and 16-bit ADCs, respectively (Table 7).[25] Using the 100-MHz spectrometer, the amount of CH_3NO_2 was determined successfully up to an intensity ratio for OCH_3 (PMMA) to CH_3NO_2 of 14 800. The 500-MHz spectrometer allowed determination of a ratio as large as 250 000. Time required for the latter measurement was 25 h. The result suggests that the $\bar{M}_n$ of PMMA can be determined up to 25×10^6 as long as the polymer molecule contains just one terminal CH_3 group which shows a signal, apart from the strong signals due to the monomeric units.

Using ^{13}C NMR spectroscopy it is easier to observe end-group signals separately from main-chain signals. However, the 1.1% natural abundance

Table 6. 500-MHz ^{1}H NMR analysis of $t\text{-}C_4H_9$ group in the mixture of isotactic PMMA and radically prepared PMMA in nitrobenzene-d_5.[a]

Sample	$OCH_3/t\text{-}C_4H_9$		M_n[b]
	Expected	Observed	
1	—	89.4	26 000
2	1 094	1 136	341 000
3	11 570	10 230	3 068 000

From Ref. 28.
[a]Measured at 80°C.
[b]Expected M_n from observed $OCH_3/t\text{-}C_4H_9$ ratio.

Table 7. ^{1}H NMR determination of a small amount of CH_3NO_2 in nitrobenzene-d_5 solution of PMMA.[a]

Taken	Found[b]	
	100 MHz	500 MHz
46.8	46.8 (2.1)	49.3 (5.3)
210.0	199.8 (4.9)	204.7 (2.5)
913	897 (1.8)	950 (4.0)
6940	7215 (4.0)	7254 (4.5)
14791	13040 (11.8)	14207 (3.9)
30401		27767 (8.7)
61649		67944 (10.2)
250337		228181 (8.9)

From Ref. 25.

[a]Figures in the table indicate intensity ratios of OCH_3/CH_3NO_2.

[b]Figures in parentheses are percentage accuracy.

of ^{13}C in carbon compounds and the low concentration of the end-groups make the analysis of high molecular weight polymers relatively difficult. One approach is to prepare low molecular weight polymers or to isolate them from whole polymer samples. An alternative approach includes the use of a ^{13}C-labelled initiator and preparation and analysis of end-labelled polymers of relatively high molecular weight, as described in Section 3.2. The limit of detection of end-group by ^{13}C NMR depends on the structure of the end-group. Methyl groups in t-C_4H_9 are relatively easy to observe. The ^{13}C NMR signal of t-C_4H_9 in isotactic PMMA with an M_n of 11600 could be observed when the spectrum was measured in nitrobenzene-d_5 at 100°C under gated decoupling condition (concentration 10%, 3600 scans, pulse repetition 20 s).[28] The relative intensities of CH_2 and α-CH_3 to CH_3 in the t-C_4H_9 group corresponded to $\bar{M}_n$ values of 11960 and 12030, respectively, which are consistent with the $\bar{M}_n$ values determined by ^{1}H NMR. ^{13}C NMR spectroscopic molecular weight determination was applied to poly(oxy-2,6-dimethyl-1,4-phenylene) (M_n = 1600–3200).[32] Lanthanide shift reagent ($Pr(fod)_3$) was used to identify the end-groups.

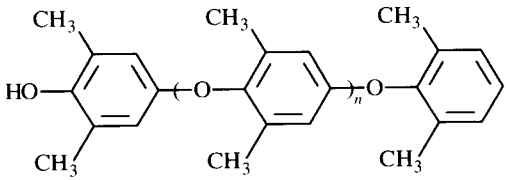

3. ANALYSIS OF END-GROUPS AND DEFECTS IN POLYMER CHAINS

3.1. Deuterated monomer method for detection of initiator fragment

Analysis of end-groups or abnormal[33] linkages in polymer chains is a powerful technique for studying the mechanism of polymerization as reviewed by Bevington *et al.*[34] and Axelson and Russell.[35] It has been demonstrated using ^{14}C-labelled α,α'-azobisisobutyronitrile (AIBN) that polystyrene radicals terminate exclusively by combination at temperatures up to 60°C, while PMMA radicals undergo substantial disproportionation.[36,37] However, the use of ^{14}C-labelled initiator only gives information on the number of initiator fragments and is not sensitive to how the fragment is incorporated into the polymer chain. Recently stable and NMR-sensitive isotope-labelled initiators were used to study initiation and termination steps especially in radical polymerization and copolymerization as described in Section 3.2. NMR methods enabled us to determine not only the number but also the structures of initiator fragments, which gave us valuable information for the understanding of mechanism of polymerization.

In a slightly different approach we studied the incorporation of the fragments of initiator and terminating reagent in a polymer molecule by polymerizing totally deuterated monomer with undeuterated initiator and analysing the resulting polymer by ^{1}H NMR spectroscopy for the fragments. Here the results of analyses on ionic polymerizations as well as radical polymerizations will be described.

3.1.1. Radical polymerization of MMA and styrene

Totally deuterated MMA (MMA-d_8) was polymerized with AIBN at 60°C in bulk and the resultant polymer was analysed for initiator fragments by ^{1}H NMR spectroscopy. The NMR spectrum of the polymer is shown in Fig. 5. The doublet at $\delta = 1.27$ ppm disappeared when the polymer was prepared with benzoyl peroxide (BPO). The ^{1}H spin-lattice relaxation time, T_1, for this doublet was 1.0 s. This indicates that the doublet is due to the methyl protons of the initiator fragment, 1-cyano-1-methylethyl group, located at the beginning of polymer chain. The T_1 value eliminates the possibility that the doublet arises from contaminants of small molecules ($T_1 \simeq 10$ s) or the protons of the groups within the polymer chain ($T_1 \simeq 0.1$ s). The splitting into two peaks is due to the adjacent asymmetric carbon in the polymer chain. The hydrogen content for this group was calculated as 0.0298 mmol/g polymer from the ratio of the doublet intensity to the signal due to the remaining protons in the nitrobenzene-d_5 used as a solvent for the measurement. The remaining proton content of the nitrobenzene-d_5 was determined using the precision coaxial tubing method as described in Section 2.3. Thus, the number of initiator

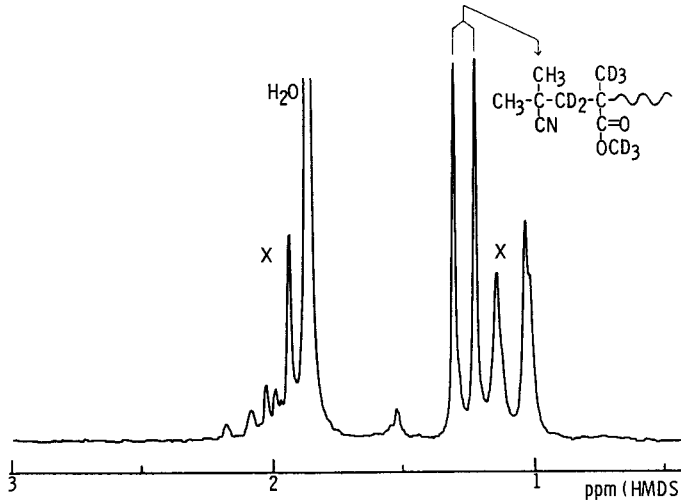

Fig. 5. ^{1}H NMR spectrum of poly(MMA-d_8) prepared in bulk by AIBN at 60°C (nitrobenzene-d_5, 110°C, 100 MHz). X = Signals due to remaining protons in the monomeric units. (From Ref. 38.)

fragments per polymer molecule was calculated to be 1.15 from the hydrogen content and the number average molecular weight of the polymer. The precision of the measurements for five determinations was 2.7%.[38]

It is well-known that the chain transfer reaction to initiator is of no importance in the polymerization of MMA with AIBN. The transfer constant to the MMA monomer is of the order of 10^{-5}; that is, one transfer reaction to the monomer occurs for 10^5 propagation reactions. The degree of polymerization of the polymers is less than 4×10^2; therefore, transfer to the monomer can also be neglected. Then, the number of initiator fragments, 1.15, means that 85% of the polymer molecules are formed through disproportionation reaction, and that half of them should contain a double bond at the chain end.

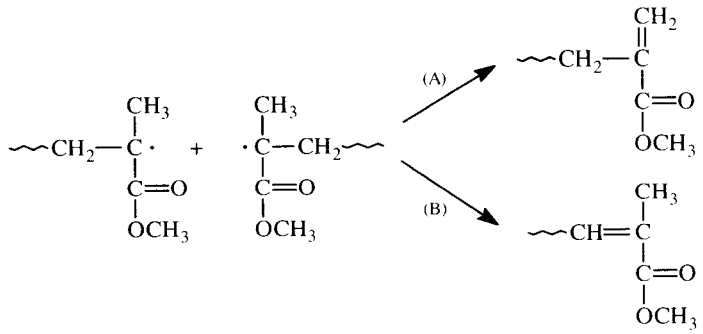

^{1}H NMR analysis of radically prepared undeuterated PMMA clearly indicated that the disproportionation proceeded through route A of the reaction as described in Section 3.3.1.[38]

In the polymerization of vinyl monomer with BPO, initiation occurs through the attack of the monomer by phenyl and benzoyloxy radicals. The poly(MMA-d_8) prepared with BPO showed the ^{1}H NMR signals due to the phenyl and benzoyloxy groups separately.[39] Intensity measurements indicated that the ratios of the benzoyloxy group to the phenyl group at the beginning of the chain were 72/28 and 21/79 for the polymer prepared in bulk and in benzene (monomer concentration, $[M]_0 =$ 0.91 mol/litre) at 60°C, respectively. The ratios roughly agree with those obtained with ^{14}C-labelled BPO (91/9 and 21/79)[40] for the PMMA prepared in bulk and at a monomer concentration of 0.91 mol/litre, respectively.[38,39]

The polymer prepared in tetrahydrofuran (THF) with BPO did not show any detectable NMR signal in the aromatic proton region, indicating that the polymer chain was not initiated by the phenyl or benzoyloxy radicals. In the spectrum there exist two small multiplets at 3.2–3.9 and 1.4–1.8 ppm; the former was assigned to the α-protons and the latter to the β-methylene protons of the THF fragments incorporated into the polymer chain. A possible mechanism of initiation is as follows:

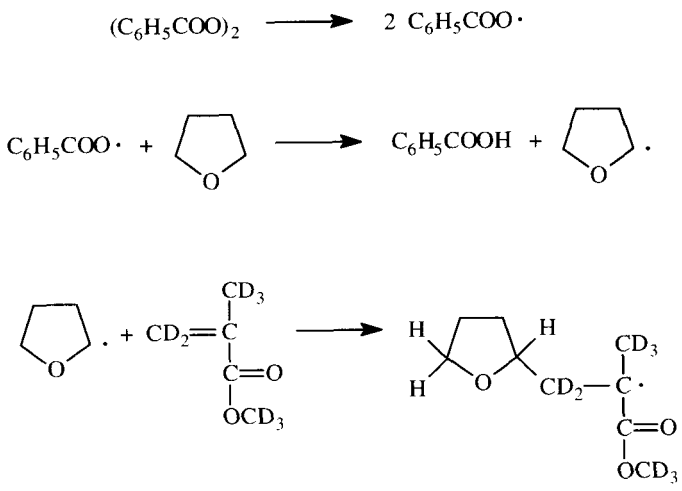

The number of THF fragments was determined to be 0.96 per polymer molecule.[41]

The termination reaction in the radical polymerization of styrene has been known to proceed only through a combination reaction:

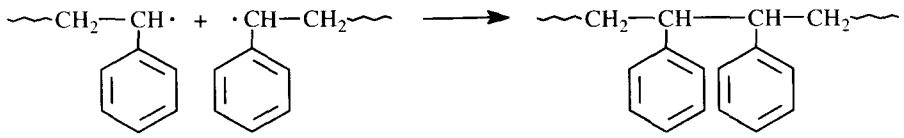

Then, the polystyrene molecule obtained should contain two initiator fragments per molecule in the absence of any chain transfer reactions. Detailed investigation of this termination reaction was carried out using totally deuterated styrene.[42] The ^{1}H NMR spectrum of poly(styrene-d_8) prepared with AIBN in bulk at 60°C is shown in Fig. 6 together with the spectrum of polystyrene prepared under the same conditions. The resonances centred at 0.94 and 1.11 ppm showed a ^{1}H-T_1 of 0.94 and 0.96 s, respectively, but were not observed when the polymer was prepared with AIBN-d_{12}. Thus, the resonances were assigned to the initiator fragment, the 1-cyano-1-methylethyl group located at the chain end of the polymer molecule. The splitting into two peaks at 0.94 and 1.11 ppm of equal intensities is due to the existence of an adjacent asymmetric centre in the polymer chain. Further splittings of these peaks may be due to the tacticity of the first few monomer sequences at the chain end.

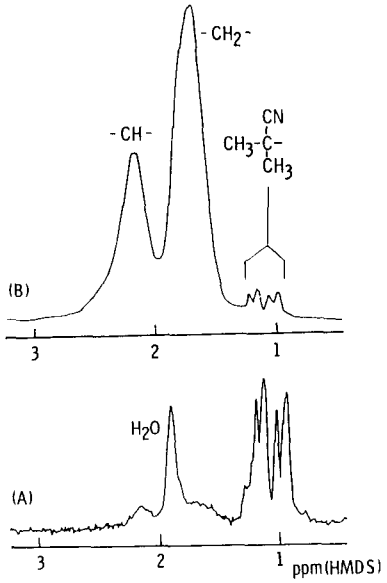

Fig. 6. ^{1}H NMR spectra of (A) poly(styrene-d_8) and (B) polystyrene prepared by AIBN in bulk at 60°C (nitrobenzene-d_5, 110°C, 100 MHz). (From Ref. 42.)

The number of initiator fragments per polymer molecule was calculated to be 1.59, indicating that there are two types of polymer molecules which contain one and two initiator fragments, respectively. Analysis of the polystyrene prepared with ^{2}H- and ^{13}C-labelled AIBN also showed that the polystyrene molecule contained 1.65[42] and 1.7–1.8[43] initiator fragments, respectively (cf. Section 3.2.1).

Undeuterated polystyrene ($\bar{M}_n = 18\,400$) prepared in bulk with AIBN at 60°C showed small NMR peaks at 1.01 and 1.18 ppm (Fig. 6B), which were assigned by Johns *et al.* to the methyl protons of initiator fragments.[44] The number of initiator fragments per chain was calculated to be 1.52. From the polystyrene, lower ($\bar{M}_n = 7760$) and higher ($\bar{M}_n = 41\,300$) molecular weight portions were fractionated using GPC. Analysis of the fractions revealed that the former had 1.44 initiator fragments per chain and the latter 1.77. This shows that the

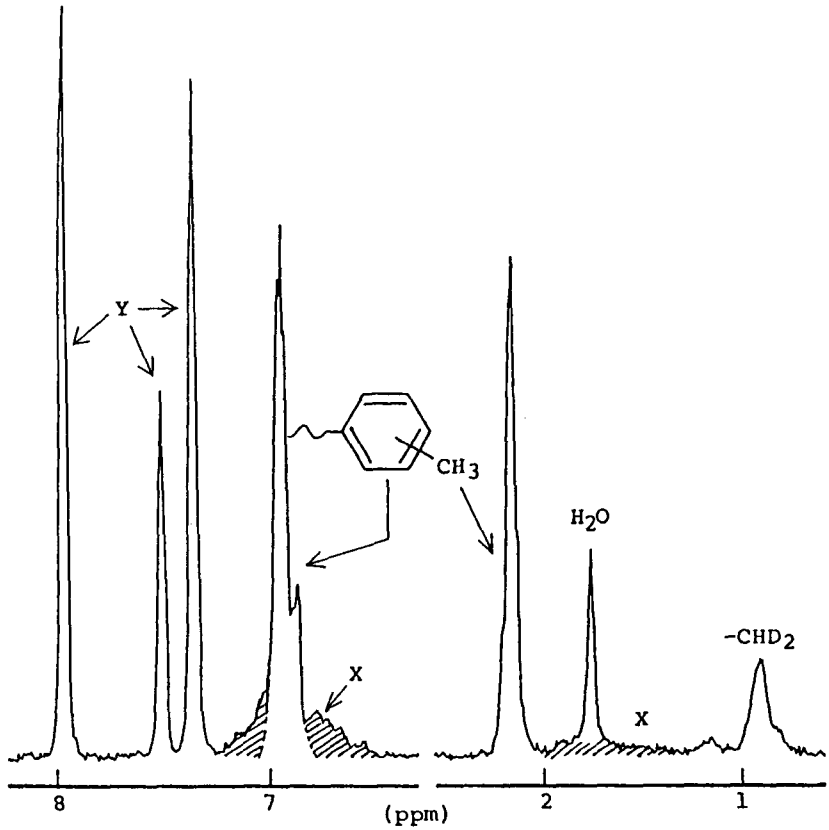

Fig. 7. ^{1}H NMR spectrum of the poly(styrene-d_8) prepared in toluene with $TiCl_4$. X and Y: Signals due to the remaining protons in the styrene-d_8 and nitrobenzene-d_5, respectively. (From Ref. 50.)

polymer molecules containing two initiator fragments, one on each end, are higher in molecular weight than those containing one initiator fragment.

From the results given above, it was concluded that in the radical polymerization of styrene, termination reaction by combination is predominant but that disproportionation is not of negligible importance. The accuracy of the determination of number of initiator fragments per chain might not be high since cumulative errors are associated with the determination of molecular weight and intensity of NMR signals. However, all the results obtained clearly indicated a number of initiator fragments per chain of less than 2.0. This, taken together with the fractionation data, should be strong evidence for the coexistence of disproportionation and combination in the termination reaction in the radical polymerization of styrene.

3.1.2. Cationic polymerization of styrene

In the cationic polymerization of styrene in aromatic solvents such as toluene, the chain transfer reaction to a solvent molecule usually occurs as follows:[45–49]

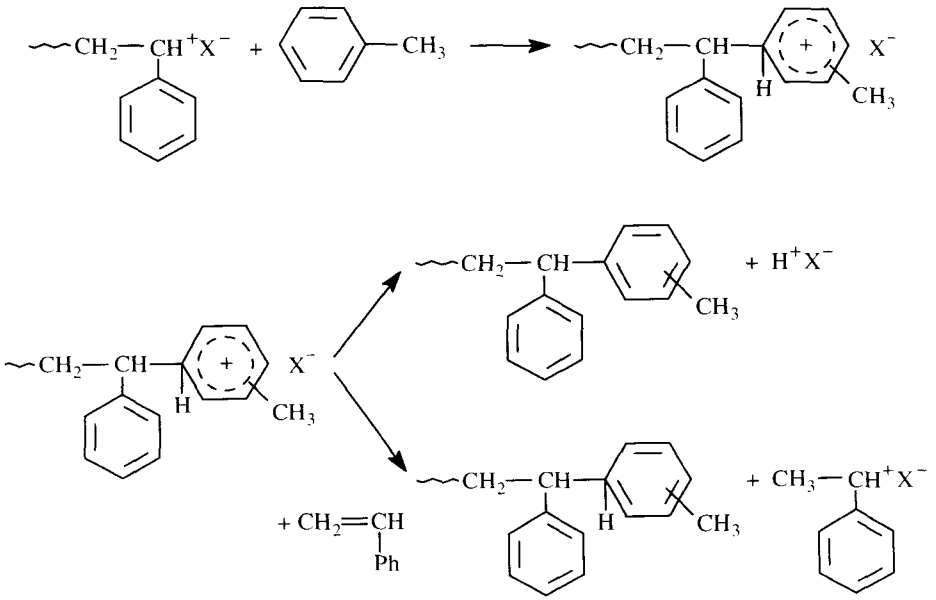

The initiation and chain transfer reactions were studied using totally deuterated monomer.[50] Figure 7 shows the ^{1}H NMR spectrum of the polymer prepared in toluene at −78°C by $TiCl_4$. There appear to be three signals at 6.92, 2.15 and 0.97 ppm, with ^{1}H-T_1 values of 2.1, 0.89 and 4.6 s, respectively. The first two peaks were assigned to the phenyl and methyl protons of the toluene fragments incorporated into the polymer chain. The T_1 values indicate that

these two peaks did not come from the protons of the toluene molecules as contaminant. The intensities of the peaks show that the polymer prepared by $TiCl_4$ contained 0.64 of toluene fragments per polymer molecule: 64% of the polymer molecules were formed through the chain transfer reaction to the solvent toluene. It follows that the residual 36% of the polymer molecules was formed through the monomer transfer reaction. From the results the ratios of the rate constants of k_M/k_p and k_s/k_p were estimated to be 0.0023 and 0.0035, respectively, where k_p, k_M and k_s are the rate constants for propagation, monomer transfer and solvent transfer reactions. The ratios thus obtained agree with the values determined kinetically.[51]

If the chain transfer to solvent occurs through the reaction shown above, the regenerated active chain should contain a CHD_2 group at the beginning of the chain:

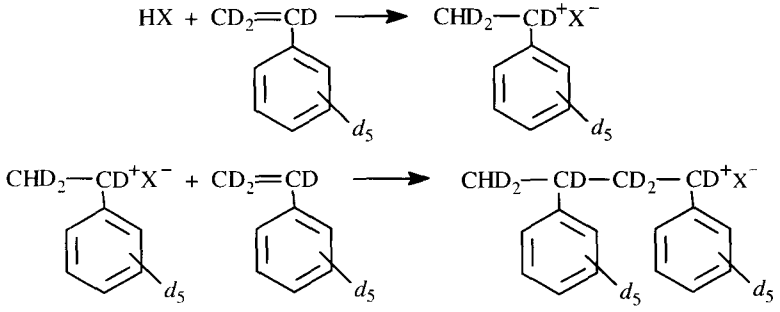

The peak at 0.97 ppm in the spectrum in Fig. 7 should be due to the proton of this partially deuterated methyl group. As mentioned above, the T_1 for this peak was much longer than those for other two peaks. The longer T_1 should be due to the loss of dipolar relaxation from the two protons in the methyl group. The amount of CHD_2 group was determined to be 0.71 per polymer molecule. On the other hand, some coinitiator is usually necessary for the cationic polymerization of styrene by metal halide.[52] In this work the coinitiator was a small amount of water which was admitted incidentally into the reaction mixture.

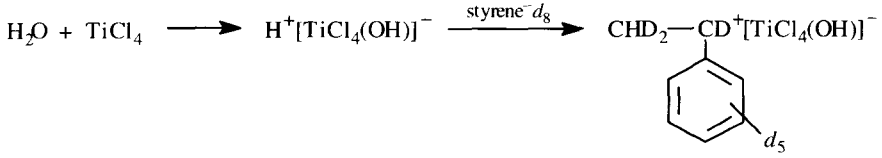

This means that the partially deuterated methyl group was introduced into the polymer chain by the initiation reaction as well as the chain transfer reaction. The difference between the number of terminal CHD_2 groups and the number of toluene fragments corresponds to the amount of water which

existed in the reaction mixture and functioned as a coinitiator at the beginning of the polymerization. It was calculated to be about 0.1 mg.

3.1.3. Anionic polymerization of methyl methacrylate

The polymerization of MMA by alkyllithium has been studied in greater detail than that by any other initiator. For bulky alkyllithiums such as 1,1-diphenylhexyllithium, the polymerization in THF proceeds in an ideal manner to give a living polymer:

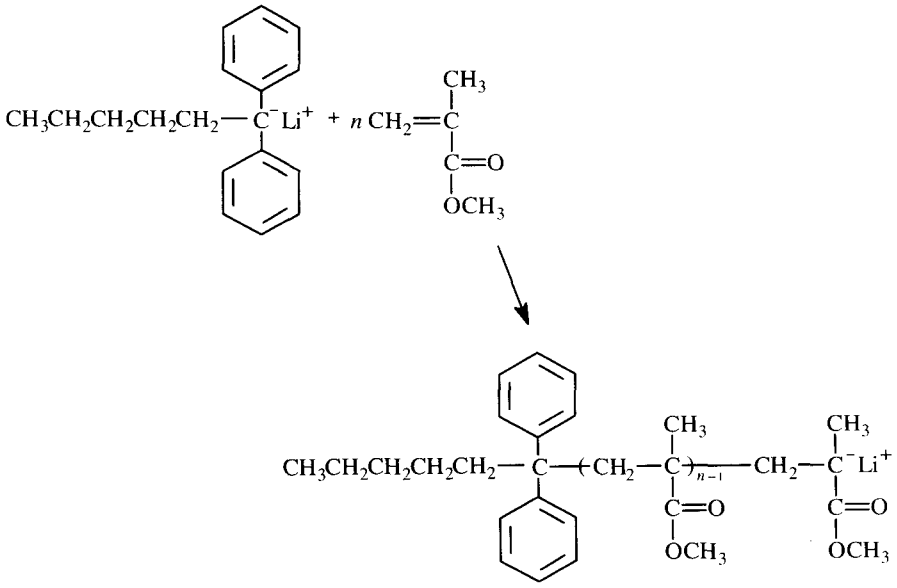

However, for polymerization with smaller alkyllithiums such as n-C_4H_9Li, there were a number of unsolved problems caused by side-reactions, as reviewed by Bywater[53] and Hatada *et al.*[54]

Polymerization of MMA with n-C_4H_9Li usually gives a methanol–insoluble polymer and a methanol-soluble oligomer. All the n-C_4H_9Li used could not be accounted for if each polymer molecule were assumed to contain one n-C_4H_9Li residue. Wiles and Bywater[55–57] reported the formation of $LiOCH_3$ in the polymerization of MMA with n-C_4H_9Li through the attack of the initiator on the ester group of the monomer:

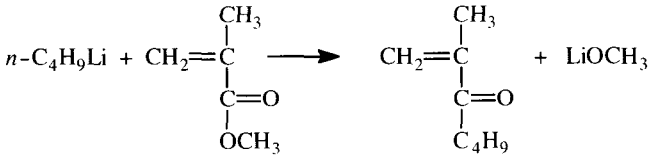

However, the structural survey of the low molecular weight products by Kawabata and Tsuruta[58] seems to indicate that carbonyl addition was not a predominant side-reaction since the amount of butyl isopropenyl ketone (BIPK) formed was very small, particularly in the polymerization in toluene. The problem was solved almost completely by totally deuterated monomer technique.[59–63] The poly(MMA-d_8) prepared with n-C_4H_9Li in toluene showed in ^1H NMR signals due to the methyl (0.79 ppm) and methylene

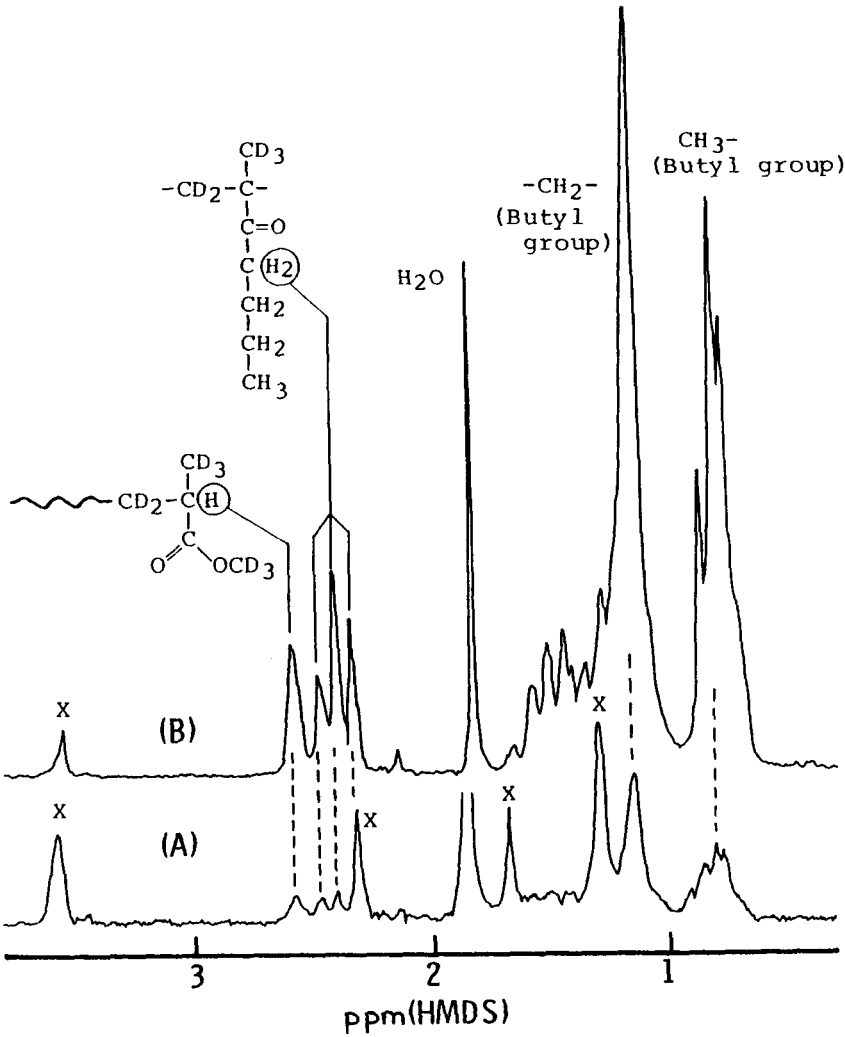

Fig. 8. ^1H NMR spectra of the polymer (A) and oligomer (B) of MMA-d_8 prepared in toluene with BuLi at −78°C. X: Signals due to the remaining protons in the monomer unit of the chain. (From Ref. 59.)

(1.15 ppm) protons of the butyl groups which were incorporated into the polymer chain from the initiator (Fig. 8). The triplet signal at 2.40 ppm was assigned to the protons of the methylene group adjacent to the carbonyl group (α-methylene protons, $-COC\underline{H}_2-CH_2CH_2CH_3$). The resonance turned out a singlet by irradiation at 1.4 ppm, where a weak multiplet appeared, indicating that the latter resonance was ascribed to the β-methylene group. These results clearly indicate the incorporation of BIPK into the PMMA chain through the copolymerization.[59] This is the reason why the ketone was not detected in the search of the low molecular weight products by Kawabata,[58] whereas $LiOCH_3$ was found in Bywater's work.[56,57,64] From the intensity measurements of the signals the polymer and oligomer molecules were found to contain roughly two butyl groups, one incorporated at the beginning of the chain through the initiation reaction and the other in an in-chain or terminating end BIPK unit. Mass spectroscopic analysis of the fractionated oligomers showed that most of the BIPK units were located at the terminating chain end:

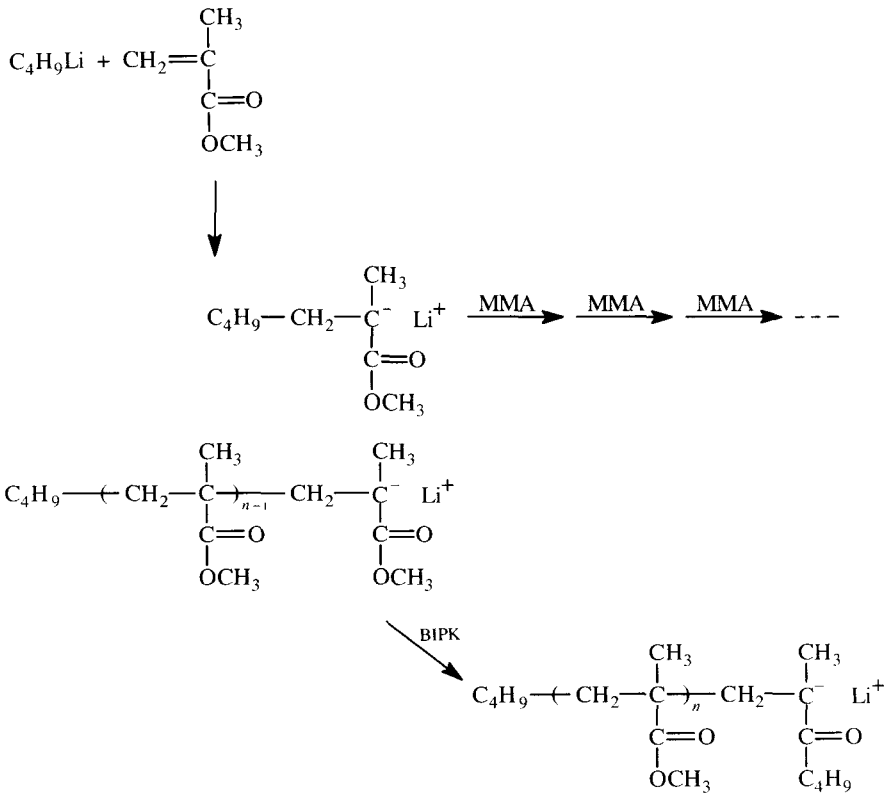

This is due to the lower reactivity of the BIPK anion at the propagating chain end as compared with the PMMA anion.[60] A small amount of butane was

found in the polymerization product by gas chromatographic analysis; the butane was formed by protonation of unreacted n-C_4H_9Li molecule when the polymerization was terminated. By taking these results into account, the fate of the initiator was almost completely clarified for this polymerization.[59]

The singlet peak at 2.57 ppm in Fig. 8 was first assigned to both the methine protons attached to the MMA (MMA-H) and BIPK (BIPK-H) units located at the terminating chain end.[59] Recently, the chemical shifts of MMA–H and BIPK–H were confirmed as 2.45 and 2.57 ppm for the poly(MMA-d_8)s prepared with the initiators which did or did not give BIPK during polymerization.[62]

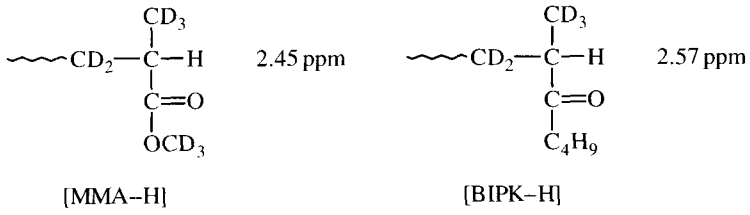

[MMA–H] [BIPK–H]

Quantitative determination of these two methine protons in PMMA prepared with n-C_4H_9Li would allow estimation of the amount of each of the two terminal units. Unfortunately, the signals due to the α-methylene protons of BIPK at terminating chain end and in-chain sequence[60] overlap with MMA-H and BIPK-H signals, respectively.

The problem was solved by the use of α-methylene-d_2 butyllithium ($CH_3CH_2CH_2CD_2Li$) as an initiator.[63] Figure 9 shows the 270-MHz ^1H NMR spectra of the polymer and oligomer of MMA-d_8 prepared with $CH_3CH_2CH_2CD_2Li$ in toluene at $-78°C$. The resonances in the methine proton region show that the polymer and oligomer molecules contained both MMA-H and BIPK-H units at the terminating chain end. The existence of the BIPK units in the chain can be realized from the two multiplets at 1.476 and 1.532 ppm, which were assigned to the β-methylene protons of the BIPK units located at the chain end and in in-chain sequences, respectively, as shown in Fig. 9. The multiplets show that most of the BIPK units were located at the chain end. From the results the following four types of polymeric chains were assumed to exist and the mechanism of polymerization was discussed in some detail.[63]

$$n\text{-}C_4H_9\text{-}(\text{MMA})_o\text{BIPK-}(\text{MMA})_p\text{BIPK-H}$$

$$n\text{-}C_4H_9\text{-}(\text{MMA})_o\text{BIPK-}(\text{MMA})_p\text{MMA-H}$$

$$n\text{-}C_4H_9\text{-}(\text{MMA})_o\text{BIPK-H}$$

$$n\text{-}C_4H_9\text{-}(\text{MMA})_o\text{MMA-H}$$

Polymerization of MMA with n-C_4H_9Li in THF at $-78°C$ was also

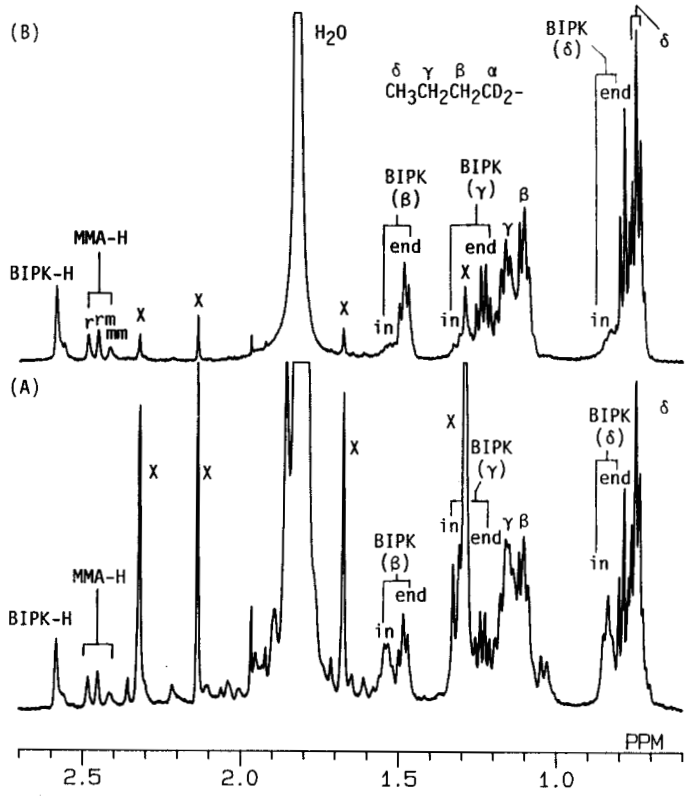

Fig. 9. 270-MHz ^{1}H NMR spectra of polymer (CH_3OH-insoluble) (A) and oligomer (CH_3OH-soluble and *n*-hexane-insoluble) (B) of MMA-d_8 prepared by $CH_3CH_2CH_2CD_2Li$ in toluene at −78°C (nitrobenzene-d_5, 110°C). X = Signals due to the remaining protons in the monomeric unit. Methylene and methyl protons of butyl(-d_2) group at the initiating chain end are designated as β, γ and δ, and those of butyl(-d_2) group of the BIPK unit as BIPK(β), BIPK(γ) and BIPK(δ) as shown in the figure. For the BIPK unit, those at the terminating end and in in-chain sequence are designated as "end" and "in", respectively. Two types of terminal methine protons are differentiated as MMA-H and BIPK-H. (From Ref. 63.)

investigated using MMA-d_8 and $CH_3CH_2CH_2CD_2Li$. The ^{1}H NMR spectra of the polymer and oligomer are shown in Fig. 10.[63] Again, BIPK formed in the early stage of polymerization was found to be incorporated into the polymer and the oligomer chains.

The spectra clearly indicated all the polymer and oligomer molecules contained terminal BIPK units besides the in-chain BIPK units, the amount of which appeared to depend on the degree of polymerization. The numbers of in-chain BIPK units in the polymer and oligomer molecules were found to be about 3 and 1, respectively, from the intensity measurement of the signals.

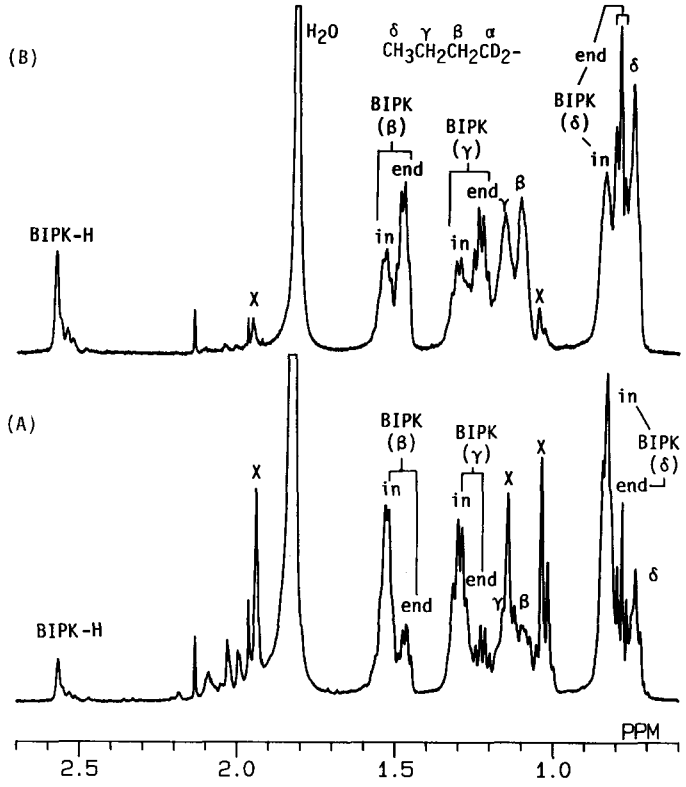

Fig. 10. 500-MHz ^{1}H NMR spectra of the polymer (CH_3OH-insoluble) (A) and oligomer (CH_3OH-soluble and *n*-hexane-insoluble) (B) of MMA-d_8 prepared with $CH_3CH_2CH_2CD_2Li$ in THF at −78°C (nitrobenzene-d_5, 110°C). See Fig. 9 for the designation of signals. (From Ref. 63.)

The structure of the polymer can thus be depicted as follows:

$$n\text{-}C_4H_9\text{-}\{\text{MMA}\}_o\,\text{BIPK}\text{-}\{\text{MMA}\}_p\,\text{BIPK}\text{-}\{\text{MMA}\}_q$$
$$\text{BIPK}\text{-}\{\text{MMA}\}_r\,\text{BIPK}\text{-H}$$

The structure indicates that the polymer anion repeatedly experiences two different states of reactivity: BIPK anion and MMA anion. The lower reactivity of the BIPK anion is expected to greatly reduce the polymerization rate. In fact, a large fraction of the polymer molecules formed after most of the BIPK monomer had been consumed, and it took about 4 h for completion of polymerization to occur, even at a high initiator to monomer ratio of 0.1 mol/mol.[60,63]

Polymerizations of MMA with Grignard reagents were also studied using the totally deuterated monomer technique.[26,27,63,65–68] *n*-Butylmagnesium chloride reacts with the C=O double bond of MMA as well as the C=C double bond

during the initiation reaction and gives a PMMA with a broad molecular weight distribution.[65] As the alkyl group becomes bulkier, the molecular weight distribution becomes narrower. In the polymerization with *s*-C_4H_9MgBr and *t*-C_4H_9MgBr the bulky alkyl groups prevent the Grignard reagents from participating in the side-reactions, leading to the formation of PMMA with a narrow molecular weight distribution.[26,27,66] The poly(MMA-d_8) prepared with *t*-C_4H_9MgBr in toluene at −78°C shows ^1H NMR signals only due to the *t*-C_4H_9 group at the beginning of the chain and the methine proton at the terminating chain end; no sign of side-reaction was observed. The intensity measurement indicated that the polymer molecule contained one *t*-C_4H_9 group and one methine proton at both chain ends, respectively.[26]

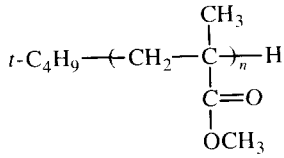

Highly syndiotactic PMMA with a narrow molecular weight distribution was prepared by the polymerization of MMA in toluene at low temperatures initiated with *t*-C_4H_9Li combined with trialkylaluminium.[69] Detailed inspection of the ^1H NMR spectra of the polymers indicated that the polymerization was initiated with the *t*-C_4H_9 anion and not with the alkyl anion from trialkylaluminium, and proceeded in a living manner. The evidence for the initiation reaction with the *t*-C_4H_9 anion was obtained from the ^1H NMR spectrum of the polymer of MMA-d_8 prepared with *t*-$C_4H_9Li/(C_2H_5)_3Al(1/3)$ in which there is a signal due to the *t*-C_4H_9 group at the initiating chain end but no signal due to the ethyl group.

3.2. End-group analysis using labelled initiator

As described in the previous section, end-group analysis of polymers provides important information on polymerization mechanisms. In radical polymerization the ^{14}C-labelling technique has long been used to study initiation and termination mechanisms, in which determination of the number of initiator fragments in a polymer molecule is the key procedure. Since the late 1970s, stable and NMR-detectable isotope-labelled initiators have been replacing radioisotope-labelled initiators. Among the various stable isotopes, ^{13}C-labelling has been most widely used for this purpose. Bevington *et al.* evaluated quantitative aspects of end-group analysis using ^{13}C-labelled initiator.[34] In the ^{13}C NMR spectrum of PMMA ($M_n = 60\,000$) prepared with AIBN enriched with ^{13}C at CH_3 carbons (46.87%), CH_3 signals due to the initiator fragment could be clearly observed among the monomer unit signals. Relative peak intensity measurements gave an $\bar{M}_n$ of 54 500, assuming

an average number of initiator fragments per polymer molecule of 1.1. Moad *et al.*[70] claimed that the accuracy of end-group analysis for polystyrene prepared with $^{13}C{=}O$-labelled BPO was 10%.

^{2}H-, ^{15}N- or ^{19}F-labelled initiators are also used to study the initiation step in radical polymerization and copolymerization. ^{2}H NMR may suffer from lower sensitivity, broadness of signals and smaller chemical shift ranges than ^{13}C NMR. However, there are several advantages of ^{2}H NMR spectroscopy in end-group analysis:[71–73] (1) the preparation of ^{2}H-labelled initiators such as AIBN-d_{12} is easier and/or less expensive than that of initiators enriched with other isotopes such as ^{3}H, ^{13}C, ^{14}C or ^{15}N, and also than the preparation of totally deuterated monomers; (2) the natural abundance of deuterium is so small that the NMR signals for ^{2}H-enriched groups in a polymer are hardly affected by "background" signals due to contaminants and/or the remainder of the polymer molecules; and (3) the much smaller spin-lattice relaxation times of the ^{2}H nucleus permits shorter duration of observed pulses and a larger number of scans, partly compensating for the lower sensitivity. The high reliability of quantitative analysis by ^{2}H NMR was proved by using a partially deuterated anionic initiator[73] as described in Section 3.2.2.

The chemical shift range of ^{19}F NMR is so large that more detailed structural information around the end-group can be obtained with ^{19}F-labelling of initiator.[74,75] ^{15}N-labelled AIBN was used for the polymerization and copolymerization of MMA and styrene.[71]

3.2.1. Radical polymerization and copolymerization

Moad *et al.*[70] have prepared polystyrene using BPO 90% enriched at the carbonyl carbon and analysed benzoyl carbonyl carbon signals by referring to ^{13}C NMR data for various benzoate esters. They found that at least four types of benzoyloxy groups were attached to the polymer:

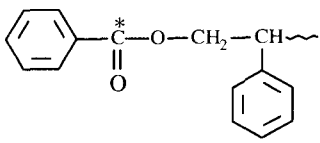

(166.2, 166.3 ppm)
(a) Tail addition

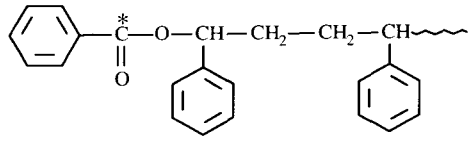

(165.6 ppm)
(b) Head addition

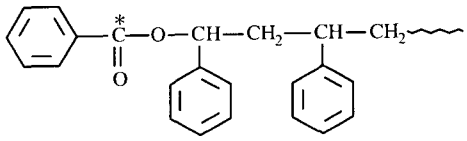

(165.3 ~ 165.5 ppm)
(c) Transfer to BPO or primary radical termination

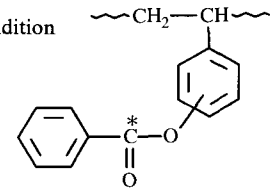

(164.8 ~ 165.0 ppm)
(d) Transfer to polymer

Structure (c) forms via chain transfer to BPO or primary radical termination and thus its amount increases with increasing concentration of BPO (14% of the total end-groups at $[I]_0 = 0.1$ M). Structure (d) was detected in the polystyrene formed at high conversion (80%), and there were more than two benzoyloxy groups per chain.

Polystyrene formed at 8% conversion with $[I]_0 = 0.4$ M was found to contain 1.7 benzoyloxy groups per chain. Most of these were introduced via regular tail addition (a) but 5% of them via head addition (b). The end-group derived from the phenyl radical, which could not be detected in this method, does not exceed 4% of the end-groups and thus the meanings of the results are hardly affected by the presence of the phenyl end-group.

AIBN enriched with ^{13}C at the α-position was also used for styrene polymerization.[43,76] Initiator fragments detected by ^{13}C NMR were all due to tail addition. A suspected initiation from the keteneiminyl radical $(CH_3)_2C{=}C{=}N$ was denied by the absence of signals ascribable to the corresponding fragment. The number of AIBN fragments per chain were $1.7 \sim 1.8$.[43] Polystyrene formed at 60 or 85% conversion was found to contain methacrylonitrile units, which should have been introduced by the copolymerization of methacrylonitrile formed through disproportionation of the primary radicals of AIBN.

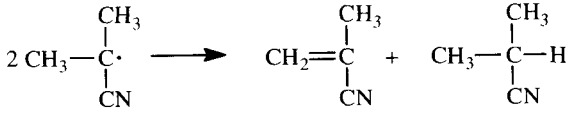

The number of initiator fragments could also be determined by ^2H NMR analysis of polystyrene prepared with AIBN-d_{12}.[42] The value (1.65) is consistent with those obtained by other methods,[42,43,70] and suggests that the disproportionation is not of negligible importance in the radical polymerization of styrene.

The deuterium-labelled initiator method was also applied to the polymerization of macromonomer to determine the number of initiator fragments in a polymacromonomer chain (N) and initiator efficiency (f).[77] Isotactic and syndiotactic PMMA macromonomers having a styrene group as polymerizable function were polymerized with AIBN-d_{12} in toluene at 60°C and the resultant polymacromonomers were analysed by ^2H NMR spectroscopy (Table 8). The N values were less than unity ($0.50 \sim 0.72$), indicating some kind of chain transfer reaction in the radical polymerization of macromonomer. The f values were $0.18 \sim 0.28$ and much smaller than those for styrene polymerization ($0.5 \sim 0.7$). The isotactic macromonomer gave larger N and f values than the syndiotactic

Table 8. End-group analysis of poly(PMMA macromonomer) prepared with AIBN-d_{12} in toluene at 60°C for 24 h.

	Macromonomer (mmol)	AIBN-d_{12} (mmol)	Toluene (ml)	Conversion[a] (%)	M_n[b]	$\frac{M_w}{M_n}$[b]	N[c]	f[d]
Isotactic	0.350	0.0174	6.1	42	55 700	1.70	0.72	0.28
Syndiotactic	0.765	0.0383	13.6	49	69 600	1.18	0.65	0.22
Syndiotactic	0.0541	0.00270	0.84	46	124 000	1.31	0.50	0.18

From Ref. 77.

[a]Determined by GPC.

[b]Determined by GPC-LALLS.

[c]Number of initiator fragment per polymacromonomer determined by ^{2}H NMR spectroscopy.

[d]Initiator efficiency.

macromonomer, suggesting that the tacticity affects the reaction pathway, probably owing to the difference in chain mobility between isotactic and syndiotactic PMMAs.

Substitution of fluorine for hydrogen in the initiator molecule can sometimes be a useful method of labelling. PMMA formed with *p*-fluorobenzoyl peroxide showed two ^{19}F NMR signals 10 ppm apart, which corresponded to *p*-fluorobenzoyloxy and *p*-fluorophenyl groups.[74] The ratio of the amounts of these groups were close to the corresponding ratio in the case of BPO (see Section 3.1.1).

Radical polymerization of vinyl acetate was carried out in benzene at 60°C with AIBN ^{13}C-labelled at the CN carbon.[78] The polymer showed CN carbon signals at 124.3 and 122.4 ppm due to the end-groups incorporated through tail and head additions, respectively:

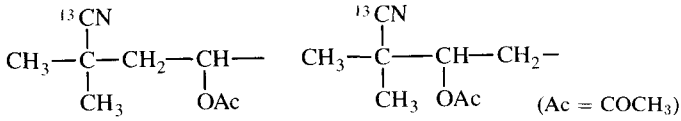

Tail addition Head addition

The results indicated that the contribution of head addition in the initiation was 20%.

When vinyl chloride was polymerized with AIBN-^{13}CN, the polymer formed exhibited CN signals due not only to the initiating chain end-group but also to the in-chain unit (methacrylonitrile unit). The latter was incorporated by the copolymerization of methacrylonitrile formed through disproportionation of the primary radicals.[79] The authors claimed that ^{14}C-labelling could not distinguish these two types of initiator residues and thus leads to misunderstanding of the polymerization mechanism.

Application of labelled initiator in copolymerization provides information on relative reactivities of comonomers A and B toward the initiator radical in the initiation process.

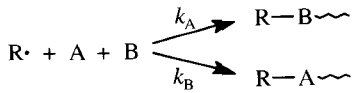

(R·: primary radical) (3)

Bevington *et al.* have investigated the end-groups of various copolymers prepared with $^{13}CH_3$-labelled AIBN. When the chemical shifts of the signals

due to the $^{13}CH_3$ groups attached to monomer units A and B differ from each other, the relative abundance of R–A– and R–B–, N_A/N_B, can be determined. From equation (4) the relative rate constant of initiation, k_A/k_B, can be estimated:

$$\frac{k_A}{k_B} = \frac{N_A[B]}{N_B[A]} \tag{4}$$

where [A] and [B] are the initial concentrations of monomers A and B. The relative rate constants for various monomers could be estimated as follows: styrene (1.0), acenaphthylene (2.24),[80] methyl vinyl ketone (1.34),[81] α-methylstyrene (0.95),[82] methyl isopropenyl ketone (0.78),[81] MMA (0.56),[83] α-methoxystyrene (0.47),[84] methacrylonitrile (0.34),[83] ethyl acrylate (0.30)[72] and vinyl chloride (0.041).[85]

Moad *et al.* reported that, for the copolymer of MMA and styrene prepared with ^{13}C=O-labelled BPO, C=O carbon showed clear splittings not only due to the difference of the first monomer unit but also due to the second monomer unit.[86] Detailed analysis of the sequences may afford monomer reactivity ratios at the beginning of the copolymerization.

Tirrell and co-workers studied copolymerization of styrene (S) and acrylonitrile (A) using 1,1′-azobis(1-phenylethane)-α,α'-^{13}C, which generates a monomeric styrene radical, 1-phenylethyl radical:[87]

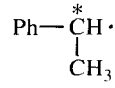

Assuming the initiation reaction with this radical is a propagation step involving the styrene radical, the relative initiation rate constant k_S/k_A may represent the monomer reactivity ratio $k_{SS}/k_{SA} = r_S$:

$$\frac{k_S}{k_A} = \frac{k_{SS}}{k_{SA}} = r_S = 0.20 \pm 0.02 \tag{5}$$

A similar experiment with 1,1′-azobis(1-cyanoethane)-α,α'-^{13}C generating radical

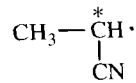

provided the reactivity ratio r_A:[88]

$$\frac{k_S}{k_A} = \frac{k_{AS}}{k_{AA}} = r_A = 0.12 \pm 0.03 \tag{6}$$

The obtained values are close to the reactivity ratios r_{SS} (0.23) and r_{SA} (0.09) based on the penultimate model, rather than those of the terminal model ($r_A = 0.05$, $r_S = 0.33$).[89] This means that the two radicals have similar reactivities to the propagating radicals $\sim\sim$ SS· and $\sim\sim$ SA·, respectively.

1,1′-Azobis(1-phenylethane)-α,α'-^{13}C was also used to study the reactivities of styrene, methyl acrylate, methyl methacrylate, methyl isopropenyl ketone, methyl vinyl ketone, and 2-vinylpyridine towards the radical

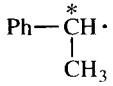

at 100°C using acenaphthylene as the reference monomer. The relative reactivities match their relative reactivities towards polystyrene radical as deduced from monomer reactivity ratios for the copolymerizations with styrene.[90]

trans-Stilbene has been known to exhibit high reactivity towards the bezoyloxy radical.[91] When MMA or styrene was polymerized at 60°C with ^{13}C=O-labelled BPO as initiator in the presence of stilbene at low concentration, it was confirmed from end-group analysis that many of the end-groups in the copolymer consist of benzoyloxy groups attached to the stilbene units, while the total incorporation of stilbene was small.[92,93] For example, in the copolymer formed at the ratio MMA/stilbene = 100, 40% of end benzoyloxy groups attached to stilbene units.[92] ^{19}F NMR spectroscopy was also used to investigate this peculiar behaviour of stilbene using *p*-fluorobenzoyl peroxide and *p*-fluorostilbene.[75]

3.2.2. Anionic polymerization

Polymerization of MMA with *t*-C_4H_9MgBr in toluene at low temperature proceeds in a living manner to give highly isotactic PMMA which contains exactly one *t*-C_4H_9 group at its chain end. By taking this synthetic advantage, accuracy of ^{2}H NMR analysis in regard to signal intensity of end-group has been examined using a partially deuterated *t*-butylmagnesium bromide, *t*-$CH_3(CD_3)_2MgBr$:[73]

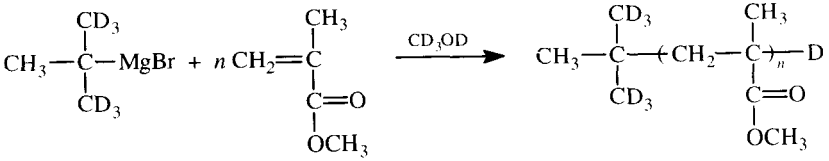

Analysis of the deuterated initiator fragments was carried out for the solution of a known amount of the polymer containing an intensity standard. the M_n of the PMMA can be calculated from the equation $M_n = 6c/s \cdot R$, where c is the concentration (g sample/g solvent) of the polymer sample solution, s is the concentration (g ^{2}H/g solvent) of a ^{2}H-labelled compound added to the sample solution as an intensity standard, and R is the relative intensity of the ^{2}H NMR signal of interest to that of the standard. The principal feature of this experiment is that the degree of polymerization, p.p. of the identical sample can also be determined by means of ^{1}H NMR spectroscopy from the intensity ratio of the ^{1}H NMR signals due to the $CH_3(CD_3)_2C$ and the CH_3O groups.

Figure 11 shows the 500-MHz ^{1}H and 61.3-MHz ^{2}H NMR spectra of the

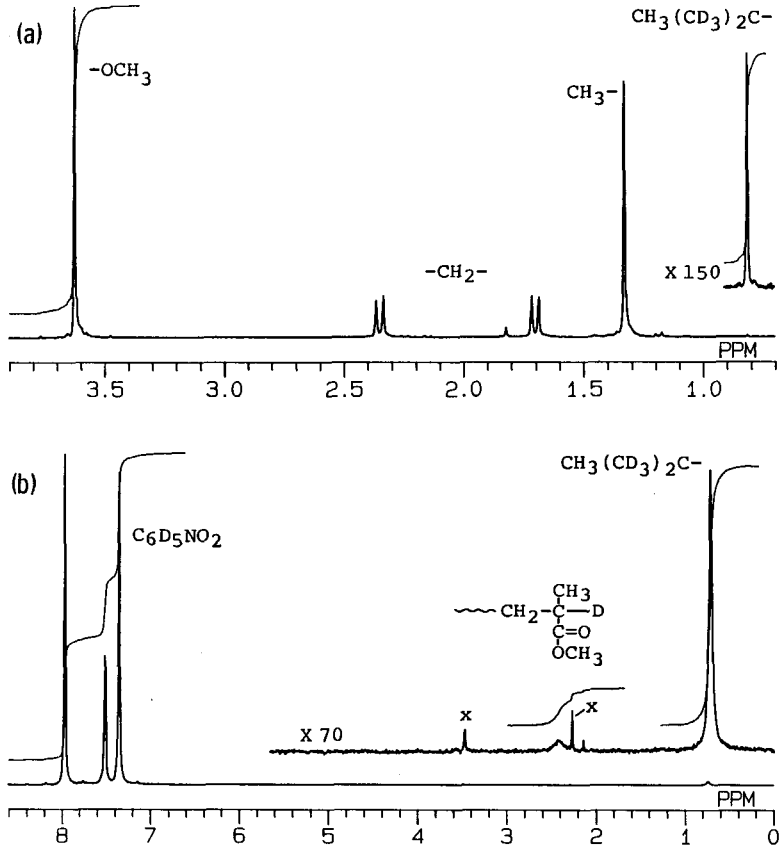

Fig. 11. ^{1}H and ^{2}H NMR spectra of PMMA (PMMA-23K) prepared with *t*-butylmagnesium-d_6 bromide in toluene at −78°C. (a) 500-MHz ^{1}H NMR spectrum measured in nitrobenzene-d_5 at 110°C; (b) 61.3-MHz ^{2}H NMR spectrum measured in nitrobenzene/nitrobenzene-d_5 (95/5) at 110°C. (From Ref. 73.)

PMMA prepared with $CH_3(CD_3)_2CMgBr$ in toluene at −78°C. In the ^2H NMR spectrum, signals at 0.83 and 2.44 ppm were assigned to $CH_3(CD_3)_2C$ and methine deuterium, respectively. Those appearing at 7.3–8.0 ppm are attributable to nitrobenzene-d_5 added as an intensity standard. The $\bar{M}_n$ of the polymer was determined as 23 890 on the basis of the ^2H NMR spectrum. In the ^1H NMR spectrum of the same polymer, the signals due to the $CH_3(CD_3)_2C$ and CH_3O groups were observed at 0.823 and 3.636 ppm, respectively, and the M_n was calculated to be 22 930. The $\bar{M}_n$ determined by VPO was 22 280. These results clearly indicate good accuracy of ^2H NMR measurement.

Relatively short NMR relaxation times of ^2H nuclei (e.g. ^2H-T_1 = 0.173 s and ^1H-T_1 = 1.38 s, for the $CH_3(CD_3)_2C$ group in PMMA measured in nitrobenzene-d_5 at 110°C) allows shorter repetition time, and the lower sensitivity of ^2H nuclei can be partly compensated by a larger number of accumulations for a certain period of time.

Transfer agent can be incorporated into the polymer chain end. Thus deuterium labelling of transfer agent provides the opportunity to study reaction mechanism through end-group analysis by ^2H NMR. Condensates of organotin and alkyl phosphate such as condensate of dibutyltin oxide (Bu_2SnO) and tributyl phosphate (Bu_3PO_4) are air-stable, efficient initiators for ring opening polymerization of oxirane compounds.[94] The addition of methanol into this polymerization has been considered to cause frequent transfer reactions to give low molecular weight polymers. When a small amount of CD_3OD was added to the polymerization of propylene oxide with a Bu_2SnO–Bu_3PO_4 (1/2) condensate, the obtained polymer showed two ^2H NMR signals due to CD_3O groups attached to the chain ends in different manners, α-cleavage and β-cleavage of the oxide ring:

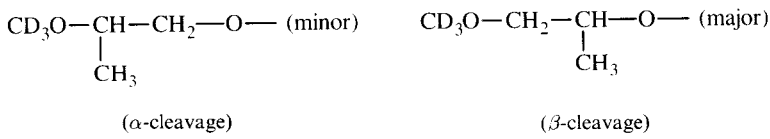

(α-cleavage) (β-cleavage)

The polymerization itself proceeds almost exclusively in the β-cleavage manner. The results of end-group analysis showed that the addition of methoxide ion to propylene oxide preferred the β-cleavage but in a less-specific way than that of the propagating oxide anion.[95]

End-labelling of the active centres with diphenyl chlorophosphate, combined with ^{31}P NMR spectroscopy, was shown to be an effective method for the determination of structure and concentration of the active species in the polymerization of several oxirane compounds.[96–98] The chemical shifts of ^{31}P signals from the diphenylphosphoryl end-groups are sensitive to the structure of polymer chain end to which it is attached. Thus the ^{31}P NMR spectrum provides information whether the propagating anion is secondary or primary. A similar

method using chlorodiphenylphosphine was recently utilized to distinguish butyllithium and lithium butoxide.[99]

Hogen-Esch and co-workers have studied the stereochemistry of anionic polymerization of vinylpyridines and related monomers. They applied end-labelling of living anion of 2- and 4-vinylpyridines and 2-isopropenylpyridine with $^{13}CH_3I$ to investigate the chain-end stereochemistry.[100,101] Triad tacticities at the chain end, $\sim\sim mm$, $\sim\sim mr$, $\sim\sim rm$ and $\sim\sim rr$, were determined from split signals of the $^{13}CH_3$ end-groups. Stereochemical assignments are based on the spectra of $^{13}CH_3$-end-labelled oligomers of known stereochemistry (see Section 5.1).

3.2.3. Ziegler polymerization

In Ziegler–Natta catalysts comprising transition metal compounds and coinitiators such as alkylaluminium, the active species consists of metal–carbon bonds formed by the alkylation of the transition metal with the coinitiator. Initiation occurs by monomer insertion to the metal–carbon bond. Therefore, labelling of coinitiator may provide an opportunity to investigate the structure of end-groups and thus the initiation mechanism.

Zambelli *et al.* studied the stereochemistry of the initiation step in propylene polymerization with an isotactic-specific Ziegler-type catalyst, δ-$TiCl_3$–AlR_3–ZnR_2, where R is a ^{13}C-labelled methyl or ethyl group.[102–104] ZnR_2 promotes transfer reaction to give a rather low molecular weight polymer and facilitates end-group analysis.

With δ-$TiCl_3$–$Al(^{13}CH_3)_3$–$Zn(^{13}CH_3)_3$, initiation occurs exclusively in primary insertion and thus the polymer formed contains an isopropyl group at its initiating chain end.

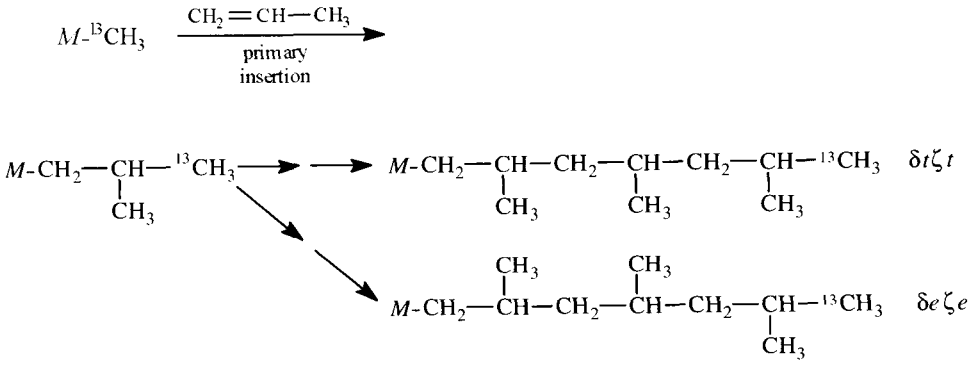

The terminal $^{13}CH_3$ in the isopropyl group may show four signals due to triad tacticity at the chain end.[103–105] As seen in the spectrum shown in Fig. 12b, only two peaks due to the terminal $^{13}CH_3$ are observed at 20.69 and 21.76 ppm in

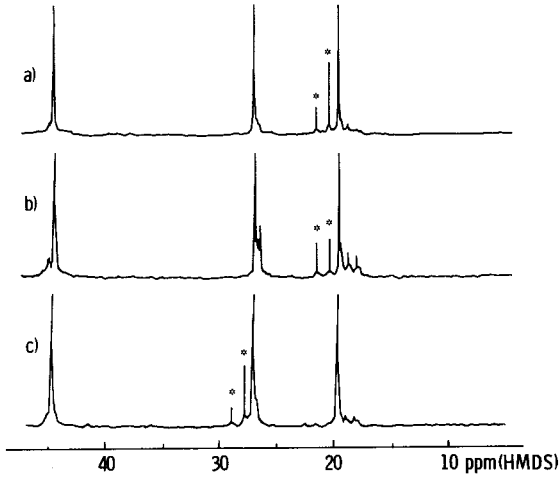

Fig. 12. ^{13}C NMR spectra of boiling heptane-soluble and boiling pentane-insoluble fraction of polypropylene prepared with (a) δ-$TiCl_3$–$Al(^{13}CH_3)_2I$; (b) δ-$TiCl_3$–$Al(^{13}CH_3)_3$–$Zn(^{13}CH_3)_2$; (c) δ-$TiCl_3$–$Al(^{13}CH_2CH_3)_3$–$Zn(^{13}CH_2CH_3)_2$. The asterisked resonances are due to ^{13}C-enriched carbons of the end-group. (From Ref. 103.)

equal intensity. The former ($\delta t\zeta t$) is assigned to a *threo* methyl group relative to both the methyl groups in the second and third monomer units, and the latter is assigned ($\delta e\zeta e$) to an *erythro* methyl group. The results indicate non-stereoselectivity in the initiation step with δ-$TiCl_3$–$Al(^{13}CH_3)_3$–$Zn(^{13}CH_3)_3$ and high stereoselectivity in the third monomer insertion. The non-selectivity in the initiation step was explained by the similar steric bulkiness of the methyl and chlorine group bonded to Ti, leading to a smaller asymmetric environment around the active sites.[103]

When $Al(^{13}CH_2CH_3)_3$ and $Zn(^{13}CH_2CH_3)_3$ were used as coinitiator, $^{13}CH_2CH_3$ signals in the 2-methylbutyl end-group were observed at 27.72 and 28.82 ppm, which correspond to the configurations of $\delta t\zeta t$ and $\delta e\zeta e$, respectively (Fig. 12c). The higher intensity of the signal of $\delta t\zeta t$ indicates the higher content of isotactic diad at the chain end.[103] The steric difference between ethyl and chlorine groups produces an asymmetric environment around Ti, which should be responsible for the higher stereoselectivity. The correlation between in-chain tacticity and *erythro* selectivity [*e*] was found for the polymerization of propylene with various ^{13}C-labelled catalyst systems as shown in Table 9.[106] TiI_3–$Al(^{13}CH_3)_3$ exhibits *erythro* selectivity [*e*] of 0.67.[107] Much higher *erythro* selectivity of δ-$TiCl_3$–$Zn(C_6H_5)_2$ was evidenced by the C-1 carbon signals of the end phenyl groups.[108] The *erythro* selectivity also depends on the structure of olefin monomers; with $TiCl_3$–$Al(^{13}CH_2CH_3)_3$ initiator, propylene [*e*] = 0.77, 1-butene 0.69 and 1-pentene 0.66.[109] Investigations along these lines with $TiCl_3$–$Al(^{13}CH_3)_3$ have been carried out for 3,7-

Table 9. *Erythro* selectivity [*e*] in the initiation process and main chain tacticity of propylene polymerization.

Catalyst system			Tacticity (%)			[*e*]	P_{DD}[a]
Ti compound	Al alkyl	Zn alkyl	*mm*	*mr*	*rr*		
δ-$TiCl_3$	$Al(^{13}CH_3)_2Cl$	—	76	12	12	0.50	0.92
δ-$TiCl_3$	$Al(^{13}CH_3)_3$	$Zn(^{13}CH_3)_3$	79	11	10	0.52	0.93
δ-$TiCl_3$	$Al(^{13}CH_3)_2I$	—	82	10	8	0.75	0.94
δ-$TiCl_3$	$Al(^{13}CH_2CH_3)_3$	$Zn(^{13}CH_2CH_3)_3$	91	5	4	0.79	0.97
$TiCl_4$–$MgCl_2$[b]	$Al(^{13}CH_2CH_3)_3$	$Zn(^{13}CH_2CH_3)_3$	89	6	5	0.80	0.96

From Ref. 106.

[a] Probability of D insertion on the D-preferring sites.

[b] In the presence of ethyl benzoate.

dimethyl-1-octene ($[e] = 0.71$)[110] and (*RS*)- or (*S*)-3-methyl-1-pentene ($[e] = 0.67$).[111] For the latter monomer, the effect of the chirality in the side-chain of the monomer on the main-chain chirality was also investigated in detail.

One of the recent advances in coordination polymerization is highly active and stereospecific homogeneous catalyst systems as demonstrated by the excellent works of Ewen[112] and Kaminski.[113] Zambelli and co-workers studied the structure of end-groups in isotactic polypropylene and poly(1-butene) prepared with homogeneous catalysts based on ethylene bisindenyldimethyltitanium and methylalumoxane in the presence of $Al(^{13}CH_3)_3$ or $Al(^{13}CH_2CH_3)_3$ as transfer agent.[114] The results were very similar to those obtained for polymerization with heterogeneous Ziegler–Natta catalysts, that is, insertion of 1-butene on Ti–$^{13}CH_3$ bonds was partially enantioselective whereas insertion of propylene was not enantioselective, and insertion of propylene on Ti–$^{13}CH_2CH_3$ bonds was more enantioselective than insertion on Ti–$^{13}CH_3$ bonds. Stereocontrol of the polymerization by these homogeneous catalysts is thus based on the chirality of Ti sites.[114]

The ^{13}C-labelling method for the analysis of the initiation step was applied to the study of the effect of Lewis bases on the polymerization of propylene with $MgCl_2$-supported $TiCl_4$–$Al(^{13}CH_2CH_3)_3$.[115] Addition of ethyl benzoate or bis(2-ethylhexyl)phthalate increased isotactic productivity, which was accompanied by an increase of $[e]$. The most significant increase in isotacticity was obtained in the presence of phenyltriethoxysilane; *mm* 97%, and $[e]$ 0.89. The results evidenced the direct participation of the Lewis base in the formation of the isotactic-specific sites in the initiation step. The effect of activation procedure of supported catalyst, $MgCl_2$–$TiCl_4$–$Al(^{13}CH_2CH_3)_3$, was also studied in a similar manner.[116] The effects of triethylamine and 2,2,6,6-tetramethylpiperidine on stereocontrol in the polymerization of propylene with δ-$TiCl_3$–$Zn(^{13}CH_2CH_3)_2$ was also examined.[117]

Copolymerization of ethylene and propylene was studied using δ-$TiCl_3$–$Al(^{13}CH_3)_3$–$Zn(^{13}CH_3)_2$.[118] The chemical shift of the $^{13}CH_3$ end-group was sensitive to the sequences of the three monomer units at the chain end (Fig. 13). The monomer selectivity at the first, second and third addition steps in this copolymerization could be estimated from the relative abundances of these end-groups as follows; $k_1/k_2 = 4 \sim 4.4$, $k_{11}/k_{12} = 26 \sim 29$, $k_{21}/k_{22} = 25 \sim 27$, $k_{221}/k_{222} = 27 \sim 35$ (subscripts 1 and 2 represent ethylene and propylene, respectively). Except for the initiation step, the remaining addition steps exhibit high selectivity for ethylene. Monomer selectivities of the same catalyst have been determined for various pairs of α-olefins.[119] The relative reactivity is found to decrease with increasing bulkiness of the

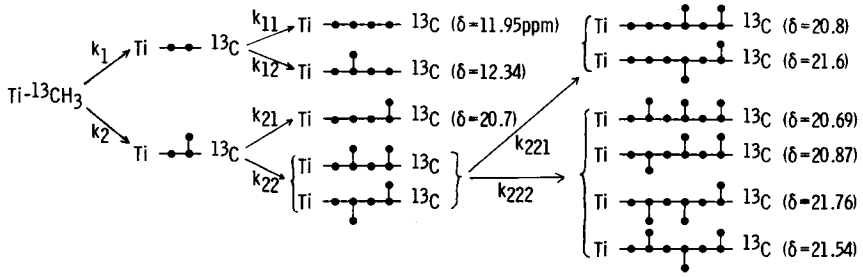

Fig. 13. Assignments of $^{13}CH_3$ end-groups in ethylene–propylene copolymer prepared with δ-$TiCl_3$–$Al(^{13}CH_3)_3$–$Zn(^{13}CH_3)_2$. (From Ref. 118.)

monomer, suggesting the importance of the steric factor in the coordination of the monomers to the active sites. Recently, Locatelli *et al.* noted the inhomogeneity of isotactic-specific sites in the copolymerization of propylene and 1-butene with $TiCl_3$–$Al(^{13}CH_2CH_3)_3$.[120,121] The fractionated copolymers were analysed by ^{13}C NMR in regard to composition, tacticity and chain-end stereochemistry. Chain-end m/r ratio observed from $^{13}CH_2CH_3$ signals was found to change from 1.6 to 8, accompanied by an increase in isotacticity of the copolymer.

In the polymerization of propylene with VCl_4–$(^{13}CH_3)_2AlCl$ at $-78°C$, the propagation reaction proceeds in a secondary insertion mechanism to give a syndiotactic polymer, as examined in terms of end-group structure.[122] The ^{13}C NMR spectrum of the polymer shows four resonances of comparable intensities at 20.60, 20.79, 21.46, and 21.69 ppm, all of which are assignable to $^{13}CH_3$ of the isobutyl group in different stereochemical configurations but not to $^{13}CH_3$ of the *sec*-butyl group expected for secondary insertion.

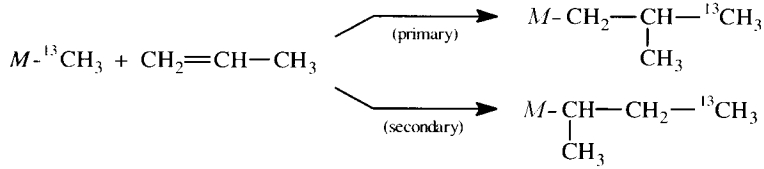

The results suggest that the insertion of propylene to V–$^{13}CH_3$ bonds is primary and that the subsequent monomer addition proceeds in a stereo-irregular fashion.[122]

3.3. Direct analysis of end-groups and defects in vinyl polymers

3.3.1. Poly(methyl methacrylate)

Propagating radicals in the polymerization of methyl methacrylate (MMA) predominantly terminate through disproportionation as described in Section 3.2.1. The reaction should give two types of chain-end structures: saturated and unsaturated terminals.

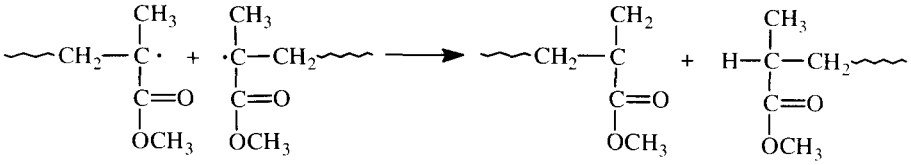

The ^{1}H NMR spectrum of PMMA prepared with AIBN at 60°C showed vinylidene proton signals at 5.4 and 6.14 ppm[38] (Fig. 14). No inner olefin proton signal was observed. The intensity measurement indicated that 36% of the polymer molecules contained the unsaturated terminal. The thermal stability of radically prepared PMMA was discussed in relation to the

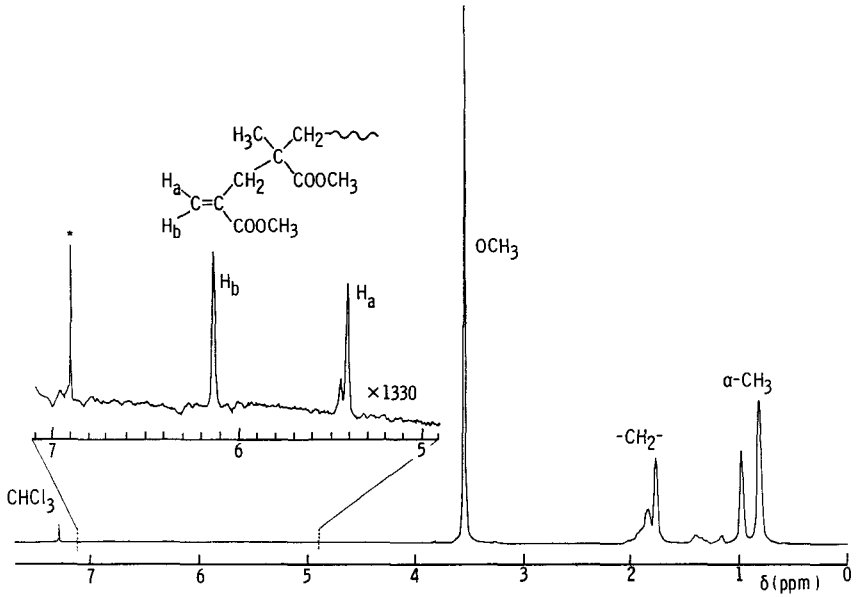

Fig. 14. ^{1}H NMR spectrum of PMMA prepared with AIBN in bulk at 60°C ($CDCl_3$, 55°C, 270 MHz). * ^{13}C satellite band of $CHCl_3$. (From Ref. 38.)

unsaturated end-group or head-to-head linkage along the chain.[39,123] Kashiwagi *et al.* reported that thermal degradation of the PMMA proceeds in three steps of weight loss: the least stable step is initiated by scissions of head-to-head linkages, the second step by scissions at the chain-end initiation from the unsaturated end-groups, and the most stable step by random scission within the main chain.[39] However, Meisters *et al.* did not observe the least stable step of degradation using PMMA with head-to-head linkage in the middle of the chain.[123]

Cobalt tetraphenylporphyrin complex promotes a chain-transfer reaction in the radical polymerization of MMA to give an MMA oligomer with vinylidene unsaturation at the chain end.[124] An alternative method of introducing the terminal unsaturation was disclosed by Meijs *et al.*[125] Substituted allylic sulphides are used as chain transfer agents in which sulphide groups act as leaving group as follows:

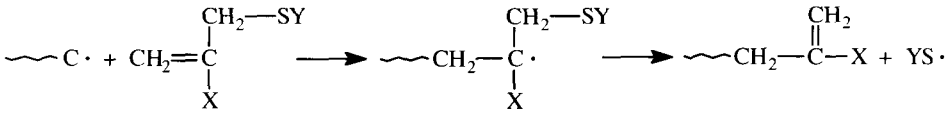

(X = COOEt, Ph, CN)

By selecting the sulphide group SY, various difunctional PMMAs and polystyrenes were prepared. The end-functionality determined by ^{1}H NMR scattered from 0.8 to 1.4.[125b]

Independently, Yamada and Otsu found a similar addition-fragmentation reaction of α-bromomethylacrylates, which produces polymers with bromomethyl and vinylidene groups at both ends:[126,127]

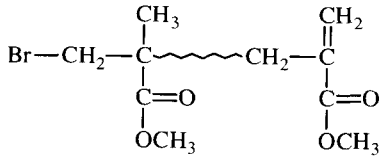

3.3.2. Poly(vinyl acetate)

It has long been known that vinyl acetate polymerizes more rapidly in ethyl acetate than in aromatic solvents such as benzene.[128] One explanation

for this phenomenon is that the benzene molecule copolymerizes with vinyl acetate, which causes a decrease in the apparent rate of polymerization.[129] Recently, Kamachi and co-workers attributed the rate decrease in aromatic solvents to the formation of a complex between the propagating radical and the π-electron system of the solvent molecule.[130] To clarify the possibility of copolymerization of aromatic solvents, poly(vinyl acetate)s prepared with AIBN in benzene, chlorobenzene and ethyl acetate were analysed for terminal groups by ^{1}H NMR spectroscopy.[131] The results are shown in Table 10.

The polymer formed in benzene showed a small signal at 7.31 ppm, whose ^{1}H-T_1 was 0.72 s and assigned to a phenyl group attached at the chain end. The intensity measurement of the signal showed that only 15% of the polymer chain contained one phenyl group at the chain end. The possibility of benzene copolymerization was thus neglected. The polymer formed in chlorobenzene was found to contain 0.28 of the solvent fragment per polymer molecule. This amount is about twice the amount in the polymer formed in benzene, and almost corresponds to the fact that the ratio of the chain-transfer constants of chlorobenzene and benzene is 2.82,[132] indicating the incorporation of the aromatic molecule through the chain-transfer reaction.

The numbers of AIBN fragment are larger than unity for the polymers formed in benzene and chlorobenzene, but that for the polymer formed in ethyl acetate is only 0.42, indicating the higher frequency of transfer reactions in ethyl acetate. By counting the end-groups generated through reinitiation from the solvent radicals

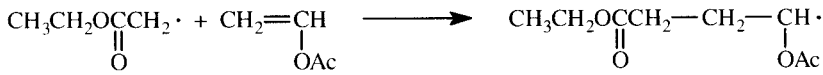

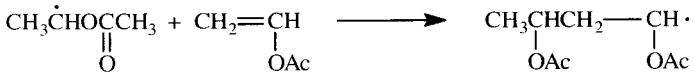

those formed by the termination reaction of the propagating radicals

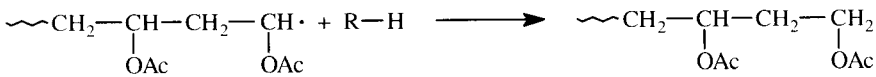

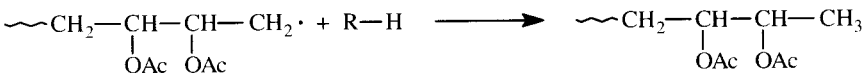

Table 10. Analysis of the terminal group in poly(vinyl acetate) prepared with AIBN at 60°C in benzene, chlorobenzene and ethyl acetate.

Solvent	$\bar{M}_n$ (VPO)	Terminal group (mol/mol)[a]		
		AIBN	Solvent	$CH_3COOC\underline{H}_2CH_2-$
Benzene	15 700	1.24	0.15	0.56
Chlorobenzene	12 100	1.20	0.28	0.41
Ethyl acetate	23 900	0.42	more than 0.43	1.24

From Ref. 131.

[a]Represents the number of terminal groups per polymer molecule.

and the AIBN fragment introduced at the chain end through the initiation reaction, the total end-groups per molecule amounts to 2.73. Thus the polymer should have at least 0.7 branches per polymer molecule. The total numbers of end-groups in the polymers formed in benzene and chlorobenzene are 1.95 and 1.89, respectively, indicating that the polymers have no branching. These results are consistent with the explanation that the propagating radicals in aromatic solvents are stabilized through π-complex formation with the aromatic rings.

The end-groups and in-chain defects in poly(vinyl alcohol) have been studied thoroughly.[133–138] The number of 1,2-glycol units can be determined by ^{13}C[136–138] and ^1H NMR[138] spectroscopy. The 1,2-glycol unit at the chain end is distinguished from that in the chain by the 500-MHz ^1H NMR spectrum. The analysis for the polymer obtained from poly(vinyl acetate) prepared at 60°C indicates that the contents of the end-chain and in-chain 1,2-glycol units are 0.06 and 1.7 mol %. This means that chain transfer from the primary radicals occurs every 50 times of head addition.[135]

3.3.3. Poly(vinyl chloride)

Poly(vinyl chloride) usually contains various defects such as branching, regio-irregular units and unsaturated units, because of the high reactivity of the propagating radical.[139] Besides direct analysis by ^1H NMR,[140–142] ^{13}C NMR analysis after reduction with Bu_3SnH provides structural information on branching and end-groups by referring the spectral data of polyethylene.[143–147]

1,2-Dichloride linkage at the chain end, $ClCH_2-CHCl\sim\sim\sim$, can be identified by ^1H NMR spectra of low molecular weight extracts, the signal of which resonating at 3.65 ppm can be distinguished from the signals due to the $ClCH_2-CH_2\sim\sim\sim$ group (3.8 ppm).[140] Almost all the 1,2-dichloride linkages were found to exist at the chain end, and should form through reinitiation reaction by chlorine radical:

$$Cl\cdot + CH_2{=}CHCl \rightarrow ClCH_2-CHCl\cdot \rightarrow ClCH_2-CHCl-CH_2-CHCl\cdot$$

The unsaturated chain end-group, $ClCH_2-CH=CH-$, is identified by ^1H NMR; the $ClCH_2$ proton signal resonates at 4.05–4.10 ppm. Its formation is explained by the following reaction scheme: as a head-to-head addition occurs, the radical isomerizes to a secondary radical, which releases a chlorine radical to form the allylic end-group.[139]

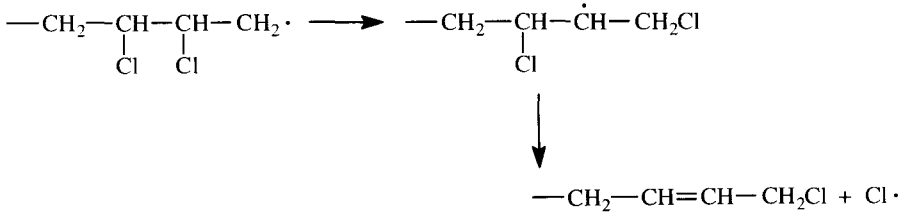

Transfer to monomer is an important process in the radical polymerization of vinyl chloride so that the number of initiator fragment in a polymer chain is less than unity. For example, poly(vinyl chloride)s prepared with AIBN in 1,2-dichloroethane at 40°C were found to contain 0.17 ~ 0.34 AIBN fragments per chain from the ^{13}C NMR analysis of the polymer reduced with Bu_3SnH. The polymers also contained a CN group in the chain (0.025 ~ 0.12 per chain), suggesting the copolymerization of methacrylonitrile which was formed *in situ* or admitted as an impurity in the starting AIBN.[79]

3.3.4. Polyolefins

End-group analysis of polyolefins prepared with Ziegler-type catalysts can be performed for relatively low molecular weight samples. ^{13}C NMR spectra of isotactic polypropylene prepared with either racemic ethylenebis(4,5,6,7-tetrahydro-1-indenyl)dichlorozirconium or racemic ethylenediindenyldichlorozirconium and methylalumoxane showed the presence of vinylidene and *n*-propyl end-groups in equal amounts, indicating that the chain-transfer process mainly involved β-hydrogen abstraction from a regio-regular monomer unit followed by initiation of a new polymer chain on a metal–hydrogen bond via primary insertion.[148]

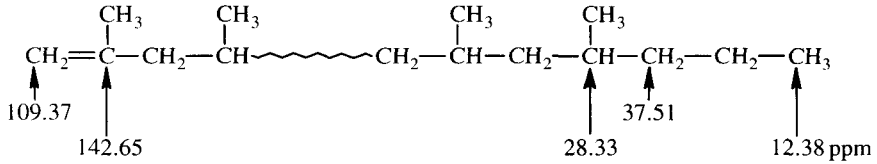

Homogeneous catalyst systems without methylalumoxane, which consists of $(CH_3)_3Al$, $(CH_3)_2AlF$ and group IV metallocenes, such

as (dicyclopentadienyl)diphenyltitanium, ethylenediindenyldichlorotitanium, ethylenediindenyldichlorozirconium or ethylenebis(4,5,6,7-tetrahydro-1-indenyl)dichlorozirconium, give isotactic polypropylene. The polymers obtained have *n*-propyl end-groups similar to the polymer obtained in the presence of methylalumoxane and the metallocenes.[149] The ^{13}C NMR spectra of the former polymers also showed signals due to two methyl groups of isobutyl end-group (20.55 and 21.80 ppm), which formed through chain transfer to $(CH_3)_3Al$:

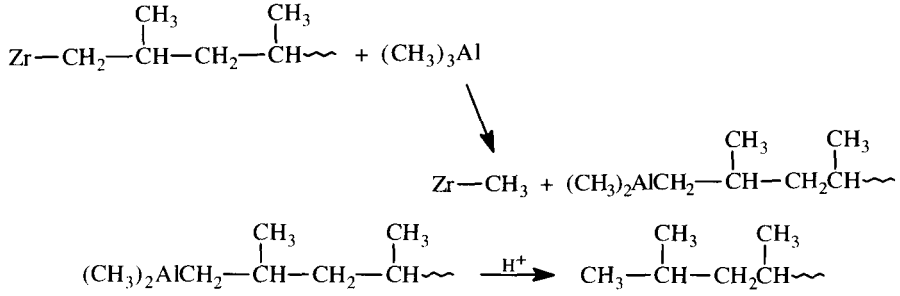

The splitting of the methyl signals occurs because of the presence of an asymmetric carbon in the neighbouring monomeric unit.

In his first article on soluble metallocene/methylalumoxane catalyst systems producing isotactic polypropylene,[112] Ewen reported the ^{13}C NMR analysis of the end-groups of the atactic polypropylene formed with bis(cyclopentadienyl)zirconium dichloride or bis(pentamethylcyclopentadienyl) zirconium and methylalumoxane. The polymer formed at 50°C contained *n*-propyl and vinylidene end-groups in 1 : 1 ratio, consistent with β-hydrogen elimination from the metal–primary carbon bond and subsequent reinitiation via primary insertion:

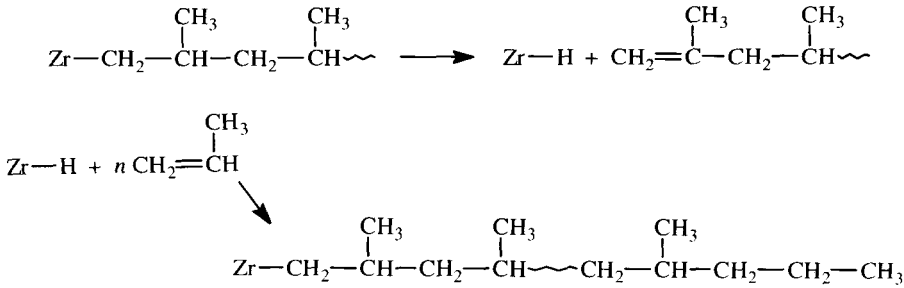

The chain end of a polypropylene formed at −30°C was exclusively isopropyl groups, which form through primary insertion of the monomer into the $Zr-CH_3$ bond both in the initiation and in the termination of the primary chain end.

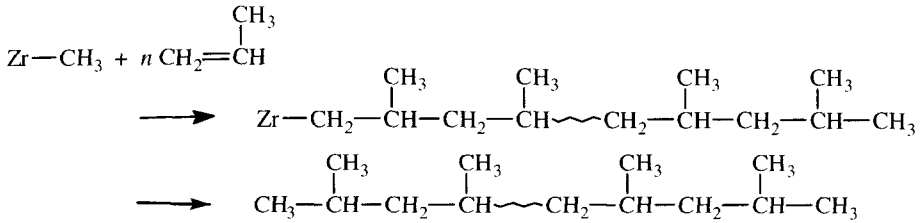

Polypropylene prepared by δ-$TiCl_3$–$(C_2H_5)_2AlCl$ in the presence of hydrogen was found to contain four types of end-groups;[150] two of which – propyl (45.9%) and ethyl (4.1%) ends – are produced by the initiation reactions with Ti–H and Ti–C_2H_5, respectively, and the other two – methyl (40.1%) and butyl (9.9%) ends – which are produced by the transfer reaction of primary and secondary chain ends to hydrogen. The reason why the transfer reaction of the secondary chain end to hydrogen forms a butyl group is that the secondary insertion occurred at the primary chain end, mostly followed by the chain-transfer reaction:

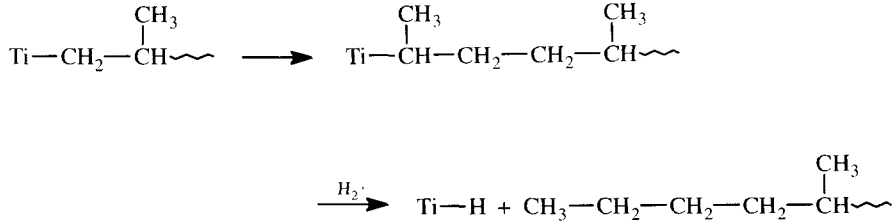

The split peaks of the carbons in the end-groups due to triad and tetrad stereosequences were assigned by the chemical shifts calculation via the γ-effect. The tetrad fractions in the initiating chain end were analysed for the heptane-soluble fraction ($\bar{M}_n = 1000$) in terms of the two-sites model.[151,152] The results showed that the steric controls in the initiation process were as strong as those in the propagation step.

Polymerization of propylene with vanadium tris(acetylacetonate)–$(C_2H_5)_2Cl$ at low temperature proceeds in a living manner to give a syndiotactic polymer.[153] A V–C bond of the living polypropylene end reacts quantitatively with iodine molecule to yield an iodine–polymer bond. The iodine-terminated polypropylenes of low molecular weight ($\bar{M}_n = 630$–3200) were found by ^1H and ^{13}C NMR spectroscopy to have a secondary structure at the chain end.[154]

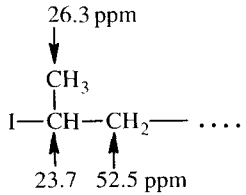

The other chain-end structure was either ethyl or propyl, suggesting the initiation reaction with the V–C_2H_5 bond is non-regiospecific:

$$V-CH_2CH_3 + CH_2=\underset{\displaystyle CH_3}{\underset{|}{CH}} \rightarrow V-CH_2-\underset{\displaystyle CH_3}{\underset{|}{CH}}-CH_2-CH_3 \text{ or}$$

$$V-\underset{\displaystyle CH_3}{\underset{|}{CH}}-CH_2-CH_2-CH_3$$

Syndiotactic polystyrene prepared with tetrabenzyltitanium or tetrabenzylzirconium and methylalumoxane was analysed by ^{13}C NMR in regard to end-groups.[155] A boiling butanone-soluble low molecular weight fraction shows signals due to both chain ends as shown below:

$$CH(C_6H_5)=CH-CH(C_6H_5)\sim\sim\sim CH_2-CH(C_6H_5)CH_3$$

132.8 127.4 43.8 35.7 20.9 ppm

The unsaturated end is formed through β-hydrogen transfer

$$\text{Metal}-CH(C_6H_5)-CH_2CH(C_6H_5) \sim\sim\sim\rightarrow$$

$$CH(C_6H_5)=CH-CH(C_6H_5) \sim\sim\sim + \text{Metal}-H$$

and another chain end is formed by reinitiation with Metal–H:

$$\text{Metal}-H + CH_2=CH(C_6H_5) \rightarrow \text{Metal}-CH(C_6H_5)-CH_3$$

The structures of both chain ends indicate that the insertion of the monomer on the metal–carbon or metal–hydrogen bonds of the catalytic complexes is secondary and that β-hydrogen abstraction is the most important chain-transfer process.

4. TACTICITY DETERMINATION

4.1. Reliability of tacticity determination and reproducibility of the polymerization of methyl methacrylate

Tacticity is one of the most valuable parameters obtained from NMR spectra, and the stereochemical assignments of ^1H and ^{13}C NMR spectra of various vinyl polymers have been established.[156] As discussed in Section 2.1, reliability of signal intensity is of prime importance in the determination of tacticity by NMR spectroscopy, since no other analytical means provide quantitative data on tacticity.

Table 11. Effect of pulse repetition time on relative peak intensity and tacticity determination for radically prepared PMMA by 500-MHz ^{1}H NMR.[a]

Pulse repetition (s)	Relative intensity[b]		Tacticity (%)		
	OCH_3	CH_2	*mm*	*mr*	*rr*
15.0	3.02	1.99	3.7	35.3	61.0
10.0	2.99	2.01	3.8	35.2	61.0
6.0	2.91	2.01	3.8	35.2	61.0
4.0	2.79	1.99	3.7	35.0	61.3
2.0	2.36	1.98	3.8	35.0	61.2
1.0	1.78	1.88	3.7	34.9	61.4
0.3	1.18	1.62	3.3	34.4	62.3

From Refs 157 and 158.

[a]Solvent $CDCl_3$; conc. 10 % w/v; temperature 55°C; pulse width 90°; number of scans 4–16.

[b]Relative intensity against α-CH_3 signals whose intensity is set to be 3.00.

The effects of operation conditions on FT-NMR measurements of tacticity have been examined using a radically prepared PMMA. Table 11[157,158] shows the relative intensities of OCH_3 and CH_2 proton signals, and triad tacticity determined from α-CH_3 proton signals. The measurements were made with various pulse repetition times. A pulse repetition time of at least 10 s is needed to obtain accurate intensities of OCH_3 and CH_2 proton signals relative to α-CH_3 signals when 90° pulse is used. However, the tacticity values obtained with repetition times from 1 to 15 s are in good agreement with each other, that is, a repetition time of 1 s is sufficient for tacticity determination with high accuracy, even though saturation of the signals may occur.

The reproducibility of the tacticity data for PMMA was examined by ^{1}H and ^{13}C NMR. Table 12[157] summarizes the mean values of tacticity for five runs obtained from various signals. For ^{13}C NMR, the data obtained under complete decoupling and the gated decoupling conditions showed no appreciable difference. The *mm* triad value obtained from ^{1}H NMR is slightly larger than the other values. This deviation comes from overlapping of the initiator fragment signals to *mm* and *mr* triad signals of α-CH_3 protons. Figure 15 shows 500-MHz and 100-MHz ^{1}H NMR spectra of PMMA prepared with AIBN.[159] In the 500-MHz spectrum two methyl proton signals due to the initiator fragment, 1-cyano-1-methylethyl group, can be distinguished from the *mm* and *mr* triad signals. The assignment of the initiator fragment signals was confirmed by comparing the spectrum with that of poly(methyl methacrylate-d_8) prepared with AIBN[38] (Fig. 5). The triad tacticity of the PMMA was corrected by omitting the contribution of the initiator fragment signals. The values thus obtained are close to those obtained from ^{13}C NMR signals.

It has been reported that the tacticity of PMMA prepared with benzoyl peroxide (BPO) deviates slightly from Bernoullian statistics while that of PMMA

Table 12. Mean values of tacticity of PMMA determined from various NMR signals.

NMR signal		Tacticity (%)			$4(mm)(rr)$
		mm	*mr*	*rr*	mr^2
α-$C\underline{H}_3$		3.77	34.76	61.47	0.767
		(3.50	34.80	61.64	0.710)[a]
α-$\underline{C}H_3$	COM[b]	3.52	36.06	60.42	0.654
	NNE[c]	3.52	35.06	61.42	0.703
Quat.	COM[b]	3.10	34.31	62.59	0.659
	NNE[c]	3.34	33.69	62.97	0.741
C=O	COM[b]	3.55	34.03	62.42	0.765
	NNE[c]	3.38	34.50	62.12	0.707
Average		3.40	34.65	61.95	0.702

From Ref. 157.
[a]Corrected for AIBN fragment signal.
[b]Complete decoupling condition.

formed with AIBN is consistent with the Bernoullian.[3,160] The tacticities of PMMAs prepared with AIBN and BPO under the same conditions were slightly different, especially in *mm* triad fractions. However, the values after correction for ABIN fragment signals were very close to each other. When the degree of polymerization of PMMA exceeds 1000, the contribution of the AIBN fragment signals can be neglected since the relative fraction of the AIBN signals becomes negligibly small.

All the data included in Table 12 indicate that the values of $4(mm)(rr)/(mr)^2$, which is expected to be unity if stereoregulation obeys Bernoullian statistics,[161] are less than unity as reported by several investigators.[3,4,10,38,160,162,163]

From the assessment of the reliability of NMR data sponsored by the Society of Polymer Science, Japan (SPSJ), the tacticity data on a PMMA sample were compiled as shown in Table 13.[10] Mean values derived from intensity ratios of split signals due to α-CH_3 protons, α-CH_3 carbon and quaternary carbon are in good agreement with each other, although the values from quaternary carbon signals show larger standard deviations than others. This may be due to the smaller shifts between the peaks and the narrower peak widths; the latter leading to a smaller number of data point defining the lineshape. The values for $4(mm)(rr)/(mr)^2$ are again less than unity.

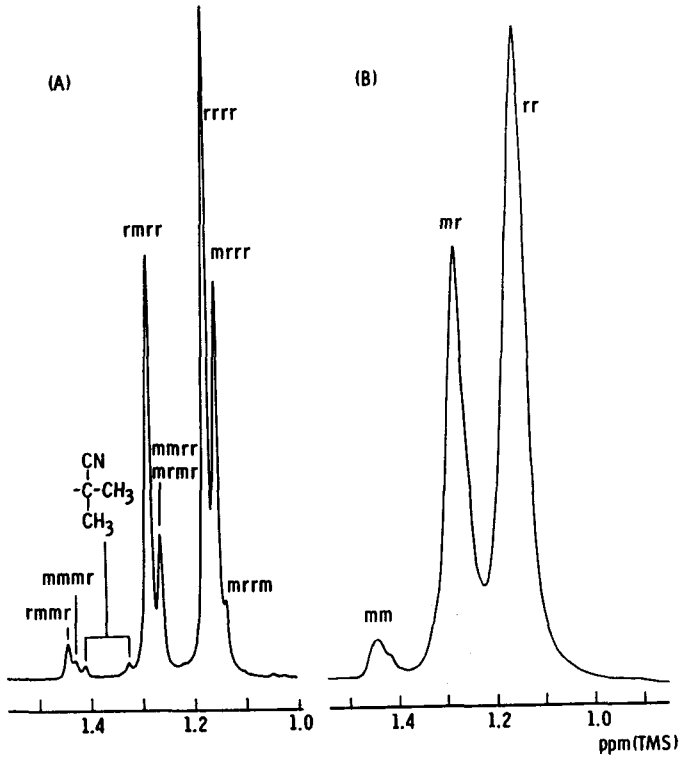

Fig. 15. 500-MHz spectrum (A) and 100-MHz (B) ^{1}H NMR signals of α-CH_3 protons of PMMA prepared with AIBN in benzene at 60°C. (From Ref. 159.)

Table 13. Mean values ($\bar{X}$) and standard deviations (σ) of tacticity of PMMA determined by ^{1}H and ^{13}C NMR spectroscopy.

Signal	n^a		Tacticity (%)			$\frac{4(mm)(rr)}{(mr)^2}$
			mm	*mr*	*rr*	
α-CH_3	17	$\bar{X}$	4.0	34.7	61.3	0.815
		σ	0.9	1.0	1.5	
α-CH_3	17	$\bar{X}$	3.0	34.8	62.2	0.616
		σ	1.3	1.6	2.0	
Quat.C	15	$\bar{X}$	3.8	35.0	61.3	0.761
		σ	1.3	3.1	3.4	

From Ref. 10.
[a]Number of determinations.

In order to determine whether a system obeys first-order Markovian statistics, a knowledge of pentad tacticity is required to a high degree of experimental accuracy. This is very difficult for the case of radically polymerized PMMA, since the fraction of *mm* triads is usually less than 5% of the total.

Moad *et al.*[163] overcame this difficulty using PMMA from MMA in which the carbonyl carbon was enriched with ^{13}C. An enrichment level of 10% was chosen to avoid confusion of the spectra by ^{13}C–^{13}C spin coupling. In the 62.9-MHz ^{13}C NMR spectra of the PMMA prepared in benzene with AIBN at 60°C measured in toluene-d_8, eight of ten pentad signals are resolved, while six pentad signals show baseline resolution when the spectrum was measured in $CDCl_3$. The first-order Markov model rather than Bernoullian's gives an excellent fit to the observed fractions of triad, pentad and heptad sequences. It is worth noting that both models predict similar proportions of the *rr*-centred pentads and that the differences between the two models are most apparent with the *mm* triads and the *mm*- and *mr*-centred pentads. The facts clearly demonstrate that there is a significant penultimate effect in the stereoregulation of polymerization of MMA in benzene at 60°C.

Non-Bernoulian behaviour of tacticity was also reported for poly(vinyl chloride) obtained at 5°C and −30°C.[164] After careful assessment of the precision and accuracy in tacticity determination, triad and tetrad fractions were found to be well-explained by the first-order Markovian statistics.

Reliable NMR data on polymer structure may afford valuable information about the polymerization mechanism, if the reproducibility of the polymerization reaction is not poor. Along with the survey of the precision and accuracy of tacticity data of PMMA from ^1H NMR, we examined the reproducibility of MMA polymerization with AIBN or n-C_4H_9Li.[4] The results of the MMA polymerization with n-C_4H_9Li by five students were fairly scattered and the fluctuation was much larger than that in the radical polymerization. However, the n-C_4H_9Li polymerization results from five runs by the same student were very precise and precision was nearly equal to that of the NMR measurements. The fluctuation of the results by different investigators might be ascribed to different levels of contamination, control of polymerization temperature, and mixing of monomer and initiator. To examine the effect of mixing condition, a special technique of anionic polymerization was invented, called "slow growth polymerization". In this technique the initiator solution is placed on the monomer solution so that it rests on top of it as a separate liquid phase and the polymerization is allowed to proceed without stirring. The initiation then occurs at the interface between the initiator and monomer solutions, and the polymerization reaction proceeds from top to bottom. The PMMA prepared by slow growth polymerization initiated by n-C_4H_9Li had a higher isotacticity and molecular weight than the polymer obtained by the ordinary method.[165–168]

4.2. NMR techniques for stereochemical assignment and tacticity determination

Tacticity determination of vinyl polymer by ^1H NMR spectroscopy was first achieved for PMMA by Nishioka[169] and Bovey.[170] ^{13}C NMR chemical shifts of carbons in PMMA show higher sensitivities to longer stereosequences.[163,171–173] The carbonyl carbons in many polymethacrylates exhibit a splitting pattern similar to that in PMMA. However, a recent report on ^{13}C NMR spectra of polymers of various chlorophenyl methacrylates indicates that the number and positions of the chloro substituent strongly affect the spectral patterns, and the carbonyl carbon signal of poly(2,4,6-trichlorophenyl methacrylate) does not show a splitting due to tacticity.[174]

To confirm the stereochemical assignments, it is advisable to check the necessary relationships among the probabilities of occurrence of the various stereosequences observed;[175] these are completely general and do not depend on the statistics of the polymerization process.

Epimerization is uniquely effective where highly isotactic and syndiotactic polymers are available which can be epimerized by any chemical reactions.[176–181] Successful examples are the analyses of polypropylene[176,179] and polystyrene.[177,178,180] Isotactic and syndiotactic polypropylenes are epimerized by the addition of 1% dicumyl peroxide and 4% tris(2,3-dibromopropyl) phosphate, resulting in well-separated inversions of configuration at low conversion. The inversion gives $\cdots mmmrrmmm \cdots$ for isotactic polypropylene and $\cdots rrrmmrrr \cdots$ for syndiotactic polypropylene. Thus epimerization of each stereoregular polypropylene produces three new pentad resonances (*mmrr* : *mmmr* : *mrrm* or *mmrr* : *mrrr* : *rmmr*) in the CH_3 carbon region spectra with an intensity ratio of 2 : 2 : 1. The *mrrm* and *rmmr* resonances are easily assigned to the peaks with the smaller intensities. The *mmrr* resonances should be commonly observed in both epimerized polypropylenes and can thus be identified by comparison of the spectra. The *mrrr* and *rmmm* resonances are then assigned by default. At this stage seven of the ten possible pentad stereosequences are assigned, i.e. *mmmm*, *rrrr*, *mmmr*, *mmrr*, *mrrm*, *mrrr* and *rmmr*.

Two of the three pentad sequences, *mmrm* and *rmrr*, can be assigned by consideration of the necessary pentad–pentad relations:

$$2\,rmmr + mmmr = mmrm + mmrr$$

$$2\,mrrm + mrrr = mmrr + rmrr$$

Finally, the last one should be *mrmr*.

Spectra of model compounds are also utilized to assign stereochemical sequences in polymer.[182] However, model compounds with defined stereochemical configurations are rather difficult to obtain. Zambelli *et al.*[183] reported that heptad models for polypropylene, 3(*S*), 5(*R*), 7(*RS*), 9(*RS*),

11(*RS*), 15(*S*)-heptamethylheptadecane (A) and a mixture of A with 3(*S*), 5(*R*), 7(*RS*), 9(*RS*), 11(*RS*), 15(*S*)-heptamethylheptadecane, all ^{13}C-enriched at the 9-CH_3 position, permitted the assignment of nine pentad stereosequences. Sato *et al.*[184,185] separated diastereomers of tetramers and pentamers of styrene by chromatography and assigned pentad resonances due to C-1 carbons of the phenyl group.

NMR chemical shift prediction by quantum chemical calculation and the γ-gauche effect method has become a useful approach for stereochemical assignment of vinyl polymers.[186,187] Recently ^{13}C NMR assignments based on γ-effect and the rotational isomeric model were demonstrated successfully for a series of polyolefins, poly(1-pentene) to poly(1-octene).[188]

Derivation of polymer also serves as a useful method for tacticity determination. Poly(triphenylmethyl methacrylate) is easily converted to PMMA by hydrolysis and the subsequent methylation with diazomethene. The polymers obtained by anionic polymerization not only in toluene but also in tetrahydrofuran are highly isotactic.[189] Even the radical polymerization of the monomer gives an isotactic polymer.[189]

Methoxy proton signals of poly(methyl α-phenylacrylate) split into three peaks assignable to *mm*, *mr* and *rr* from low to high magnetic field.[190] The ^{1}H chemical shift of methoxy protons of poly[methyl α-(*p*-bromophenyl)acrylate] is sensitive to longer stereosequences, making the tacticity determination difficult. Reduction of the polymer with $LiAlH_4$ was attempted to obtain poly(methyl α-phenylacrylate) but resulted in the reduction of the ester group as well as the bromophenyl group to form poly(2-phenylallyl alcohol). Fortunately, the carbonyl carbon of the acetylated polymer, poly(2-phenylallyl acetate), showed three split signals assignable to triad stereosequences:[191]

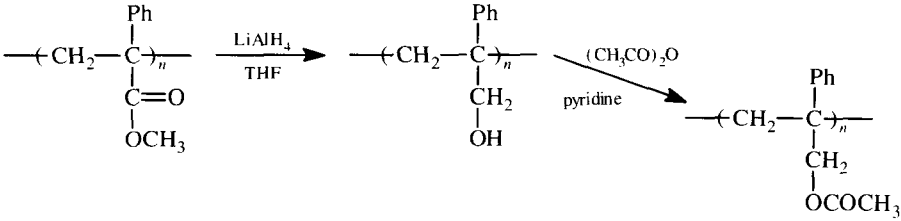

In these types of polymer reaction, quantitative conversion is a definite requirement; otherwise, there would be a possibility that the tacticity of the derived polymer differs from the original one owing to the tacticity dependence of the reaction.

In the ^{1}H NMR spectrum of the polymer of alkyl methacrylates other than MMA, the resonance of an ester group often overlaps with the α-methyl signals and obscures the splittings due to the tacticity of the polymer. ^{1}H-T_1 values of poly(alkyl methacrylate) are in the order of backbone methylene $<$ α-methyl $\ll$ ester group (see Section 6.2).[192] We can capitalize on this large

difference in T_1 values of protons in α-methyl and ester groups to eliminate the ester group resonance overlapped with the α-methyl signal by using inversion-recovery pulse sequence $(180°–t–90°–T)_n$.[193] The value of t is adjusted such that the longitudinal magnetization of the protons of the ester group is zero.

This technique, called the peak elimination method, is a modification of WEFT (water eliminated Fourier transform) NMR.[194] An example of the method is demonstrated in Fig. 16 for poly(ethyl methacrylate). In the ^{1}H NMR spectrum measured in $CDCl_3$, the α-methyl signal is obscured by overlapping with the signal of methyl protons in the ester ethyl group. When the spectrum was taken by using a pulse sequence of (180°–0.8 s–90°–20 s), the ester methyl signal was eliminated and the three splittings in the α-methyl resonance clearly appeared as shown in Fig. 16B. Triad fractions thus obtained were consistent with diad fractions observed from methylene proton signals. The magnetization of α-methyl protons did not recover completely under the condition $t = 0.8$ s, but the accurate determination of tacticity is possible owing to relatively small difference among the T_1 values of α-methyl protons in the three different triads. The T_1 values of the protons in the ester group of polymethacrylate are generally much longer than those in the α-methyl group[193] and the peak-elimination method is widely applicable to the measurements of triad tacticity of various polymethacrylates.

Changing the NMR solvent is another choice. In ^{1}H NMR spectra of poly(ethyl methacrylate), *mr* and *rr* triad signals of α-methyl protons can be distinguished from methyl signals due to the ester group when measured in $CDCl_3$ (Fig. 16B), and *mm* and *mr* triad signals can be distinguished when measured in toluene-d_8 (Fig. 16C). Thus, the comparison of these two spectra provides triad tacticity data.

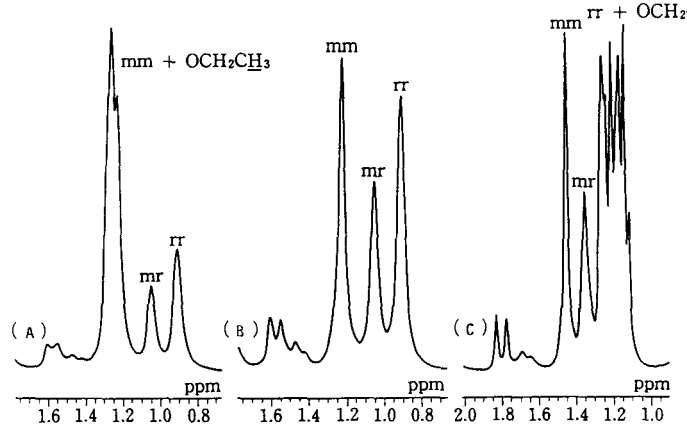

Fig. 16. 270-MHz ^{1}H NMR spectra of poly(ethyl methacrylate) in $CDCl_3$ at 55°C. (A) Normal spectrum. (B) Spectrum obtained with a pulse sequence of (180°–0.8 s–90°–20 s). (C) Normal spectrum measured in toluene-d_8 at 110°C.

Two-dimensional (2D) NMR spectroscopy has recently been used to make absolute tacticity assignments without any other supports.[195–208] An early successful example is ^{1}H COSY analysis of poly(vinyl alcohol).[198,199] Figure 17 shows a broad-band decoupled ^{1}H COSY spectrum of poly(vinyl alcohol)[199] and illustrative assignments for the correlations between triad peaks of methine proton and tetrad peaks of methylene protons. Expected connectivities between triad and tetrad are as follows:

Triad	Tetrad
mm	*mmm*, *mmr*
mr	*mmr*, *rmr*, *mrr*, *mrm*
rr	*rrr*, *mrr*

The assignments shown in Fig. 17B are made based on the connectivities shown above and on consideration of the magnetic equivalency of the methylene protons. The ^{1}H NMR assignments have been extended to ^{13}C NMR assignment using the ^{13}C–^{1}H heteronuclear shift-correlated 2D NMR technique (^{13}C–^{1}H COSY).[199]

^{13}C–^{1}H COSY has been used to provide unambiguous assignments for tacticity-sensitive splittings of C=O carbon and CH_2, α-CH_3 and OCH_3 proton resonances of PMMA, ^{13}C-enriched on the C=O carbon.[205] Chang *et al.*

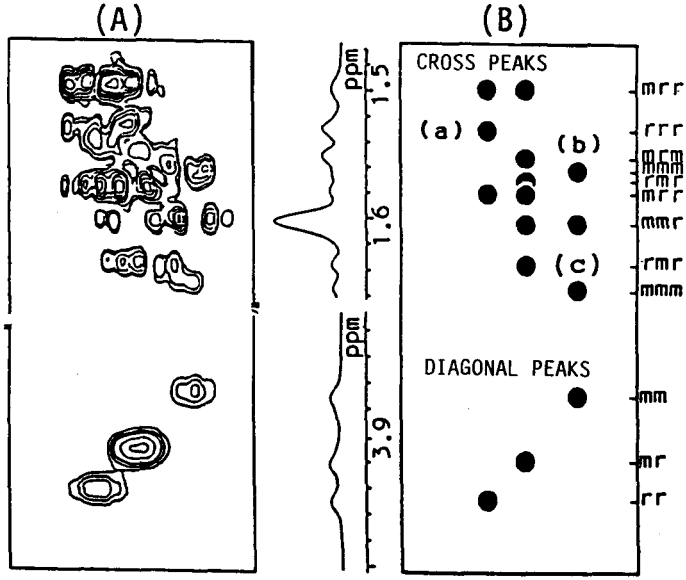

Fig. 17. 500-MHz broad-band decoupled COSY spectra of PVA in D_2O at 80°C. (A) Expansion of CH–CH_2 cross-peaks and diagonal peaks of CH. (B) Schematic representation of spectrum A. (From Ref. 199.)

applied ^{13}C–^{1}H COSY to identify the ^{1}H and ^{13}C resonances belonging to the *m* and *r* diads in poly(vinylamine).[204] Unambiguous assignments of tacticity-sensitive peaks for poly(vinyl chloride) were made by heteronuclear spin-lock relay experiment,[197] which involves magnetization pathways ^{a}H–^{b}H–^{b}C and ^{b}H–^{a}H–^{a}C, and allows identification of neighbouring carbons (^{a}C–^{b}C) by recognition of the shared protons:

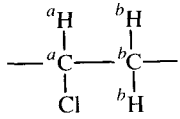

From this experiment, connectivities between tetrad (CH_2) and pentad (CH) signals were identified.

2D INADEQUATE (incredible natural abundance double-quantum transfer experiment) enables direct observation of neighbouring ^{13}C–^{13}C correlation and has been applied to poly(vinyl alcohol)[199] and polypropylene.[206] For example, the CH carbon in the *rrrr* pentad has two cross-peaks with hexad methylenes of *rrrrr* and *rrrrm*.

Stereochemical assignments have also been made at the pentad level for poly(vinyl fluoride) from the ^{19}F COSY spectrum, in which the cross-peaks arise from four-bond scalar coupling (about 7 Hz) between the central pair of fluorines in the pentad sequences that share a common hexad.[200]

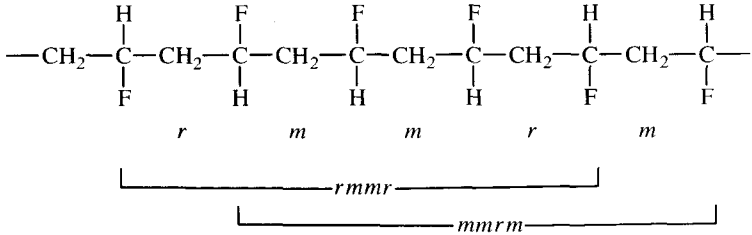

The ^{1}H COSY spectrum of isotatic PMMA enables unambiguous assignment of *erythro* and *threo* methylene protons based on the fact that only the *erythro* proton is capable of forming with α-methyl protons a "W"-shaped four-bond path of long-range coupling.[203] Tetrad–pentad correlation was also observed in the ^{1}H COSY spectrum of radically prepared PMMA.[203]

Configurational structures of both the chain ends of highly isotactic PMMA prepared with t-C_4H_9MgBr were investigated extensively using ^{1}H and ^{13}C–^{1}H COSY spectra.[208,209] The ^{1}H COSY experiment was carried out with a delay time of 200 ms for long-range enhancement; this enhances the signals from the polymer ends. Window functions such as sine-bell and sine-square func-

tions, commonly employed in Fourier transform of 2D NMR data matrices in order to suppress peak-broadening, also served to emphasize the correlation peaks originating from the end-groups, since relaxation times of the protons in in-chain monomeric units are very different from those of polymer end-groups. The ^{1}H and ^{13}C NMR signals of α-CH_3 and CH_2 groups in the first three and the last three monomeric units of the chain were assigned as indicated in Fig. 18.[209] The assignments were made by following cross peaks from the terminating chain-end (right-end) methine proton signals and from the initiating chain-end (left-end) *t*-butyl signals. In the first report,[208] the assignment for right-end tacticity was made, as in-chain tacticity, by the assumption that the chemical shift between *meso* methylene proton signals is larger than that between the signals of two *racemo* methylene protons. This assumption was found not to be applicable to the right-end tacticity; the chemical shift between two methylene proton peaks is larger for *racemo* sequence than for *meso* sequences at the right end. This was confirmed by X-ray crystallographic analysis of the *mm* trimer[210] as described in Section 5. The assignments shown in Fig. 18 have been corrected.[209]

The signals from the first three and the last three monomeric units at the left and right ends overlap with the in-chain α-CH_3 signals as shown in the figure. In order to determine the exact triad tacticity from the α-CH_3 signals, these overlapped signals should be taken into consideration.[208] The isotacticity of in-chain units, when corrected for the overlapped signals due to end-groups, is independent of the molecular weight of the polymer. Without correction, the isotacticity seems to increase with molecular weight and would lead to misunderstanding of the polymerization reaction.

4.3. Cotacticity and comonomer sequence distribution of copolymers

The properties of a copolymer depend on its composition, monomer sequence and stereochemical structure. Although compositional analysis can be achieved by several methods other than NMR spectroscopy, quantitative data on monomer sequence distribution can only be obtained from NMR spectroscopy. ^{13}C NMR chemical shifts of C=O carbons of PMMA are sensitive to pentad to heptad stereochemical sequences. The C=O carbon signals for the copolymers of methacrylates are also sensitive to triad comonomer sequence. Thus it should be difficult to assign both tactic and comonomer sequence signals, especially in the case of copolymers with low stereoregularity.

The high stereoregularity of block and random copolymers prepared with *t*-C_4H_9MgBr or *t*-C_4H_9Li–R_3Al simplifies the spectrum and permits us to distinguish the peak splittings due to tacticity from those due to monomer sequence distribution.[69,211,212] Figure 19[211] shows 125-MHz ^{13}C NMR

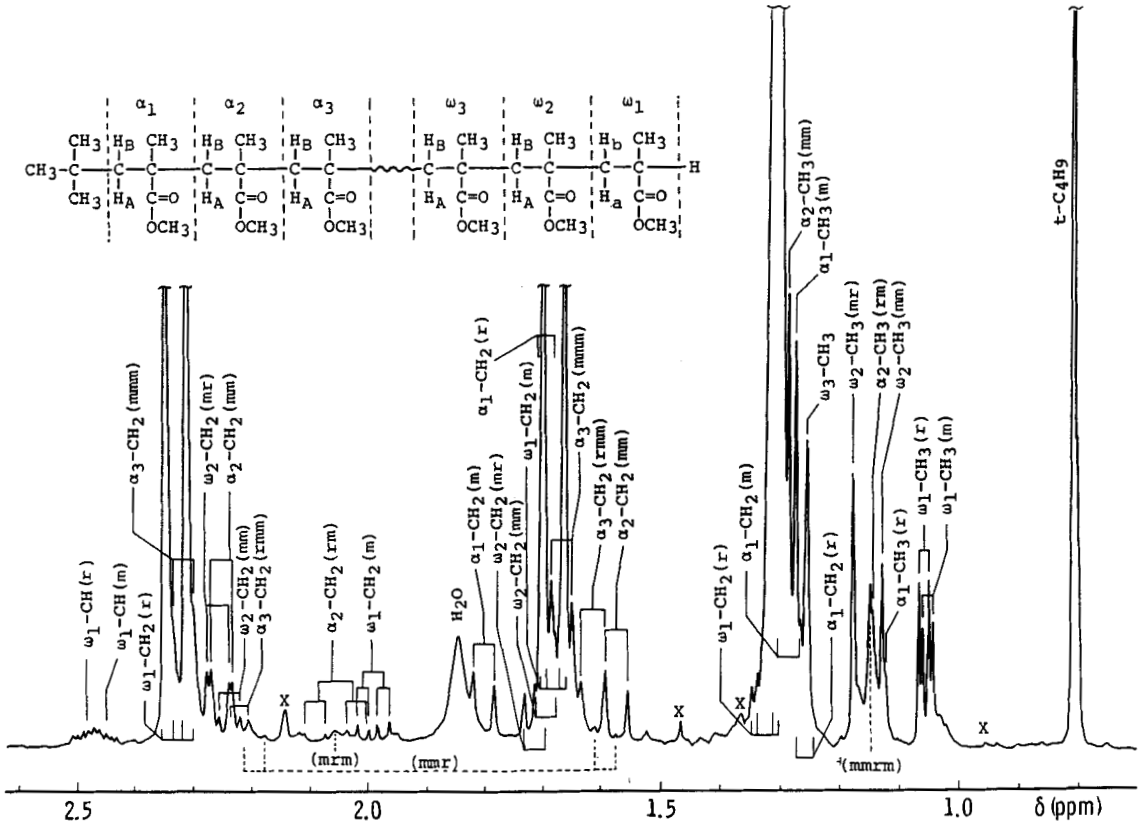

Fig. 18. ^{1}H NMR spectrum of isotactic PMMA ($\bar{M}_n = 2530$) prepared with t-C_4H_9MgBr in toluene at $-78°C$. Signals due to the end-groups and monomeric units at and near the left and right ends are indicated according to the numbering system shown in the figure. X denotes signals due to impurities. (From Ref. 209.)

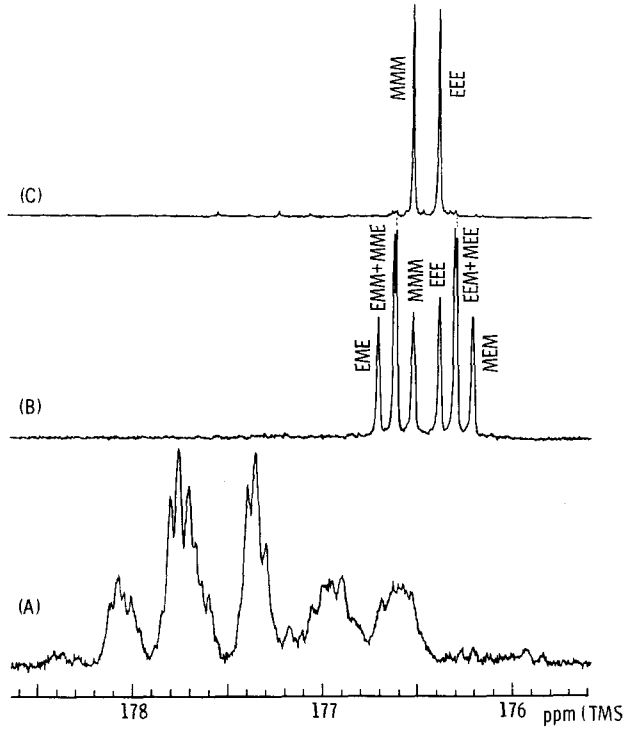

Fig. 19. Carbonyl carbon NMR signals of highly isotactic poly(MMA)-*block*-poly(EMA). (A), highly isotactic poly(MMA-*co*-EMA) (B), both prepared with *t*-C_4H_9MgBr in toluene at −60°C, and poly(MMA-*co*-EMA) (C) prepared by AIBN in toluene at 60°C. M and E represent MMA and EMA units, respectively. (125 MHz, $CDCl_3$, 55°C.) (From Ref. 211.)

spectra of C=O carbons of highly isotactic block and random copolymers of MMA and ethyl methacrylate (EMA) prepared by *t*-C_4H_9MgBr in toluene at −60°C. In the spectrum of the copolymer obtained from an equimolar mixture of MMA and EMA (Fig. 19B), the signals of MMA and EMA centred sequences in *mmmm* configurational pentad show splitting due to the triad monomer sequences. Small splittings in the peaks assigned to (MME + EMM) and (MEE + EEM) (M: MMA unit; E: EMA unit) might be due to the effect of longer sequences or different conformations.

The diblock copolymer shows two strong signals at 176.51 and 176.37 ppm, with weak signals of equal intensities at 176.60 and 176.28 ppm (Fig. 19a). The first two strong signals were assigned to the MMM and EEE triads in isotactic pentad configuration, *mmmm*, respectively, by referring to the spectra of isotactic PMMA and isotactic poly(EMA). The latter signals were assigned to MME and MEE triads in *mmmm* configuration by comparing the spectrum with that of the random copolymer, which should exist at the switching point of

MMA and EMA sequences:

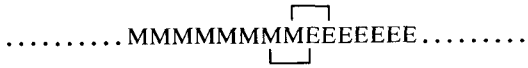

Some other small peaks ascribable to chain-end units were also observed in the spectrum.

The C=O carbon spectrum of MMA and butyl methacrylate copolymer exhibits similar spectral features, that is, splittings due to both monomer sequence and stereosequence,[213,214] although the signal assignments for the 25-MHz ^{13}C NMR spectra based on only monomer sequence distribution[215] had been made erroneously.

Figure 20 illustrates the 500-MHz ^1H NMR spectra of highly isotactic poly(MMA-*ran*-EMA), PMMA-*block*-poly(EMA), poly(EMA)-*block*-PMMA, and a 1 : 1 mixture of PMMA and poly(EMA), all of which were prepared with t-C_4H_9MgBr.[216] In the spectra of the block copolymers methylene protons showed two sets of AB quartet signals due to PMMA block and poly(EMA) block (Fig. 20B, C), clearly indicating that both blocks are highly isotactic. The corresponding signals of methylene protons in the random copolymer (Fig. 20A) showed much more complicated splittings (1.75 ppm) or broadening (2.4 ppm) owing to the presence of different types of monomer sequences. Similar spectral differences between the block and random copolymers are also observed in the other signals. Thus, these ^1H NMR signals are good and clear indications for distinguishing the block and random copolymers of MMA and EMA. Lochmann *et al.*[217] reported that block and statistical copolymers of MMA and butyl methacrylate could be distinguished from the α-methyl proton signals in their ^1H NMR spectra.

NMR spectra of the block copolymers are expected to be almost the superimpositions of the spectra of the corresponding homopolymers. However, the signals due to initiator fragments (0.8 $\sim$ 0.9 ppm) provide the information for distinguishing the block copolymers from the mixture. The PMMA-*block*-poly(EMA) (Fig. 20B) and poly(EMA)-*block*-PMMA (Fig. 20C) showed single t-C_4H_9-signals at 0.823 and 0.852 ppm, respectively, which are assigned to the initiator fragments attached to the PMMA and poly(EMA) sequences, respectively. On the other hand, the mixture of PMMA and poly(EMA) prepared with the same initiator t-C_4H_9MgBr shows signals of two types of initiator fragments as indicated in Fig. 20D. It is worth noting that the t-C_4H_9 signals in the two block copolymers also provide the information whether the block copolymer was prepared from the PMMA anion or the poly(EMA) anion.[216]

The advantages of 2D NMR spectroscopy in monomer sequence analysis have been demonstrated for several copolymers.[218–225] The copolymer of vinylidene chloride (V) and isobutylene (I) shows no correlation in the ^1H COSY spectrum, since it has no J-coupled protons. However, 2D NOE spectroscopy

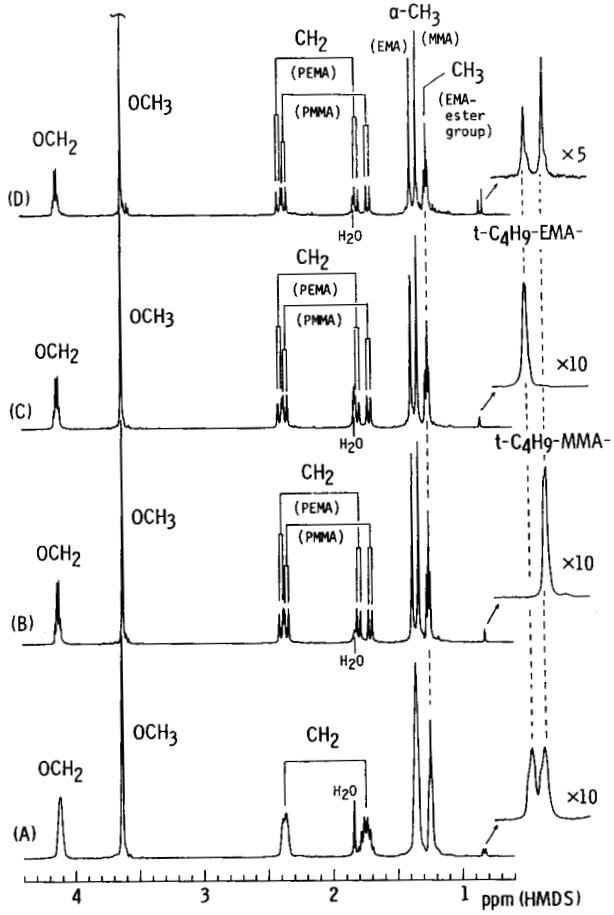

Fig. 20. 500-MHz ^{1}H NMR spectra of highly isotactic copolymers of MMA and EMA prepared with t-C_4H_9MgBr in toluene at −60°C, measured in nitrobenzene-d_5 at 110°C. (A) Poly(MMA-*ran*-EMA); (B) PMMA-*block*-poly(EMA); (C) poly(EMA)-*block*-PMMA; (D) PMMA + poly(EMA) (MMA/EMA = 1/1). (From Ref. 216.)

(NOESY) has been successfully used to assign the monomer sequence of this copolymer.[219] For example, in the VVVVI pentad shown below,

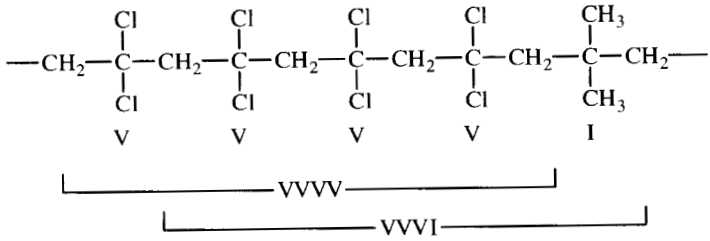

there is a proton–proton Overhauser effect between the two central methylene groups, and then we would expect to observe a cross-peak between the overlapping VVVV and VVVI tetrads, which constitute the common VVVVI pentad.

NOESY has also been used to elucidate the chain conformation of poly(styrene-*alt*-MMA).[220,221] 2D INADEQUATE has been applied to studies of monomer sequence distribution in ethylene–propylene copolymer.[223] Additivity rules for the ^{13}C chemical shifts of ethylene–propylene copolymer were devised for configurational sequences as well as substituent effects.[226]

Monomer reactivity ratios r_1 and r_2 in copolymerization can be determined from a single sample of copolymer as long as the mole fraction of each diad is obtained.[227,228]

$$r_1 = \frac{[M_2]_0}{[M_1]_0}\frac{2(M_1M_1)}{(M_1M_2)} \qquad r_2 = \frac{[M_1]_0}{[M_2]_0}\frac{2(M_2M_2)}{(M_1M_2)} \tag{7}$$

Similarly, the ratios r_{ij} ($i, j = 1$ or 2) can be determined from triad monomer sequence distribution data:

$$r_{11} = \frac{[M_2]_0}{[M_1]_0}\frac{2(M_1M_1M_1)}{(M_1M_1M_2)} \qquad r_{21} = \frac{[M_2]_0}{[M_1]_0}\frac{(M_1M_1M_2)}{2(M_2M_1M_2)}$$

$$r_{12} = \frac{[M_1]_0}{[M_2]_0}\frac{(M_1M_2M_2)}{2(M_1M_2M_1)} \qquad r_{22} = \frac{[M_1]_0}{[M_2]_0}\frac{2(M_2M_2M_2)}{(M_1M_2M_2)} \tag{8}$$

Recently, the Research Group on NMR, SPSJ, assessed reliability of copolymer analysis by NMR using three samples of radically prepared copolymers of MMA and acrylonitrile with different compositions. ^1H and ^{13}C NMR spectra of the copolymers were collected from 46 NMR spectrometers (90 ~ 500 MHz) and the composition and sequence distribution were determined.[232] Table 14 summarizes the monomer reactivity ratios determined by ^{13}C NMR analysis. The large difference between r_{11} and r_{21} indicates the presence of a penultimate effect in this radical copolymerization, as previously reported.[233] The values of r_{ij}, especially r_{11}, depended on the comonomer feed ratio, suggesting higher order of neighbouring unit effect on the reactivity of chain-end radicals.

Configurational sequences, so-called cotacticity, of methacrylate copolymers have been studied extensively in connection with their stereoregular polymerization by radical and anionic initiators.[234–239] To elucidate stereoregulation in the cross-propagation step in copolymerization, at least two independent parameters, σ_{12} and σ_{21}, should be taken into consideration. Here σ_{ij} is the probability of generating a *meso* diad when a monomer unit M_j is formed at the M_i end of a growing chain as proposed by Bovey and Tiers.[240] In the reports[234–239] mentioned above, however, the two configurational parameters were assumed to be equal. The assumption is

Table 14. Monomer reactivity ratios in the copolymerization of MMA (M_1) and acrylonitrile (M_2).[a]

No.	MMA content		r_1	r_2	r_{11}	r_{21}	r_{12}	r_{22}
	Feed	Copolymer[b]						
1	0.206	0.375	1.55	0.34	1.44	1.59	0.34	0.34
2	0.347	0.520	1.41	0.34	1.24	1.55	0.34	0.33
3	0.548	0.671	1.27	0.38	1.13	1.52	0.38	0.39

From Ref. 232.
[a]In dimethyl sulphoxide at 50°C.
[b]Average data of ^{1}H NMR analysis.

unavoidable even if the NMR signals of methylene protons show splittings due to tacticity, since it is impossible to distinguish the two methylene units originated from M_1 and M_2 in the NMR spectrum as can be seen from the following formula:

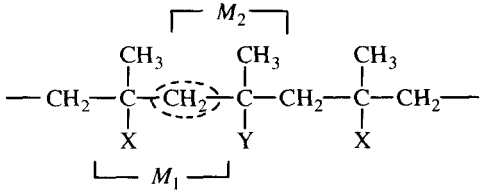

The assigned coisotactic parameters, σ_{12} and σ_{21}, were determined unequivocally by use of a totally deuterated monomer.[241,242] The copolymer of MMA-d_8 (M_1) with a small amount of undeuterated triphenylmethyl methacrylate (M_2) was prepared in toluene by AIBN at 60°C and converted into the

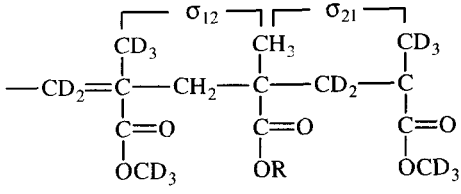

R = $C(C_6H_5)_3$

copolymer of MMA-d_8 with undeuterated MMA by selective hydrolysis of triphenylmethyl mechacrylate units and subsequent methylation with diazomethane. Figure 21 shows the ^{1}H NMR spectra of the copolymer. The initiator fragment signals overlapping with α-CH_3 signals could be eliminated in the partially relaxed FT spectrum (Fig. 21B). The predominant existence of the $M_1M_2M_1$ triad among the M_2-centred triads allows us to

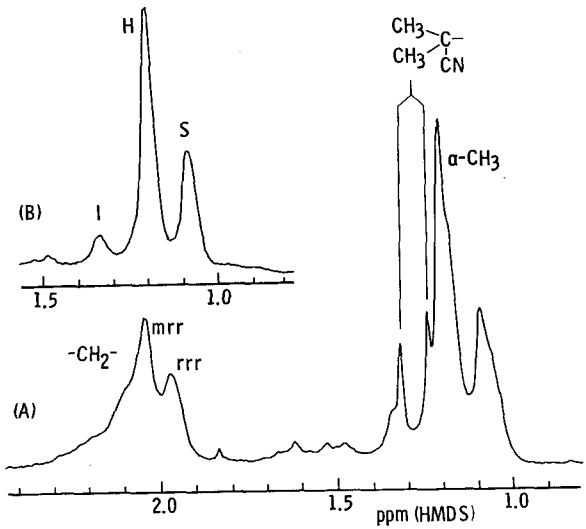

Fig. 21. ^{1}H NMR spectra of the copolymer of MMA-d_8 with MMA derived from the copolymer of MMA-d_8 with triphenylmethyl methacrylate: normal spectrum (A), partially relaxed spectrum (B) (pulse sequence 180°–0.6 s–90°–10 s). (Nitrobenzene-d_5, 110°C, 100 scans, 100 MHz.) (From Ref. 242.)

approximate the intensities of the ^{1}H NMR signals of the α-CH_3 protons as follows:

$$[mm] = 0.063 = \sigma_{12} \cdot \sigma_{21}$$
$$[mr] = 0.620 = \sigma_{12}(1 - \sigma_{21}) + \sigma_{21}(1 - \sigma_{12})$$
$$[rr] = 0.317 = (1 - \sigma_{12})(1 - \sigma_{21}) \qquad (9)$$

The resonance of the backbone methylene protons, which belonged originally to the triphenylmethyl methacrylate units, indicated that σ_{12} was less than 0.5. Then, the σ_{12} and σ_{21} were determined to be 0.10 and 0.65, respectively. Similar results were obtained on the copolymers of MMA-d_8 with diphenyl-2-pyridylmethyl and phenyl-2-pyridyl-*o*-tolylmethyl methacrylate.[242] Analysis of the homopolymers and a copolymer of MMA-d_8 (M_1) and MMA (M_2) gave $\sigma_{11} = 0.22$, $\sigma_{12} = 0.20$, $\sigma_{21} = 0.22$, and $\sigma_{22} = 0.21$, showing the validity of this deuterated monomer technique. These results indicate that the propagating radical of the bulky methacrylate is favourable to isotactic placement of the incoming small methacrylate monomer, MMA, even if the bulky monomer unit is located alone at the end of a fairly long chain of MMA units. The isotactic placement may be controlled by the rigid conformation of the bulky methacrylate radical, as suggested by Kamachi *et al.* from ESR spectroscopic observation of the propagating radicals.[243,244]

Recently, this type of deuterated monomer method was applied to the copolymerization of MMA and styrene in the presence of BCl_3 at low temperature, which gives a heterotactic-rich alternating copolymer.[245,246] Using styrene-β-d_2, Goto *et al.* revealed that the addition of MMA to the styrene radical is syndiotactic-specific while the addition of styrene to the MMA radical is isotactic-specific, and that the alternation of these addition steps gives rise to the formation of a heterotactic-rich alternating sequence.

5. STEREOCHEMISTRY OF OLIGOMERS

NMR study of polymers has frequently been undertaken using appropriate model compounds possessing known chemical and stereochemical structures.[247] Close inspection of the configurational sequence of oligomers leads to a clear understanding of polymerization stereochemistry. Notable efforts include the oligomerization of methyl vinyl ether,[248] styrene,[249–255] 2- and 4-vinylpyridines,[256–258] 2- and 4-isopropenylpyridines,[259,260] vinyl phenyl sulphoxide,[261–263] methyl methacrylate,[208–210,264–274] triphenylmethyl methacrylate,[275,276] chloral[277–282] and phenol-acetaldehyde novolacs.[283] Among these, the oligomers most widely studied by NMR are the methyl methacrylate oligomers.

5.1. Oligomers of methyl methacrylate and other vinyl monomers

Recently, several laboratories have reported stereochemical analysis using NMR spectroscopy of series of MMA oligomers (from unimer to pentamer) prepared by radical polymerization with tetraphenylethane initiators,[266] by radical telomerization with thiophenol,[267] and by group transfer polymerization.[268] These polymerization systems are not stereospecific (rather syndiotactic) and thus the resultant MMA oligomers consist of comparable amounts of some stereoisomers. Cacioli and co-workers[267] prepared MMA oligomers by radical telomerization with cobalt (II) tetraphenyl porphyrin, and studied them using two-dimensional NMR. They isolated three of four possible stereoisomers of the pentamer ($n = 3$):

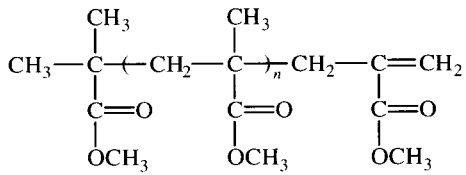

Volpe *et al.*[270] prepared the "symmetric" oligomer of MMA by initiation with lithium and sodium enolates derived from methyl isobutyrate in THF followed by termination with methyl iodide. They then produced a ^{13}C NMR spectrum of the mixture of three of six possible stereoisomers of the hexamer ($n = 4$):

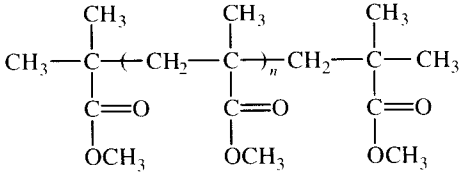

Isolation of pure stereoisomers from an oligomer mixture becomes increasingly difficult as the degree of polymerization increases. Stereoregular living polymerization offers an effective means of preparing stereoregular oligomers. The polymerization of MMA initiated with *t*-C_4H_9MgBr in toluene at $-78°C$ gives highly isotactic PMMA ($mm \geq 97\%$) with a narrow molecular weight distribution,[27] whereas the living polymerization with *t*-C_4H_9Li–trialkylaluminium complex in toluene at $-78°C$ affords highly syndiotactic PMMA ($rr \geq 90\%$).[69] The pure-isotactic and pure-syndiotactic MMA oligomers which are composed exclusively of *meso* (*m*) and *racemo* (*r*) dyads, respectively, can be prepared and isolated effectively through these polymerization systems by the aid of high-performance liquid chromatography (HPLC). Even the octamers for which 128 diastereomers are theoretically possible, are isolated in stereochemically almost pure states.[272] It should be noted that these polymerization systems provide the polymers and oligomers carrying the same terminal groups. It is now possible to isolate pure stereoisomers of MMA oligomers exceeding the 20mer level by supercritical fluid chromatography.[274,284]

Figure 22 shows ^1H NMR spectra of the MMA trimers 3*mm*, 3*mr*, 3*rm*, and 3*rr*.[271,272] The configurational assignments for the monomeric sequences in the oligomers can usually be made on the basis of the non-equivalency of the methylene protons; the chemical shift difference between the two methylene protons (H_A and H_B) in a given monomeric unit should be larger for *meso* sequences than for *racemo* sequences.

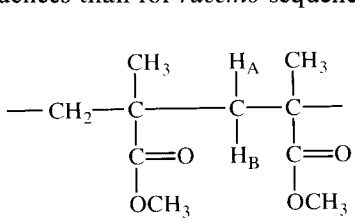

meso sequence

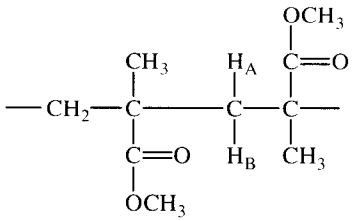

racemo sequence

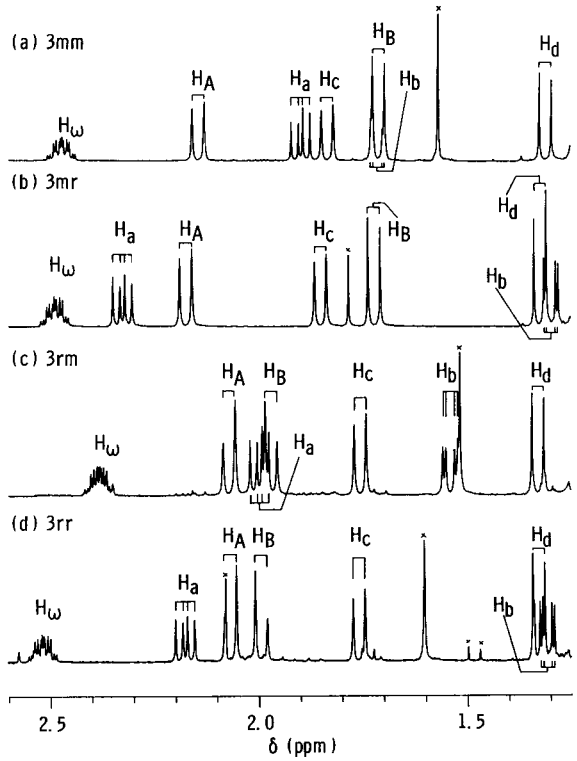

Fig. 22. ^{1}H NMR spectra (methine and methylene protons region) of the *mm*, *mr*, *rm* and *rr* trimers of methyl methacrylate (chloroform-*d*, 35°C, 500 MHz). (From Ref. 272.)

Nishioka[169] and Bovey[170] succeeded in the assignments of ^{1}H NMR spectra of isotactic and syndiotactic PMMAs based on the assumption that the methylene protons of the *meso* sequence are magnetically non-equivalent while those of the *racemo* sequence are equivalent. However, this was found not to be the case for the terminal unit; the chemical shift difference between the non-equivalent methylene protons (H_a and H_b) in the terminal monomeric unit is larger for the *r* diad than for the *m* diad. The assignments were established for the *mm* trimer, *rrm* tetramer and *mmmm* pentamer whose configurations were determined by X-ray single-crystal analysis, and adopted for other oligomers.[272,285] Both the *meso*- and *racemo*-terminal units of the oligomers in solution assume *trans-gauche* (*tg*) conformation along the skeletal sequence C–C–C–C–H_ω, as evidenced from the vicinal coupling constants between H_ω and two methylene protons,

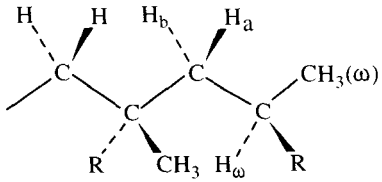

meso-terminal (*tg*)

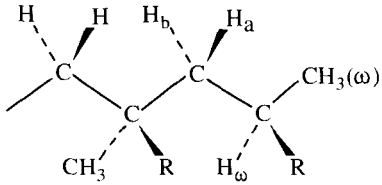

racemo-terminal (*tg*)

H_a and H_b, which were 8.4 and 3.4 Hz. Another possibility of *tg* conformation (tg^-) should be rejected by the fact that ^4J connectivity through "W"-shape coupling between $CH_3(\omega)$ protons and the methylene proton H_a was not observed in the COSY spectra. These *meso*- and *racemo*-terminal conformations explain the larger non-equivalency of the methylene protons of the *racemo*-terminal than those in the *meso*-terminal.

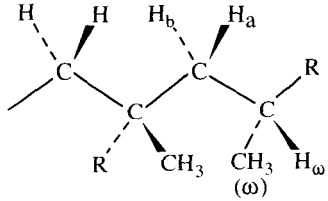

meso-terminal (tg^-)

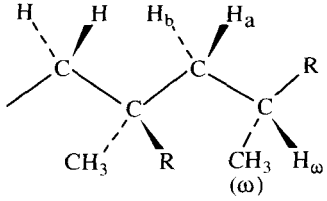

racemo-terminal (tg^-)

The assignments of the methyl and methylene proton signals can be made by the use of a network of correlation peaks starting from the strong singlet at 0.85 ppm due to the t-C_4H_9 group and ending with the multiplet at 2.45 ppm due to the terminal methine proton (H_ω) (Fig. 23). The chemical shifts of protons and carbons in the monomeric units of the third and farther positions from the end-groups were nearly the same as those in the corresponding stereosequences of high molecular weight PMMA. Methylene protons of the syndiotactic oligomers are non-equivalent in the first and second monomeric units from the end-groups, while the non-equivalency almost disappeared in the third and farther monomeric unit from the end-groups. The chemical shift of the methylene protons of the fourth monomeric unit agreed with those of

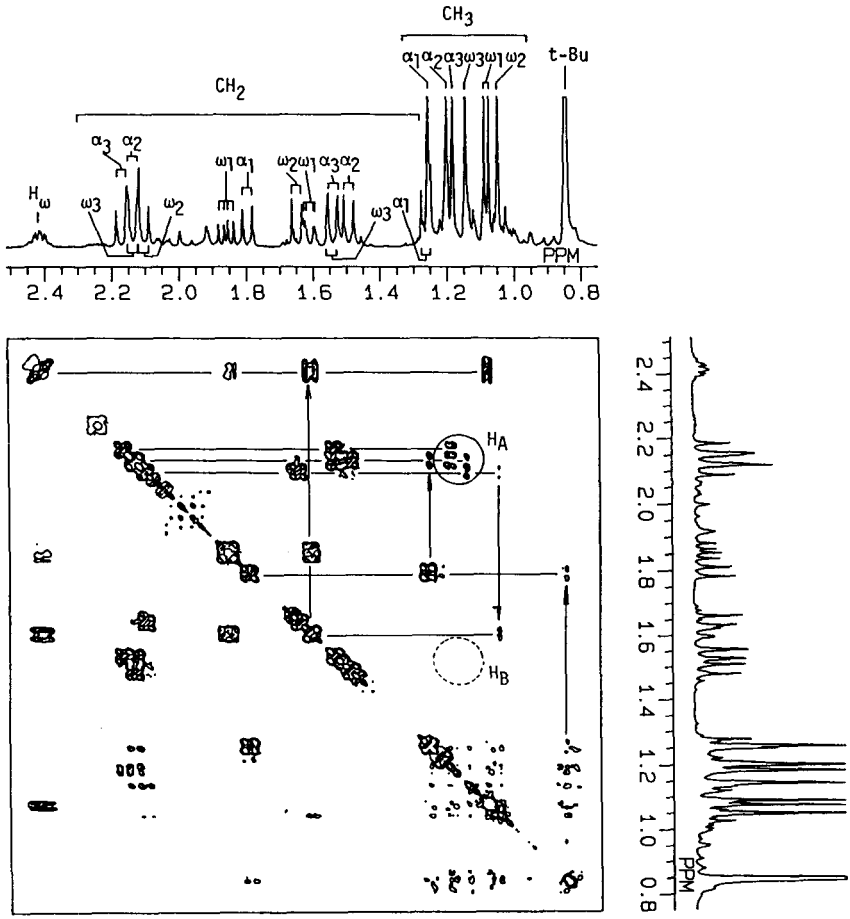

Fig. 23. Double-quantum filtered COSY of the pure isotactic hexamer (*mmmmm*-) of methyl methacrylate. (From Ref. 272.)

the methylene protons in highly syndiotactic PMMA (*rrr* tetrad). These results indicate that the magnetic environments in the third and farther monomeric units from the chain ends are very similar to those in the polymer chain. Therefore, the pentamers and the higher oligomers should be fairly good models in the NMR studies of stereoregular PMMA.

The ^{13}C-T_1 values for the isotactic (*mmmmm*) and syndiotactic (*rrrrr*) hexamers were measured in toluene-d_8 at 35°C (125 MHz).[272] The results are shown in Fig. 24. The T_1 values of the carbonyl, methylene, quaternary and methyl carbons in each monomeric unit decreased gradually as the monomeric unit detached from the terminal groups. However, the T_1 values were much longer than those for PMMA, even in the third monomeric units. The T_1 values for the syndiotactic hexamer were smaller than those for the isotactic antipode as to the corresponding carbon of the corresponding monomeric unit. This suggests that the syndiotactic oligomers have a lower segmental mobility than the isotactic ones, even at the hexamer level (see Section 6.2).

Optically active oligomers of methyl methacrylate were obtained by the asymmetric polymerization of triphenylmethyl methacrylate, followed by the substitution of methyl for triphenylmethyl, and subsequent GPC separation[275] and optical resolution.[276] Detailed study on the stereostructure of the oligomer made it possible to discuss precisely the mechanism of polymerization leading to the formation of polymer with one-handed helical conformation.

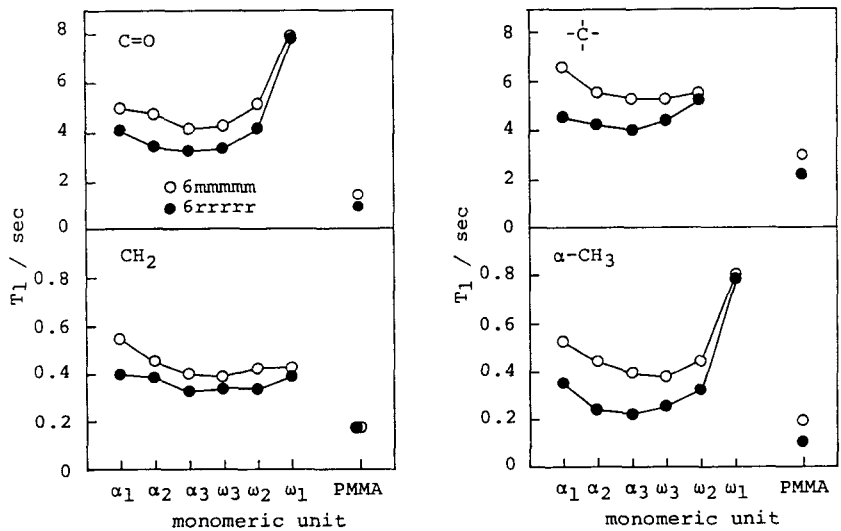

Fig. 24. ^{13}C-T_1 values for the pure isotactic (*mmmmm*-) and the pure syndiotactic (*rrrrr*-) hexamers of methyl methacrylate and for the isotactic and syndiotactic poly(methyl methacrylate)s measured in toluene-d_8 at 35°C (125 MHz). (From Ref. 272.)

^{1}H NMR spectroscopy provides sufficient information regarding not only the configuration but also the conformation of the MMA oligomers. Schilling and co-workers[203] observed in the ^{1}H COSY spectrum of isotactic PMMA a cross-peak between the *mmmm* methyl resonance and the *mmm erythro* methylene resonance but not the *mmm threo* resonance, and interpreted this cross-peak as arising from weak ^4J(HH) couplings through a "W"-shaped four-bond planar path. In a similar manner, inspection of long-range ^4J(HH) connectivities observed in ^{1}H DQF-COSY of the isotactic (*mmmmm*) hexamer measured in $CDCl_3$ (Fig. 23) indicated the all-extended conformation of the isotactic oligomers. Of the two non-equivalent methylene protons in each monomeric unit, only one of them showed correlation peaks with the protons of the two neighbouring methyl groups due to ^4J(HH) coupling. For instance, the ^4J(HH) correlation was observed between CH_3 and H_A (one of the non-equivalent methylene protons resonating at the higher frequency) but not between CH_3 and H_B (the other one) in the COSY spectrum. This indicates the four-bond planar "W" arrangement between the respective protons in a highly preferred conformation of the MMA units.

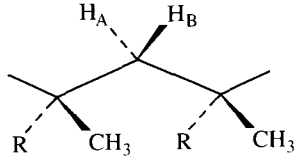

R = CO_2CH_3

The "W" arrangement in all the CH_2-C-CH_3 groups in a chain requires that one of the methylene protons and the methyl carbon should be in the *trans* state, that is, that the main-chain backbone should be in the repeated *tt* conformation. Similar ^4J(HH) connectivities were reported for the telomers of MMA prepared by radical polymerization in the presence of cobalt(II) tetraphenylporphyrin as chain transfer reagent.[269,286]

Oligomers of 2-vinylpyridine initiated with Li, Na, K and Rb salts of ^{13}C-labelled or -unlabelled 2-ethylpyridine and terminated with ^{13}C-labelled or -unlabelled methyl iodide were analysed by ^{13}C NMR spectra of the initial or terminal CH_3 group.[256,257] The ^{13}C NMR of the methyl end-groups is sensitive to the stereochemistry of the two or three adjacent diads (Fig. 25). As a result, the stereochemistry of the addition of the terminal monomer unit and the stereochemistry of methylation can be determined as a function of chain length. The effects of the size of the metal ion and its inter- or intramolecular coordination on the stereochemistry were remarkable in the isotactic living oligomerization of 2-vinylpyridine but not in the oligomerization of 4-vinylpyridine which gives stereo-irregular products.[260] These results were consistent with the occurrence of intramolecular coordination of the metal counterion with the 2-pyridyl group of the penultimate asymmetric centre.

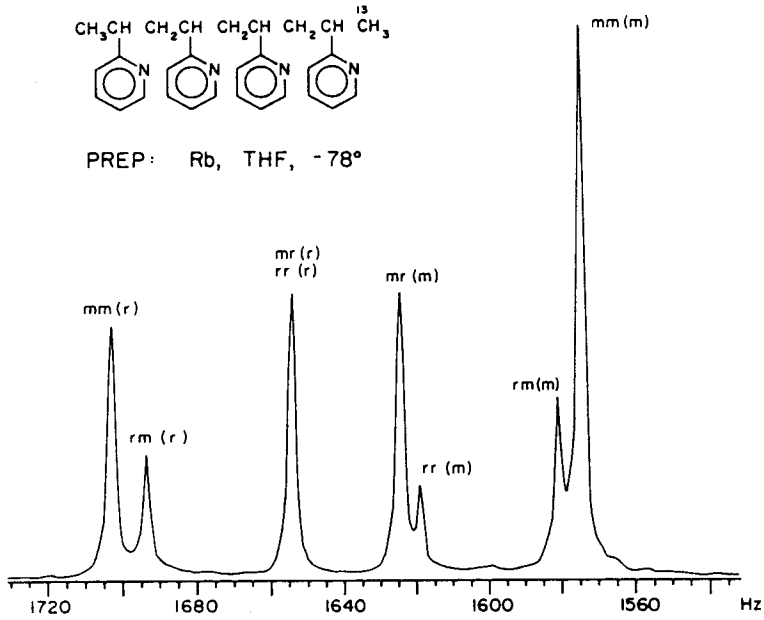

Fig. 25. ^{13}C NMR spectrum of the 2-vinylpyridine tetramer terminated with labelled $^{13}CH_3$ group (DMSO-d_6, 75 MHz). (From Ref. 257.)

The oligomers of methyl vinyl ether were synthesized by the successive addition of methyl vinyl ether to the corresponding dimethyl acetal in the presence of BF_3OEt_2 in toluene; the steric course of each addition step was studied by ^1H NMR spectroscopic analysis of the oligomers from dimer to pentamer.[248] The *meso*-diad probability of each addition step was found to be almost constant, indicating that the stereoregulation obeys Bernoullian statistics.

Although symmetrical oligomers such as 2,4-diphenylpentane,[249,250] 2,4,6-triphenylheptane,[251] and 2,4,6,8-tetraphenylnonane[252] have been investigated as model compounds of polystyrene, ^1H and ^{13}C NMR spectra of these compounds have supplied only little information concerning the analysis of the spectrum of polystyrene. The poor applicability of these compounds is attributed to the end-groups: the methyl end-groups of the model compounds provide a conformation which is different from that of the corresponding polymer. The symmetrical dimer to pentamer with propyl end-groups have been demonstrated to be useful models for the ^1H[253] and ^{13}C[254,255] NMR analysis of polystyrene.

Among spectroscopic methods, ^1H and ^{13}C NMR spectroscopies are the most useful diagnostic techniques for the configurational analysis of oligomers. However, these techniques alone do not always provide sufficient information for unambiguous differentiation of diastereomeric oligomers, especially those from monomers other than vinyl and α-substituted vinyl

monomers such as aldehyde.[277–283] In such a case, single-crystal X-ray analysis appears to be an indispensable tool to solve this structural problem, as demonstrated in the following section.

5.2. Chloral oligomers

Some isotactic polymers such as polychloral[287,288] and poly(triphenylmethyl methacrylate)[289] are known to exist only in purely helical conformation. The helical structure of the polymers is rigid even in solution, owing to the bulkiness of the side-groups. This has been demonstrated by the measurement of high optical activity of the polymers prepared by asymmetric polymerizations; the optical activity is based on a one-handed helical conformation of the polymer chain.

The stereostructures of the linear chloral oligomers have been determined by X-ray single-crystal analysis (Fig. 26).[280] The chloral oligomers from dimer to hexamer were isolated by distillation and by GPC fractionation from the oligomer mixture prepared with t-C_4H_9OLi initiation and acetate end-capping. The dimer fraction was a diastereomeric mixture of the *racemo* and *meso* isomers ($m/r = 3/1$). Subsequent propagating steps of monomer addition force the reaction to become stereospecific toward *meso* addition

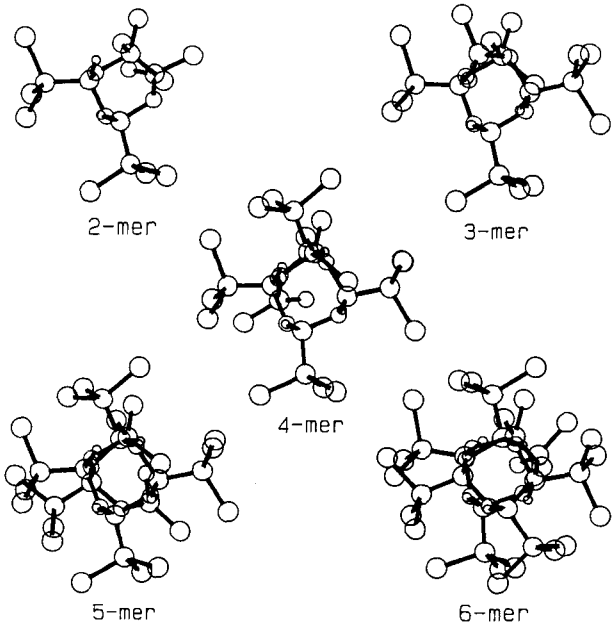

Fig. 26. X-ray molecular structure of the isotactic chloral oligomers from dimer to hexamer. (From Ref. 280.)

because of the tendency of the oligomer anion to form a rigid helical conformation. The higher oligomer fractions ($n \geq 3$) each contained a single diastereomer consisting exclusively of *meso* diads.

The backbone arrangements of the dimer to the hexamer are essentially identical and approximate a 4/1 helix with repeat *gauche*(−)–*skew*(+) sequences from the *t*-C_4H_9O group to the acetyl terminal group (for *R*-configurations). In order to get information on the backbone conformation in solution, long-range ^3J(COCH) coupling constants observed in ^{13}C NMR spectra of the oligomers were examined.[280] The ^3J(COCH) coupling constant depends on the dihedral angle ψ in the ^{13}C–O–C–^{1}H arrays[290,291] and this Karplus type relationship is applicable to the conformational analysis of the chloral oligomers.

$$^3J(\mathrm{COCH}) = 2.21\cos 2\phi - 1.03\cos\phi + 3.64 \qquad (10)$$

Figure 27 shows the ^{1}H-coupled ^{13}C NMR spectrum of the pentamer measured in chloroform-*d* at 35.0°C (acetal and trichloromethyl carbons region).[280] The ^{13}C signals due to the acetal carbons are split into two peaks by ^1J(CH) coupling (171.4–180.3 Hz) from the acetal proton, and the peaks showed further splitting due to the long-range ^3J(COCH) coupling from the acetal protons in the neighbouring monomeric units. For example, the signal due to C(2) splits into four peaks by ^3J(COCH) couplings from the acetal protons

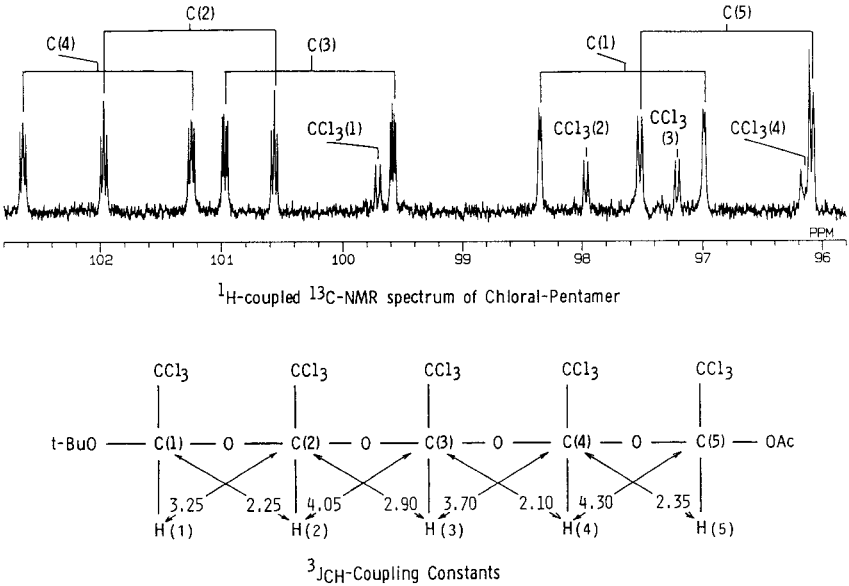

Fig. 27. ^{1}H-coupled ^{13}C NMR spectrum of the chloral pentamer $(CH_3)_3CO[CH(CCl_3)_3O]_5COCH_3$ measured in $CDCl_3$ at 35°C (acetal and trichloromethyl carbons region, at 125 MHz). (From Ref. 280.)

H(1) and H(3), and the signal due to C(5) splits into four peaks by ^3J(COCH) from H(3) and H(5); when the acetal proton H(3) was weakly irradiated, the splittings by the ^3J(COCH) coupling from H(3) disappeared and the remaining splitting of the C(2) and C(5) signals was attributed to the ^3J(COCH) coupling from H(1) and H(5), respectively. The ^3J(COCH) coupling constants thus determined agreed approximately with the values estimated from the dihedral angles in the crystal. These results suggested that the 4/1-helical conformation of the chloral oligomers was maintained even in solution. The (*R,R,R,R,R*)-(−)-pentamer was found to adopt the right-handed helix in solution at 35°C as well as in the crystalline state.[277] The helix-sense preference was ascribed to the conformational energy difference between the right- and left-handed helices.

The isotactic pentamer carrying a methyl group at both ends is the "*meso*(±)-" isomer in which the right- and left-handed helices are no longer diastereomeric but are enantiomeric states with equal probability. A 500-MHz

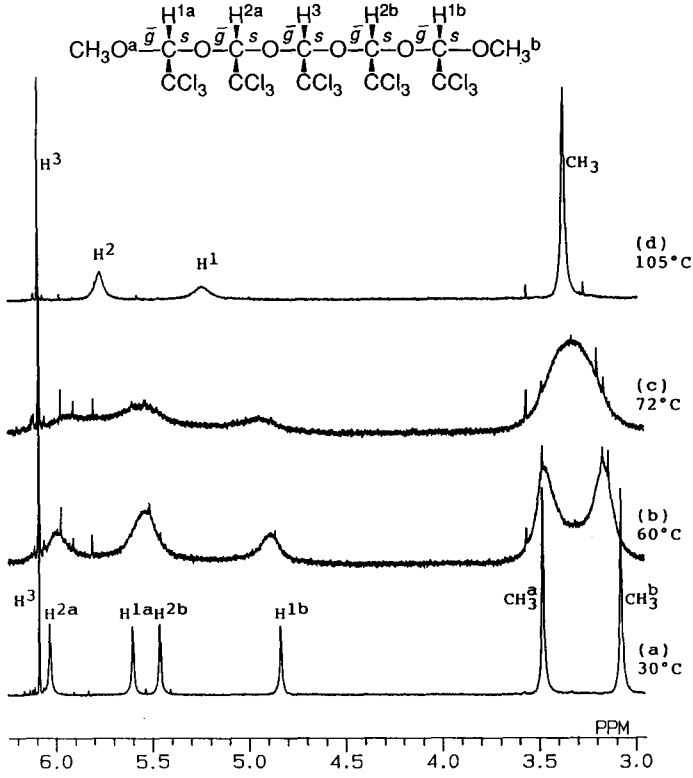

Fig. 28. 500-MHz ^{1}H NMR spectra of the isotactic pentamer of chloral $CH_3O[CH(CCl_3)O]_5CH_3$ in toluene-d_8 at 30°C (a), 60°C (b), 72°C (c), and 105°C (d). (From Ref. 278.)

^{1}H NMR spectrum of the symmetrical pentamer measured in toluene-d_8 at 30°C showed signals due to methyl groups at 3.08 and 3.48 ppm and those due to methine protons at 4.84, 5.46, 5.60, 6.03 and 6.09 ppm (Fig. 28a);[278] these peaks, except for the peak at 6.09 ppm, are relatively broad. The sharp signal at 6.09 ppm is attributed to the methine proton of the central monomer unit (H^3). The non-equivalency of the two methyl groups and of the two sets of acetal methine protons indicates that the pentamer exists in solution at 30°C in a highly preferred conformation, probably the 4/1-helix approximating the repeat *gauche*(−)–*skew*(+) sequences. The signals, except for the signal due to H^3, became broader at 60°C (Fig. 28b) and the signals due to methyl groups coalesced at 72°C (Fig. 28c); the spectrum finally appeared as four signals with an intensity ratio of 6 : 2 : 2 : 1 at 105°C (Fig. 28d). Cooling the sample solution to 35°C again completely reproduced the spectrum shown in Fig. 28a. The results clearly show that the rate of helix sense reversal becomes too fast at 72°C for the time scale of 500-MHz NMR to distinguish the right-$(gs)_5$ and left-handed $(sg)_5$ helical states of the pentamer. From the spectra, the activation energy for the helix inversion ($\Delta G^{\ddagger}$) was determined to be 16.4 kcal/mol.

In a similar manner, the coalescence temperature for the methyl groups of the tetramer was determined as 4°C. $\Delta G^{\ddagger}$ was calculated as 12.7 kcal/mol which was 3.7 kcal/mol smaller than that for the pentamer. The hexamer showed a total of seven signals with narrow linewidth due to two methyl groups and six methine protons even at 70°C, indicating that the rate of helix sense reversal is much slower than the rate for the pentamer. This suggests the possibility that the symmetrical oligomers over the pentamer level may be optically resolved at room temperature based entirely on conformational asymmetry. This was confirmed by the chiral HPLC technique using (+)poly(triphenylmethyl methacrylate) as a stationary phase.[282]

The ethoxy-initiated, methoxy-terminated oligomer of chloral has a small energy difference between the right-handed and left-handed helical states ($\Delta H = 0.498$ kcal/mol, $\Delta S = 0.238$ cal/mol K for the hexamer). It was possible to determine the fraction of both states in solution by NMR spectroscopy at temperatures below the coalescence point.[282]

The purely isotactic oligomers of chloral provides unique and ideal models for the quantitative investigation of the properties of helical polymers because the oligomers have a high tendency to crystallize and have very simple ^{1}H and ^{13}C NMR spectra. As far as we are aware, there is no other analogue of linear low-molecular compounds showing such slow interconversion between enantiomeric helical states.

6. NMR RELAXATION PARAMETERS AND TACTICITY

6.1. Reliability and frequency dependence of spin-lattice relaxation time and NOE factor for PMMA in solution

Nuclear magnetic relaxation parameters give important information on molecular motion and have become increasingly familiar to NMR users since the introduction of Fourier transform (FT) method into NMR technology. Relaxation parameters are also essential in adjusting data acquisition conditions in FT-NMR measurement to obtain quantitative data. In particular, reliable spin-lattice relaxation time (T_1) and nuclear Overhauser enhancement (NOE) factor determinations are required for the correct setting of measurement conditions. It is also important to know whether or not the accuracy of determination of these parameters allows us to treat them as one of the characteristics of a polymer.

From this point of view, ^{1}H- and ^{13}C-T_1 and ^{13}C NOE factors of radically prepared PMMA ($\bar{M}_n = 28\,500$) in $CDCl_3$ were collected from 27 NMR spectrometers by the Research Group on NMR, Society of Polymer Science, Japan through a "round-robin" method.[11] The observing frequencies ranged from 60 to 500 MHz for ^{1}H NMR and from 15 to 125 MHz for ^{13}C NMR. As a result, the frequency dependences of T_1 and NOE were obtained for a very wide range of frequencies.

The reproducibility of the ^{1}H-T_1 values of α-methyl and backbone methylene protons is less than 5%. These T_1 values can be regarded as characteristic data for the polymer as long as they are obtained under the specified conditions. ^{1}H-T_1 data for methoxy protons showed fairly large standard deviations, partly due to the long T_1 value. The ^{1}H-T_1 values of all sorts of protons increase linearly with increasing resonance frequency.

The standard deviations for the measurement of ^{13}C-T_1 values were larger than those for ^{1}H-T_1 values and exceeded 10% in some cases. The T_1 values of all carbons except for the carbonyl carbon increase as the observing frequency increases. This requires a longer pulse duration for the measurement at higher magnetic field strengths and thus results in less efficient accumulation of the spectra within a limited period of time. ^{13}C-T_1 values for the carbonyl carbon decrease with increasing resonance frequencies above 25 MHz. A significant contribution of chemical shift anisotropy to the relaxation of the carbonyl carbon was suggested.

The precision of the NOE measurements were as good as those for ^{13}C-T_1. NOE values obtained at or below 25 MHz are close to the theoretical maximum for all but carbonyl carbons. At higher frequencies NOE values decrease with increasing magnetic field strength. This is another disadvantage to the measurement of the spectrum at higher magnetic field strength. Compared at each frequency, the NOE value for each carbon is in the order of α-CH_3 > quaternary carbon $\sim$ OCH_3 $\sim$ CH_2 > carbonyl carbon. The dif-

ferences between the NOE values of these carbons increase with increasing resonance frequency, leading to inaccurate intensity ratios in the spectrum measured by complete ^{13}C–^{1}H decoupling with NOE. It is worth noting that the quaternary carbon, which has no directly attached hydrogens, shows a similar NOE value to those for other carbons with directly attached hydrogens. The relaxation of quaternary carbon seems to be governed mainly by dipole–dipole interaction with its neighbouring protons in methyl and methylene groups. The carbonyl carbon shows distinctively smaller NOE values than other carbons and the values come close to unity at 100 and 125 MHz as seen in Fig. 29.

The frequency dependences of ^{13}C-T_1 and NOE values were analysed using various molecular motional models; box-type, $\log\chi^2$, 2τ and 3τ models.[292] The three-tau (3τ) model, which describes three kinds of independent superposed motions of the C–H internuclear vector, seems most suitable for describing the frequency dependences. However, multiple correlation time models with more than four kinds of motions are considered to be necessary for detailed analyses of the side-groups since they should be subjected to additional inner rotations compared to the backbone carbons.[292]

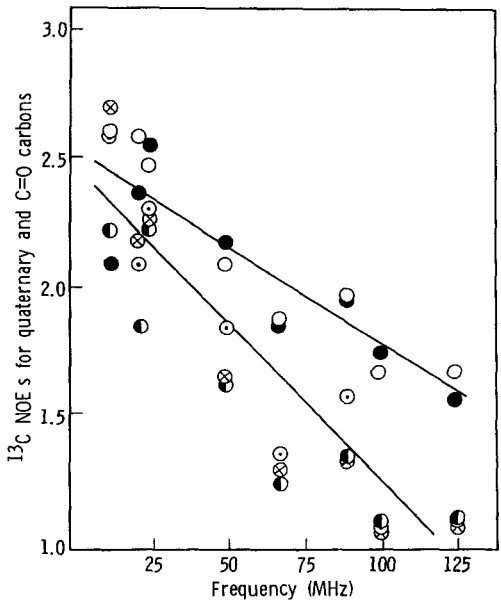

Fig. 29. Frequency dependence of ^{13}C NOE values for quaternary and carbonyl carbons of PMMA measured in $CDCl_3$ at 55°C: ○, quaternary (*rr*); ●, quaternary (*mr*); ◐; carbonyl (*rrrm*); ⊙, carbonyl (*mmrr* + *rmmr*); ⊗, carbonyl (*rrrr*). (From Ref. 11.)

6.2. Tacticity dependence of ^{1}H- and ^{13}C-T_1 values of vinyl polymers in solution

NMR relaxation data of stereochemically shifted nuclei should give valuable information about local molecular motion of stereosequences or stereoregular polymers. Earlier reports on the ^{13}C-T_1 values of polymers showed equal relaxation times for the corresponding carbons in different steric configurations for the solutions of polyacrylonitrile,[293,294] polystyrene[293] and poly(vinyl chloride).[294] Tacticity dependence of vinyl polymer T_1 values was first reported by Hatada and co-workers using PMMA in toluene-d_8 at 110°C and 100 MHz.[192] The findings are that the ^{1}H-T_1 values are longer for an isotactic PMMA than for a syndiotactic PMMA and also longer for an isotactic triad than for a syndiotactic triad. A similar dependence of ^{1}H-T_1 values on tacticity was found for poly(*R*,*S*-α-methylbenzyl methacrylate)s, poly(MMA-*alt*-methyl α-phenylacrylate) and poly(α-methylstyrene).[192] Later, many papers were published on relaxation times in solutions, particularly on the ^{13}C-T_1 of polymethacrylates differing in tacticity.[272,295–311] The ^{13}C-T_1 of carbon in isotactic polymethacrylates has been found to be consistently longer than that of the corresponding carbon in the syndiotactic polymers.[11,272,295–301,303,309–311] The ^{13}C-T_1 values for various poly(alkyl methacrylate)s measured in toluene-d_8 at 110°C and at 25 MHz are shown in Table 15. The NOE for each carbon is close to the theoretical maximum under these conditions, indicating that the segmental motion could be characterized by a single correlation time and the extreme narrowing condition is satisfied. Then the correlation time, τ, can be calculated by the following equation:

$$\tau = \frac{\gamma_C^{-2}\gamma_H^{-2}\hbar^{-2}}{T_1 \sum_i r_i^{-6}} \tag{11}$$

where γ_C and γ_H are the gyromagnetic ratios of ^{13}C and ^{1}H nuclei, respectively, and r_i is the internuclear distance between carbon and hydrogen. The calculated correlation times, τ are also shown in Table 15.[296] The results strongly indicate that the isotactic polymer chain has a greater segmental mobility than the syndiotactic chain. The segmental mobility seems to decrease with an increase in the bulkiness of the ester group in both isotactic and syndiotactic polymers. The α-methyl group in the isotactic polymers also has a greater freedom of internal rotation than that in syndiotactic ones.[296] The ^{13}C NMR relaxation data obtained at 38°C in $CDCl_3$ for the methylene carbons of isotactic and syndiotactic PMMAs suggested that a distribution of correlation times rather than a single correlation time characterizes the backbone segmental motion in the PMMA molecule. Both Cole–Cole distribution[312] and log χ^2 distribution[313] were found to provide reasonable fits for the experimental data; however, a broader distribution was required to fit the results for syndiotactic PMMA than those for isotactic PMMA. The T_1

Table 15. ^{13}C-T_1 values and correlation times (τ) of various poly(alkyl methacrylate)s in toluene-d_8 at 110°C.

Ester group		T_1 (s)				$\tau \times 10^{11}$ (s)	
		CH_2	α-CH_3	C=O	C-4	CH_2	α-CH_3
CH_3	Isotactic	0.28	0.49	7.85	2.96	8.4	3.1
	Syndiotactic	0.10	0.22	3.03	1.63	22.4	7.1
C_2H_5	Isotactic	0.19	0.42	3.50	2.38	12.1	3.7
	Syndiotactic	0.086	0.22	2.95	1.34	27.1	7.1
i-C_3H_7	Isotactic	0.13	0.35	2.88	2.36	18.1	4.5
	Syndiotactic	0.077	0.18	2.33	1.01	30.2	8.9
t-C_4H_9	Isotactic	0.074	0.24	2.60	1.07	31.5	6.6
	Syndiotactic	0.036	0.13	1.84	0.67	64.7	11.8

From Ref. 296.

results for the α-methyl carbons again suggest that the constraint to methyl internal rotation in the isotactic chain is less than that in the syndiotactic chain.[298]

As the ester group of polymethyacrylate became bulkier, the difference in ^{13}C-T_1 values between the isotactic and syndiotactic polymers decreased. A similar trend was observed in the alkyl α-chloroacrylate polymers, and the isotactic and syndiotactic poly(isopropyl α-chloroacrylate)s showed almost the same T_1 values.[310] In the cases of the polymers of benzyl and α-methylbenzyl methacrylates, the isotactic polymers generally show larger ^{13}C-T_1 values than the syndiotactic polymers in toluene-d_8 at 110°C, although the differences are small. However, most of the carbons in isotactic poly(diphenylmethyl methacrylate) showed smaller T_1 values than the corresponding carbons in the syndiotactic polymer at 110°C. Temperature dependence of the ^{13}C-T_1 values for the methylene and α-methyl carbons indicated that the T_1 values observed at 110°C lay in the region of the left side to the T_1 minimum, where T_1 is inversely proportional to the correlation time. Thus, the larger T_1 values for the syndiotactic poly(diphenylmethyl methacrylate) indicate the higher segmental mobility of the syndiotactic polymer than the isotactic one. NOE values at 110°C were higher for the syndiotactic polymer than for the isotactic one, also supporting the above results. It is believed that the isotactic polymer chain tends to take a helical structure. If this is the case for poly(diphenylmethyl methacrylate), more restricted mobility of the isotactic chains would be ascribed to interactions among the phenyl groups in the neighbouring ester functions, which make the helical conformation rigid.[310]

Extensive ^{13}C NMR relaxation measurements on poly(*n*-butyl methacrylate) were carried out at 45°C and at 90.6, 37.8 and 20.0 MHz in a variety of solvents and a semiquantitative relationship between polymer side-chain motion and the

solubility parameter was established. The diamond-lattice conformational jump model[314–316] has been modified to explain successfully both backbone motion and side-chain multiple internal rotations.[302]

The difference in ^{13}C-T_1 between polymers with different tacticities but the same chemical structure results not only from differences in the chain segmental motion between stereoregular polymers or sequences but also from differences in preferred conformations between the stereoregular polymers or sequences which lead to different average distances for the interaction of a carbon with a proton of a neighbouring monomeric unit.[298] The solvent dependence of ^{13}C-T_1 for stereoregular PMMAs has been explained by the solvent-dependent conformation of the polymer chain.[299–301] In the case of ^{1}H-T_1 the mechanism of relaxation is rather complicated and the observed T_1 cannot be directly related to the segmental mobility of the polymer chains. However, the ^{1}H-T_1 values of poly(alkyl methacrylate)s were found to be parallel with the ^{13}C-T_1 values, i.e. the T_1 of the protons in the isotactic polymer was always larger than that of the comparable protons in the syndiotactic polymer.[296]

In the analysis of ^{1}H-T_1 relaxation times, in addition to intra-group dipolar interaction, other contributions have also to be considered:

$$T_{1(\text{obsd})}^{-1} = T_{1(\text{intra})}^{-1} + T_{1(\text{inter})}^{-1} \tag{12}$$

where $T_{1(\text{obsd})}^{-1}$ is the observed rate of relaxation, $T_{1(\text{intra})}^{-1}$ is the contribution from the interaction within the given group, and $T_{1(\text{inter})}^{-1}$ is the contribution from the interactions with the protons of other groups in the same and nearby monomeric units of the chain.

The relaxation rate of methylene protons due to the partner methylene proton $T_{1(\text{intra})}^{-1}$ is expressed by the following equation:[317]

$$T_{1(\text{intra})}^{-1} = N\frac{3}{10}\frac{\gamma_H^{-4}\hbar}{r^6}\left(\frac{\tau}{1+\omega_H^2\tau^2} + \frac{4\tau}{1+4\omega_H^2\tau^2}\right) \tag{13}$$

where γ and N are the distances between protons interacting with each other and the number of interacting protons, respectively, and $N = 1$ in this case. If we assume the same correlation time for methylene carbon and protons, $T_{1(\text{intra})}^{-1}$ can be calculated from the correlation time, τ, estimated from ^{13}C-T_1. Then, $T_{1(\text{other})}^{-1}$ can also be estimated from the comparison of intra- and inter-group contributions to the relaxation rate of backbone methylene protons for isotactic and syndiotactic PMMAs in CD_3CN and $CDCl_3$ at 27°C. The inter-group interactions in isotactic PMMA were found to be larger than those in syndiotactic PMMA, which may be a consequence of the regular helix structure of isotactic PMMA. The inter-group contribution in $CDCl_3$ is considerably larger than that in CD_3CN, especially for syndiotactic PMMA. This implies that the conformational structure of a sequence of monomer units in stereoregular PMMAs, especially in syndiotactic

PMMA, is different in $CDCl_3$ and in CD_3CN.[301] Similar results were obtained for isotactic and syndiotactic PMMAs in toluene-d_8, nitrobenzene-d_5 and *N*,*N*-dimethylformamide-d_7 at 110°C and 60°C, and in $CDCl_3$ and nitromethane-d_3 at 60°C.[310]

The magnitudes of the intra- and inter-group contributions of ^1H relaxation in isotactic and syndiotactic PMMAs were determined in toluene-d_8 at 110°C using four types of copolymers of totally deuterated MMA with a small amount of undeuterated MMA and of the following three specifically deuterated MMAs:[303]

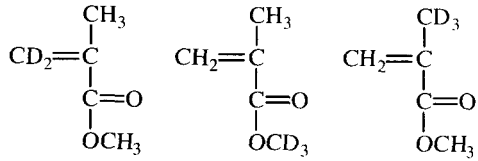

The results are shown in Table 16. The spin-lattice relaxations of the α-methyl and methoxy protons were found to arise mainly from the dipolar interactions between the protons in the methyl group itself. In the relaxation of backbone methylene protons the contributions from the protons in the neighbour-

Table 16. Contributions to observed relaxation times and rates of protons in poly(methyl methacrylate) (PMMA).

Type of protons	Component of T_1[a]	Isotactic PMMA[b]		Syndiotactic PMMA[b]	
		T (s)	$1/T$ (s^{-1})	T (s)	$1/T$ (s^{-1})
α-CH_3	T_{CH_3}	0.50	2.0 (65)	0.24	4.2 (74)
	$T_{CH_3-CH_2}$	3.3	0.31 (20)	2.3	0.44 (16)
	$T_{CH_3-OCH_3}$	10	0.10 (3)	2.7	0.37 (7)
	$T_{other(CH_3)}$	2.7	0.37 (12)	6.3	0.16 (3)
OCH_3	T_{OCH_3}	0.95	1.05 (80)	0.59	1.7 (87)
	$T_{OCH_3-CH_2}$	19	0.053 (8)	23	0.044 (4)
	$T_{OCH_3-CH_3}$	14	0.074 (6)	18	0.057 (3)
	$T_{other(OCH_3)}$	13	0.077 (6)	9.1	0.11 (6)
CH_2	T_{CH_2}	0.42	2.4 (53)	0.23	4.3 (45)
	$T_{CH_2-CH_3}$	2.6	0.39 (17)	1.5	0.67 (14)
	$T_{CH_2-OCH_3}$	71	0.014 (1)	3.3	0.30 (6)
	$T_{other(CH_2)}$	0.75	1.3 (29)	0.29	3.4 (35)

From Ref. 303.

[a] T_{CH_3}, $T_{CH_3-CH_2}$ and $T_{CH_3-OCH_3}$ are the contributions to the T_1 of α-methyl protons from the partner protons (intra-group contribution) and from the methylene and the methoxy protons of the nearest neighbour, respectively. $T^{-1}_{other(CH_3)} = {}^{PMMA}T^{-1}_{CH_3} - (T^{-1}_{CH_3} + 2T^{-1}_{CH_3-CH_2} + T^{-1}_{CH_3-OCH_3})$. Other symbols are defined similarly.

[b] Numbers in parentheses are percentages of the total relaxation rate of the protons in PMMA.

ing α-methyl and methylene groups as well as the intra-group contributions were significant. The correlation times of the α-methyl and methylene protons in PMMAs were calculated from the values of T_{CH_3} and T_{CH_2}, respectively, using equation (13). The correlation time for isotactic PMMA is consistently shorter than the corresponding correlation time for syndiotactic PMMA. The results mean that the greater segmental mobility of isotactic PMMA could also be definitely evidenced from the ^{1}H NMR relaxation data.[303]

^{1}H-T_1 values for isotactic[305] and syndiotactic[304] PMMAs were analysed in terms of backbone conformational transition and methyl rotation. The results for the backbone methylene protons roughly agreed with the results given in Table 16.

^{1}H and ^{13}C NMR relaxation studies in concentrated chloroform solution[307,308] and ^{13}C relaxation studies of cross-linked gels in benzene-d_6[309] were carried out on PMMA. The dependence of the segmental mobility on stereosequence was not affected by the presence of covalent cross-links in the chain. The isotactic sequences are more mobile than the syndiotactic sequences.[309]

Completely isotactic and completely syndiotactic oligomers of MMA from dimers to octamers were isolated from stereoregular living polymerization systems of MMA in toluene at -78°C with t-C_4H_9MgBr and t-C_4H_9Li–$(C_2H_5)_3Al$, respectively.[271] The ^{13}C-T_1 values for the isotactic hexamer were found to be larger than those for the syndiotactic hexamer for any carbon in any monomeric unit, indicating higher segmental mobility of the isotactic oligomers than that of the syndiotactic oligomers (see Section 5.1).

The tacticity dependence of the ^{13}C-T_1 values was also observed for the methine carbons of polypropylene and poly(1-butene). Smaller T_1 values were observed for the syndiotactic polymers as compared with the corresponding values for the isotactic polymers. The difference is small but significant and tends to be larger when the comparison is done on the correlation times determined with the $\log \chi^2$ distribution model.[318]

^{13}C-T_1 values of isotactic-rich poly(alkyl vinyl ether)s (alkyl = CH_3, C_2H_5, *iso*-C_3H_7, *iso*-C_4H_9, t-C_4H_9) were measured in toluene at 110°C and 100 MHz.[319] The T_1 values for syndiotactic sequences are consistently larger than those for isotactic sequences, in contrast to the cases of polymethacrylates and polypropylenes mentioned above. The NOE values for the polymers of methyl and t-butyl vinyl ethers are close to the theoretical maximum. These results indicate that the syndiotactic sequences have higher mobility than the isotactic sequences.

Carbon-13 NMR spectra of 1,4-polyisoprenes in solid state have been studied above their glass transition temperatures[320,321] and the ^{13}C-T_1 values of individual carbons were found to be larger for *trans*-polyisoprene than for *cis*-polyisoprene. The reverse relationship was reported for 1,4-polybutadiene in both solid and solution.[322] The results of measurements of ^{13}C-T_1 values for

1,4-polyisoprenes in $CDCl_3$ solution at 27°C[323] are the reverse of the results obtained by Schaefer[320] in solid state; *cis*-polyisoprene showed slightly but meaningfully larger ^{13}C-T_1 values than the *trans*-polymer except for methyl carbon. The results indicate the higher segmental mobility of the *cis*-polymer chain. The T_1 of methyl carbon is much larger for the *trans*-polymer than for the *cis*-polymer, indicating the greater freedom of the internal rotation of the methyl group in *trans*-polyisoprene. The tacticity dependence of T_1 is independent of the solution concentration up to about 50%. So the structure dependence of ^{13}C-T_1 for solid polyisoprene may be different from that for polyisoprene in solution.

The ^{13}C-T_1 values of *cis–trans* isomerized polyisoprenes with different compositions were measured in $CDCl_3$ at 27°C.[323] The methyl carbon in the *trans* unit showed consistently larger T_1 values than that in the *cis* unit and the T_1 values in each unit are nearly constant regardless of the *cis–trans* composition of the polymer. On the other hand, the T_1 values of the backbone carbons depend on the *cis–trans* composition and increase with an increase in the *cis*-unit content, indicating that the segmental mobility of the 1,4-polyisoprene increases, as a whole, with an increase in the *cis* content. The T_1 for the methine carbon in the *trans* unit is longer than that in the *cis* unit of the same polymer and the T_1 for the $CH_2(1)$ methylene carbon in the *trans–trans* dyad is also longer than that in the *cis–cis* dyad. This is rather strange since the T_1 times of these carbons in *trans*-polyisoprene are shorter than those of the corresponding carbons in *cis*-polyisoprene. However, a similar phenomenon was observed for *cis–trans*-polybutadiene and was explained by the effect of the rotational barrier of the neighbouring monomer unit.[322] The relatively low activation energy for the T_1 of the *trans* unit in *cis–trans*-polybutadiene was explained as the effect of the lower rotational barrier of the neighbouring *cis* unit, and vice versa.[322] A similar explanation might apply to the results of our *cis–trans* isomerized polyisoprenes, although more detailed study is needed to confirm this.

^{13}C NMR spin-lattice relaxations in solid PMMAs of different tacticity were studied by CP/MAS NMR spectroscopy.[324–328] The relaxation proceeds more slowly in isotactic PMMA than in syndiotactic PMMA even in the solid state; this is because of the faster reorientation of the α-CH_3 group in the isotactic chain.[135] The ^{13}C-T_1 times of the α-methyl carbons of PMMAs with different tacticities were measured over a wide range of temperatures by cross polarization, magic-angle spinning, dipole dephasing (CP/DD) ^{13}C NMR spectroscopy.[325,326] The T_1 minimum was clearly observed and the T_1 value at the minimum increased with increasing isotactic content, whilst the temperature giving the minimum shifted concomitantly to a lower temperature. The data could not be interpreted by a single correlation time model and were analysed by a modified 3τ model introducing a three-fold potential minimum around the rotational axis of the methyl group. The activation energy of the α-methyl rotation is 5.9 kJ/mol for

the isotactic PMMA and 16.8 kJ/mol for the syndiotactic polymer.[325,326] The tendency for the activation energy to increase with increasing syndiotacticity has also been observed by ^{1}H NMR spectroscopy[329] and the quasi-elastic neutron scattering method.[330,331] The increased mobility of the polymer in the presence of a plasticizer was not reflected in significant changes in ^{13}C-T_1.[324]

The broad resonance of the α-methyl carbon observed in the CP/MAS/DD ^{13}C NMR spectrum of atactic PMMA can be decomposed to three peaks corresponding to different tacticities by taking advantage of the differences in the rotational motions of the α-methyl carbons in different stereosequences.[327]

7. ON-LINE GPC/NMR ANALYSIS OF STEREOREGULAR POLYMERS AND OLIGOMERS

7.1. Instrumentation and performance of GPC/NMR

Recent developments in the sensitivity and resolution of NMR spectrometers permitted us to use one as a real-time detector for high-performance liquid chromatography as demonstrated in recent review articles.[332,333] Recently we developed an on-line GPC/NMR system in which a 500-MHz ^{1}H NMR spectrometer was used as a detector.[334–339] By using on-line GPC/NMR the molecular weight of a polymer can be determined without a calibration curve if the polymer sample contains a known amount of end-group per polymer molecule.

The molecular weight dependence of polymer structures such as tacticity or copolymer composition can also be easily evaluated by on-line GPC/NMR. Data on the molecular weight dependence of polymer structures are very useful for understanding the mechanism of polymerization or the properties of polymers, and are usually collected by the fractionation of the polymer and the subsequent structural analysis of each fraction. However, this method requires a lot of time and rather a large polymer sample. The on-line GPC/NMR method is very useful for this purpose; it needs only a few hours and a very small sample (0.5–1.0 mg).

Our on-line GPC/NMR system consists of a JASCO TRI ROTAR-V chromatograph and a JEOL JNM-GX500 spectrometer (a 16-bit A/D converter was installed). A 2- or 3-mm (i.d.) glass tubing with tapered structure at both ends is employed as an NMR observation flow cell (Fig. 30); the detection volumes are 0.060 and 0.140 ml, respectively. A similar type of flow cell was used in the on-line HPLC/NMR experiments.[340,341] The tapered structures at both ends are needed to prevent turbulent flow in the inlet path of the cell, which would cause broadening of the elution band. When a cell without tapering was used, some broadening of the band was observed.[334]

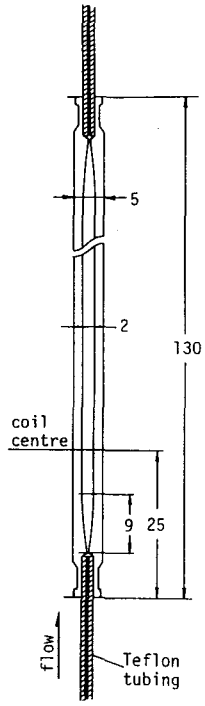

Fig. 30. Schematic diagram of the 5-mm glass tubing using for the NMR observation flow cell. The figures indicate lengths in millimetres. (From Ref. 335.)

The flow cell is mounted in the proton probe designed specially for the GPC/NMR system. The connections between the chromatograph equipped with a GPC column and the flow cell are made with a 3-m Teflon tubing (0.3 mm i.d.).

Chloroform-*d* containing 0.5% ethanol-d_6 is usually used as an eluent. The background signals due to the small amounts of impurities in the eluent, except for the H_2O signal, can be eliminated by subtracting the baseline absorbance.

The ^1H NMR data, each consisting of 8192 data points covering 4500 Hz, are collected over the entire chromatographic peak and stored as n coadded scans every t s; the repetition time and the time resolution of the chromatogram are t/n and t s, respectively. The 45° pulse is usually used. One of the characteristic features of on-line GPC/NMR is the use of the flow cell. Table 17[342] shows the effect of flow rate on the resolution of the peak of the proton of $CHCl_3$ in the deuterated chloroform. The resolution is represented both by the half-height width $W_{1/2}$ and the linewidth at the ^{13}C-satellite level W_s. The $W_{1/2}$ values are almost the same up to a flow rate of 0.5 ml/min and then become worse. The values of W_s become better as the flow rate

Table 17. Flow-rate dependency of line width of the ^1H NMR signal due to $CHCl_3$ in the eluent.[a]

	Ordinary probe (5 mm) Spinning rate (Hz)		GPC probe (2 mm i.d. cell) Flow rate (ml/min)					
	0	15	0.0	0.1	0.2	0.5	1.0	2.0
$W_{1/2}$ (Hz)[b]	1.11 (2.7)	0.69 (1.8)	0.79 (9.5)	0.77 (5.4)	0.80 (6.2)	0.88 (3.3)	0.97 (5.0)	1.55 (2.7)
W_s (Hz)[c]	25.9 (3.2)	14.4 (0.87)	18.4 (9.2)	17.7 (4.8)	14.3 (13.5)	14.0 (11.6)	12.8 (1.6)	21.8 (20.8)

From Ref. 342.

[a]Deuterated chloroform containing 5% $CHCl_3$ was used as an eluent. The mean values of five linewidth determinations are shown. The figures in parentheses are the relative standard deviation (%). Digital resolution 0.07 Hz; broadening factor 0.03 Hz.

[b]The linewidth at half-height level.

[c]The linewidth at ^{13}C-satellite level.

increases up to 1.0 ml/min. Therefore, flow rates of 0.1–0.5 ml/min were used for the measurements. It should be noted that the resolution obtained by the flow cell is much better than the resolution obtained in the ordinary measurement without spinning and not as low as that in the ordinary measurement with spinning.

For the accurate determination of signal intensities using a flow cell the volume of the cell has to be large enough for the premagnetization to be located just before that part of the cell used for signal detection. When a 90° pulse is used, a residence time longer than $5T_{1\,max}$ is needed for accurate results ($T_{1\,max}$: the largest T_1 among the T_1 values of protons in the sample).[342]

7.2. Molecular weight determination of polymers with well-defined structure

As mentioned in the previous section, determination of molecular weight by GPC requires a calibration curve, which is usually prepared using a set of standard polystyrenes with a narrow molecular weight distribution (MWD). Preparation of other standard polymers with different molecular weights and narrow MWD are generally difficult or laborious, and much attention has been given to empirical means of deriving calibrations for other polymers from that for polystyrene.[343] The only exception at present is dual detection of a GPC chromatogram by a combination of UV or refractive index (RI) method with low angle light-scattering, in which the weight-average molecular weight (M_w) of a given polymer can be determined without a calibration curve.[344]

The usefulness of a polymer having a known amount of chromophore groups per chain for absolute molecular weight calibrations in GPC has

been noted recently.[345] The technique was applied to the determination of instrumental broadening in GPC using a polystyrene polymerized with bis(3-phenylazo)benzoyl peroxide and a chromatograph equipped with a variable-wavelength UV detector which is sensitive to both the chromophore and polymer.[346]

NMR spectrometers are sensitive to mass concentration and also to the number average molecular weight ($\bar{M}_n$) of the solute polymer if the polymer molecule contains a known amount of end-groups per chain and can be used as a dual detector for GPC. Here the results of a molecular weight determination for a highly isotactic PMMA by on-line GPC/NMR technique are shown. The isotactic PMMAs were prepared by the living and isotactic polymerization of MMA with t-C_4H_9MgBr in toluene at $-78°C$. The polymer molecules contain one t-C_4H_9 group at the left end of the chain,[26,27]

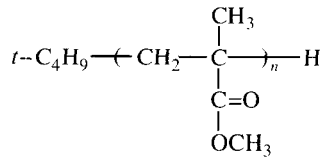

and the $\bar{M}_n$ can be determined from the relative intensities of the ^1H NMR signals due to t-C_4H_9 and CH_3O groups.

Figure 31 shows the GPC/NMR data of the isotactic PMMA with $\bar{M}_n$ of 12 600. The signals due to $-OCH_3$, CH_2, α-CH_3 and t-C_4H_9 protons resonate at 3.60, 2.13 and 1.52, 1.20 and 0.86 ppm, respectively. All the cross-sections at the peak positions give ^1H NMR-detected GPC chromatograms. The ^1H NMR-detected GPC chromatograms of the three PMMA samples are shown

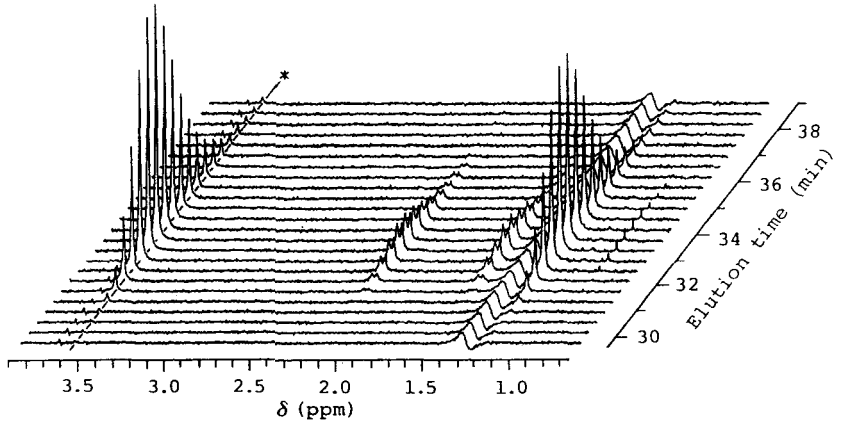

Fig. 31. On-line GPC/NMR data of isotactic PMMA (M_n = 12 600). (From Ref. 335.)

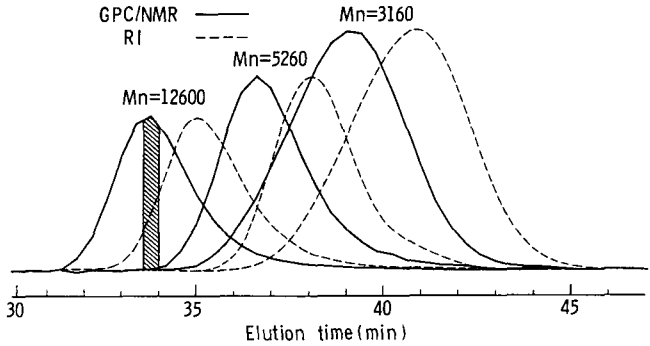

Fig. 32. The ^{1}H NMR-detected GPC curves of the isotactic PMMAs with M_n values of 12600 ($\bar{M}_w/\bar{M}_n = 1.18$), 5260 ($\bar{M}_w/\bar{M}_n = 1.13$), and 3160 ($\bar{M}_w/\bar{M}_n = 1.19$). These curves were obtained by plotting the intensity of the methoxy proton signal (3.60 ppm). The RI-detected GPC curves are also shown. (From Ref. 335.)

in Fig. 32, together with those recorded using an RI detector. The peak shapes of the ^{1}H NMR-detected and RI-detected chromatograms are very similar. The differences in elution times are due to differences in the void volume of the connecting path.

For example, the ^{1}H NMR spectrum of the PMMA ($\bar{M}_n = 12\,600$) stored as a single file for elution times from 33.6 to 34.0 min (cf. Fig. 32) has a signal-to-noise ratio (S/N) for the t-C_4H_9 end-group of 7.2, which is large enough to determine the $\bar{M}_n$ accurately. The $\bar{M}_n$ of the PMMA detected in this file was calculated to be 11 800. The files which exhibit the t-C_4H_9 signal with an S/N less than 5 are added with 2 or 3 contiguous files so that the ratio exceeds 5. Thus the $\bar{M}_n$ of each fraction can be determined directly from the ^{1}H NMR spectrum. This is one of the great advantages of the on-line GPC/NMR system over dual-detection systems such as UV–RI detectors or a variable wavelength UV detector, which requires calibration of the detected intensity of absorption due to end-groups and monomeric units in the polymer chains for the real molecular weight.

When the $\log(\bar{M}_n)$ determined from the ^{1}H NMR spectrum in each file is plotted against the elution time, the plots for all three PMMA samples fall on a single straight line. The linear relation of the $\log(\bar{M}_n)$ versus elution time obtained by the on-line GPC/NMR experiment should be the most accurate calibration curve for highly isotactic PMMA. The $\bar{M}_w/\bar{M}_n$ values calculated from the GPC/NMR method agreed well with those obtained from the normal GPC/RI method using standard polystyrenes.

It is worth noting that a single sample with a broad MWD is enough to make the calibration curve if the number of end-groups per chain is well-defined. On-line detection by ^{1}H NMR offers not only an absolute calibration curve but also information on the molecular weight dependency of some polymer properties such as tacticity or copolymer composition at the same time. Thus, efforts

directed towards the preparation of polymers of controlled structure should be encouraged in order to provide on-line GPC/NMR with suitable polymer samples.

7.3. Molecular weight dependence of tacticity and copolymer composition

The on-line GPC/NMR technique is also useful for studying the molecular weight dependence of polymer properties such as tacticity and copolymer composition. This type of information is very important for an understanding of the mechanism of polymerization. The polymerization of MMA by anionic initiators often involves multiple active species with different reactivities and stereospecificities. For example, Grignard reagent exists in the Schlenk equilibrium:

$$2RMgX \rightleftharpoons R_2Mg + MgX_2 \tag{14}$$

"RMgX" gives highly isotactic PMMA and "R_2Mg" gives syndiotactic PMMA with much higher reactivity than the former.[347] This means that the tacticity of the PMMA prepared by Grignard reagent depends strongly on the amount of

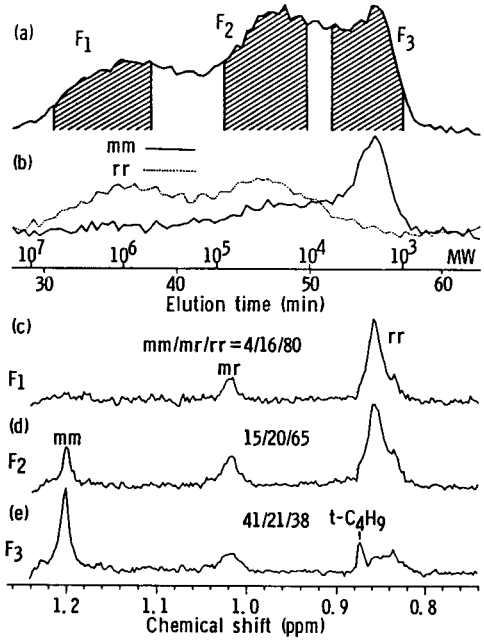

Fig. 33. The ^{1}H NMR-detected GPC traces obtained by monitoring the methoxy proton resonance at 3.60 ppm (a) and the α-methyl proton resonances at 0.86 ppm (·····) and 1.20 ppm (————) due to *rr* and *mm* triads, respectively (b). The NMR signals due to α-methyl protons of the PMMA eluted in the elution periods F_1 (c), F_2 (d) and F_3 (e) are also shown. (From Ref. 336.)

MgX_2 in the initiator solution. A t-C_4H_9MgBr solution with an $[Mg^{2+}]/[t\text{-}C_4H_9Mg]$ ratio larger than 1.5 gives a highly isotactic polymer with a narrow molecular weight distribution and that with a ratio less than unity gives a less isotactic or syndiotactic polymer.[27] Figure 33a shows the ^1H NMR-detected GPC trace of a PMMA prepared with t-C_4H_9MgBr ($[Mg^{2+}]/[t\text{-}C_4H_9Mg] = 0.87$) in toluene at $-78°C$. The chromatogram was obtained by monitoring the OCH_3 resonance at 3.60 ppm. The polymer has a trimodal molecular weight distribution, and the ^1H NMR spectra acquired in the elution periods F_1, F_2 and F_3 (cf. Fig. 33a) show that the tacticity of the higher molecular weight part is syndiotactic (Fig. 33c) while those of the lower molecular weight parts are less syndiotactic (Fig. 33d) or stereoblock-like (Fig. 33e). The molecular weight dependence of tacticity can also be illustrated in a continuous form by plotting the signal intensities of the α-CH_3 resonances at 0.86 and 1.20 ppm due to the *rr* and *mm* triads, respectively, against elution time (Fig. 33b). It is clear that the fraction of syndiotactic triad increases with an increase in molecular weight of the polymer. The results suggest that the high molecular weight part with high syndiotacticity was produced from the species generated by "$(t\text{-}C_4H_9)_2Mg$" and that the isotactic part, which has lower molecular weight and relatively narrow MWD, was produced from the species generated mainly by "t-C_4H_9MgBr".[336]

Polymerization of MMA with t-C_4H_9Li in toluene at $-78°C$ gave isotactic-rich PMMA with a broad but unimodal MWD.[69,348] Addition of trialkylaluminium to t-C_4H_9Li changes the initiator activity for MMA to syndio-

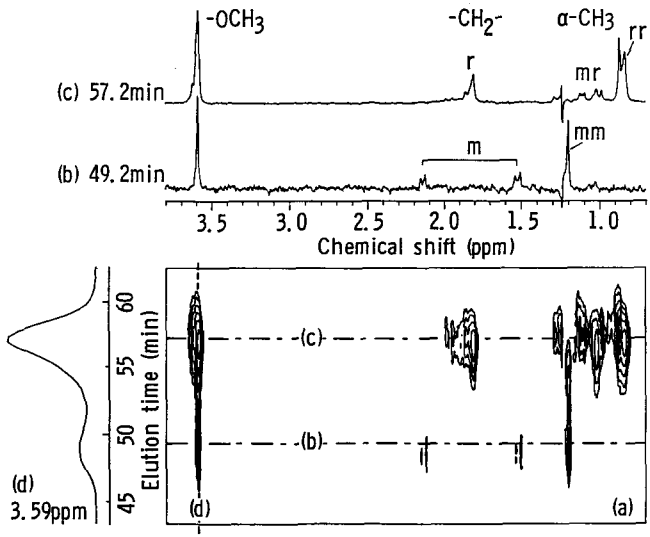

Fig. 34. A contour plot (a) and cross-sections (b–d) of the on-line GPC/NMR data for PMMA prepared with t-C_4H_9Li–$(n\text{-}C_4H_9)_3Al$ Al/Li = 1.0) in toluene at $-78°C$. (From Ref. 336.)

tactic specific and the polymerization with t-C_4H_9Li–$(n$-$C_4H_9)_3Al$ ($Al/Li \geq 2$) in toluene at −78°C gives highly syndiotactic PMMAs.[69,348] The t-C_4H_9Li–$(n$-$C_4H_9)_3Al$ ($Al/Li = 1$) system gives a stereoblock-like PMMA in toluene at −78°C. The contour plot of the GPC/NMR data for this PMMA is shown in Fig. 34a. The cross-section at the chemical shift of the OCH_3 peak (Fig. 34d) indicates the polymer has a bimodal MWD. The cross-sections at elution times of 49.2 and 57.2 min (Fig. 34b and c) clearly show that the lower molecular weight part of the polymer is syndiotactic and the higher molecular weight part is isotactic; that is, isotactic- and syndiotactic-specific propagating species exist concomitantly in the polymerization system.[336]

The on-line GPC/NMR also gives valuable information on the molecular weight dependence of copolymer composition. GPC/NMR analysis was carried out for a highly isotactic block copolymer of PMMA and poly(n-butyl methacrylate), which has a bimodal MWD. The copolymer was obtained by polymerizing n-butyl methacrylate (n-BuMA) with the PMMA living anion, which was prepared by the polymerization of MMA with t-C_4H_9MgBr in toluene at −78°C. The cross-sections at 3.59 ppm (OCH_3 of MMA unit) and 3.95 ppm (OCH_2 of n-BuMA unit) give us changes of the contents of MMA and n-BuMA units, respectively, in the copolymer along with a change of the molecular weight, indicating larger n-BuMA content in the higher molecular weight part. This is important information for understanding the mechanism of polymerization.[337]

Poly(vinyl alcohol) is usually prepared by the hydrolysis of poly(vinyl acetate) and often contains a small number of unreacted vinyl acetate units. The on-line GPC/NMR analysis of several commercial poly(vinyl alcohol)s revealed that the number of vinyl acetate units depended on the molecular weight of the polymer, lower molecular weight fractions containing larger numbers of acetate units than the higher molecular weight fractions.[338]

7.4. Simple and accurate analysis of oligomers

The on-line GPC/NMR technique also provides structural data about homologous components in oligomers if a GPC column with a small porosity is employed. The on-line GPC/NMR data were collected for a mixture of chloral oligomers. The oligomers were prepared by polymerizing chloral with t-C_4H_9OLi slightly below the ceiling temperature of polymerization and end-capping the anion with an acetate group. The trimer and the higher oligomers have been found to be completely isotactic.[280,281,349–351]

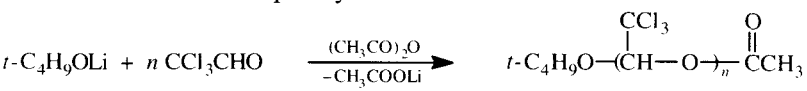

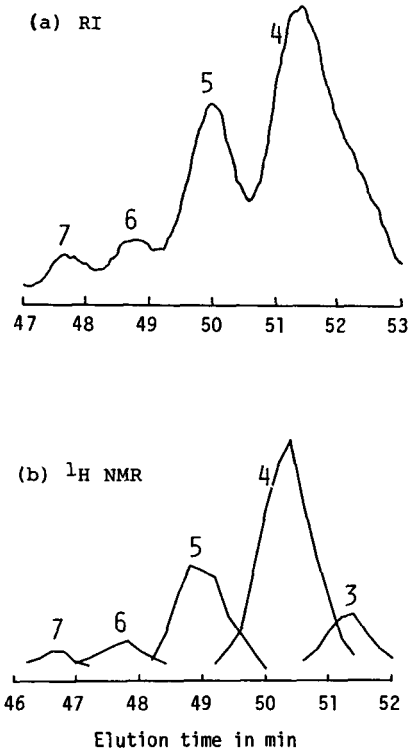

Fig. 35. The RI-detected (a) and ^{1}H NMR-detected (b) GPC curves of the mixture of chloral oligomers. (From Ref. 339.)

Figure 35 shows the GPC/NMR-detected chromatogram for the chloral oligomers together with an RI-detected chromatogram. The ^{1}H NMR detection was carried out by monitoring peak intensity of the acetal proton signals resonating at 5.92 ppm (trimer), 5.71 ppm (tetramer), 5.84 ppm (pentamer), 5.68 ppm (hexamer) and 6.23 ppm (heptamer). The peaks selected for monitoring were chosen so as to minimize any overlap effect. When the spectra recorded at elution times from 48.6 to 49.4 min are accumulated, the spectrum of the pure pentamer is obtained with a much improved S/N ratio, in spite of the incomplete separation by chromatography. This is one of the great advantages of on-line GPC/NMR. It should also be noted that in the NMR-detected GPC curves the extent of overlap of the peaks can be easily realized from the chromatogram and the relative peak intensities reflect accurately the molar fractions of the oligomer components. This is another advantage of the on-line GPC/NMR method when applied to the analysis of oligomers.

8. NMR PARAMETERS AND MONOMER REACTIVITY

Several attempts have been made to correlate the reactivities of vinyl monomers in polymerization or copolymerization with their spectral data. The studies are important and useful for understanding the mechanisms of polymerization as well as for estimating the reactivity without or prior to performing the experiments.

In radical copolymerization the Alfrey–Price Q–e scheme has been proposed for systematizing a large amount of data and for correlating the reactivity of a monomer to its chemical structure. In this scheme the monomer reactivity ratios are given by the following equations:

$$r_1 = Q_1/Q_2 \exp\{-e_1(e_1 - e_2)\} \tag{15}$$

$$r_2 = Q_2/Q_1 \exp\{-e_2(e_2 - e_1)\} \tag{16}$$

where Q is a crude measure of the resonance stabilization of monomer and e is associated with the polarity of the double bond or the propagating radical. Several attempts using UV[352] and IR[353,354] spectroscopy have been published to establish correlations between reactivity parameters in copolymerization and spectral data. The polarographic half-wave potential of reduction for vinyl and diene monomers was also found to be correlated to the Q and e values.[355]

The chemical shifts of the carbons in vinyl groups have been reported to be mainly controlled by the π-electron density,[356–358] and, therefore, it is expected that the chemical shifts for vinyl carbons and the e value can be correlated by a linear relationship. This was demonstrated by Hatada and co-workers.[359] The linear relationships clearly indicate that the chemical shift of β-carbon ($\delta C\beta$) shifts to a lower field and the shift of α-carbon ($\delta C\alpha$) to higher field as the e value of the monomer becomes larger; the π-electron density of the β-carbon decreases and that of the α-carbon increases when the e value of the monomer increases. So the results are considered to be convincing proof for the validity of the e value as a measure of polarity.

Herman and Teyssie[360] reported that a plot of $\delta C\beta$ against e for 21 substituted styrenes gave a linear relationship. Borchardt and Dalrymple[361] generated equations relating Q and e values to β- and α-carbon values by the use of a multiple-correlation analysis program. The resulting model equation is as follows:

$$\begin{aligned} e =, Q = {} & a\alpha + b\beta + c(\alpha - \beta) + d(\alpha/\beta) + f/(\alpha - \beta)^8 \\ & + g(\alpha/\beta)^{1/2} + h(\alpha^2 - \beta^2) + i\alpha^2 + j\beta^2 + k\alpha\beta \\ & + 1/\alpha + m/\beta + n\alpha^{1/2} + o\beta^{1/2} + p(\alpha^2 + \beta^2)^{1/2} \\ & + r/(\alpha^2 - \beta^2)^8 + s(\alpha - \beta)^4 + t(\alpha - \beta)^2 + u(\beta/\alpha) \\ & + v(\alpha - \beta)^3 + w/(\alpha - \beta)^{10} + \text{intercept} \end{aligned} \tag{17}$$

Separate equations for eight groups of monomers such as styrenes, chlorinated olefins, acrylates and methacrylates were developed and the correlation coefficients for most of the equations were greater than 0.99. The method has been extended to the calculation of the monomer reactivity ratios from the ^{13}C NMR spectra of the monomers for which no Q and e values are known.[362]

Hatada and co-workers studied the relationship between the monomer reactivity ratio and the ^{13}C chemical shifts of the double bond of the monomer to elucidate the meaning of e values.[363] Equation (15) can be rewritten as follows:

$$\log(1/r_1) - \log Q_2 = -0.4343e_1e_2 + 0.4343e_1^2 - \log Q_1 \qquad (18)$$

where the quantity $\log(1/r_1) - \log Q_2$ is plotted against the $\delta C\beta$ referred from TMS of various monomers M_2 in the radical copolymerization of styrene, acrylonitrile or methyl methacrylate (M_1), a linear relation is obtained; the slope of the plot is positive for styrene and negative for the other two monomers. The plots of the slope against the $\delta C\beta$ of the M_1 give a linear relation with a negative slope. As seen from equation (18), the values of these slopes should correspond to the e value of the propagating radical ending with M_1. So the results are an indication that polarity induced on the radical end by a given substituent is proportional to the polarity of the double bond of the corresponding monomer.

From equations (15) and (16) the following relation can also be obtained:

$$\log(r_1r_2) = -0.4343(e_2 - e_1)^2 \qquad (19)$$

When $\log(r_1r_2)$ in the copolymerizations of styrene or acrylonitrile (M_1) with various monomers (M_2) is plotted against $(\delta C\beta M_2 - \delta C\beta M_1)^2$, a linear relation is obtained as shown in Fig. 36. The slopes of these two straight lines are almost the same, giving support for the validity of the approximation that the e values of a monomer and its corresponding propagating radical are equal.[363]

Figure 37 shows plots of Q against the chemical shift of carbonyl carbon of the various methacrylates. The linear relation indicates that π-electron density on the carbonyl carbon increases as Q becomes larger. This should indicate that Q is a measure of the resonance stabilization of the monomers.[364] The plot of Q against the difference between the chemical shifts of two β-methylene protons of methacrylates gave a straight line with negative slope, indicating that the s-character of the vinylidene double bond is reduced as the Q value becomes larger. This is additional evidence for Q values as a measure of resonance stabilization.[364]

A much clearer indication of the meaning of Q was obtained by the measurement of the spin–spin coupling constants for methacrylates. Figure 38 shows plots of Q against the coupling constants between α- and β-carbon ($J(C\alpha\text{-}C\beta)$) and carbonyl carbon ($J(C\alpha\text{-}CO)$). As Q becomes larger,

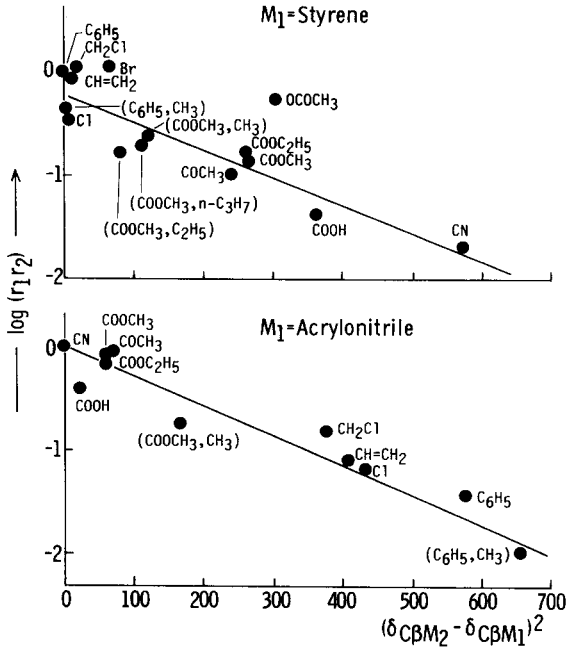

Fig. 36. Plots of $\log(r_1 r_2)$ against $(\delta C\beta M_2 - \delta C\beta M_1)^2$ in the copolymerization of styrene or acrylonitrile (M_1) with various monomers $H_2C{=}CXY$ (M_2) at about 60°C. (From Ref. 363.)

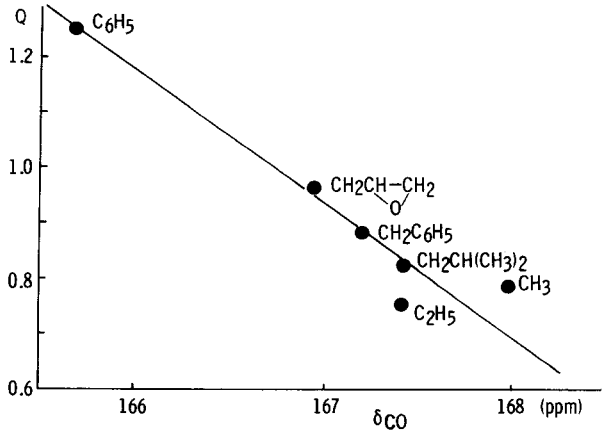

Fig. 37. Plots of Q value against the chemical shift of carbonyl carbon of the various methacrylates. (From Ref. 364.)

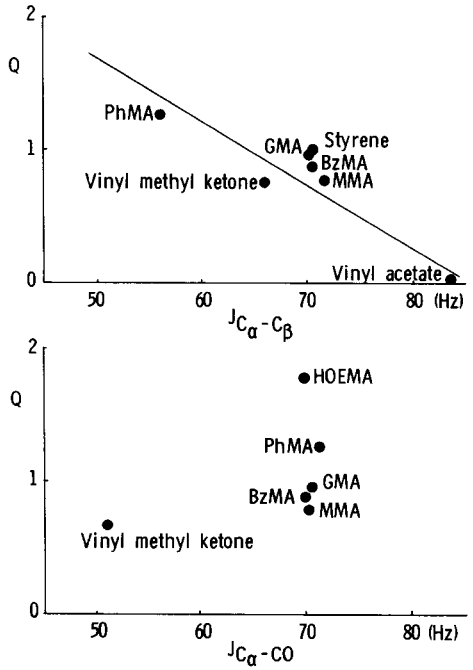

Fig. 38. Plots of Q values against $J(C\alpha\text{-}C\beta)$ and $J(C\alpha\text{-}CO)$ for several methacrylates. (From Ref. 365.)

$J(C\alpha\text{-}C\beta)$ becomes smaller and $J(\alpha\text{-CO})$ larger, indicating that the extent of resonance stabilization in methacrylate becomes larger as Q increases.[365]

^{13}C Chemical shift values also give information on the reactivity of vinyl monomers in homopolymerization by radical mechanism. In the radical polymerization of styrene and *p*-substituted styrene a participation of the following ionic structure in the transition state of the propagation reaction was suggested:[366]

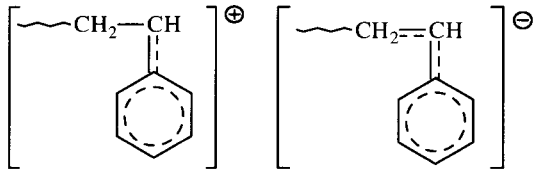

Plots of k_p for these polymerizations against $\delta C\beta$ of the corresponding monomer gave a straight line which indicates that k_p increased as $\delta C\beta$ shifted to lower field. This shows that the lower electron density on the β-carbon of the monomer, the more easily electron transfer from the polymer radical to the monomer occurs and, consequently, the higher the reactivity of

the monomer.[363] Similar analysis for the reactivity of vinyl monomers including styrenes was made using ^{1}H NMR spectra; the signals of the β-methylene protons shifted to low field with increasing monomer reactivity.[367,368]

The low polymerizability of *t*-butyl isopropenyl ketone in radical and anionic polymerizations can be explained in terms of the high electron density on the β-carbon resulting from distortion of the usual planar *s-cis* or *s-trans* conformation. The evidence is that the β-carbon of this monomer resonates at a very high field (117.7 ppm), much closer to that of the corresponding alkenes (109–117 ppm) and much higher than any of the other vinyl ketones (125–129 ppm), and that the carbonyl carbon resonates at a lower field (208.7 ppm), in the same range as the saturated ketones (208–217 ppm) and lower than the conjugative enones (198–202 ppm).[369]

Examination of the relationship between the reactivity of monomers and NMR data is also of significance to the understanding of the mechanism of ionic polymerization. Plots of the relative reactivity of substituted styrenes (M_2), $\log 1/r_1$ against $\delta C\beta$ in the cationic copolymerization of styrene as M_1 by $SnCl_4$ at 0°C are linear, and indicate that the relative reactivity is larger for the substituted styrene having the higher π-electron density on the β-carbon.[363] A similar result was also reported by Higashimura.[370] These results indicate that the attack of the growing carbonium ion on the β-carbon of the monomer is the rate-determining step in this copolymerization. Similar relations between the reactivity of the vinyl monomer and $\delta C\beta$ value were observed in the cationic copolymerization of benzyl vinyl ether with the substituted benzyl vinyl ether[371] and of phenyl vinyl ether with the substituted one.[372]

The rate constant k_{ij} of the addition reaction of substituted styrenes to the living polystyrene anion has been measured in tetrahydrofuran at 25°C.[373] When $\log k_{ij}$ was plotted against $\delta C\beta$ of the substituted styrene, a linear correlation was obtained, showing that the lower the π-electron density on the β-carbon, the higher the reactivity of the substituted styrene toward the polystyrene anion.[363]

Natta and co-workers[374] studied the copolymerization of styrene (M_1) with several substituted styrenes by Ziegler catalysts at 40°C and suggested that the coordination of the monomer to the more electron-deficient part of the catalyst complex is one of the fundamental stages in this stereospecific polymerization. By plotting the relative reactivity, $\log(1/r_1)$ against the $\delta C\beta$ of the substituted styrene a linear relationship was obtained, which exhibited a typical feature of ordinary cationic polymerization. This is direct evidence for Natta's suggestion and also a clear indication that the vinyl group of the monomer is bound to the catalyst complex at the β-position in the coordination step.[363]

In the cationic copolymerization of alkyl vinyl ethers (M_1 = *n*-butyl vinyl ether) by $EtAlCl_2$ in toluene at −78°C, the relative reactivity, $\log(1/r_1)$,

is in the order: alkyl = $CH_3 < C_2H_5 < n\text{-}C_3H_7 < n\text{-}C_4H_9 < n\text{-}C_6H_{13} < i\text{-}C_4H_9 < C_6H_5CH_2 < i\text{-}C_3H_7 < C_6H_{11} < t\text{-}C_4H_9$. The reactivity of the monomer becomes higher when the β-carbon resonates at the lower field while the α-carbon is at the higher field. This indicates that the attack of the carbonium ion on the β-carbon of the monomer is not the rate-determining step.[375,376] It has been suggested that alkyl vinyl ethers may take the following resonance form resulting from a partial double bond character in the C–O bond:[357,377]

$$\bar{C}H_2-CH=\overset{+}{O}-R$$

As the relative reactivity, $\log(1/r_1)$ becomes larger, the difference between the chemical shifts of the two β-methylene protons increases linearly. The geminal coupling constant between the two β-methylene protons, which can be used as a measure of the *s*-character of the C–H bond,[378] increases mostly with an increase in the reactivity. These results indicate that the contribution of the resonance form is greatest in methyl vinyl ether, which is the least reactive, and is least in *t*-butyl vinyl ether, which is the most reactive; resonance stabilization in alkyl vinyl ether may play some important role in determining the reactivity.[377]

Thus NMR studies of monomers are an important tool for understanding the basic problems in radical and ionic polymerization reactions.

REFERENCES

1. K. Hatada and Y. Terawaki, *Kogyo Kagaku Zasshi*, 1968, **71,** 1163.
2. K. Hatada, K. Ota, Y. Terawaki and H. Yuki, *Kogyo Kagaku Zasshi*, 1968, **71,** 1168.
3. K. Hatada, Y. Terawaki, H. Okuda, S. Niinomi and H. Yuki, *Kobunshi Kagaku*, 1971, **28,** 293.
4. K. Hatada, Y. Terawaki, J. Oshima and H. Yuki, *Kobunshi Kagaku*, 1972, **29,** 391.
5. K. Müllen and P.S. Pregosin, *Fourier Transform NMR Techniques: A Practical Approach*. Academic Press, London 1976.
6. D.H. Hoult, *Topics in Carbon-13 NMR Spectroscopy*, Vol. 3 (ed. G.C. Levy), p. 16, John Wiley & Sons, New York, 1979.
7. (a) B. Thiault and M. Mersseman, *Org. Magn. Reson.*, 1975, **7,** 575;
   (b) B. Thiault and M. Mersseman, *Org. Magn. Reson.*, 1976, **8,** 28.
8. J.C. Randall, *Polymer Sequence Determination—Carbon-13 NMR Method*, Chap. 5. Academic Press, London, 1977.
9. K. Hatada, Y. Terawaki, T. Kitayama and K. Ute, *Polym. Prep. Jpn*, 1989, **38,** 845; English edition, E345.
10. R. Chûjô, K. Hatada, R. Kitamaru, T. Kitayama, H. Sato and Y. Tanaka, *Polym. J.*, 1987, **19,** 413.
11. R. Chûjô, K. Hatada, R. Kitamaru, T. Kitayama, H. Sato, Y. Tanaka, F. Horii and Y. Terawaki, *Polym. J.*, 1988, **20,** 627.
12. R. Chûjô, H. Matsuo and Y. Inoue, *Polym. J.*, 1977, **9,** 569.
13. P.M. Henrichs, J.M. Hewitt, L.J. Schwartz and D.B. Bailey, *J. Polym. Sci., Polym. Chem. Ed.*, 1982, **20,** 775.

14. K. Hatada, Preprint of meeting of research group on NMR, January, p. 5. Society of Polymer Science, Japan, 1981.
15. W.B. Smith, *J. Chem. Educ.*, 1964, **41,** 97.
16. S. Barcza, *J. Org. Chem.*, 1963, **28,** 1914.
17. A.F. Cockerill, R.C. Harden, G.L.O. Davies and D.M. Rackham, *Org. Magn. Reson.*, 1974, **6,** 452.
18. K. Hatada, Y. Terawaki, H. Okuda, K. Nagata and H. Yuki, *Anal. Chem.*, 1969, **41,** 1518.
19. K. Hatada, Y. Terawaki and H. Okuda, *Org. Magn. Res.*, 1977, **9,** 518.
20. J.R. Zimmerman and M.R. Foster, *J. Phys. Chem.*, 1957, **61,** 282.
21. K. Frei and H.J. Bernstein, *J. Chem. Phys.*, 1962, **37,** 1891.
22. (a) K. Hatada, Y. Terawaki and H. Okuda, *Bull. Chem. Soc. Jpn.*, 1969, **42,** 1781.
(b) K. Hatada, Y. Terawaki and H. Okuda, *Bull. Chem. Soc. Jpn.*, 1972, **45,** 3720.
23. Y. Terawaki, K. Ute and K. Hatada, unpublished results.
24. W.C. Dickinson, *Phys. Rev.*, 1951, **81,** 717.
25. K. Hatada, Y. Terawaki and T. Kitayama, *Kobunshi Ronbunshu*, 1992, **49,** 335.
26. K. Hatada, K. Ute, K. Tanaka, T. Kitayama and Y. Okamoto, *Polym. J.*, 1985, **17,** 977.
27. K. Hatada, K. Ute, K. Tanaka, Y. Okamoto and T. Kitayama, *Polym. J.*, 1986, **18,** 1037.
28. K. Hatada, T. Kitayama, K. Ute, Y. Terawaki and N. Fujimoto, *Polym. Prep. Jpn.*, 1991, **40,** 1119; English edition, E457.
29. K. Hatada, T. Kitayama, K. Ute and Y. Terawaki, *Polym. Prep. Jpn.*, 1987, **36,** 3112.
30. J.W. Cooper, *Topics in Carbon-13 NMR Spectroscopy*, Vol. 2 (ed. G.C. Levy), p. 411. John Wiley & Sons, New York, 1976.
31. C.H. Sotak, C.L. Dumoulin and G.C. Levy, *Anal. Chem.*, 1983, **55,** 782.
32. J. Reuben and A. Biswas, *Macromolecules*, 1991, **24,** 648.
33. D.H. Solomon, *J. Macromol. Sci. -Chem.*, 1982, **A17,** 337.
34. J.C. Bevington, J.R. Ebdon and T.N. Huckerby, *Eur. Polym. J.*, 1985, **21,** 685.
35. D.E. Axelson and K.E. Russell, *Prog. Polym. Sci.*, 1985, **11,** 221.
36. J.C. Bevington, H.W. Melville and R.P. Taylor, *J. Polym. Sci.*, 1954, **12,** 449.
37. J.C. Bevington, H.W. Meville and R.P. Taylor, *J. Polym. Sci.*, 1954, **14,** 463.
38. K. Hatada, T. Kitayama and E. Masuda, *Polym. J.*, 1986, **18,** 395.
39. T. Kashiwagi, A. Inada, J.E. Brown, K. Hatada, T. Kitayama and E. Masuda, *Macromolecules*, 1986, **19,** 2160.
40. J.C. Bevington, *Proc. R. Soc. Lond. A*, 1951, **231,** 420.
41. K. Hatada, T. Kitayama and H. Yuki, *Makromol. Chem., Rapid Commun.*, 1980, **1,** 51.
42. K. Hatada, T. Kitayama and E. Masuda, *Polym. J.*, 1985, **17,** 985.
43. G. Moad, D.H. Solomon, S.R. Johns and R.I. Willing, *Macromolecules*, 1984, **17,** 1094.
44. S.R. Johns, E. Rizzardo, D.H. Solomon and R.I. Willing, *Makromol. Chem., Rapid Commun.*, 1983, **4,** 29.
45. P.H. Plesch, *J. Chem. Soc.*, 1953, 1659.
46. C.G. Overberger and G.F. Endres, *J. Polym. Sci.*, 1955, **16,** 283.
47. C.G. Overberger, G.F. Endres and A. Monaci, *J. Am. Chem. Soc.*, 1956, **78,** 1969.
48. T. Higashimura and S. Okamura, *Kobunshi Kagaku*, 1956, **13,** 397.
49. T. Higashimura, T. Yonezawa, K. Fukui and S. Okamura, *Kobunshi Kagaku*, 1956, **13,** 431.
50. K. Hatada, T. Kitayama and H. Yuki, *Polym. Bull.*, 1980, **2,** 15.
51. Y. Sakurada, T. Higashimura and S. Okamura, *J. Polym. Sci.*, 1958, **33,** 496.
52. P.H. Plesch (Ed.), *The Chemistry of Cationic Polymerization*, p. 241. Pergamon Press, New York, 1963.
53. S. Bywater, *Adv. Polym. Sci.*, 1965, **4,** 66.
54. K. Hatada, T. Kitayama and K. Ute, *Prog. Polym. Sci.*, 1988, **13,** 189.
55. D.M. Wiles and S. Bywater, *Chem. Ind.*, 1963, 1209.
56. D.M. Wiles and S. Bywater, *J. Phys. Chem.*, 1964, **68,** 1983.
57. D.M. Wiles and S. Bywater, *Trans. Faraday Soc.*, 1965, **61,** 150.

58. N. Kawabata and T. Tsuruta, *Makromol. Chem.*, 1965, **86,** 231.
59. K. Hatada, T. Kitayama, K. Fujikawa, K. Ohta and H. Yuki, *ACS Symp. Series*, 1981, **166,** 327.
60. K. Hatada, T. Kitayama, S. Okahata and H. Yuki, *Polym. J.*, 1981, **13,** 1045.
61. K. Hatada, T. Kitayama, S. Okahata and H. Yuki, *Polym. J.*, 1982, **14,** 971.
62. T. Kitayama, K. Ute and K. Hatada, *Polym. J.*, 1984, **16,** 925.
63. K. Ute, T. Kitayama and K. Hatada, (to be published).
64. B.J. Cottam, D.M. Wiles and S. Bywater, *Can. J. Chem.*, 1963, **41,** 1905.
65. K. Ute, T. Kitayama and K. Hatada, *Polym. J.*, 1986, **18,** 249.
66. K. Hatada, K. Ute, K. Tanaka, T. Kitayama and Y. Okamoto, *Recent Advances in Anionic Polymerization* (ed. T.E. Hogen-Esch and J. Smid), p. 195. Elsevier, Amsterdam, 1987.
67. K. Hatada, H. Nakanishi, K. Ute and T. Kitayama, *Polym. J.*, 1986, **18,** 581.
68. Zun-Kui Cao, K. Ute, T. Kitayama, Y. Okamoto and K. Hatada, *Kobunshi Ronbunshu*, 1986, **43,** 435.
69. T. Kitayama, T. Shinozaki, T. Sakamoto, M. Yamamoto and K. Hatada, *Makromol. Chem., Suppl.*, 1989, **15,** 167.
70. G. Moad, D.H. Solomon, S.R. Johns and R.I. Willing, *Macromolecules*, 1982, **15,** 1188.
71. J.C. Bevington, T.N. Huckerby and N.W.E. Hutton, *Eur. Polym. J.*, 1982, **18,** 963.
72. J.C. Bevington, T.N. Huckerby and N.W.E. Hutton, *Eur. Polym. J.*, 1984, **20,** 525.
73. K. Hatada, K. Ute and M. Kashiyama, *Polym. J.*, 1990, **22,** 853.
74. J.C. Bevington, T.N. Huckerby and N. Vickerstaff, *Makromol. Chem., Rapid Commun.*, 1983, **4,** 349.
75. J.C. Bevington, T.N. Huckerby and N. Vickerstaff, *Makromol. Chem., Rapid Commun.*, 1988, **9,** 791.
76. J.C. Bevington, J.R. Ebdon, T.N. Huckerby and N.W.E. Hutton, *Polym. Commun.*, 1982, **23,** 163.
77. T. Kitayama, S. Kishiro, E. Masuda and K. Hatada, *Polym. Bull.*, 1991, **25,** 205.
78. J.C. Bevington, S.W. Breuer, E.N.J. Heseltine, T.N. Huckerby and S.C. Varma, *J. Polym. Sci., Polym. Chem.*, 1987, **25,** 1085.
79. W.H. Starnes, Jr., I.M. Plitz, F.C. Schilling, G.M. Villacorta, G.S. Park and A.H. Saremi, *Macromolecules*, 1984, **17,** 2507.
80. J.C. Bevington and T.N. Huckerby, *J. Macromol. Sci.-Chem.*, 1983, **A20,** 753.
81. K. Behari, J.C. Bevington and T.N. Huckerby, *Polymer*, 1988, **29,** 1867.
82. K. Behari, J.C. Bevington and T.N. Huckerby, *Makromol. Chem.*, 1987, **188,** 2441.
83. J.C. Bevington, T.N. Huckerby and N.W.E. Hutton, *J. Polym. Sci., Polym. Chem. Ed.*, 1982, **20,** 2655.
84. K. Behari, J.C. Bevington, S.W. Breuer and T.N. Huckerby, *Eur. Polym. J.*, 1988, **24,** 187.
85. G. Ayrey, K. Jumangt, J.C. Bevington and T.N. Huckerby, *Polym. Commun.*, 1983, **24,** 2758.
86. G. Moad, E. Rizzardo and D.H. Solomon, *Polym. Bull.*, 1984, **12,** 471.
87. D.A. Cywar and D.A. Tirrell, *Macromolecules*, 1986, **19,** 2908.
88. G.S. Prementine and D.A. Tirrell, *Macromolecules*, 1987, **20,** 3034.
89. D.J.T. Hill, J.H. O'Donnell and P.W. O'Sullivan, *Macromolecules*, 1982, **15,** 960.
90. J.C. Bevington, D.A. Cywar, T.H. Huckerby, E. Senogles and D.A. Tirrell, *Eur. Polym. J.*, 1990, **26,** 41.
91. J.C. Bevington and C.S. Brooks, *Makromol. Chem.*, 1958, **28,** 173.
92. J.C Bevington and T.N. Huckerby, *Macromolecules*, 1985, **18,** 176.
93. J.C. Bevington, S.W. Breuer and T.N. Huckerby, *Macromolecules*, 1989, **22,** 55.
94. T. Nakata, *Coordination Polymerization* (ed. C.C. Price and E.J. Vanderberg), p. 55. Plenum, New York, 1983.
95. K. Miura, T. Kitayama, K. Hatada and T. Nakata, *Polym. J.*, 1990, **22,** 671.
96. S. Sosnowski, A. Duda, S. Slomkowski and S. Penczek, *Makromol. Chem., Rapid Commun.*, 1984, **5,** 551.

97. S. Penczek and S. Sosnowski, *Recent Advances in Anionic Polymerization* (ed. T.E. Hogen-Esch and J. Smid), p. 275. Elsevier, Amsterdam, 1987.
98. H. Keul, H. Höcker, E. Leitz, K.-H. Ott and L. Morbitzer, *Makromol. Chem.*, 1990, **191,** 1975.
99. M. Basko, A. Nyk, P. Klosinski, J. Libiszowski, P. Kubisa and S. Penczek, *Polym. Bull.*, 1991, **26,** 63.
100. S.S. Huang, A.H. Soum and T.E. Hogen-Esch, *J. Polym. Sci., Polym. Lett. Ed.*, 1983, **21,** 559.
101. A.H. Soum and T.E. Hogen-Esch, *Macromolecules*, 1985, **18,** 690.
102. A. Zambelli, P. Locatelli, M.C. Sacchi and E. Rigamonti, *Macromolecules*, 1980, **13,** 798.
103. A. Zambelli, P. Locatelli, M.C. Sacchi and G. Zannoni, *Macromolecules*, 1982, **15,** 211.
104. A. Zambelli, P. Locatelli and G. Bajo, *Macromolecules*, 1979, **12,** 154.
105. A. Zambelli, P. Locatelli and E. Rigamonti, *Macromolecules*, 1979, **12,** 156.
106. A. Zambelli, P. Locatelli, M.C. Sacchi and I. Tritto, *Macromolecules*, 1982, **15,** 831.
107. M.C. Sacchi, P. Locatelli, A. Zambelli and I. Tritto, *Makromol. Chem., Rapid Commun.*, 1984, **5,** 661.
108. P. Locatelli, M.C. Sacchi, I. Tritto, G. Zannoni, A. Zambelli and V. Piscitelli, *Macromolecules*, 1985, **18,** 627.
109. P. Locatelli, I. Tritto and M.C. Sacchi, *Makromol. Chem., Rapid Commun.*, 1984, **5,** 495.
110. M.C. Sacchi, P. Locatelli, I. Tritto and D.R. Ferro, *Makromol. Chem., Rapid Commun.*, 1984, **5,** 731.
111. A. Zambelli, P. Locatelli, M.C. Sacchi, P. Ammendola and G. Zannoni, *Macromolecules*, 1983, **16,** 341.
112. J.A. Ewen, *J. Am. Chem. Soc.*, 1984, **106,** 6355.
113. W. Kaminski, K. Kulper, H. Brintzinger and F.R.W.P. Wild, *Angew. Chem. Int. Ed., Eng.*, 1985, **24,** 507.
114. P. Longo, A. Grassi, C. Pellecchia and A. Zambelli, *Macromolecules*, 1987, **20,** 1015.
115. M.C. Sacchi, C. Shan, P. Locatelli and I. Tritto, *Macromolecules*, 1990, **23,** 383.
116. I. Tritto, M.C. Sacchi, P. Locatelli and G. Zannoni, *Macromolecules*, 1989, **22,** 2535.
117. I. Tritto, M.C. Sacchi, P. Locatelli and G. Zannoni, *Macromolecules*, 1988, **21,** 384.
118. P. Ammendola, A. Vitagliano, L. Oliva and A. Zambelli, *Makromol. Chem.*, 1984, **185,** 2421.
119. P. Ammendola and A. Zambelli, *Makromol. Chem.*, 1984, **185,** 2451.
120. P. Locatelli, M.C. Sacchi, I. Tritto and F. Forlini, *Macromolecules*, 1990, **23,** 2406.
121. P. Locatelli, M.C. Sacchi, I. Tritto and G. Zannoni, *Makromol. Chem., Rapid Commun.*, 1988, **9,** 575.
122. P. Locatelli, M.C. Sacchi, E. Rigamonti and A. Zambelli, *Macromolecules*, 1984, **17,** 123.
123. A. Meisters, G. Moad, E. Rizzardo and D.H. Solomon, *Polym. Bull.*, 1988, **20,** 499.
124. N.S. Enikolopyan, B.R. Smirnov, G.V. Ponomarev and I.M. Belgovskii, *J. Polym. Sci. Polym. Chem. Ed.*, 1981, **19,** 879.
125. (a) G.F. Meijs, E. Rizzard and S.H. Thang, *Macromolecules*, 1988, **21,** 3122.
(b) G.F. Meijs, T.C. Morton, E. Rizzard and S.H. Thang, *Macromolecules*, 1991, **24,** 3689.
126. B. Yamada and T. Otsu, *Makromol. Chem. Rapid Commun.*, 1990, **11,** 513.
127. B. Yamada, E. Kato, S. Kobatake and T. Otsu, *Polym. Bull.*, 1991, **25,** 423.
128. G.M. Burnett and G.M. Melville, *Discuss. Faraday Soc.*, 1947, **2,** 322.
129. W.H. Stockmayer and L.H. Peebles, Jr., *J. Am. Chem. Soc.*, 1953, **75,** 2278.
130. (a) M. Kamachi, D.J. Liaw and S. Nozakura, *Polym. J.*, 1979, **11,** 921.
(b) M. Kamachi, J. Satoh and D.J. Liaw, *Polym. Bull.*, 1979, **1,** 581.
131. K. Hatada, Y. Terawaki, T. Kitayama, M. Kamachi and M. Tamaki, *Polym. Bull.*, 1981, **4,** 451.
132. S. Palit and S.K. Das, *Proc. Roy. Soc.*, 1954, **A226,** 82.
133. S. Amiya, *Bunseki*, 1984, 850.
134. S. Amiya, *Kobunshi*, 1987, **36,** 722.
135. S. Amiya, *Kobunshi-Kako* (*Polymer Applications*), 1989, **38,** 388.
136. S. Amiya and M. Uetsuki, *Macromolecules*, 1982, **15,** 166.

137. D.W. Ovenall, *Macromolecules*, 1984, **17,** 1458.
138. S. Amiya and M. Uetsuki, *Anal. Sci.*, 1985, **1,** 91.
139. A. Guyot, *Pure Appl. Chem.*, 1985, **57,** 833.
140. T. Hjertberg, E. Sörvik and A. Wendel, *Makromol. Chem., Rapid Commun.*, 1983, **4,** 175.
141. C.J.M. van den Heuvel and A.J.M. Weber, *Makromol. Chem.*, 1983, **184,** 2261.
142. C.J.M. van den Heuvel and A.J.M. Weber, *Makromol. Chem., Rapid Commun.*, 1984, **5,** 57.
143. W.H. Starnes, Jr., *Pure Appl. Chem.*, 1985, **57,** 1001.
144. W.H. Starnes, Jr., G.M. Villacorta, F.C. Schilling, I.M. Plitz, G.S. Park and A.H. Saremi, *Macromolecules*, 1985, **18,** 1780.
145. W.H. Starnes, Jr., F.C. Schilling, I.M. Plitz, R.E. Cais, D.J. Freed, R.L. Hartless and F.A. Bovey, *Macromolecules*, 1983, **16,** 790.
146. M.F. Llauro-Darricades, N. Bensemra, A. Guyot and R. Petiaud, *Macromol. Chem. Macromol. Symp.*, 1989, **29,** 171.
147. W.H. Starnes, F.C. Schilling, K.B. Abbas, R.E. Cais and F.A. Bovey, *Macromolecules*, 1979, **12,** 556.
148. A. Grassi, A. Zambelli, L. Resconi, E. Albizzati and R. Mazzocchi, *Macromolecules*, 1988, **21,** 617.
149. A. Zambelli, P. Longo and A. Grassi, *Macromolecules*, 1989, **22,** 2186.
150. T. Hayashi, Y. Inoue, R. Chûjô and T. Asakura, *Macromolecules*, 1988, **21,** 2675.
151. A. Zambelli, P. Locatelli, A. Provasoli and D.R. Ferro, *Macromolecules*, 1980, **13,** 267.
152. R. Chûjô, *Kagaku*, 1980, **36,** 420.
153. (a) Y. Doi, S. Ueki and T. Keii, *Macromolecules*, 1979, **12,** 814.
(b) Y. Doi, S. Suzuki and K. Soga, *Macromolecules*, 1986, **19,** 2896.
154. Y. Doi, F. Nozawa, M. Murata, S. Suzuki and K. Soga, *Makromol. Chem.*, 1985, **186,** 1825.
155. A. Zambelli, P. Longo, C. Pellecchia and A. Grassi, *Macromolecules*, 1987, **20,** 2035.
156. J.C. Randall, *Polymer Sequence Determination—Carbon-13 NMR Method*, Chap. 6. Academic Press, New York, 1977.
157. K. Hatada, Y. Terawaki, T. Kitayama and K. Ute, *Polym. Prep. Jpn*, 1989, **38,** 845; English edition E345.
158. K. Hatada, *Kobunshi Sokuteiho* (in Japanese). The Society of Polymer Science, Japan, p. 5. Kyoritsu Shuppan, Tokyo, 1990.
159. K. Hatada, T. Kitayama, Y. Terawaki and R. Chûjô, *Polum. J.*, 1987, **19,** 1127.
160. I. Ando and A. Nishioka, *Kogyo Kagaku Zasshi*, 1970, **73,** 375.
161. R. Chûjô, *J. Phys. Soc. Jpn*, 1966, **21,** 2669.
162. M. Reinmollen and T.G. Fox, *Polym. Prep., Am. Chem. Soc., Div. Polym. Chem.*, 1966, **7,** 999.
163. G. Moad, D.H. Solomon, T.H. Spurling, S.R. Johns and R.I. Willing, *Austr. J. Chem.*, 1986, **39,** 43.
164. J. King, D.I. Bower, W.F. Maddams and H. Pyszora, *Makromol. Chem.*, 1983, **184,** 879.
165. H. Yuki, K. Hatada and S. Kokan, *Polym. J.*, 1973, **5,** 329.
166. K. Hatada, S. Kokan and H. Yuki, *J. Polym. Sci., Polym. Lett. Ed.*, 1975, **13,** 721.
167. K. Hatada, M. Furomoto and H. Yuki, *Makromol. Chem.*, 1978, **179,** 1107.
168. K. Hatada, M. Furomoto, T. Kitayama, Y. Tsubokura and H. Yuki, *Polym. J.*, 1980, **12,** 193.
169. A. Nishioka, H. Watanabe, K. Abe and Y. Sono, *J. Polym. Sci.*, 1960, **48,** 241.
170. F.A. Bovey and G.V.D. Tiers, *J. Polym. Sci.*, 1960, **44,** 173.
171. Y. Inoue, A. Nishioka and R. Chûjô, *Polym. J.*, 1971, **2,** 535.
172. I.R. Peat and W.F. Reynolds, *Tetrahedron Lett.*, 1972, 1359.
173. R.C. Ferguson and D.W. Ovenall, *Polym. Prep., Am. Chem. Soc., Div. Polym. Chem.*, 1985, **26,** 182.
174. W.-G. Hiller, H. Pasch and I.V. Lampe, *Makromol. Chem.*, 1991, **192,** 1431.
175. H.L. Frisch, C.L. Mallows and F.A. Bovey, *J. Chem. Phys.*, 1966, **45,** 1565.
176. F.C. Stehling and J.R. Knox, *Macromolecules*, 1975, **8,** 595.
177. D.Y. Yoon and P.J. Flory, *Macromolecules*, 1977, **10,** 562.
178. L. Schepherd, T.K. Chen and H.J. Harwood, *Polym. Bull.*, 1979, **1,** 445.

179. U.W. Suter and P. Neuenschwander, *Macromolecules*, 1981, **14,** 528.
180. H.J. Harwood, T.K. Chen, A. DasGupta, J.F. Kinstle, E.R. Saufee, L. Shepherd and F.-T. Lin, *Polym. Prep., Am. Chem. Soc., Div. Polym. Chem.*, 1985, **26**(1), 39.
181. A. Dworak, W.J. Freeman and H.J. Harwood, *Polym. J.*, 1985, **17,** 351.
182. F.A. Bovey, *Chain Structure and Conformation of Macromolecules*, p. 40. Academic Press, New York, 1982.
183. A. Zambelli, P. Locattelli, G. Bajo and F.A. Bovey, *Macromolecules*, 1975, **8,** 687.
184. H. Sato, Y. Tanaka and K. Hatada, *Makromol. Chem. Rapid Commun.*, 1982, **3,** 181.
185. H. Sato and Y. Tanaka, *Macromolecules*, 1984, **17,** 1964.
186. I. Ando and T. Asakura, *Ann. Reports NMR*, 1980, **10A,** 81.
187. A.E. Tonnelli, *NMR Spectroscopy and Polymer Microstructure: The Conformational Connection*, p. 84. VCH Publishers, New York, 1989.
188. T. Asakura, M. Demura and Y. Nishiyama, *Macromolecules*, 1991, **24,** 2334.
189. H. Yuki, K. Hatada, T. Niinomi and Y. Kikuchi, *Polym. J.*, 1970, **1,** 36.
190. H. Yuki, K. Hatada, T. Niinomi, M. Hashimoto and J. Ohshima, *Polym. J.*, 1971, **2,** 629.
191. K. Hatada, Y. Okamoto, H. Ise, S. Yamaguchi and H. Yuki, *J. Polym. Sci., Polym. Lett. Ed.*, 1975, **13,** 731.
192. K. Hatada, Y. Okamoto, K. Ohta and H. Yuki, *J. Polym. Sci. Polym. Lett. Ed.*, 1976, **14,** 51.
193. K. Hatada, K. Ohta, Y. Okamoto, T. Kitayama, Y. Umemura and H. Yuki, *J. Polym. Sci., Polym. Lett. Ed.*, 1976, **14,** 531.
194. F.W. Benz, J. Feeney and G.C.K. Roberts, *J. Magn. Reson.*, 1972, **8,** 114.
195. S. Macura and L.R. Brown, *J. Magn. Reson.*, 1983, **53,** 529.
196. P.A. Mirau and F.A. Bovey, *Macromolecules*, 1986, **19,** 210.
197. M.W. Crowther, N.M. Szeverenyi and G.C. Levy, *Macromolecules.*, 1986, **19,** 1333.
198. G.P. Gippert and L.R. Brown, *Polym. Bull.*, 1984, **11,** 585.
199. K. Hikichi and M. Yasuda, *Polym. J.*, 1987, **19,** 1003.
200. M.D. Bruch, F.A. Bovey and R.E. Cais, *Macromolecules*, 1984, **17,** 2547.
201. H.N. Cheng and G.H. Lee, *Polym. Bull.*, 1985, **13,** 549.
202. M.D. Bruch, F.A. Bovey, R.E. Cais and J.H. Noggle, *Macromolecules*, 1985, **18,** 1253.
203. F.C. Schilling, F.A. Bovey, M.D. Bruch and S.A. Kozlowski, *Macromolecules*, 1985, **18,** 1418.
204. C. Chang, D.D. Muccio and T. St. Pierre, *Macromolecules*, 1985, **18,** 2334.
205. G. Moad, E. Rizzardo, D.H. Solomon, S.R. Johns and R.I. Willing, *Macromolecules*, 1986, **19,** 2494.
206. M. Kakugo, T. Miyatake, Y. Kawai, Y. Seki and K. Hikichi, *Polym. Prep. Jpn*, 1986, **35,** 3420.
207. F.A. Bovey and P.A. Mirau, *Acc. Chem. Res.*, 1988, **21,** 37.
208. K. Hatada, K. Ute, K. Tanaka, M. Imanari and N. Fujii, *Polym. J.*, 1987, **19,** 425.
209. K. Hatada, K. Ute, T. Kitayama, K. Tanaka, M. Imanari and N. Fujii, *Polym. J.*, 1989, **21,** 447.
210. K. Ute, T. Nishimura, Y. Matsuura and K. Hatada, *Polym. J.*, 1989, **21,** 231.
211. T. Kitayama, K. Ute, M. Yamamoto, N. Fujimoto and K. Hatada, *Polym. J.*, 1990, **22,** 386.
212. T. Kitayama, K. Ute and K. Hatada, *Br. Polym. J.*, 1990, **23,** 5.
213. G. Moad and R.I. Willing, *Polym. J.*, 1991, **23,** 1401.
214. T. Kitayama, T. Nishiura, M. Yamamoto and K. Hatada, *Polym. Bull.*, to be submitted.
215. A.S. Brar and G.S. Kapur, *Polym. J.*, 1988, **20,** 811.
216. T. Kitayama, K. Ute, M. Yamamoto, N. Fujimoto and K. Hatada, *Polym. Bull.*, 1991, **25,** 683.
217. L. Lochmann, J. Kolarik, D. Doskocilova, S. Vozka and J. Trekoval, *J. Polym. Sci., Polym. Chem. Ed.*, 1979, **17,** 1727.
218. H.N. Cheng and G.H. Lee, *Polym. Bull.*, 1984, **12,** 463.
219. M.D. Bruch and F.A. Bovey, *Macromolecules*, 1984, **17,** 978.
220. S.A. Heffner, F.A. Bovey, L.A. Verge, P.A. Mirau and A.E. Tonelli, *Macromolecules*, 1986, **19,** 1628.
221. M.D. Bruch and W.G. Payne, *Macromolecules*, 1986, **19,** 2712.

222. P.A. Mirau, F.A. Bovey, A.E. Tonelli and S.A. Heffner, *Macromolecules*, 1987, **20,** 1701.
223. K. Hikichi, T. Hiraoki, M. Ikura, K. Higuchi, K. Eguchi and M. Ohuchi, *Polym. J.*, 1987, **19,** 1317.
224. T. Hayashi, Y. Inoue, R. Chûjô and T. Asakura, *Polym. J.*, 1988, **20,** 895.
225. G.J. Ray, R.E. Pauls, J.J. Lewis and L.B. Rogers, *Makromol. Chem.*, 1985, **186,** 1135.
226. H.N. Cheng and M.A. Bennett, *Makromol. Chem.*, 1987, **188,** 135.
227. V.U. Johnsen and K. Kolbe, *Makromol. Chem.*, 1968, **116,** 173.
228. R. Chûjô, H. Ubara and A. Nishioka, *Polym. J.*, 1972, **3,** 670.
229. J. Cattiaux, T. Suzuki and H.J. Harwood, *J. Appl. Polym. Sci., Polym. Symp.*, 1978, **34,** 1.
230. T.A. Gerken and W.M. Ritchey, *J. Appl. Polym. Sci., Appl. Polym. Symp.*, 1978, **34,** 17.
231. Y.S. Jo, Y. Inoue, R. Chûjô, K. Saito and S.M. Miyata, *Macromolecules*, 1985, **18,** 1850.
232. K. Hatada, T. Kitayama, T. Terawaki and H. Sato, *Polym. Prep. Jpn*, 1991, **40,** 3946; English edition E1496.
233. A. Guyot and J. Guillot, *J. Macromol. Sci., Chem.*, 1968, **A2,** 889.
234. K. Ito, T. Sugie and Y. Yamashita, *Makromol. Chem.*, 1969, **125,** 291.
235. J.C. Bevington, D.O. Harris and F.S. Rankin, *Eur. Polym. J.*, 1970, **6,** 725.
236. P. Vlcek, D. Doskocilova and J. Trekoval, *J. Polym. Sci., Polym. Symp.*, 1973, **42,** 231.
237. A. Yamada and J. Tanaka, Preprint of 23rd Symposium of Polymer Science, Japan, Tokyo, 1974, p. 253.
238. Y. Okamoto, S. Nakashima, K. Ohta, K. Hatada and H. Yuki, *J. Polym. Sci., Polym. Lett. Ed.*, 1975, **13,** 273.
239. H. Yuki, Y. Okamoto, Y. Shimada, K. Ohta and K. Hatada, *J. Polym. Sci., Polym. Chem. Ed.*, 1979, **17,** 1215.
240. F.A. Bovey and G.V.D. Tiers, *Fortshr. Hochpolym. Forsch.*, 1963, **3,** 139.
241. K. Hatada, T. Kitayama, K. Fujikawa, K. Ohta and H. Yuki, *Polym. Bull.*, 1978, **1,** 97.
242. K. Hatada, T. Kitayama, T. Ochi and H. Yuki, *Polym. J.*, 1987, **19,** 1105.
243. M. Kamachi, M. Kohno, D.-J. Liaw and S. Katsuki, *Polym. J.*, 1978, **10,** 69.
244. M. Kamachi, Y. Kuwae, S. Nozakura, K. Hatada and H. Yuki, *Polym. J.*, 1981, **13,** 919.
245. Y. Gotoh and H. Hirai, *Current Topics in Polymer Science*, Vol. 1 (ed. R.H. Ottenbrite, L.A. Utradi and S. Inoue) p. 151. Hanser, Munich, 1987.
246. Y. Gotoh, M. Yamashita, M. Nakamura, N. Toshima and H. Hirai, *Chem. Lett.*, 1991, 53.
247. F.A. Bovey, *High Resolution NMR of Macromolecules*, Academic Press, New York, 1972.
248. K. Hatada, T. Hasegawa, T. Kitayama and H. Yuki, *J. Polym. Sci., Polym. Lett. Ed.*, 1976, **14,** 395.
249. F.A. Bovey, F.P. Hood III, E.W. Anderson and L.C. Snyder, *J. Chem. Phys.*, 1965, **42,** 3900.
250. D. Doskocilová and B. Schneider, *J. Polym. Sci., B*, 1965, **3,** 213.
251. D. Lim, M. Kolinsky, J. Petranek, D. Doskocilovà and B. Schneider, *J. Polym. Sci., B*, 1966, **4,** 645.
252. B. Jasse, F. Lauprêtre and L. Monnerie, *Makromol. Chem.*, 1977, **178,** 1987.
253. Y. Tanaka, H. Sato, K. Saito and K. Miyashita, *Makromol. Chem., Rapid Commun.*, 1980, **1,** 551.
254. H. Sato, Y. Tanaka and K. Hatada, *Makromol. Chem., Rapid Commun.*, 1982, **3,** 175.
255. H. Sato, Y. Tanaka and K. Hatada, *J. Polym. Sci., Polym. Phys. Ed.*, 1983, **21,** 1667.
256. S.S. Huang, C. Mathis and T.E. Hogen-Esch, *Macromolecules*, 1981, **14,** 1802.
257. S.S. Huang and T.E. Hogen-Esch, *J. Polym. Sci.*, 1985, **23,** 1203.
258. M.A. Buese and T.E. Hogen-Esch, *Macromolecules*, 1984, **17,** 118.
259. C.C. Meverden and T.E. Hogen-Esch, *J. Polym. Sci., Polym. Chem. Ed.*, 1985, **23,** 159.
260. T.E. Hogen-Esch, R.A. Smith, D. Ades and M. Fontanille, *J. Polym. Sci., Polym. Lett. Ed.*, 1981, **19,** 309.
261. K. Hashimoto and T.E. Hogen-Esch, *Macromolecules*, 1983, **16,** 1805, 1809.
262. M.A. Buese and T.E. Hogen-Esch, *J. Am. Chem. Soc.*, 1985, **107,** 4509.
263. M.A. Buese and T.E. Hogen-Esch, *Recent Advances in Anionic Polymerization* (ed. T.E. Hogen-Esch and J.C. Smid), p. 231. Elsevier, Amsterdam, 1987.

264. S. Fujishige, *Makromol. Chem.*, 1976, **177,** 375.
265. S. Fujishige, *Makromol. Chem.*, 1978, **179,** 2251.
266. A. Bledzki, H. Balard and D. Braun, *Makromol. Chem.*, 1988, **189,** 2807.
267. J.-M. Bessiere, B. Boutevin and L. Sarraf, *J. Polym. Sci.*, 1988, **A26,** 3275.
268. T. Konishi, Y. Tamai, M. Fujii, Y. Einaga and H. Yamakawa, *Polym. J.*, 1989, **21,** 329.
269. P. Cacioli, D.G. Hawthorne, S.R. Johns, D.H. Solomon, E.Rizzardo and R.I. Willing, *J. Chem. Soc., Chem. Commun.*, 1985, 1355.
270. R. Volpe and T.E. Hogen-Esch, *Macromolecules*, 1990, **23,** 4196.
271. K. Hatada, K. Ute, K. Tanaka and T. Kitayama, *Polym. J.*, 1987, **19,** 1325.
272. K. Ute, T. Nishimura and K. Hatada, *Polym. J.*, 1989, **21,** 1027.
273. K.A. Holland, I.D. Rae and J.A. Weigold, *Magn. Reson. Chem.*, 1991, **29,** 59.
274. K. Hatada, K. Ute, T. Nishimura, M. Kashiyama, T. Saito and M. Takeuchi, *Polym. Bull.*, 1990, **23,** 157.
275. G. Wulff, R. Sczepan and A. Steigel, *Tetrahedron Lett.*, 1986, **27,** 1991.
276. (a) Y. Okamoto, E. Yashima, T. Nakano and K. Hatada, *Chem. Lett.*, 1987, 759.
(b) T. Nakano, Y. Okamoto and K. Hatada, *J. Am. Chem. Soc.*, 1992, **114,** 1318.
277. K. Ute, K. Oka, Y. Okamoto, K. Hatada, F. Xi and O. Vogl, *Polym. J.*, 1991, **23,** 1419.
278. K. Ute, K. Hirose, H. Kashimoto, K. Hatada and O. Vogl, *J. Am. Chem. Soc.*, 1991, **113,** 6305.
279. K. Ute, K. Oka, M. Kashiyama, K. Hatada, F. Xi and O. Vogl, *Makromol. Chem.*, 1991, **192,** 35.
280. K. Ute, T. Nishimura, K. Hatada, F. Xi, F. Vass and O. Vogl, *Makromol. Chem.*, 1990, **191,** 557.
281. K. Hatada, K. Ute, T. Nakano, F. Vass and O. Vogl, *Makromol. Chem.*, 1989, **190,** 2217.
282. K. Ute, K. Hirose, H. Kashimoto, H. Nakayama, K. Hatada and O. Vogl, *Polym. Prep. Jpn*, 1991, **40,** 3883; English edition E1475.
283. G. Casiraghi, M. Cornia, G. Ricci, G. Casnati, G.D. Andreetti and L. Zetta, *Macromolecules*, 1984, **17,** 19.
284. K. Ute, N. Miyatake, T. Asada and K. Hatada, *Polym. Bull.*, 1992, **28,** 561.
285. K. Ute, N. Miyatake and K. Hatada, *J. Macromol. Sci.-Chem.*, 1992, **A29,** 589.
286. S.R. Johns, R.I. Willing and D.A. Winkler, *Makromol. Chem., Rapid Commun.*, 1987, **8,** 17.
287. O. Vogl, H.C. Miller and W.H. Sharkey, *Macromolecules*, 1972, **5,** 658.
288. L.S. Corley and O. Vogl, *Polym. Bull.*, 1980, **3,** 211.
289. Y. Okamoto, K. Suzuki, K. Ohta, K. Hatada and H. Yuki, *J. Am. Chem. Soc.*, 1979, **101,** 4763.
290. G.K. Hamer, F. Balza, N. Cyr and A.S. Perlin, *Can. J. Chem.*, 1978, **56,** 3109.
291. R. Yamada and I. Ando, *Polym. Prep. Jpn*, 1983, **32,** 835.
292. F. Horii, M. Nakagawa and R. Kitamaru, *Polym. Prep. Jpn*, 1987, **36,** 3151; English edition E435.
293. J. Schaefer and D.F.S. Natusch, *Macromolecules*, 1972, **5,** 416.
294. Y. Inoue, A. Nishioka and R. Chûjô, *J. Polym. Sci., Polym. Phys. Ed.*, 1973, **11,** 2237.
295. J.R. Lyerla Jr. and T.T. Horikawa, *J. Polym. Sci., Polym. Lett. Ed.*, 1976, **14,** 641.
296. K. Hatada, T. Kitayama, Y. Okamoto, K. Ohta, Y. Umemura and H. Yuki, *Makromol. Chem.*, 1978, **179,** 485.
297. K. Hatada, T. Kitayama, K. Saunders and R.W. Lenz, *Makromol. Chem.*, 1981, **182,** 1449.
298. J.R. Lyerla, Jr., T.T. Horikawa and D.E. Johnson, *J. Am. Chem. Soc.*, 1977, **99,** 2463.
299. Y. Inoue, T. Konno, R. Chûjô and A. Nishioka, *Makromol. Chem.*, 1977, **178,** 2131.
300. Y. Inoue and T. Konno, *Makromol. Chem.*, 1978, **179,** 1311.
301. J. Spevácek and B. Schneider, *Polymer*, 1978, **19,** 63.
302. G.C. Levy and D. Wang, *Macromolecules*, 1986, **19,** 1013.
303. K. Hatada, H. Ishikawa, T. Kitayama and H. Yuki, *Makromol. Chem.*, 1977, **178,** 2753.
304. F. Heatley and M.K. Cox, *Polymer*, 1980, **21,** 381.
305. F. Heatley and M.K. Cox, *Polymer*, 1981, **22,** 190.
306. F. Heatley and M.K. Cox, *Polymer*, 1981, **22,** 288.

307. J. Zajicek, H. Pivcová and B. Schneider, *Makromol. Chem.*, 1981, **182,** 3169.
308. J. Zajicek, H. Pivcová and B. Schneider, *Makromol. Chem.*, 1981, **182,** 3177.
309. T. Asakura, K. Suzuki, K. Horie and S. Mita, *Makromol. Chem.*, 1981, **182,** 2289.
310. K. Hatada, T. Kitayama, Y. Terawaki, K. Ohta, Y. Okamoto, H. Yuki and R.W. Lenz, *Bull. Inst. Chem. Res. Kyoto Univ.*, 1988, **66,** 115.
311. S.H. Oh, R. Ryoo and M.S. Jhon, *J. Polym. Sci., Polym. Chem. Ed.*, 1989, **27,** 1383.
312. T.M. Connor, *Trans. Faraday Soc.*, 1964, **60,** 1574.
313. J. Schaefer, *Macromolecules*, 1973, **6,** 882.
314. B. Valeur, J.P. Jarry, F. Geny and L. Monnerie, *J. Polym. Sci., Polym. Phys. Ed.*, 1975, **13,** 667.
315. B. Valeur, L. Monnerie and J.-P. Jarry, *J. Polym. Sci., Polym. Phys. Ed.*, 1975, **13,** 675.
316. B. Valeur, J.-P. Jarry, F. Geny and L. Monnerie, *J. Polym. Sci., Polym. Phys. Ed.*, 1975, **13,** 2251.
317. A. Carrington and A.D. McLachlan, *Introduction to Magnetic Resonance*, Chap. 11. Harper & Row, New York, 1967.
318. T. Asakura and Y. Doi, *Macromolecules*, 1983, **16,** 786.
319. K. Hatada, T. Kitayama, N. Matsuo and H. Yuki, *Polym. J.*, 1983, **15,** 719.
320. J. Schaefer, *Macromolecules*, 1972, **5,** 427.
321. R.A. Komoroski, J. Maxfield and L. Msandelkern, *Macromolecules*, 1977, **10,** 545.
322. W. Gronski and N. Murayama, *Makromol. Chem.*, 1976, **177,** 3017.
323. K. Hatada, T. Kitayama, Y. Terawaki, Y. Tanaka and H. Sato, *Polym. Bull.*, 1980, **2,** 791.
324. H.T. Edzes and W.S. Veeman, *Polym. Bull.*, 1981, **5,** 255.
325. B. Gabrys, F. Horii and R. Kitamaru, *Macromolecules*, 1987, **20,** 175.
326. F. Horii, Y. Chen, M. Nakagawa, B. Gabrys and R. Kitamuru, *Bull. Inst. Chem. Res., Kyoto Univ.*, 1988, **66,** 317.
327. H. Tanaka, M.A. Gomez and A.E. Tonelli, *Macromolecules*, 1988, **21,** 2934.
328. H. Tanaka, *J. Appl. Polym. Sci.*, 1982, **27,** 2197.
329. T.M. Connor and A. Hartland, *Phys. Lett.*, 1966, **23,** 662.
330. J.S. Higgins, G. Allen and P.N. Brier, *Polymer*, 1972, **13,** 157.
331. G. Allen, C.J. Wright and J.S. Higgins, *Polymer*, 1974, **15,** 319.
332. H.C. Dorn, *Anal. Chem.*, 1984, **56,** 747A.
333. D.A. Laude Jr. and C.L. Wilkins, *Trends Anal. Chem.*, 1986, **5,** 230.
334. K. Hatada, K. Ute, Y. Okamoto, M. Imanari and N. Fujii, *Polym. Bull.*, 1988, **20,** 317.
335. K. Hatada, K. Ute, M. Kashiyama and M. Imanari, *Polym. J.*, 1990, **22,** 218.
336. K. Hatada, K. Ute, T. Kitayama, T. Nishimura, M. Kashiyama and N. Fujimoto, *Polym. Bull.*, 1990, **23,** 549.
337. K. Hatada, K. Ute, T. Kitayama, M. Yamamoto, T. Nishimura and M. Kashiyama, *Polym. Bull.*, 1989, **21,** 489.
338. M. Hotta, K. Ute and K. Hatada, *Polym. Prep. Jpn*, 1991, **40,** 1123; English edition E459.
339. K. Ute, M. Kashiyama, K. Oka, K. Hatada and O. Vogl, *Makromol. Chem., Rapid Commun.*, 1990, **11,** 31.
340. J.F. Haw, T.E. Glass and H.C. Dorn, *Anal. Chem.*, 1981, **53,** 2327.
341. K. Albert and E. Bayer, *Trends Anal. Chem.*, 1988, **7,** 288.
342. K. Ute, M. Kashiyama and K. Hatada, unpublished results.
343. Z. Grubisic, P. Rempp and H. Benoit, *J. Polym. Sci.*, 1967, **B5,** 753.
344. W. Kaye and A.J. Havlik, *Appl. Optics*, 1973, **12,** 541.
345. H.A. Andreetta, I.H. Sorokin and R.V. Figini, *Makromol. Chem., Rapid Commun.*, 1985, **6,** 419.
346. T.Q. Nguyen and H.H. Kausch, *J. Chromatogr.*, 1988, **449,** 63.
347. K. Matsuzaki, H. Tanaka and T. Kanai, *Makromol. Chem.*, 1981, **182,** 2905.
348. T. Kitayama, T. Shinozaki, E. Masuda, M. Yamamoto and K. Hatada, *Polym. Bull.*, 1988, **20,** 505.

349. O. Vogl, *The Chemist*, 1985, **62,** 16.
350. J. Zhang, G.D. Jaycox and O. Vogl, *Polymer*, 1988, **29,** 707.
351. O. Vogl, K. Ute, T.Nishimura, F. Xi, F. Vass and K. Hatada, *Macromolecules*, 1989, **22,** 4658.
352. T. Ito, T. Otsu and M. Imoto, *J. Polym. Sci., Part B*, 1966, **4,** 81.
353. Yu. D. Semchikov, A.N. Egorochkin and A.V. Ryabov, *Vysokomol. Soedin., Ser. B*, 1973, **15**(12), 993; *Chem. Abstr.*, **81,** 64049c.
354. H. Fujihara, K. Matsuzaki, Y. Matsubara, M. Yishihara and T. Maeshima, *J. Macromol. Sci. Chem.*, 1979, **13,** 1081.
355. S.A. Voronov, V.A. Puchin, L.A. Kosik, V.S. Tokarev and E.M. Kisilev, *Vysokomol. Soedin. Ser. B*, 1978, **20,** 577. *Chem. Abstr.*, 1978, **89,** 164033b.
356. G.E. Maciei, *J. Phys. Chem.*, 1965, **69,** 1947.
357. T. Higashimura, S. Okamura, I. Morishima and T. Yonezawa, *Polym. Lett.*, 1969, **7,** 23.
358. M. Karplus and J.A. Pople, *J. Chem. Phys.*, 1963, **38,** 2803.
359. K. Hatada, K. Nagata and H. Yuki, *Bull. Chem. Soc. Jpn*, 1970, **43,** 3267.
360. J.J. Herman and Ph. Teyssie, *Macromolecules*, 1978, **11,** 839.
361. J.K. Borchardt and E.D. Dalrymple, *J. Polym. Sci., Polym. Chem. Ed.*, 1982, **20,** 1745.
362. J.K. Borchardt, *J. Macromol. Sci. Chem.*, 1985, **A22,** 1711.
363. K. Hatada, K. Nagata, T. Hasegawa and H. Yuki, *Makromol. Chem.*, 1977, **178,** 2413.
364. K. Hatada, T. Kitayama and T. Masuki, unpublished results.
365. K. Ute, T. Kitayama and K. Hatada, unpublished results.
366. M. Imoto, M. Kinoshita and M. Nishigaki, *Makromol. Chem.*, 1965, **86,** 217.
367. A.V. Chernobai, N.S. Pivnenko, I.A. Goncharenko and N.N. Florinskaya, *Zh. Prikl. Spektrosk.*, 1982, **36,** 329.
368. V.M. Sutyagin, V.P. Lopatinskii and V.D. Filimonov, *Vysokomol. Soedin., Ser. B*, 1984, **26,** 904.
369. H. Ito, S.A. MacDonald, C.G. Willson, J.W. Moore, H.M. Gharapetian and J.E. Guillet, *Macromolecules*, 1986, **19,** 1839.
370. T. Higashimura, *Cationic Polymerization* (in Japanese), p. 222. Kagakudojin, Kyoto, 1971.
371. H. Yuki, K. Hatada, K. Nagata and T. Hasegawa, unpublished data.
372. T. Fueno, T. Okuyama, I. Matsumura and J. Furukawa, *J. Polym. Sci., Part A-1*, 1969, **7,** 1447.
373. M. Shima, D.N. Bhattacharyya, J. Smid and M. Szwarc, *J. Am. Chem. Soc.*, 1963, **85,** 1306.
374. G. Natta, F. Danusso and D. Sianesi, *Makromol. Chem.*, 1959, **30,** 238.
375. H. Yuki, K. Hatada, K. Nagata and T. Emura, *Polym. J.*, 1979, **1,** 269.
376. K. Hatada, K. Nagata and H. Yuki, *Bull. Chem. Soc. Jpn*, 1970, **43,** 3195.
377. H. Yuki, K. Hatada and M. Takeshita, *J. Polym. Sci., Part A-1*, 1969, **7,** 667.
378. J.A. Pople and A.A. Bothner-By, *J. Chem. Phys.*, 1965, **42,** 1339.

The Application of Cation NMR to Living Systems: ^{87}Rb NMR

JONATHAN L. ALLIS*

MRC Biochemical and Clinical Magnetic Resonance Unit, John Radcliffe Hospital, Headington, Oxford, OX3 9DU, UK

1. INTRODUCTION

Sodium (Na^+) and potassium (K^+) play an integral role in the processes associated with living tissues. They are mostly present as free cations, unequally distributed across cell membranes. Sodium is actively excluded

* Present address: Oxford Magnet Technology, Wharf Road, Eynsham, Oxford OX8 1BP, UK.

ANNUAL REPORTS ON NMR SPECTROSCOPY
VOLUME 26 ISBN 0-12-505326-6

from cells, giving rise to high extracellular (~ 150 mM) and low intracellular (~ 10 mM) sodium concentrations. The opposite is true of potassium. The energy stored in their distribution across cell membranes fuels a multitude of membrane transport processes and provides the basis for the neural depolarization and repolarization upon which all nervous activity is based. Both ions have NMR-detectable isotopes, ^{23}Na and ^{39}K respectively. They exhibit a non-zero quadrupolar moment, which accounts for their rapid, biexponential relaxation.

Under normal conditions the resonant frequencies of intra- and extracellular species of an ion are the same, implying that, for example, the conventional ^{23}Na magnetic resonance spectrum of a biological sample consists of a single peak. The various populations of ions in tissue do exhibit different relaxation characteristics, and early studies by Cope and Damadian[1] and Berendsen and Edzes[2] utilized these differences in an attempt to elucidate the behaviour of ions within living tissues. Degani and Elgavish[3] used a complex of the paramagnetic ion gadolinium, $Gd(EDTA)^-$, to broaden the extracellular ^{23}Na and ^{7}Li resonances in phosphatidylcholine vesicles such that they detected only the intracellular signal. Subsequently, Riddell and Southon[4] used complexes of lanthanum for a similar purpose, showing that the extracellular ^{87}Rb NMR signal in a suspension of red cells could be broadened to such an extent that only the intracellular signal was visible.

In the early 1980s membrane-impermeable chemical shift reagents were developed which frequency shifted the extracellular cation resonances, thus allowing measurement of the transmembrane distributions of Na^+ and K^+.[5–7] Early experiments on erythrocytes showed that intra- and extracellular $^{23}Na^+$[5] and $^{39}K^+$ resonances[8] could be resolved by the shift reagent dysprosium tripolyphosphate, $Dy(PPP)_2^{7-}$. In subsequent studies $Dy(PPP)_2^{7-}$ and dysprosium triethylenetetraamine-hexa-acetic acid, $Dy(TTHA)^{3-}$[7] were used to resolve intra- and extracellular sodium, lithium and potassium resonances in phospholipid vesicles,[9,10] yeast,[11] red cells,[5,12,13] and a variety of mammalian tissues: kidney tubules,[14,15] heart[16,17] and muscle.[5,18] These studies established that NMR was capable of measuring the concentration of intracellular cations, though the results obtained did not always agree with those obtained by other analytical techniques.

The rate of cation flux from one compartment to another is obviously a more useful parameter than the static transmembrane distribution of cations. Directional fluxes can be studied by a variety of NMR methods:[19] lineshape analysis, magnetization transfer, or by following the kinetics of a suitable congener. Each of these techniques applies to a different exchange rate regime. Lineshape analysis is applicable to very rapid exchange processes, and has been used extensively by Riddell to measure the transport of cations into phospholipid vesicles by antibiotics such as monensin[9] and salinomycin.[20] Magnetization transfer experiments[21,22] rely on magnetically labelling a group of spins by saturating or inverting them, and then observing their transfer to another

resonance in the spectrum. In order for the saturation or inversion transfer experiments to work, the pseudo first-order rate of exchange from one compartment to the other must be of the same order of magnitude as the NMR relaxation rates of the exchanging species. For quadrupolar nuclei, with short relaxation times, this requires a large transfer rate constant, k. For $^{23}Na^+$, T_1 in tissue is ~ 20 ms, and thus k must be at least 5 or $10\,s^{-1}$ for the transfer to be detectable. In addition, the exchanging resonances must be well-resolved and must not be too broad, or else relaxation effects will not allow selective saturation or inversion. It has been shown that the Na^+ and Li^+ flux through monensin-induced channels in lipid vesicles can be measured by both the inversion transfer and the 2D-NOESY experiment.[23–25] The rates of exchange in these experiments were very high (between 10 and $70\,s^{-1}$) and the chemical shift between the intra- and extracellular resonances were large, thus allowing magnetization transfer techniques to be used. To the author's knowledge, no measurements of Na^+ flux by magnetization transfer have yet been successfully performed in biological tissue, and it is very unlikely that the transmembrane Na^+ flux in biological tissues will ever allow such experiments to be performed. The same arguments, compounded by the poor NMR sensitivity, apply to the measurement of the transmembrane K^+ flux.

For slow exchange a method of measuring the transmembrane cation flux by NMR is to follow the kinetics of a suitable Na^+ or K^+ congener. As Na^+ is predominantly an extracellular ion, the intracellular concentration of a suitable Na^+ congener will not be large, and unless it has a very high NMR sensitivity, its uptake kinetics will be difficult to follow. K^+, on the other hand, shows considerable promise, as its high intracellular concentration implies that a good K^+ congener will also exist at a high intracellular concentration. Both rubidium (Rb^+) and caesium (Cs^+) have been identified as congeners of K^+.[26] Cs^+ enters red cells at $\sim 1/3$ the rate of K^+,[27] whilst Rb^+ is indistinguishable from K^+ in uptake studies, as the transport protein Na^+–K^+-ATPase is unable to differentiate between K^+ and Rb^+. The efflux of Rb^+ from cells has been reported to be slower than that of K^+,[28] which is adequately explained by the fact that the Rb^+ ion is larger than the K^+ ion, and thus less able to pass through pores and channels "designed" to permit the passage of K^+ ions.

Within a few years of its identification as a chemical element the possible applications of Rb^+ to biology and medicine were being investigated, culminating in Ringer's experiments on isolated frog heart, which suggested that Rb^+ and K^+ had similar effects on contractility.[26] It was noted that the acute intravenous injection of Rb^+ or K^+ produced cardiotoxic death, and that chronic loading of animals with 7 mM Rb^+/kg per day appeared to produce hyperirritability, tetanic spasms and eventually death. The relationship between irritability and Rb^+ is the basis of its use in psychiatry as an antidepressant drug.[29] Radioactive $^{86}Rb^+$ is the mainstay of research on K^+ fluxes into cells and organs,[30,31] and recently abnormalities in *in vivo* red cell Rb^+ uptake, determined by atomic absorption spectrophotometry performed on

Table 1. The NMR properties of ^{23}Na, ^{39}K, ^{85}Rb and ^{87}Rb.

Nucleus	Spin	Magnetogyric ratio (γ)[a]	Quadrupolar moment (Q)[b]	Natural abundance (%)
^{23}Na	3/2	7.08	0.10	100
^{39}K	3/2	1.25	0.05	93
^{85}Rb	5/2	2.59	0.26	72
^{87}Rb	3/2	8.78	0.13	28

[a] The units of γ are 10^7 rad/T s.
[b] The units of Q are 10^{-28} m^2.

blood samples drawn after an oral load of RbCl, have been identified with hypertension and chronic renal failure.[32]

The large volume of literature dealing with biological ^{23}Na and ^{39}K NMR have spawned a number of review articles on the subject,[33] and in order to introduce a note of originality into this review of the biological uses of quadrupolar ions we shall concentrate on recent work on the use of ^{87}Rb NMR to measure cation fluxes in cells and whole organs.

Two isotopes of Rb^+ are detectable by NMR, ^{85}Rb and ^{87}Rb, and their NMR properties together with those of ^{23}Na and ^{39}K are shown in Table 1.[19] The low magnetogyric ratio of ^{85}Rb and corresponding low NMR receptivity has meant that ^{87}Rb is the isotope favoured for study by NMR.

We begin, in Section 2, with a detailed theoretical examination of the physics of quadrupolar, spin-$\frac{3}{2}$ nuclei, using the matrix operator formalism to discuss the various NMR experiments used in biological spectroscopy of quadrupolar ions and the biexponential relaxation of these ions. The effect of interaction of the Rb^+ ion with its chemical environment on relaxation characteristics of the ^{87}Rb nucleus is considered in Section 3. Section 4 deals with methods of differentiating between intra- and extracellular species of ions. In Section 5 we discuss the kinetics of Rb^+ in a variety of tissues, as studied by ^{87}Rb NMR. Where appropriate, studies of ^{23}Na and ^{39}K are also cited.

2. NUCLEAR MAGNETIC RESONANCE OF SPIN-$\frac{3}{2}$ NUCLEI IN LIQUIDS

2.1. Introduction

We now present a detailed discussion on the physics of quadrupolar nuclei in biological solution. Most previous treatments of quadrupolar nuclei have invoked the mathematics of irreducible tensor operators, and although this formalism does lead to a more intuitive feel for the experiments, it does require a considerable degree of mathematical sophistication.[34] Our approach will be to derive the results of a variety of NMR experiments in terms of explicit matrix

representations of the density matrix operators. We proceed as follows: the classical and quantum mechanical forms of the full quadrupolar Hamiltonian are derived, and the resulting equations of motion solved for (1) the steady-state static field, (2) hard pulses and chemical shift evolution, and (3) quadrupolar T_2 relaxation. In order to do this the quantum mechanical machinery of the density matrix is introduced. There follows an analysis of the simple "pulse and collect", the Hahn spin-echo and the triple-quantum filtered T_2 experiment.

2.2. The classical quadrupolar Hamiltonian

A volume of charged, current-containing matter, such as an atomic nucleus, interacts with the electromagnetic field. The electric field interacts with only the nuclear charge distribution, while the magnetic field interacts with the nuclear current distribution. The interaction energy, H_E, between the electric field and the nuclear charge may be written as

$$H_E = \int \rho(\mathbf{r}) V(\mathbf{r}) \, dv \tag{1}$$

where $\rho(\mathbf{r})$ is the nuclear charge density, $V(\mathbf{r})$ is the electric potential and the integral is over all space. The coordinate system is defined to have the centre of the nucleus at $\mathbf{r} = 0$. The potential, $V(\mathbf{r})$, may be expanded as a Taylor series about $\mathbf{r} = 0$, giving

$$V(\mathbf{r}) = V(0) - \mathbf{r} \cdot \mathbf{E}(0) - 1/6 \sum_i \sum_j (3x_i x_j - r^2 \delta_{ij}) V_{ij}(0) + \ldots \tag{2}$$

where $\mathbf{E}(0) = -\nabla V(0)$; $V_{ij} = \partial^2 V / \partial x_i \partial x_j = -\partial E_i / \partial x_j$, the electric field gradient; and x_i are the components of the vector $\mathbf{r}$. Substituting (2) into (1) gives

$$H_E = qV(0) - \mathbf{p} \cdot \mathbf{E}(0) - 1/6 \sum_i \sum_j Q_{ij} \partial E_j(0) / \partial x_i + \ldots \tag{3}$$

where q is the nuclear charge, $\mathbf{p}$ is the nuclear dipole moment and Q_{ij} is the nuclear quadrupole moment, defined as

$$Q_{ij} = \int (3x_i x_j - r^2 \delta_{ij}) \rho(\mathbf{r}) \, dv \tag{4}$$

$qV(0)$ is a constant addition to the electric potential energy, and may be ignored. All nuclei have a zero dipole moment,[35] implying that $\mathbf{p} \cdot \mathbf{E}(0)$ is zero. The first non-zero contribution to the electric potential energy of the nucleus is the quadrupole moment. Although higher multipole moments are theoretically allowed, no nuclei with octupolar moments are known to occur naturally, and so the quadrupolar term may be regarded as the only term of the electric

Hamiltonian, i.e.

$$H_E = -1/6 \sum_i \sum_j Q_{ij} \partial E_j(0)/\partial x_i \tag{5}$$

By direct analogy with the electric case the interaction energy of the magnetic field with the nuclear current distribution may be written as a sum of multipoles.[36] The dominant contribution is the interaction between the nuclear dipole moment, $\boldsymbol{\mu}$, and the magnetic field, $\mathbf{B}$, giving

$$H_M = -\boldsymbol{\mu} \cdot \mathbf{B} \tag{6}$$

The full classical quadrupolar Hamiltonian is thus given by

$$H = -\boldsymbol{\mu} \cdot \mathbf{B} - 1/6 \sum_i \sum_j Q_{ij} \partial E_j(0)/\partial x_i \tag{7}$$

2.3. The quantum mechanical quadrupolar Hamiltonian

The quantum mechanical nuclear dipole moment is defined as

$$\boldsymbol{\mu} = \gamma \hbar \mathbf{I} \tag{8}$$

where γ is the magnetogyric ratio and $\mathbf{I}$ is the angular momentum spin operator. The magnetic component of the quantum mechanical Hamiltonian is thus

$$H_M = -\gamma \hbar \mathbf{I} \cdot \mathbf{B} \tag{9}$$

The quadrupolar term is more complicated, but after judicious application of the Wigner–Eckhart theorem,[37] the electric Hamiltonian, for cylindrical symmetry, may be written as

$$H_E = \frac{eQV_{zz}}{4I(2I-1)} [3\mathbf{I}_z^2 - \mathbf{I}^2] \tag{10}$$

where e is the proton charge, Q is the quantum mechanical expectation value of the quadrupolar moment, V_{zz} is the z component of the electric field gradient and $\mathbf{I}_z$ is the z component of the quantum mechanical spin operator, $\mathbf{I}$. The full quantum mechanical form of the quadrupolar Hamiltonian is given by

$$H = H_M + H_E = -\gamma \hbar \mathbf{I} \cdot \mathbf{B} + \frac{eQV_{zz}}{4I(2I-1)} [3\mathbf{I}_z^2 - \mathbf{I}^2] \tag{11}$$

The methods employed to solve the equations of motion, which evolve under the Hamiltonian given in (11), are as follows. The magnetic field is composed of the large static field, B_0, in the z direction, and the radio frequency (rf) B, field orthogonal to it in the xy plane. H_M may therefore be further subdivided into, H_0, the static field Hamiltonian, and, H_{RF}, the rf field Hamiltonian. H_0 is much larger than either H_{RF} or H_E, and they may be treated as perturbations of the H_0 Hamiltonian. For ions in solution, the time average of H_E is zero, implying that H_E contributes only to the relaxation of the nucleus and not to the static

energy level structure. During a hard rf pulse, H_{RF} is, by definition, $\gg H_E$, implying that there is little relaxation during the pulse. Thus during the application of rf pulses, the Hamiltonian is the sum of H_0 and H_{RF}, while during chemical shift evolution and relaxation delays, it is the sum of H_0 and H_E.

Assuming that the molecular and laboratory principal axes coincide, a matrix representation of the spin operators $\mathbf{I}_x$, $\mathbf{I}_y$, $\mathbf{I}_z$ and $\mathbf{I}^2$ is as follows:[38]

$$\mathbf{I}_x = \begin{pmatrix} 0 & \sqrt{3}/2 & 0 & 0 \\ \sqrt{3}/2 & 0 & 1 & 0 \\ 0 & 1 & 0 & \sqrt{3}/2 \\ 0 & 0 & \sqrt{3}/2 & 0 \end{pmatrix}$$

$$\mathbf{I}_y = \begin{pmatrix} 0 & -i\sqrt{3}/2 & 0 & 0 \\ i\sqrt{3}/2 & 0 & -i & 0 \\ 0 & i & 0 & -i\sqrt{3}/2 \\ 0 & 0 & i\sqrt{3}/2 & 0 \end{pmatrix}$$

$$\mathbf{I}_z = \begin{pmatrix} 3/2 & 0 & 0 & 0 \\ 0 & 1/2 & 0 & 0 \\ 0 & 0 & -1/2 & 0 \\ 0 & 0 & 0 & -3/2 \end{pmatrix}$$

$$\mathbf{I}^2 = 15/4 \begin{pmatrix} 1 & 0 & 0 & 0 \\ 0 & 1 & 0 & 0 \\ 0 & 0 & 1 & 0 \\ 0 & 0 & 0 & 1 \end{pmatrix} \tag{12}$$

Let $|n\rangle$ be the nth eigenvector of the spin operator $\mathbf{I}^2$, then,

$$\mathbf{I}^2|n\rangle = I(I+1)|n\rangle \tag{13}$$

and

$$\mathbf{I}_z|n\rangle = m_1|n\rangle \tag{14}$$

For the spin-$\frac{3}{2}$ case, $I = \frac{3}{2}$, and m_1 may take on one of four possible eigenvalues, $-3/2$, $-1/2$, $1/2$ or $3/2$.

The eigenvalues of H_0 are now easily obtained. From equations (9), (12) and (14),

$$H_0|n\rangle = -\gamma\hbar B_0 \mathbf{I}_z|n\rangle = -\gamma\hbar B_0 n|n\rangle = E_n|n\rangle \tag{15}$$

There are four energy levels, $E_n = \gamma\hbar B_0 3/2, \gamma\hbar B_0 1/2, -\gamma\hbar B_0 1/2$ and $-\gamma\hbar B_0 3/2$.

The quantum mechanical equation of motion for an ensemble of nuclei may be written in terms of the reduced density matrix, σ,[37] which is defined as, $\sigma = \sum_k p_k |\psi_k(t)\rangle\langle\psi_k(t)|$, where $|\psi_k(t)\rangle$ is a possible wave function for the ensemble of nuclear spins and p_k is the probability of the nuclei being in that state. The equation of motion is,

$$\frac{d\sigma}{dt} = \frac{i}{\hbar}(\sigma\mathbf{H} - \mathbf{H}\sigma) \tag{16}$$

where $\mathbf{H}$ is the Hamiltonian of the whole nuclear system. If $\mathbf{H}$ is independent of time, then,

$$\sigma(t) = \exp(-i\mathbf{H}t/\hbar)\sigma(0)\exp(i\mathbf{H}t/\hbar) \tag{17}$$

The quantum mechanical expectation value of an operator A, is given by

$$\langle A\rangle = \mathrm{Tr}(\sigma A) = \mathrm{Tr}(A\sigma) = \sum_n \sum_k \sigma_{nk} A_{kn} = \sum_n \sum_k A_{nk}\sigma_{kn} \tag{18}$$

This result is now applied to calculating which elements of the density matrix actually contribute to the detectable signal. Assuming quadrature detection, the detectable magnetization is proportional to $\langle \mathbf{I}_x + i\mathbf{I}_y\rangle$, which according to equation (18) is $\mathrm{Tr}(\sigma(\mathbf{I}_x + i\mathbf{I}_y))$. Using equation (12) it is simple to show that

$$\langle \mathbf{I}_x + i\mathbf{I}_y\rangle = \sqrt{3}\sigma_{21} + 2\sigma_{32} + \sqrt{3}\sigma_{43} \tag{19}$$

The thermal equilibrium density matrix is calculated from the definition of the density matrix and the Boltzmann equilibrium spin distribution.[39] Ignoring all constants, $\sigma(0)$, the unperturbed, equilibrium density matrix, is simply equal to $\mathbf{I}_z$, as expected.

2.4. Hard pulses and chemical shift evolution

For the discussion of hard pulses and chemical shift evolution, the Hamiltonian is transformed into the rotating frame. The only change is in the form of the magnetic Hamiltonian $\mathbf{H}_M$, which becomes[35]

$$\mathbf{H}_M = -\hbar[\Delta\omega\mathbf{I}_z + \gamma B_1 \mathbf{I}\cdot\mathbf{n}] \tag{20}$$

where $\Delta\omega$ is the difference between the B_1 irradiation frequency, ω_z, and the nuclear Larmor frequency, γB_0, B_1 is the magnitude of the rf field and $\mathbf{n}$ its direction. Hard pulses are defined as having $\gamma B_1 \gg \Delta\omega$, which simplifes equation (20) to

$$\mathbf{H}_M = -\hbar\gamma B_1 \mathbf{I}\cdot\mathbf{n} \tag{21}$$

Substituting (21) into (17) shows the effect of a hard pulse of duration t on the evolution of the density matrix, i.e.

$$\sigma(t) = \exp(i\omega_1 t\mathbf{I}\cdot\mathbf{n})\sigma(0)\exp(-i\omega_1 t\mathbf{I}\cdot\mathbf{n}) \tag{22}$$

where $\gamma B_1 = \omega_1$. The product $\omega_1 t$ is simply θ, the angle of nutation about the **n** axis. As the quantum mechanical rotation operator $\mathbf{R}_\mathbf{n}(\theta)$ is of the form $\exp(-i\theta\mathbf{I}\cdot\mathbf{n})$,[36] (22) may be written as

$$\boldsymbol{\sigma}(+) = \mathbf{R}_\mathbf{n}(-\theta)\boldsymbol{\sigma}(-)\mathbf{R}_\mathbf{n}(\theta) \tag{23}$$

where $\boldsymbol{\sigma}(-)$ and $\boldsymbol{\sigma}(+)$ is the density matrix before and after the pulse. The calculation of a matrix representation for $\exp(-i\theta\mathbf{I}\cdot\mathbf{n})$ is not always simple; fortunately general formulae do exist.[40] Some of the more commonly used ones are: $\mathbf{R}_\mathbf{x}(\pi/2)$, $\mathbf{R}_\mathbf{x}(\pi)$, $\mathbf{R}_\mathbf{y}(\pi/2)$, $\mathbf{R}_\mathbf{y}(\pi)$, $\mathbf{R}_\mathbf{x}(-\pi/2)$, $\mathbf{R}_\mathbf{x}(-\pi)$, $\mathbf{R}_\mathbf{y}(-\pi/2)$ and $\mathbf{R}_\mathbf{y}(-\pi)$.

$$\mathbf{R}_\mathbf{x}(\pi/2) = \frac{\sqrt{2}}{4}\begin{pmatrix} 1 & -i\sqrt{3} & -\sqrt{3} & i \\ -i\sqrt{3} & -1 & -i & -\sqrt{3} \\ -\sqrt{3} & -i & -1 & -i\sqrt{3} \\ i & -\sqrt{3} & -i\sqrt{3} & 1 \end{pmatrix}$$

$$\mathbf{R}_\mathbf{x}(\pi) = \begin{pmatrix} 0 & 0 & 0 & i \\ 0 & 0 & i & 0 \\ 0 & i & 0 & 0 \\ i & 0 & 0 & 0 \end{pmatrix}$$

$$\mathbf{R}_\mathbf{y}(\pi/2) = \frac{\sqrt{2}}{4}\begin{pmatrix} 1 & -\sqrt{3} & \sqrt{3} & -1 \\ \sqrt{3} & -1 & -1 & \sqrt{3} \\ \sqrt{3} & 1 & -1 & -\sqrt{3} \\ 1 & \sqrt{3} & \sqrt{3} & 1 \end{pmatrix}$$

$$\mathbf{R}_\mathbf{y}(\pi) = \begin{pmatrix} 0 & 0 & 0 & -1 \\ 0 & 0 & 1 & 0 \\ 0 & -1 & 0 & 0 \\ 1 & 0 & 0 & 0 \end{pmatrix}$$

$$\mathbf{R}_\mathbf{x}(-\pi/2) = \frac{\sqrt{2}}{4}\begin{pmatrix} 1 & i\sqrt{3} & -\sqrt{3} & -i \\ i\sqrt{3} & -1 & i & -\sqrt{3} \\ -\sqrt{3} & i & -1 & i\sqrt{3} \\ -i & -\sqrt{3} & i\sqrt{3} & 1 \end{pmatrix}$$

$$\mathbf{R}_\mathbf{x}(-\pi) = \begin{pmatrix} 0 & 0 & 0 & -i \\ 0 & 0 & -i & 0 \\ 0 & -i & 0 & 0 \\ -i & 0 & 0 & 0 \end{pmatrix}$$

$$\mathbf{R}_y(-\pi/2) = \frac{\sqrt{2}}{4}\begin{pmatrix} 1 & \sqrt{3} & \sqrt{3} & 1 \\ -\sqrt{3} & -1 & 1 & \sqrt{3} \\ \sqrt{3} & -1 & -1 & \sqrt{3} \\ -1 & \sqrt{3} & -\sqrt{3} & 1 \end{pmatrix}$$

$$\mathbf{R}_y(-\pi) = \begin{pmatrix} 0 & 0 & 0 & 1 \\ 0 & 0 & -1 & 0 \\ 0 & 1 & 0 & 0 \\ -1 & 0 & 0 & 0 \end{pmatrix} \tag{24}$$

As mentioned in Section 2.3, in the absence of an rf pulse the rotating frame Hamiltonian is the sum of H_0 and H_E. As these two operators commute, they may be treated independently of each other. Equation (20) shows that in the absence of an rf pulse, H_0 reduces to the chemical shift evolution (CSE) Hamiltonian, i.e.

$$\mathbf{H_M} = -\hbar\Delta\omega\mathbf{I}_z \tag{25}$$

The resulting evolution operator, $\exp(i\Delta\omega\mathbf{I}_z t)$ has the following matrix representation:

$$\mathbf{R}_z(-\Delta\omega t) = \begin{pmatrix} \exp(i3\Delta\omega t/2) & 0 & 0 & 0 \\ 0 & \exp(i\Delta\omega t/2) & 0 & 0 \\ 0 & 0 & \exp(-i\Delta\omega t/2) & 0 \\ 0 & 0 & 0 & \exp(-i3\Delta\omega t/2 \end{pmatrix} \tag{26}$$

2.5. Quadrupolar relaxation

For some quadrupolar nuclei with a very small quadrupolar moment, the dipole–dipole mechanism contributes significantly to relaxation, e.g. ^{7}Li. ^{87}Rb has a very large quadrupolar moment and Sternheimer anti-shielding factor, and thus, quadrupolar relaxation dominates completely; the same is true of ^{23}Na and ^{39}K. The Sternheimer anti-shielding factor describes how sensitive the NMR relaxation of a nucleus is to its electronic environment.[37]

The form of the rotating frame Hamiltonian, H'_E, for quadrupolar relaxation is

$$H'_E = \exp(-i\gamma B_0\mathbf{I}_z t)H_E \exp(i\gamma B_0\mathbf{I}_z t) \tag{27}$$

As H'_E is dependent on time, the solution to the density matrix is not simply given by (17). Applying second-order perturbation theory, the derivatives of the density matrix can be shown to be[41]

$$\frac{d\sigma_{\alpha\beta}(t)}{dt} = \sum_{\gamma\delta} P_{\alpha\beta\gamma\delta} \exp[i(\omega_\alpha - \omega_\beta - \omega_\gamma + \omega_\delta)]\sigma_{\gamma\delta}(0) \tag{28}$$

where $P_{\alpha\beta\gamma\delta}$ is a matrix of transition probabilities, and is a function of the relaxation Hamiltonian.

The spectral variation in H_E may be determined by computing the auto-correlation function, $R(\omega)$, which is defined as

$$R(\omega) = \int_{-\infty}^{+\infty} H_E(0)H_E(\tau) \exp(-i\omega\tau)\, d\tau \tag{29}$$

The time dependence of $H_E(0)H_E(\tau)$ is often taken as exponential, i.e.

$$R(\omega) = |H_E(0)|^2 \int_{-\infty}^{+\infty} \exp(-|\tau_c|/\tau) \exp(-i\omega\tau)\, d\tau \tag{30}$$

where τ_c is the correlation time of the quadrupolar Hamiltonian, i.e. the minimum average time during which it changes significantly. The spectral density function, $j(\omega)$, is defined as

$$j(\omega) = \int_{-\infty}^{+\infty} \exp(-|\tau_c|/\tau) \exp(-i\omega\tau)\, d\tau \tag{31}$$

which is

$$j(\omega) = \frac{\tau_c}{1 + \omega^2\tau_c^2}; \quad \text{let } j_n = j(n\omega) \tag{32}$$

The structure and meaning of τ_c is further discussed in Section 3. Returning to equation (28); the form of $P_{\alpha\beta\gamma\delta}$ has been calculated explicitly for $I = \frac{3}{2}$ nuclei by Mclachlan.[42] The submatrix of interest for transverse relaxation is

$$\frac{d}{dt}\begin{pmatrix} \sigma_{12} \\ \sigma_{23} \\ \sigma_{34} \end{pmatrix} = C\begin{pmatrix} -(j_0 + j_1 + j_2) & 0 & j_2 \\ 0 & -(j_1 + j_2) & 0 \\ j_2 & 0 & -(j_0 + j_1 + j_2) \end{pmatrix}\begin{pmatrix} \sigma_{12} \\ \sigma_{23} \\ \sigma_{34} \end{pmatrix} \tag{33}$$

where

$$C = 1/20(eV_{zz}Q/\hbar)^2 \tag{34}$$

Defining the relaxation rates, R_i, as

$$R_1 = -C[j(0) + j(\omega)] \tag{35}$$

$$R_2 = -C[j(\omega) + j(2\omega)] \tag{36}$$

$$R_3 = -C[j(0) + j(\omega) + 2j(2\omega)] \tag{37}$$

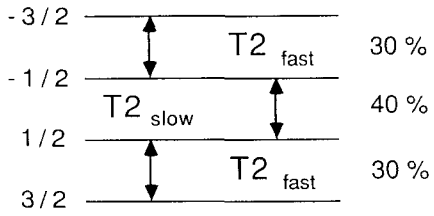

Fig. 1. Energy level and T_2 relaxation diagram for an isolated spin-$\frac{3}{2}$ nucleus. The fractions on the left are the angular momenta of each of the four energy levels. The percentages on the right are the proportion of the total signal relaxing via each of the T_2 relaxation channels. Reproduced from Ref. 95, with permission of Karger AG, Basel.

it is not difficult to show that

$$\sigma_{12}(t) = \tfrac{1}{2}[\{\sigma_{12}(0) + \sigma_{34}(0)\}\exp(-R_1 t) + \{\sigma_{12}(0) - \sigma_{34}(0)\}\exp(-R_3 t)] \quad (38)$$

$$\sigma_{23}(t) = \sigma_{23}(0)\exp(-R_2 t) \quad (39)$$

$$\sigma_{34}(t) = \tfrac{1}{2}[\{\sigma_{12}(0) + \sigma_{34}(0)\}\exp(-R_1 t) + \{\sigma_{12}(0) - \sigma_{34}(0)\}\exp(-R_3 t)] \quad (40)$$

When $\sigma_{12} = \sigma_{34}$, equations (39)–(41) simplify to

$$\sigma_{12}(t) = \sigma_{12}(0)\exp(-R_1 t) = \sigma_{12}(0)\exp(-t/T_{2F}) \quad (41)$$

$$\sigma_{23}(t) = \sigma_{23}(0)\exp(-R_2 t) = \sigma_{23}(0)\exp(-t/T_{2S}) \quad (42)$$

$$\sigma_{34}(t) = \sigma_{34}(0)\exp(-R_1 t) = \sigma_{34}(0)\exp(-t/T_{2F}) \quad (43)$$

Similar equations apply for σ_{21}, σ_{32} and σ_{43}. The energy level and T_2 relaxation diagram for spin-$\frac{3}{2}$ nuclei is shown in Fig. 1.

We now apply the above theory to modelling of the "pulse-and-collect", Hahn spin-echo and triple-quantum filtered T_2 experiments.

2.6. The pulse-and-collect experiment

The pulse sequence for this simplest of Fourier transform (FT)-NMR experiments is

$$\pi/2_x - \text{Acq.} \quad (44)$$

Before the $\pi/2_x$ pulse the density matrix is given by $\sigma(0)$, the thermal equilibrium density matrix. After the pulse,

$$\sigma_1(+) = \mathbf{R}_x(-\pi/2)\sigma(0)\mathbf{R}_x(\pi/2) \quad (45)$$

which is

$$\sigma_1(+) = 1/2\begin{bmatrix} 0 & -i\sqrt{3} & 0 & 0 \\ i\sqrt{3} & 0 & -i2 & 0 \\ 0 & i2 & 0 & -i\sqrt{3} \\ 0 & 0 & i\sqrt{3} & 0 \end{bmatrix} \quad (46)$$

By comparison with equation (12), $\boldsymbol{\sigma}_1(+)$ is simply $\mathbf{I}_y$, as expected. During the acquisition period the magnetization undergoes CSE and relaxation. Applying the CSE operator, equation (26), gives

$$\boldsymbol{\sigma}_2(t) = \mathbf{R}_z(-\Delta\omega t)\boldsymbol{\sigma}_1(+)\mathbf{R}_z(\Delta\omega t) \tag{47}$$

$\boldsymbol{\sigma}_2(t) =$

$$1/2\begin{bmatrix} 0 & -i\sqrt{3}\exp(i\Delta\omega t) & 0 & 0 \\ i\sqrt{3}\exp(-i\Delta\omega t) & 0 & -i2\exp(i\Delta\omega t) & 0 \\ 0 & i2\exp(-i\Delta\omega t) & 0 & -i\sqrt{3}\exp(i\Delta\omega t) \\ 0 & 0 & i\sqrt{3}\exp(-i\Delta\omega t) & 0 \end{bmatrix} \tag{48}$$

Relaxation of the non-zero density matrix elements are given by equations (39)–(41). Defining $F = \exp(-t/T_{2F})$ and $S = \exp(-t/T_{2S})$, the final density matrix, $\boldsymbol{\sigma}_3(t)$, is of form

$\boldsymbol{\sigma}_3(t) =$

$$1/2\begin{bmatrix} 0 & -i\sqrt{3}F\exp(i\Delta\omega t) & 0 & 0 \\ i\sqrt{3}F\exp(-i\Delta\omega t) & 0 & -i2S\exp(i\Delta\omega t) & 0 \\ 0 & i2S\exp(-i\Delta\omega t) & 0 & -i\sqrt{3}F\exp(i\Delta\omega t) \\ 0 & 0 & i\sqrt{3}F\exp(-i\Delta\omega t) & 0 \end{bmatrix} \tag{49}$$

The detected signal, $\langle \mathbf{I}_x + i\mathbf{I}_y \rangle$, is given by equation (19), i.e.

$$\langle \mathbf{I}_x + i\mathbf{I}_y \rangle = i[3\exp(-t/T_{2F}) + 2\exp(-t/T_{2S})]\exp(-i\Delta\omega t) \tag{50}$$

The general form of the FID is thus biexponential,[43] giving rise to a bi-Lorentzian, or "super-Lorentzian" lineshape.[44] The effect of field inhomogeneity broadening has been ignored in this analysis, but may be included by replacing T_{2i} with T_{2i}^* in equation (50). The initial detectable magnetization may be normalized to unity by dividing equation (50) by 5, i.e.

$$\langle \mathbf{I}_x + i\mathbf{I}_y \rangle = (i/5)[3\exp(-t/T_{2F}) + 2\exp(-t/T_{2S})]\exp(-i\Delta\omega t) \tag{51}$$

2.7. The Hahn spin-echo experiment

The pulse sequence for this experiment is

$$\pi/2_x - \tau/2 - \pi_y - \tau/2 - \text{Acq.} \tag{52}$$

Utilizing the result of the previous section gives the form of the density matrix at the end of the first evolution period:

$\sigma_3(\tau/2) =$

$$1/2\begin{bmatrix} 0 & -i\sqrt{3}F'\exp(i\Delta\omega\tau/2) & 0 & 0 \\ i\sqrt{3}F'\exp(-i\Delta\omega\tau/2) & 0 & -i2S'\exp(i\Delta\omega\tau/2) & 0 \\ 0 & i2S'\exp(-i\Delta\omega\tau/2) & 0 & -i\sqrt{3}F'\exp(i\Delta\omega\tau/2) \\ 0 & 0 & i\sqrt{3}F'\exp(-i\Delta\omega\tau/2) & 0 \end{bmatrix} \tag{53}$$

where $F' = \exp(-\tau/2T_{2F})$ and $S' = \exp(-\tau/2T_{2S})$. After the π_y pulse,

$$\sigma_4(\tau/2,+) = \mathbf{R}_y(-\pi)\sigma_3(\tau/2)\mathbf{R}_y(\pi) \tag{54}$$

$\sigma_4(\tau/2) =$

$$1/2\begin{bmatrix} 0 & -i\sqrt{3}F'\exp(-i\Delta\omega\tau/2) & 0 & 0 \\ i\sqrt{3}F'\exp(i\Delta\omega\tau/2) & 0 & -i2S'\exp(-i\Delta\omega\tau/2) & 0 \\ 0 & i2S'\exp(i\Delta\omega\tau/2) & 0 & -i\sqrt{3}F'\exp(-i\Delta\omega\tau/2) \\ 0 & 0 & i\sqrt{3}F'\exp(i\Delta\omega\tau/2) & 0 \end{bmatrix} \tag{55}$$

Note the reversal of phase due to refocusing of the CSE.

Applying the CSE operators during the second evolution period gives

$$\sigma_5(\tau) = 1/2\begin{bmatrix} 0 & -i\sqrt{3}F' & 0 & 0 \\ i\sqrt{3}F' & 0 & -i2S' & 0 \\ 0 & i2S' & 0 & -i\sqrt{3}F' \\ 0 & 0 & i\sqrt{3}F' & 0 \end{bmatrix} \tag{56}$$

Applying the relaxation operator, and defining $F' \cdot F' = f = \exp(-\tau/T_{2F})$ and $S' \cdot S' = s = \exp(-\tau/T_{2S})$,

$$\sigma_6(\tau) = 1/2\begin{bmatrix} 0 & -i\sqrt{3}f & 0 & 0 \\ i\sqrt{3}f & 0 & -i2s & 0 \\ 0 & i2s & 0 & -i\sqrt{3}f \\ 0 & 0 & i\sqrt{3}f & 0 \end{bmatrix} \tag{57}$$

During the acquisition period CSE and relaxation occur as in Section 2.9. The final density matrix is, therefore,

$\sigma_7(t,\tau) =$

$$1/2\begin{bmatrix} 0 & -i\sqrt{3}fF\exp(i\Delta\omega t) & 0 & 0 \\ i\sqrt{3}fF\exp(-i\Delta\omega t) & 0 & -i2sS\exp(i\Delta\omega t) & 0 \\ 0 & i2sS\exp(-i\Delta\omega t) & 0 & -i\sqrt{3}fF\exp(i\Delta\omega t) \\ 0 & 0 & i\sqrt{3}fF\exp(-i\Delta\omega t) & 0 \end{bmatrix} \tag{58}$$

Using equation (19), the detected signal, $\langle \mathbf{I}_x + i\mathbf{I}_y \rangle$, is

$$i[3\exp(-\tau/T_{2F})\exp(-t/T_{2F}^*) + 2\exp(-\tau/T_{2S})\exp(-t/T_{2S}^*)]\exp(-i\Delta\omega t) \tag{59}$$

which must also be normalized by dividing through by 5.

So far, biexponential relaxation has been the only aspect of the behaviour of quadrupolar nuclei which has distinguished them from the classical model of nuclear magnetism. This is because all the density matrices generated have contained only single-quantum elements, which behave classically in response to rf pulses. The order of multiple-quantum coherence for a density matrix element σ_{nm} is $|n - m|$ for the special case of a single spin. The coherence pattern for a spin-$\frac{3}{2}$ density matrix is thus,

$$\sigma = \begin{bmatrix} 0 & 1 & 2 & 3 \\ 1 & 0 & 1 & 2 \\ 2 & 1 & 0 & 1 \\ 3 & 2 & 1 & 0 \end{bmatrix} \tag{60}$$

In the next section a pulse sequence which excites both single- and triple-quantum coherences will be studied.

2.8. The triple-quantum filtered experiment

The pulse sequence for this experiment is[45]

$$\pi/2_x - \tau/2 - \pi_y - \tau/2 - \pi/2_y - \delta - \pi/2_y - \text{Acq.} \tag{61}$$

Using the result from equation (57) for the sequence up to the end of the second $\tau/2$ period, and applying the first $\pi/2_y$ pulse, gives

$$\sigma_8(\tau,+) = 1/16 \begin{pmatrix} 0 & -i4\sqrt{3}(s+f) & 0 & i12(s-f) \\ i4\sqrt{3}(s+f) & 0 & -i4(s+3f) & 0 \\ 0 & i4(s+3f) & 0 & -i4\sqrt{3}(s+f) \\ -i12(s-f) & 0 & i4\sqrt{3}(s+f) & 0 \end{pmatrix} \tag{62}$$

Comparison of equation (62) with (60) shows that both single- and triple-quantum coherences are excited. The single-quantum coherences may be eliminated by phase cycling the pulses in the manner discussed by Braunschweiler *et al.*[46] The phase cycle consists of stepping the first three pulses through phase increments of $\pi/3$, while holding the phase of the last pulse at zero, and alternating the receiver phase. Possible artefacts due to pulse imperfections may be reduced by additional phase cycling of the π pulse according to the

"Exorcycle" phase scheme.[47] The density matrix is then,

$$\sigma_9(\tau) = 1/16 \begin{pmatrix} 0 & 0 & 0 & i12(s-f) \\ 0 & 0 & 0 & 0 \\ 0 & 0 & 0 & 0 \\ -i12(s-f) & 0 & 0 & 0 \end{pmatrix} \tag{63}$$

During the δ period, the triple-quantum coherence undergoes both CSE and relaxation. Applying the CSE operator gives

$$\sigma_{10}(\tau+\delta) = 1/16 \begin{pmatrix} 0 & 0 & 0 & i12(s-f)\exp(i3\Delta\omega\delta) \\ 0 & 0 & 0 & 0 \\ 0 & 0 & 0 & 0 \\ -i12(s-f)\exp(-i3\Delta\omega\delta) & 0 & 0 & 0 \end{pmatrix} \tag{64}$$

It can be shown that the triple-quantum relaxation rate is the same as R_2, equation (36).[32] So, defining $d = \exp(-\delta/T_{2S})$, gives

$$\sigma_{11}(\tau+\delta) = 1/16 \begin{pmatrix} 0 & 0 & 0 & i12d(s-f)\exp(i3\Delta\omega\delta) \\ 0 & 0 & 0 & 0 \\ 0 & 0 & 0 & 0 \\ -i12d(s-f)\exp(-i3\Delta\omega\delta) & 0 & 0 & 0 \end{pmatrix} \tag{65}$$

Defining $a = 12 \cdot d \cdot (s-f) \cdot \exp(i3\Delta\omega\delta)$, equation (65) may be written as

$$\sigma_{11}(\tau+\delta) = 1/16 \begin{bmatrix} 0 & 0 & 0 & ia \\ 0 & 0 & 0 & 0 \\ 0 & 0 & 0 & 0 \\ -ia^* & 0 & 0 & 0 \end{bmatrix} \tag{66}$$

Equation (19) shows that only single-quantum transitions are detectable as transverse magnetization. In order to detect the ia and $-ia^*$ triple-quantum terms they must be "moved" into the single-quantum elements of the density matrix. This is the formation of the final $\pi/2_y$ pulse. The density matrix after this pulse is

$$\sigma_{12}(\tau+\delta,+) =$$

$$1/128 \begin{bmatrix} i(a-a^*) & i\sqrt{3}(a+a^*) & i\sqrt{3}(a-a^*) & i(a+a^*) \\ -i\sqrt{3}(a+a^*) & i3(a-a^*) & -i3(a+a^*) & -i\sqrt{3}(a-a^*) \\ i\sqrt{3}(a-a^*) & i3(a+a^*) & i3(a-a^*) & i\sqrt{3}(a+a^*) \\ -i(a+a^*) & -i\sqrt{3}(a-a^*) & -i\sqrt{3}(a-a^*) & -i(a-a^*) \end{bmatrix} \tag{67}$$

Including the effect of CSE and relaxation during the acquisition period, the detected magnetization, $\langle \mathbf{I}_x + i\mathbf{I}_y \rangle$, is of the form

$$(1/128)[i6(a + a^*)S - i6(a + a^*)F] \exp(-i\Delta\omega t) \tag{68}$$

It is simple to show that $(a + a^*) = 24 \cdot d \cdot (s - f) \cdot \cos(3\Delta\omega\delta)$, and substituting this into equation (68) gives

$$(9/8)[\exp(-\tau/T_{2S}) - \exp(-\tau/T_{2F})] \exp(-\delta/T_{2S}) \cos(3\Delta\omega\delta) \times$$
$$\times [\exp(-t/T_{2S}) - \exp(-t/T_{2F})] \exp(-i\Delta\omega t) \tag{69}$$

Including the normalization factor of 1/5, equation (69) becomes

$$(9/40)[\exp(-\tau/T_{2S}) - \exp(-\tau/T_{2F})] \exp(-\delta/T_{2S}) \cos(3\Delta\omega\delta) \times$$
$$\times [\exp(-t/T_{2S}) - \exp(-t/T_{2F})] \exp(-i\Delta\omega t) \tag{70}$$

Which agrees with the result obtained using the irreducible tensor formalism.[34] The triple-quantum filtration pulse sequence, applied to a spin-$\frac{3}{2}$ quadrupolar nucleus, produces almost exactly the same result as does the double-quantum filtration sequence, except for two differences. The double-quantum relaxation rate is faster than the triple-quantum relaxation rate, and the triple-quantum FID is a factor of 1.5 larger than the double-quantum FID.[34] The triple-quantum filter will thus require less than half the number of acquisitions to equal the signal-to-noise of the double-quantum sequence.

3. QUADRUPOLAR RELAXATION AND CHEMICAL EXCHANGE

3.1. Transverse relaxation of spin-$\frac{3}{2}$ nuclei

We now consider relaxation of quadrupolar ions in greater detail. The theory presented applies to any spin-$\frac{3}{2}$ quadrupolar nucleus, though the experimental examples discussed are of $^{87}Rb^+$ in agarose gels.

The simplest of all forms of single-site quadrupolar relaxation occurs for the case $(\omega\tau_c)^2 \ll 1$, known as relaxation within the motional narrowing region. All spectral density functions, $j(n\omega)$, tend to $j(0)$, which is simply equal to τ_c (see equation (32)), and there is then no difference between T_{2S} and T_{2F}. The same is also true for T_{1S} and T_{1F}, resulting in the following expression for the longitudinal and transverse relaxation times,

$$\frac{1}{T_1} = \frac{1}{T_2} = \frac{1}{20}\left[\frac{eV_{zz}Q}{\hbar}\right]^2 \tau_c \tag{71}$$

Single-site relaxation is not very biophysical, as ions in living tissues are in exchange with a multitude of molecular and membrane binding sites. The bound ions are expected to be subject to large electric field gradients and long correlation times, resulting in non-motional narrowing relaxation, i.e.

$(\omega\tau_c)^2 \gg 1$. We consider only the fast exchange case, where the time the ion spends in a bound state is much less than its transverse relaxation time. The theory of two-site exchange for spin-$\frac{3}{2}$ nuclei which we now discuss was developed by Bull.[48] Let $\alpha = 1$ or 2, and $\beta = S$ or F, then, $T_{\alpha\beta}^{\text{FREE}}$ and $T_{\alpha\beta}^{\text{BOUND}}$ are the "free" and "bound" relaxation times respectively. If τ is the average time the ion spends in the bound state, and p is the fraction of the ions in the bound state, then the measured relaxation rates, $R_{\alpha\beta}$, for $p \ll 1$, are

$$R_{\alpha\beta} = \frac{1}{T_{\alpha\beta}} = \frac{1}{T_{\alpha\beta}^{\text{FREE}}} + \frac{p}{T_{\alpha\beta}^{\text{BOUND}} + \tau} \tag{72}$$

The nuclear correlation time, τ_c, is approximately equal to τ, the average binding time. For rapid exchange, $\tau \ll T_{\alpha\beta}^{\text{BOUND}}$, and thus the τ may be dropped from equation (72), which then becomes

$$R_{\alpha\beta} = \frac{1}{T_{\alpha\beta}} = \frac{1}{T^{\text{FREE}}} + \frac{p}{T_{\alpha\beta}^{\text{BOUND}}} \tag{73}$$

where $T_{\alpha\beta}^{\text{FREE}}$ has been replaced by T^{FREE}, as in free solution the slow and fast T_1 and T_2 relaxation times are equal. This may be written solely in terms of the relaxation rates, i.e.

$$R_{\alpha\beta} = R^{\text{FREE}} + pR_{\alpha\beta}^{\text{BOUND}} \tag{74}$$

The fraction of bound ions, p, may be written as $K[S]$, where $[S]$ is the concentration of binding sites, and K is the equilibrium constant for the $(\text{ion}^+ + S)_{\text{FREE}} \leftrightarrow (\text{ion}^+S)_{\text{BOUND}}$ reaction. Equation (74) becomes

$$R_{\alpha\beta} = R^{\text{FREE}} + K[S]R_{\alpha\beta}^{\text{BOUND}} \tag{75}$$

The bound site correlation time can be calculated from this equation,[49] though for any practical situation it is unlikely that the two-site exchange model and its corresponding single-site correlation time realistically reflects the actual events in a biochemical medium. Equation (75) may be simply extended to multiple-binding sites, i.e.

$$R_{\alpha\beta} = R^{\text{FREE}} + \sum_i K_i[S_i]R_{\alpha\beta i}^{\text{BOUND}} \tag{76}$$

where i is summed over all possible sites. It is not possible to calculate the multiple correlation times from this equation without introducing further assumptions about the relaxation behaviour.[50]

Before considering the consequences of these equations theoretically, we present some experimental results which graphically illustrate the influence of the concentration of binding sites on the measured transverse relaxation rates of the $^{87}Rb^+$ nucleus.[51] An analysis of ^{23}Na NMR relaxation in a variety of model systems, including agarose, has been undertaken by Payne and Styles.[52] The triple-quantum filtration experiment was used to determine T_{2S} and T_{2F} for $^{87}Rb^+$ in gels of the carbohydrate agarose, and the dependence

of T_{2S} and T_{2F} on agarose concentration was determined. The magnetic field dependence of the agarose relaxation times was measured at 1.9, 4.2 and 7.05 T. As shown in Section 2, triple-quantum filtration of spin-$\frac{3}{2}$ nuclei gives rise to detectable magnetization, on resonance, and with $\delta \approx 0$, of the form

$$[\exp(-\tau/T_{2S}) - \exp(-\tau/T_{2F})][\exp(-t/T_{2S}) - \exp(-t/T_{2F})] \qquad (77)$$

The frequency domain signal is the difference between two Lorentzians, one corresponding to T_{2S} and the other to T_{2F}. By performing a number of experiments, each at a different τ time, a set of spectra are obtained, in which the peak amplitudes vary according to the function $[\exp(-\tau/T_{2S}) - \exp(-\tau/T_{2F})]$, yielding values for T_{2S} and T_{2F}. Experiments following this protocol were performed on agarose gels of concentration from 1 to 16 g%. All samples were prepared in 1 M RbCl. A triple-quantum filtered spectrum of RbCl in the presence of 2 g% agarose sample is shown in Fig. 2a, while Fig. 2b shows the dependence of the peak amplitudes of the triple-quantum creation time, τ. The slow and fast relaxation times of $^{87}Rb^{+}$ in agarose are plotted in Fig. 3. The field dependence of T_{2S} and T_{2F} in 4 g% agarose is plotted in Fig. 4.

Plots of R_{2S}^{BOUND} (equation (36)) and R_{2F}^{BOUND} (equation (35)) as a function of correlation time and frequency are shown in Fig. 5. For correlation times $> 1/\omega$, R_{2F}^{BOUND} increases linearly with τ_c, while R_{2S}^{BOUND} decreases slowly.

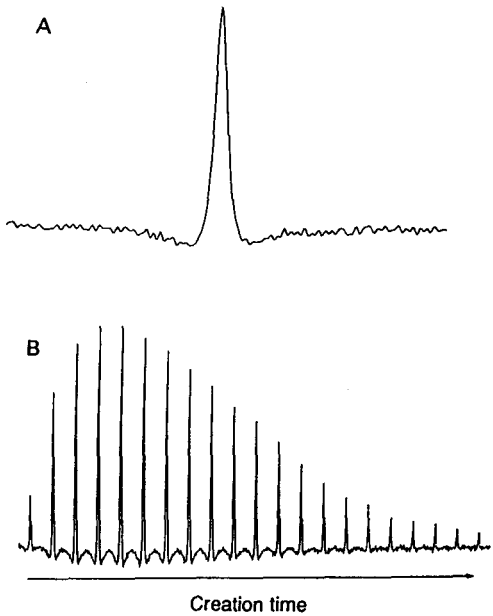

Fig. 2. (A) ^{87}Rb triple-quantum filtered NMR spectrum of 2 g% agarose in RbCl. (B) Dependence of the triple-quantum signal amplitude on the triple-quantum creation time—a biexponential fit to the peak heights of the series of spectra yields the T_{2S} and T_{2F} relaxation times. From Ref. 51, with permission.

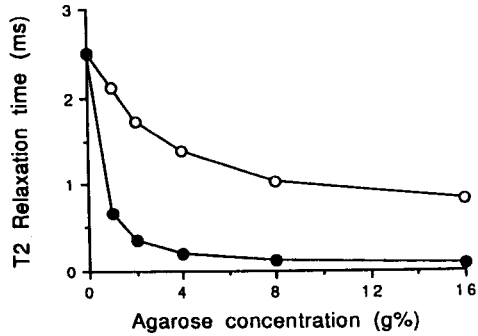

Fig. 3. ^{87}Rb T_{2S} and T_{2F} relaxation times as a function of agarose gel concentration. ●, T_{2S}; ○, T_{2F}. From Ref. 51, with permission.

This illustrates that for an ion in exchange with a binding site where τ_c is expected to be long, $T_{2F} < T_{2S}$. From equation (76) it is clear that as the concentration of possible binding sites, $[S_i]$, rises, so the measured rate of relaxation rises. $[S_i]$ is obviously proportional to the number of binding sites per molecule (n), and may be written as $[S_i] = n_i \cdot [C]$, where $[C]$ is the concentration of molecules. The measured relaxation rates may then be written as,

$$R_{2\beta} = R^{\text{FREE}} + \sum_i K_i \cdot n_i \cdot R_{2\beta}^{\text{BOUND}} \cdot [C] \tag{78}$$

A plot of $R_{2\beta}$ against $[C]$ should give a straight line of slope $\sum K_i \cdot n_i \cdot R_{2\beta}^{\text{BOUND}}$. A plot of R_{2F} against agarose concentration is shown in Fig. 6. For agarose concentrations less than 8 g% the data are linear, suggesting that the multisite exchange model adequately explains the behaviour of $^{87}Rb^+$ ions in solution. The ^{87}Rb-agarose experiments illustrate the much-reported NMR invisibility of spin-$\frac{3}{2}$ ion in tissues. As $T_{2F} \ll T_{2S}$ it is possible that a large proportion of the rapidly relaxing $|\pm 3/2\rangle \rightarrow |\pm 1/2\rangle$ transition could be lost during the rf pulse and receiver delay, or just broadened into the baseline noise

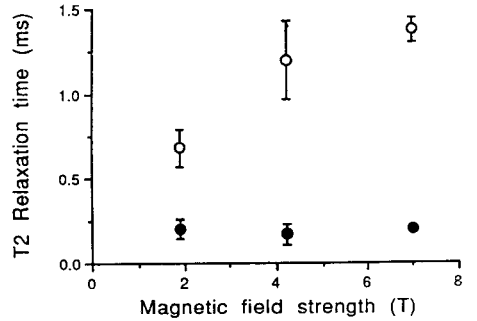

Fig. 4. Dependence of the $^{87}Rb^+$ T_{2S} and T_{2F} relaxation times in 4 g% agarose on magnetic field strength. ●, T_{2S}; ○, T_{2F}. From Ref. 51, with permission.

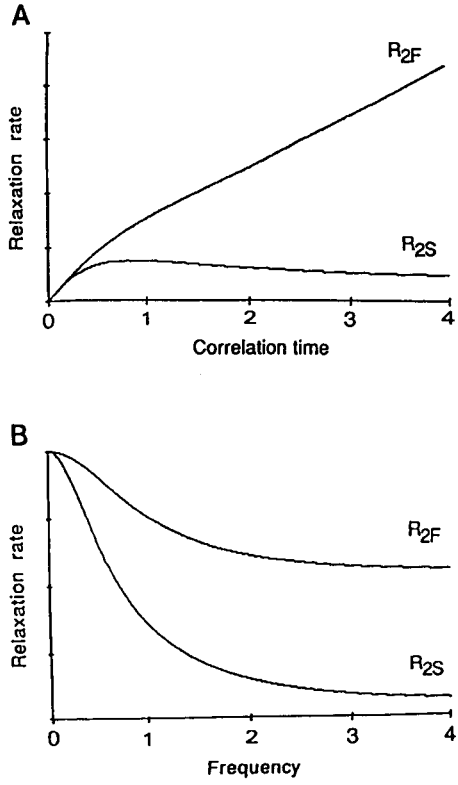

Fig. 5. Dependence of the slow, R_{2S}, and fast, R_{2F}, relaxation rates on correlation time (A) and frequency (B). The correlation time is expressed in units of $1/\omega$, and the frequency is expressed in units of $1/\tau$. The relaxation rates are in arbitrary units. From Ref. 51, with permission.

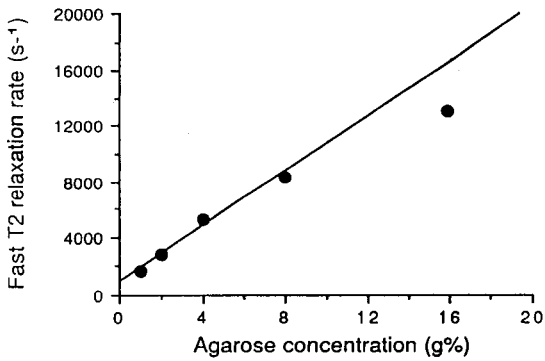

Fig. 6. The fast relaxation rate, R_{2F}, of $^{87}Rb^{+}$ in agarose. The form of the line fitted to the first 4 points is $R_{2F} = 834(\pm 359) + [\text{agarose}] \times 976(\pm 67)$. The last point was omitted as it did not fall within the linear region of the two-site exchange model.

of the spectrum. This will decrease the NMR visibility of the relevant ion. Assuming that all the signal from the rapidly relaxing transition is lost, only 40%[43] of the total amount of the spin-$\frac{3}{2}$ ion present will be detected (see equation (57)). This explanation of the apparent invisibility of $^{23}Na^+$ in animal tissues was initially proposed by Berendsen and Edzes.[2] There are numerous reports on the reduced visibility of $^{23}Na^+$, $^{39}K^+$ and $^{87}Rb^+$ in heart, kidney and muscle,[16,33,53–56] though the visibility of these ions in human erythrocytes has been shown to be 100%.[57,58] Recent work by Shinar and Navon[59] has shown that the $^{23}Na^+$ relaxation times in nucleated cells are much shorter than the relaxation times in cells devoid of a nucleus, such as the human red cell, which goes to support the observed decrease in spin-$\frac{3}{2}$ ion visibility in tissues other than erythrocytes.

3.2. Longitudinal relaxation of spin-$\frac{3}{2}$ nuclei

The equations for T_1 relaxation are[44]

$$R_{1S} = \frac{1}{T_{1S}} = \frac{1}{10}\left[\frac{eQV_{zz}}{\hbar}\right]^2 j(2\omega) \quad (20\%) \tag{79}$$

and

$$R_{1F} = \frac{1}{T_{1S}} = \frac{1}{10}\left[\frac{eQV_{zz}}{\hbar}\right]^2 j(\omega) \quad (80\%) \tag{80}$$

where R_{1S} and R_{1F} are the rates of slow and fast T_1 relaxation, and the numbers in parenthesis are the percentages of total relaxation proceeding via each channel.

The biexponential nature of the longitudinal relaxation time is very difficult to detect,[44] and T_1 may be regarded as a uniexponential process, with rate constant[48]

$$\frac{1}{T_1} = \frac{0.2}{T_{1S}} + \frac{0.8}{T_{1F}} \tag{81}$$

For a population of spins exchanging between a free and a bound state, the measured T_1 relaxation rate, by analogy to the T_2 case, is

$$R_1 = R_1^{\text{FREE}} + \sum_i K_i \cdot n_i \cdot R_1^{\text{BOUND}} \cdot [C] \tag{82}$$

where R_1^{BOUND} is given by equations (79, 80 and 81).

The experimental dependence of R_1 for $^{87}Rb^+$ as a function of agarose concentration and magnetic field strength is shown in Fig. 7, and the theoretical interpretation of these results is very similar to that used for the transverse relaxation case.

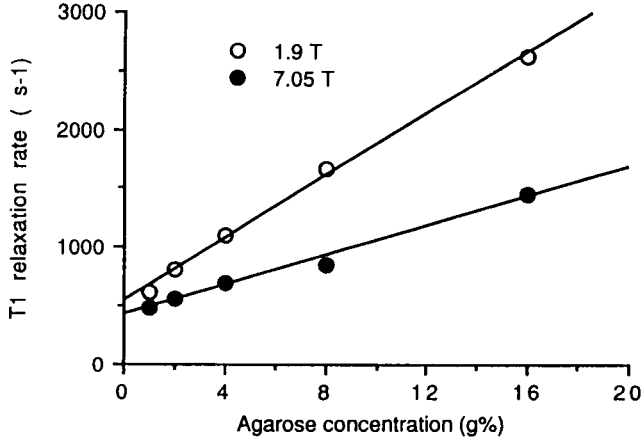

Fig. 7. The T_1 relaxation rates, R_1, of $^{87}Rb^+$ in agarose at 1.9 T (●) and 7.05 T (○). The forms of the lines are, $R_1(●) = 584(\pm 151) + [\text{agarose}] \times 126(\pm 12)$, and $R_1(○) = 417(\pm 25) + [\text{agarose}] \times 68(\pm 2)$.

4. DIFFERENTIATION BETWEEN INTRA- AND EXTRACELLULAR IONS

4.1. Introduction

In order to study the distribution of cations across cell membranes and the transmembrane flux by NMR, it is essential to differentiate between signals originating from the various intracellular and extracellular spaces. In order to do this, spins in each space must be "labelled". The magnetization in any compartment is characterized by a set of parameters: ω, T_1, T_{2S} and T_{2F}, and if these parameters differ considerably between compartments they may be used as the basis of a spectral editing or data-processing technique designed to either separate intra- and extracellular resonances or to selectively detect one of these signals, whilst suppressing the others. We shall simplify matters by assuming that the tissue is composed only of an intracellular and extracellular space. The validity of this assumption varies, depending on the tissue type under consideration.

4.2. Differentiation with respect to resonant frequency

Having the intra- and extracellular signals resonating at different frequencies in the spectrum is the simplest method of differentiating between intra- and extracellular cation resonances. This method allows the direct measurement of compartment populations, and under certain conditions, the measurement of the

flux of ions from one compartment to the other. For ions with quadrupolar nuclei the chemical shift separation of intra- and extracellular resonances may result from the interaction of the quadrupolar moment with the intracellular environment, or because of the addition of a paramagnetic shift reagent to the extracellular space. It has recently been shown that the intra- and extracellular resonances of $^{133}Cs^+$ in red cells and rat heart are separated by $\sim$ 1 ppm.[27] This intrinsic shift is presumably due to second-order perturbation effects of the quadrupolar Hamiltonian on the Zeeman energy level states.[44] Fortunately, the $^{133}Cs^+$ relaxation times are long, giving rise to narrow spectral lines, which for a 1 ppm separation at high field, are resolved. No intrinsic chemical shift of intracellular $^{23}Na^+$, $^{39}K^+$ or $^{87}Rb^+$ resonances have been observed, and we are forced to resort to more interventional methods.

4.2.1. Paramagnetic shift reagents

The paramagnetic shift reagents dysprosium tripolyphosphate, $Dy(PPP)_2^{7-}$, and dysprosium triethylenetetraamine-hexa-acetic acid, $Dy(TTHA)^{3-}$, have been used extensively to resolve intra- and extracellular $^{23}Na^+$ and $^{39}K^+$ resonances in red cells,[5,8,12,57,60] rat and frog heart,[16,17,61] rat and frog muscle,[5,18] and cat brain.[62] These anionic shift reagents do not pass through cellular membranes, nor do they have a great affinity for large macromolecules, which, under physiological conditions, are negatively charged. The hyperfine shift of the ion is induced by the paramagnetic lanthanide, Dy^{3+}, whilst the function of the negatively charged ligand is to bring the inorganic and paramagnetic ions into close proximity. See Springer[33] for a review of this topic.

The efficacy of $Dy(PPP)_2^{7-}$ and $Dy(TTHA)^{3-}$ as shift reagents for a variety of ions, including $^{23}Na^+$, $^{39}K^+$ and $^{87}Rb^+$, has been examined,[7] and the effect of temperature, osmolarity and shift reagent concentration on the chemical shift has been studied by Burnstein and Fossel.[63] The chemical shift of $^{87}Rb^+$ as a function of $Dy(TTHA)^{3-}$ concentration in the presence of 6.7 g% bovine serum albumin (BSA) is shown in Fig. 8. The BSA was included to mimic the extracellular plasma environment.

4.2.2. Halide shift reagents

All the alkali metals show significant shifts in the presence of halide ions,[64] and iodide (I) introduces $^{87}Rb^+$ shifts in excess of 50 ppm. In addition, the Rb^+–I^- interaction does not give rise to very large $^{87}Rb^+$ relaxation effects, and hence the linewidths are not significantly increased. The concentrations of I^- required to induce large shifts are in the molar range. This obviously disqualifies I^- as a shift reagent for use in biological studies, but Rb^+- and I^--containing solutions do form a very good reference for quantification studies.

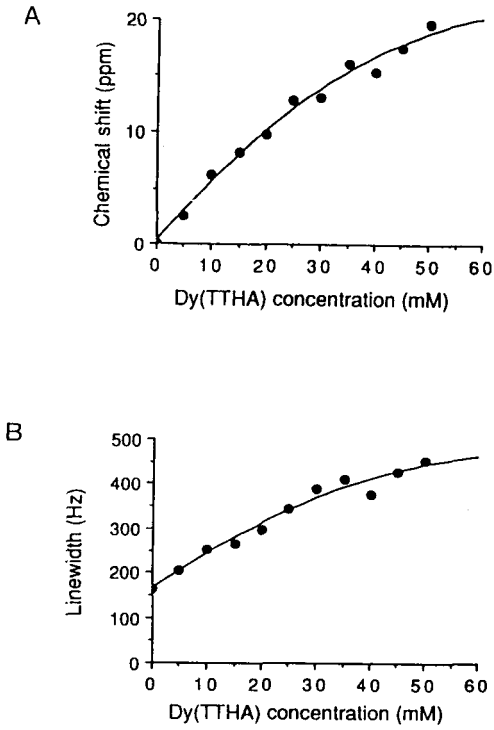

Fig. 8. (A) The chemical shift of 10 mM RbCl in 6.7 g% BSA as a function of $Dy(TTHA)^{3-}$ concentration. (B) The $^{87}Rb^{+}$ linewidths as a function of the $Dy(TTHA)^{3-}$ concentration.

4.3. Relaxation time editing of $^{87}Rb^{+}$ NMR spectra

The intra- and extracellular environments are very different in their chemical composition, and the high intracellular protein and membrane concentration suggests that the relaxation times of intracellular ions should be considerably shorter than those in the extracellular fluid. This assertion is corroborated by experimental measurements. A number of pulse techniques have been developed for the suppression of one resonance with particular relaxation times, whilst selectively detecting another resonance with different relaxation times.[65,66] All these techniques are based on the conventional inversion-recovery or spin-echo experiments, and offer the promise of resolving intra- and extracellular resonances without the addition of potentially harmful shift reagents to the system.[67] If the linewidth of the intra- and extracellular signals are very different, then simple lineshape analysis will allow differentiation between the intra- and extracellular resonances. On the basis of preliminary studies of ^{87}Rb NMR of cells and perfused organs it was clear that the

intracellular $^{87}Rb^+$ resonance was very broad ($\sim$ 900 Hz in kidney and heart at 4.2 T), while the extracellular signal was still close to the free solution linewidth ($\sim$ 150–200 Hz), this allowed computer lineshape analysis to be used to differentiate between these two resonances in studies of the perfused rat kidney.[68] A similar method of differentiating between intra- and extracellular $^{39}K^+$ resonances in the perfused salivary gland has also been developed.[69]

An alternative to exploiting natural differences between intra- and extracellular relaxation times is to generate an artificial difference by chemical means. Degani and Elgavish[3] used $Gd(EDTA)^-$ to broaden the extracellular resonances so that the intracellular $^{23}Na^+$ and $^7Li^+$ resonances in lipid vesicles could be measured. Riddell and Southon[4] used diamagnetic complexes of lanthanum and tripolyphosphate to broaden the extracellular $^{87}Rb^+$ resonance in red cells, allowing the intracellular signal to be observed.

4.4. Editing by triple-quantum filtration

It has been reported that double-quantum filtration of erythrocyte ^{23}Na spectra allows the selective detection of intracellular sodium.[70] As seen in Section 2, triple- or double-quantum filtered (TQF or DQF) signals are detectable only if $T_{2F} \ll T_{2S}$. Analysis of equation (70) shows the size of the TQF signal to be a monotonically increasing function of the T_{2S}/T_{2F} ratio.[71,72] In Section 3 we saw that the T_{2S}/T_{2F} ratio of $^{87}Rb^+$ in agarose gels rose as a function of agarose concentration, suggesting that quadrupolar ions in contact with a multiplicity of binding sites give rise to more DQF/TQF signal than those with access to fewer binding sites.[52,72] This is illustrated in Fig. 9, where DQF ^{87}Rb spectra of RbCl solutions containing increasing quantities of the protein bovine serum albumin (BSA) are shown. As the BSA concentration rises, so too does the size of the DQF signal. Note that the RbI reference does not give rise to a DQF signal.[73] In practice both intra- and extracellular ions give rise to DQF/TQF signals, as was illustrated in an elegant set of experiments by Jelicks and Gupta.[74] They showed that in the absence of any shift reagent, both intra- and extracellular red cell $^{23}Na^+$ gave rise to a DQF signal. As the extracellular shift reagent concentration rose, so the extracellular DQF resonance was decreased or "quenched", presumably due to equalization of the T_{2S} and T_{2F} relaxation times by paramagnetic relaxation. In an extension to this work they showed that submillimolar quantities of the paramagnetic relaxation agent $Gd(PPP)_2^{7-}$ could be used to quench the extracellular DQF resonance.[75,76] The DQF/TQF resonance can be quantificated, either by comparison with a calibrated DQF/TQF reference,[75] or by comparison with a conventional single-quantum spectrum containing a calibrated reference.[77]

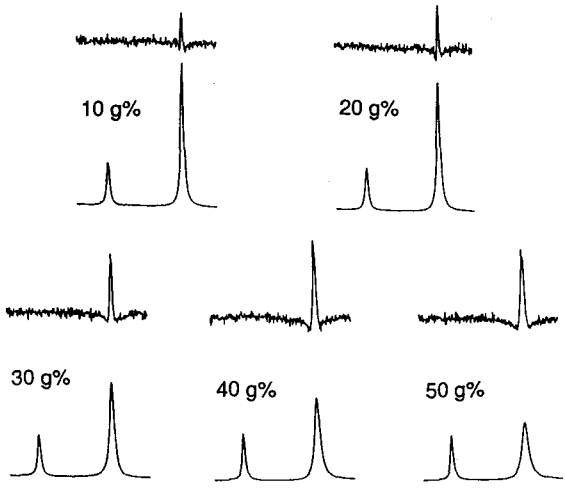

Fig. 9. Single- and triple-quantum filtered ^{87}Rb spectra as a function of BSA concentration. The triple-quantum creation time was set to τ_{max} for each sample. The triple-quantum filtered spectrum (10 240 scans) is plotted above the corresponding single-quantum spectrum (64 scans). The downfield peak in the single-quantum spectrum is a Rb and KI reference. From Ref. 72, with permission.

5. THE STUDY OF ION TRANSPORT BY METAL CATION NMR

The availability and resilience of human red cells have led to their being more intensively studied than any other mammalian cell system. The transport of a wide variety of organic metabolites and inorganic ions have been studied by high-resolution NMR. Early work utilized the techniques of ^{31}P,[78] ^{13}C[79] and ^{1}H NMR.[80] The development of membrane-impermeable, paramagnetic shift reagents, capable of differentiating between intra- and extracellular ions[5–7] greatly accelerated interest in the study of red cell ion transport by NMR. Most early work dealt with the steady-state transmembrane distribution and relaxation properties of Na^+, Li^+ and K^+.[5,8,12,13,60,81,82] Intracellular Na^+ and K^+ concentrations measured by NMR agreed with those determined by other analytical means; approximately 10 mM and 100 mM, respectively. The ouabain-sensitive Na^+ efflux and ionophore-induced influx in red cells has been studied by Ogino *et al.*[57] Measurement of the intra- and extracellular Na^+ concentration in red cells by NMR allowed Cowan and co-workers to calculate the sodium membrane potential.[83] Recent work by Shinar and Navon[59] has shed light on the nature of intracellular relaxation, showing that binding of Na^+ to the nucleus of the cell leads to a large increase in relaxation rate. This result also provides an explanation for the 100% visibility of $^{23}Na^+$ and $^{39}K^+$ ions in un-nucleated red cells, as opposed to the reduced visibility of these ions reported in most other tissues.[12,33] The relationship between efflux and

influx of K^+, Na^+ and pH (H^+) in yeast cells was investigated by Ogino and co-workers.[11] Studies of tissues include rat and frog heart,[16,17] kidney tubules,[14,15] cultured renal epithelial cells,[84] rat and frog muscle,[5,18] salivary glands[85,86] and cat brain.[62] The majority of these studies involved monitoring changes to intracellular Na^+ while carrying out some manipulation of the set of parameters affecting Na^+ transport rate. These include adding the Na^+–K^+-ATPase inhibitor, ouabain, inducing ischaemia, and changing the extracellular ion content. The NMR visibility of $^{23}Na^+$ and $^{39}K^+$ in these studies varied from 20% to 100%, depending on the identity of the tissue and the investigator. A detailed discussion of visibility of these two ions is given by Springer.[33]

5.1. Human erythrocytes

None of these studies dealt with the normal unidirectional K^+ flux across the cell membrane, and the only method of determining this flux in living tissues is to follow the kinetics of a suitable K^+ congener. Both Cs^+ and Rb^+ have been used as biological congeners of K^+.[26,28] Rb^+ most resembles K^+ and radioactive $^{86}Rb^+$ is the mainstay of much of the research into K^+ flux in cells and organs. A detailed NMR study of the kinetics of $^{133}Cs^+$ transport in red cells and perfused rat heart[27] has shown Cs^+ to be transported at about 1/3 of the rate of K^+. Before discussing ^{87}Rb NMR studies of red cell Rb^+ transport we need to develop a simple model of Rb^+ transport in cells.

Many cell types take up Rb^+ and K^+ in a very similar way; however, the efflux of Rb^+ and K^+ from cells is different, leading to intracellular Rb^+ concentrations different to that predicted on the basis of a direct substitution of Rb^+ for K^+.[28] The total flux of K^+ in human red cells may be separated into two components: one, linear with the external K^+ concentration, and assumed to be due to passive diffusion; and the other, representing the major fraction of all transport, which saturates with external K^+ concentration, and is associated with active sodium transport by the protein Na–K-ATPase. About 80–90% of the saturable component can be blocked with cardiac glycosides such as ouabain.[30] There are certainly a number of other K^+ transport channels in the red cell, but these are quiescent under normal conditions of pH, osmolarity and pressure. In studies of radioactive $^{86}Rb^+$ transport, the Rb^+ is present in tracer quantities, implying that competition between Rb^+ and K^+ may be ignored. In NMR studies of $^{87}Rb^+$ transport, the Rb^+ is present in much larger (millimolar) concentrations, which requires that competition between the two ions for transport channels be taken into account. The rate of active Rb^+ uptake, V_{Rb}, may be written as a fraction of the total rate of active transport of both Rb^+ and K^+, V_{max}:

$$V_{Rb} = \frac{V_{max} \cdot [Rb]_E}{[Rb]_E + [K]_E} \tag{83}$$

Assuming that the passive uptake and efflux rate constants, k, are equal, we may write the intracellular Rb^+ concentration as:

$$\frac{d[Rb]_I}{dt} = V_{Rb} + k[Rb]_E - k[Rb]_I \tag{84}$$

For a constant extracellular Rb^+ concentration, $[Rb]_E$, and an initial intracellular Rb^+ concentration of zero, the solution is simple.

$$[Rb(t)]_I = \frac{V_{Rb} + k[Rb]_E}{k} \cdot [1 - \exp(-kt)] \tag{85}$$

If the extracellular Rb^+ concentration changes with time, the solution is more complicated, but we will not discuss this here. If the NMR experiment allows sufficient time resolution, we can mirror radioactive tracer experiments and use the data acquired in the linear part of the exponential curve, i.e. where $t < 1/k$, as this eliminates any need to model the passive efflux part of the transport process correctly. For cellular studies at high field this is possible, but for perfused organ studies at lower field the sensitivity of the NMR experiment does not permit this, and we are forced to acquire data over a longer time period and fit equation (85) to the resulting spectral areas.

Two reports on the measurement of Rb^+ transport in red cells by $^{87}Rb^+$ NMR have been published.[58,87] Both groups used $Dy(TTHA)^{3-}$ to resolve the intra- and extracellular $^{87}Rb^+$ resonances. The relative frequency shift between intra- and extracellular red cell resonances at 7 T, in buffers containing 5, 10, 15, 20, 25, 30 and 35 mM $Dy(TTHA)^{3-}$, are shown in Fig. 10.

In experiments carried out in our laboratory, washed erythrocytes were resuspended in buffer, containing 25 mM $Dy(TTHA)^{3-}$, to a haematocrit of 50%, to which RbCl was added, resulting in an extracellular Rb^+ concentration of 10 mM. NMR spectra were acquired with a $\pi/2$ pulse applied every 12.8 ms. A spectrum was acquired every 20 min, and the bore of the magnet was maintained at 37°C during the experiment. The natural linewidth of both the intra- and extracellular resonances was $\sim$ 450 Hz. A stacked plot of Gaussian resolution-enhanced ^{87}Rb spectra as a function of time are shown in Fig. 11. Rb^+ uptake is shown to be slow, and easily monitored by ^{87}Rb NMR. Having measured the Rb^+ uptake rate from the initial linear part of the exponential uptake curve, the result was scaled to calculate the K^+ flux, using equation (83). The average K^+ flux calculated from these measurements was 1.8 ± 0.3 mmol/h litre of cells. A full analysis of the exponential uptake with time, taking account of the changing extracellular Rb^+ concentration yielded a value for the K^+ flux of 1.7 mmol/h litre of cells.[88] Both results are in good agreement with the literature values for the unidirectional K^+ flux into erythrocytes of between 1.5 and 2.1 mmol/h litre of cells.[31,89] The total integral of the $^{87}Rb^+$ NMR signal (intra- plus extracellular) did not change during the course of any of the uptake experiments, implying that the intracellular NMR visibility of $^{87}Rb^+$ is $\sim$ 100%. This is consistent with what has been found for $^{23}Na^+$ and

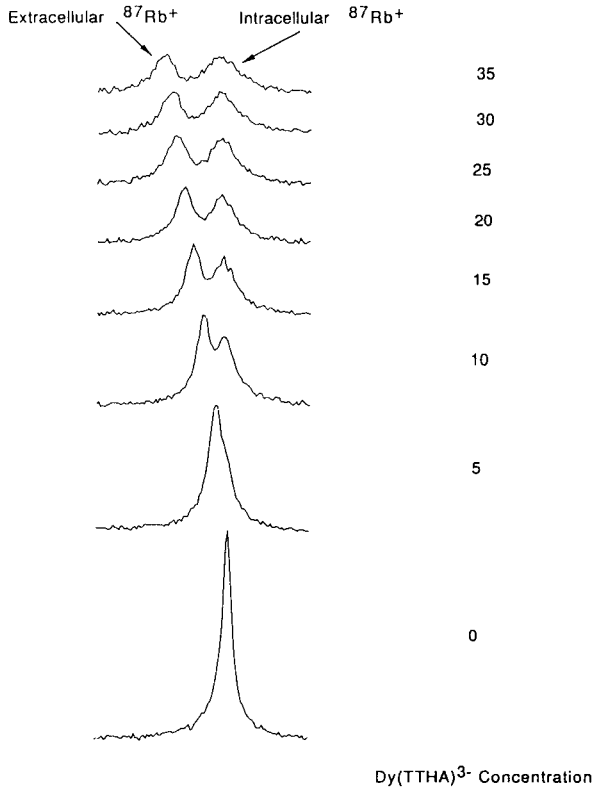

Fig. 10. ^{87}Rb NMR spectra of Rb^+-loaded erythrocytes in buffer containing Rb^+ and varying concentrations (mM) of $Dy(TTHA)^{3-}$. The spectra were acquired at 7.05 T.

$^{39}K^+$ in erythrocytes.[57] Helpern *et al.*[87] followed a similar protocol to that described above, though they performed their experiments at 9.3 T, and so were able to use a lower shift reagent concentration (10 mM $Dy(TTHA)^{3-}$). They also replaced all of the extracellular K^+ with Rb^+, leading to an extracellular Rb^+ concentration of 18 mM. On analysing their uptake data in terms of a simple kinetic model they found a Rb^+ uptake rate of 1.3 mmol/h litre of cells, which though slightly low, is still close to the literature values for Rb^+ uptake in red cells. They reported a reduced visibility for intracellular $^{87}Rb^+$, though this can probably be explained by signal loss during the long receiver delay (144 μs) used.

Assuming, for the sake of simplicity, that the transverse and longitudinal relaxation times of intracellular $^{23}Na^+$, $^{39}K^+$ and $^{87}Rb^+$ were monoexponential, Allis *et al.*[58] measured these relaxation times in red cells at 7 T, and calculated the relative NMR sensitivity of the three nuclei. The results are

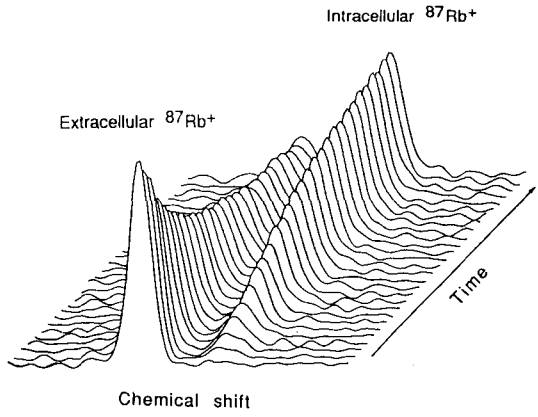

Fig. 11. A stacked plot of ^{87}Rb NMR spectra of human erythrocytes as a function of time, showing the uptake of Rb^+. The initial extracellular Rb^+ concentration was 10 mM, and the $Dy(TTHA)^{3-}$ concentration was 25 mM. Each spectrum took 4 min to acquire, and the time between spectra was 20 min. Spectra were processed with Gaussian resolution enhancement. From Ref. 58, with permission.

shown in Table 2. The sensitivities are normalized to that of ^{23}Na, which is taken as 100%.

The selective detection of intracellular $^{23}Na^+$ by double-quantum filtered NMR was discussed in Section 4.4, and it has been shown that intracellular $^{87}Rb^+$ in red cells can be selectively detected by this technique.[72] ^{87}Rb NMR has recently been used to examine the cromakalim-induced Rb^+ flux in cultivated smooth muscle cells.[90]

5.2. Perfused rat heart

Allis and co-workers[54] used ^{87}Rb NMR to measure the K^+ flux into cardiac muscle. Hearts from Wistar rats were perfused in the Langendorff mode[91,92] with modified Krebs–Henseleit buffer (KHB).[93] The heart hung freely within the radiofrequency coil, thus eliminating the problems associated with Rb^+ accumulation within any enclosing perfusion chamber. The temporal resolution between successive spectra was 250 s. Quantification of absolute amounts

Table 2. T_1 and T_2 relaxation times of $^{23}Na^+$, $^{39}K^+$ and $^{87}Rb^+$ in human erythrocytes at 7.05 T.

Nucleus	T_1 (ms)	T_2 (ms)	Sensitivity (%)
^{23}Na	20.6 ± 0.2	9.1 ± 0.1	100
^{39}K	17.1 ± 0.7	6.8 ± 0.6	3
^{87}Rb	0.95 ± 0.08	0.71 ± 0.06	56

of Rb^+ in hearts was obtained from the ratio of the heart signal to a calibrated reference consisting of Rb^+ and saturated KI. Hearts were weighed at the end of each experiment. Some hearts were freeze-clamped and their absolute Rb^+ content determined by atomic absorption spectrophotometry (AAS). The kinetic data obtained from these experiments were analysed in terms of the simple model of active and passive transport developed above. A stacked plot of ^{87}Rb spectra as a function of the duration of Rb-KHB perfusion is shown in Fig. 12. The natural linewidth of the heart ^{87}Rb spectra was ≈ 720 Hz, corresponding to a T_2^* of 450 μs. The kinetic model parameters were $V_{Rb} + kI_E = 0.41 \pm 0.07\,\mu$mol/min g and $k = 0.028 \pm 0.002\,\text{min}^{-1}$. I_{max} the equilibrium Rb^+ concentration is given by $(V_{Rb} + kI_E)/k$ or $11.9 \pm 1.9\,\mu$mol/g. The Rb^+ content of four hearts, determined by AAS, was $21.2 \pm 1.5\,\mu$mol/g. Comparing this with the NMR-measured Rb^+ concentration gave an NMR visibility of $^{87}Rb^+$ in rat heart at 4.2 T of $56 \pm 2\%$. This result elevated the true $(V_{Rb} + kI_E)$ to $0.73 \pm 0.16\,\mu$mol/min g, and I_{max} to $21.2 \pm 4.3\,\mu$mol/g. The physiological behaviour of the heart was not severely altered by the levels of intracellular Rb^+ achieved in these experiments. Relating Rb^+ and K^+ fluxes in the same way as for the red cell experiments gave a K^+ flux into the heart of $3.7 \pm 0.8\,\mu$mol/min g. This compares favourably with the K^+ flux as measured by radioactive $^{42}K^+$ of 3.3 μmol/min g.[54,94]

5.3. Perfused rat kidney

In studies performed by Endre *et al.*, rat kidneys were perfused with Rb^+-containing Krebs bicarbonate buffer.[55,95] A tracer quantity of radioactive $^{86}Rb^+$ was added to the perfusate in some experiments to evaluate the NMR visibility of the intracellular ^{87}Rb. The uptake of NMR-detectable Rb^+ into the kidney was analysed in terms of the model discussed above. The kinetic parameters obtained from three experiments were: $V_{Rb} + kI_E = 0.92 \pm 0.07\,\mu$mol/min g,

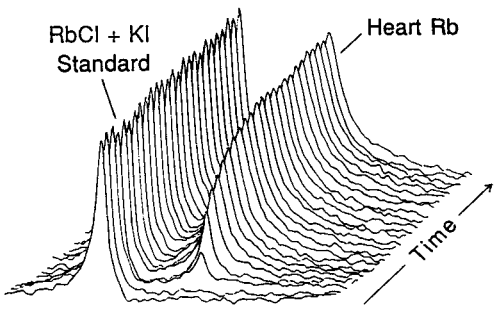

Fig. 12. Stacked plot of ^{87}Rb spectra showing the uptake of Rb^+ by a perfused rat heart. The time resolution between spectra was 4.2 min, and each spectrum was processed with 150 Hz of exponential line-broadening.

$k = 0.12 \pm 0.01\,\text{min}^{-1}$, implying that $I_{max} = 7.7 \pm 0.3$ mM. The average linewidth of renal $^{87}Rb^+$ spectra was ≈ 800 Hz, corresponding to a T_2^* of 400 μs. The proportion of tissue Rb^+ observed by NMR (NMR-visible $^{87}Rb^+$) was determined by comparing the final mass of Rb^+ measured by NMR with that measured in an aqueous extract of the kidney by radioactive $^{86}Rb^+$. The intracellular NMR visibility of $^{87}Rb^+$ in renal tissue determined by this method was $42 \pm 8\%$ ($n = 8$), which is similar to the 45% NMR visibility reported for renal $^{39}K^+$,[53] and close to the theoretical 40% visibility of quadrupolar ions in biological environments.[33] Including the $42 \pm 8\%$ NMR visibility of $^{87}Rb^+$ in renal tissue elevated I_{max} to 18.3 ± 3.6 mM and the initial uptake rate to 2.2 ± 0.4 μmol/min g. This gave a unidirectional K^+ flux into the whole kidney of 9.1 ± 1.7 μmol/min g. Literature values of K^+ flux measured using radioactive $^{42}K^+$ are between 5.8 and 8.8 μmol/min g in isolated rat kidney tubules[96] and 12.1 μmol/min g in guinea-pig kidney cortex slices.[97] These values compare favourably with the figure inferred from the ^{87}Rb NMR measurements.

5.4. Perfused rat salivary gland

The perfused rat salivary gland is a good test bed for the study of ion fluxes as the gland is quite resilient and easily stimulated by secretomotor agonists, leading to substantial Na^+ and K^+ fluxes, amongst others. Steward *et al.*[98] showed uptake of Rb^+ and changes in Rb^+ flux in response to acetylcholine. They were also able to demonstrate selective detection of intracellular $^{87}Rb^+$ by double-quantum filtered ^{87}Rb NMR.

5.5. Intact rat muscle

Syme *et al.*[56] loaded Sprague–Dawley rats with Rb^+ for 3–7 days prior to the NMR study, during which the rats were anaesthetized and placed in a 1.9 T magnet. NMR signals were acquired from the hindquarter muscle (see Fig. 13). The width of the intracellular $^{87}Rb^+$ signal was ≈ 2000 Hz, corresponding to a T_2^* of 160 μs, and twice the width of signals encountered in heart and kidney at 4.3 T. This is consistent with the field dependence of ^{87}Rb T_{2S} measured for $^{87}Rb^+$ in agarose (Section 3.1). The NMR visibility of muscle $^{87}Rb^+$ was calculated by comparing AAS measurements of the muscle Rb^+ content to the NMR measurement, and gave an NMR visibility of $41 \pm 3\%$. Syme *et al.*[99] used ^{87}Rb NMR to show that the rate of Rb^+ uptake into muscle of spontaneously hypertensive rats was three times higher than the rate of uptake into normotensive control rats.

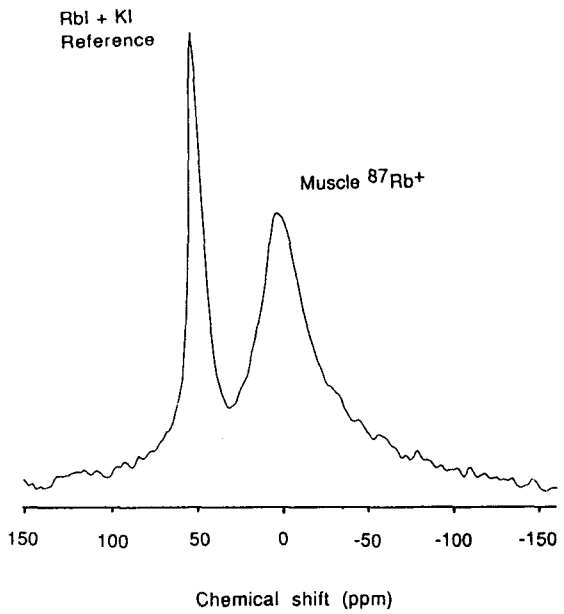

Fig. 13. ^{87}Rb NMR spectra of muscle from Rb^{+}-loaded rat, *in vivo* at 1.9 T.

6. CONCLUSION

^{87}Rb NMR provides a unique, non-destructive method for measurement of potassium fluxes in living systems. Agreement between the ^{87}Rb NMR method and the conventional ^{86}Rb tracer method is very good, providing that the reduced NMR visibility of the $^{87}Rb^{+}$ ion is taken into account. The visibility of intracellular $^{87}Rb^{+}$ is reduced in all cells, excepting human erythrocytes. The combination of ^{87}Rb, ^{23}Na and ^{31}P NMR provides an elegant, multinuclear approach to the study of ion fluxes and energetics in living tissues.

REFERENCES

1. F.W. Cope and R. Damadian, *Physiol. Chem. Phys.*, 1974, **6,** 17.
2. H.J.C. Berendsen and H.T. Edzes, *Ann. N.Y. Acad. Sci.*, 1973, **204,** 459.
3. H. Degani and G.A. Elgavish, *FEBS Lett.*, 1978, **90,** 357.
4. F.G. Riddell and T.E. Southon, *Inorg. Chim. Acta*, 1987, **136,** 133.
5. R.K. Gupta and P. Gupta, *J. Magn. Reson.*, 1982, **47,** 344.
6. M.M. Pike and C.S. Springer, *J. Magn. Reson.*, 1982, **46,** 348.
7. S.C. Chu, M.M. Pike, E.T. Fossel, T.W. Smith, J.A. Balschi and C.S. Springer, *J. Magn. Reson.*, 1984, **56,** 33.
8. P.J. Brophy, M.K. Hayer and F.G. Riddel, *Biochem. J.*, 1983, **210,** 961.
9. F.G. Riddell, S. Arumugan and B.G. Cox, *Biochim. Biophys. Acta*, 1988, **944,** 279.
10. M.M. Pike, S.R. Simon, J.A. Balshi and C.S. Springer, *Proc. Natl. Acad. Sci. USA*, 1982, **79,** 810.

11. T. Ogino, J.A. denHollander and R.G. Shulman, *Proc. Natl. Acad. Sci. USA*, 1983, **80,** 5185.
12. M.M. Pike, E.T. Fossel, T.W. Smith and C.S. Springer, *Am. J. Physiol.*, 1984, **246,** C528.
13. J.W. Pettegrew, J.F.M. Post, K. Panchalingam, G. Withers and D.E. Woessner, *J. Magn. Reson.*, 1987, **71,** 504.
14. B.M. Rayson and R.K. Gupta, *J. Biol. Chem.*, 1985, **260,** 7276.
15. S.R. Gullans, M.J. Avison, T. Ogino, G. Giebisch and R.G. Schulman, *Am. J. Physiol.*, 1985, **249,** F160.
16. E.T. Fossel and H. Hoefeler, *Magn. Reson. Med.*, 1986, **3,** 534.
17. M.M. Pike, J.C. Frazer, D.F. Dedrick, J.S. Ingwall, P.D. Allen, C.S. Spinger and T.W. Smith, *Biophys. J.*, 1985, **48,** 159.
18. H. Blum, M.D. Schnall, B. Chance and G.P. Buzby, *Am. J. Physiol.*, 1988, **255,** C377.
19. R.K. Harris, *Nuclear Magnetic Resonance Spectroscopy*. Longman, London, 1983.
20. F.G. Riddell and S.J. Tompsett, *Biochim. Biophys. Acta*, 1990, **1024,** 193.
21. S. Forsen and R.A. Hoffman, *J. Chem. Phys.*, 1963, **39,** 2892.
22. I.D. Campbell, C.M. Dobson, R.G. Ratcliffe and R.J.P. Williams, *J. Magn. Reson.*, 1978, **29,** 397.
23. G. Robinson, P.W. Kuchel, B.E. Chapman *et al.*, *J. Magn. Reson.*, 1985, **63,** 314.
24. D.C. Shungu and R.W. Briggs, *J. Magn. Reson.*, 1988, **77,** 491.
25. F.G. Riddell and S. Arumugan, *Biochim. Biophys. Acta*, 1988, **945,** 65.
26. S. Ringer, *J. Physiol.*, 1983, **6,** 370.
27. S.G. Davis, E. Murphy and R.E. London, *Biochemistry*, 1988, **27,** 3547.
28. A.S. Relman, *Yale J. Biol. Med.*, 1956, **29,** 248.
29. H.L. Meltzer and R.R. Fieve, *Curr. Devel. Psychopharmacol.*, 1975, **1,** 205.
30. L.A. Beauge and N. Adragna, *J. Gen. Physiol.*, 1971, **57,** 576.
31. L.A. Beauge and O. Ortiz, *J. Physiol.*, 1970, **210,** 519.
32. N.A. Boon, J.K. Aronson, K.F. Hallis, N.J. White, A.E.G. Raine and D.G. Grahame-Smith, *Clin. Sci.*, 1984, **66,** 569.
33. C.S. Springer, *Ann. Rev. Biophys. Biophys. Chem.*, 1987, **16,** 375.
34. G. Jaccard, S. Wimperis and G. Bodenhausen, *J. Chem. Phys.*, 1986, **85,** 6282.
35. W.N. Cottingham and D.A. Greenwood, *An Introduction to Nuclear Physics*. Cambridge University Press, Cambridge, 1986.
36. J.D. Jackson, *Classical Electrodynamics*. Wiley, New York, 1962.
37. C.P. Slichter, *Principles of Magnetic Resonance*. Springer-Verlag, Berlin, 1983.
38. I. Schiff, *Quantum Mechanics*. McGraw-Hill, New York, 1968.
39. M. Weissbluth, *Atoms and Molecules*. Academic Press, London, 1984.
40. D.M. Brink and C.R. Satchler, *Angular Momentum*. Clarendon Press, Oxford, 1962.
41. J. McConnel, *Nuclear Magnetic Resonance Relaxation in Liquids*. Cambridge University Press, Cambridge, 1986.
42. A.D. McLachlan, *Proc. Roy. Soc. Lond. A*, 1964, **280,** 271.
43. P.S. Hubbard, *J. Chem. Phys.*, 1970, **53,** 985.
44. H. Monoi, *Rev. Magn. Reson. Med.*, 1986, **1,** 73.
45. A. Bax, R. Freeman and S.P. Kempsell, *J. Am. Chem. Soc.*, 1980, **102,** 4849.
46. L. Braunschweiler, G. Robinson and R.R. Ernst, *Mol. Phys.*, 1983, **48,** 535.
47. G. Bodenhausen, R. Freeman and D.L. Turner, *J. Magn. Reson.*, 1977, **27,** 511.
48. T.E. Bull, *J. Magn. Reson.*, 1972, **15,** 344.
49. A. Delville, C. Detellier and P. Laszlo, *J. Magn. Reson.*, 1979, **34,** 301.
50. C.W.R. Mulder, J. deBleijser and J.C. Leyte, *Chem. Phys. Lett.*, 1980, **69,** 354.
51. J.L. Allis, R.M. Dixon and G.K. Radda, *J. Magn. Reson.*, 1990, **90,** 141–147.
52. G.S. Payne and P. Styles, *J. Magn. Reson.*, 1991, **95,** 253.
53. W.R. Adam, A.P. Koretsky and M.W. Weiner, *Biophys. J.*, 1987, **51,** 265.
54. J.L. Allis, C.D. Snaith, A-M.L. Seymour and G.K. Radda, *FEBS Lett.*, 1989, **242,** 215.
55. Z.H. Endre, J.L. Allis, P.J. Ratcliffe and G.K. Radda, *Kidney Int.*, 1989, **35,** 1249.

56. P.D. Syme, R.M. Dixon, J.L. Allis, J.K. Aronson, D.G. Graham-Smith and G.K. Radda, *Clin. Sci.*, 1990, **78,** 303.
57. T. Ogino, G.I. Sculman, M.J. Avison, S.R. Gullans, J.A. denHollander and R.G. Shulman, *Proc. Natl. Acad. Sci. USA*, 1985, **82,** 1099.
58. J.L. Allis, R.M. Dixon, A.M. Till and G.K. Radda, *J. Magn. Reson.*, 1989, **85,** 524–529.
59. H. Shinar and G. Navon, *Biophys. J.*, 1991, **59,** 203.
60. J.W. Pettegrew, D.E. Woesner, N.J. Minshew and T. Glonek, *J. Magn. Reson.*, 1984, **57,** 185.
61. D. Burnstein and E.T. Fossel, *J. Magn. Reson. Med.*, 1987, **4,** 261.
62. M.D. Schnall, K. Yoshizaki, B. Chance and J.S. Leigh, *J. Magn. Reson. Med.*, 1988, **6,** 15.
63. D. Burnstein and E.T. Fossel, *J. Magn. Reson.*, 1987, **73,** 150.
64. C. Deverell and R.E. Richards, *Mol. Phys.*, 1966, **10,** 551.
65. I.D. Campbell, C.M. Dobson, R.J.P. Williams and A.V. Xavier, *J. Magn. Reson.*, 1973, **11,** 172.
66. K.R. Metz, P.J. Stankiewicz, J.W. Sassani and R.W. Briggs, *Magn. Reson. Med.*, 1985, **3,** 575.
67. Z.H. Endre, J.L. Allis and G.K. Radda, *J. Magn. Reson. Med.*, 1989, **11,** 267.
68. J.L. Allis, Z.H. Endre and G.K. Radda, *Biochem. Soc. Trans.*, 1988, **16,** 806.
69. Y. Seo, M. Murakami, E. Suzuki and H. Watari, *J. Magn. Reson.*, 1987, **75,** 529.
70. J. Pekar, P.F. Renshaw and J.S. Leigh, *J. Magn. Reson.*, 1987, **72,** 159.
71. W.D. Rooney, T.M. Barbara and C.S. Springer, *J. Am. Chem. Soc.*, 1988, **110,** 674.
72. J.L. Allis and G.K. Radda, *J. Magn. Reson.*, 1989, **84,** 372–375.
73. J. Pekar and J.S. Leigh, *J. Magn. Reson.*, 1986, **69,** 582.
74. L. Jelicks and R.K. Gupta, *J. Magn. Reson.*, 1989, **81,** 586.
75. L. Jelicks and R.K. Gupta, *J. Magn. Reson.*, 1989, **83,** 146.
76. L. Jelicks and R.K. Gupta, *J. Biol. Chem.*, 1989, **264,** 15230.
77. J.L. Allis, A-M.L. Seymour and G.K. Radda, *J. Magn. Reson.*, 1991, **93,** 71.
78. R.B. Moon and J.H. Richards, *J. Biol. Chem.*, 1973, **248,** 7276.
79. R.E. London, C.T. Gregg and N.A. Matwiyoff, *Science*, 1975, **188,** 266.
80. F.F. Brown, I.D. Campbell, P.W. Kuchel and D.C. Rabenstein, *FEBS Lett.*, 1977, **82,** 12.
81. Y. Boulanger, P. Vinay and M. Derorches, *Biophys. J.*, 1985, **47,** 553.
82. H. Shinar and G. Navon, *Biophys. Chem.*, 1984, **20,** 275.
83. B.E. Cowan, D.Y. Sze, M.T. Mai and O. Jardetzky, *FEBS Lett.*, 1985, **184,** 130.
84. A.W.H. Jans, R. Willem, E.R. Kellenbach and R.K.H. Kinne, *J. Magn. Reson. Med.*, 1988, **7,** 292.
85. Y. Seo, M. Murakami and H. Watari, *Biochem. Biophys. Acta*, 1990, **1034,** 142.
86. Y. Seo, M. Murakami, E. Suzuki, S. Kuki, K. Nagayama and H. Watari, *Biochemistry*, 1990, **29,** 599.
87. J.A. Helpern, K.M.A. Welch and H.R. Halvorson, *NMR Biomed.*, 1989, **2,** 47.
88. J.L. Allis, D.Phil thesis, Oxford University, 1989.
89. R. Whittam, *Transport and Diffusion in Red Blood Cells*. Edward Arnold, Baltimore, Maryland, 1964.
90. M.P. Williamson, *FEBS Lett.*, 1989, **254,** 171.
91. Langendorff, *Pflügers Arch*, 1895, **61,** 291.
92. P.B. Garlick, G.K. Radda and P.J. Seeley, *Biochem J.*, 1979, **184,** 547.
93. H.A. Krebs and K. Henseleit, *Hoppe-Seyler's Z. Physiol. Chem.*, 1932, **210,** 33.
94. E.S. Blesa, G.A. Langer, A.J. Brady and S.D. Serena, *Am. J. Physiol.*, 1970, **219,** 747.
95. J.L. Allis, Z.H. Endre and G.K. Radda, *Renal Physiol. Biochem.*, 1989, **12,** 171–180.
96. M.B. Burg, E.F. Grollman and J. Orloff, *Am. J. Physiol.*, 1964, **206,** 483.
97. R. Whittam and R.E. Davies, *Biochem. J.*, 1954, **56,** 445.
98. M.C. Steward, Y. Seo, M. Murakami and H. Watari, *Proc. Roy. Soc. Lond. B*, 1991, **243,** 115.
99. P.D. Syme, R.M. Dixon, J.K. Aronson, D.G. Graham-Smith and G.K. Radda, *J. Hypertension*, 1990, **8,** 1161.

Multinuclear NMR of Azo Dyestuffs

A. LYČKA

Research Institute of Organic Syntheses, 532 18 Pardubice-Rybitví, Czech Republic

1. INTRODUCTION

Azo dyes of the common formula X–N=N–Y represent a very important class of dyestuffs,[1] with more than 50% of commercial dyestuffs based on this type of compound. Nuclear magnetic resonance (NMR) spectroscopy, especially in its multinuclear form, is a powerful technique for the characterization of such compounds and also for the description of azo–hydrazone tautomerism, a property which is indivisibly linked with this group of dyes. This chapter reports on high-resolution ^{1}H, ^{13}C, ^{14}N, ^{15}N, ^{17}O, ^{19}F and ^{31}P NMR spectra of azo dyestuffs measured in solutions.

2. NMR PROPERTIES OF THE NUCLEI USED

Table 1 gives the properties[2] of the nuclei used in this study pertinent to the NMR experiments.

ANNUAL REPORTS ON NMR SPECTROSCOPY
VOLUME 26 ISBN 0-12-505326-6

Table 1. NMR properties of nuclei included in present chapter.

Isotope	Natural abundance (%)	Spin number, I	Receptivity	
			Related to hydrogen	Related to carbon
^{1}H	99.99	1/2	1.0	5680
^{13}C	1.11	1/2	1.76×10^{-4}	1
^{14}N	99.63	1	1.0×10^{-3}	5.69
^{15}N	0.37	1/2	3.85×10^{-6}	0.02
^{17}O	0.037	5/2	1.08×10^{-5}	0.06
^{19}F	100	1/2	0.833	4730
^{31}P	100	1/2	0.066	377

3. ^{1}H NMR SPECTROSCOPY

3.1. ^{1}H NMR data

^{1}H Spectroscopy is the method of primary choice and importance for the characterization of azo dyes, because of its high sensitivity (Table 1) and its ability to characterize aromatic substitution patterns, aliphatic side-chains and acidic protons. From the point of view of modern NMR spectroscopy, azo dyes are small molecules;[3] most of them have molecular weights of less than 500 Da. This should make the NMR analyses easy. On the other hand, protons (as well as carbons) often resonate in a very narrow range of chemical shifts and the solubility of many compounds is rather low. The use of as high a field as possible for recording of NMR spectra is recommended because it provides both greater chemical shift dispersion and higher sensitivity.[4]

The simplest azo dyes include the substituted azobenzenes of type **1** and **2**.

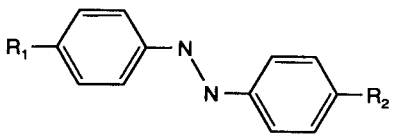

1

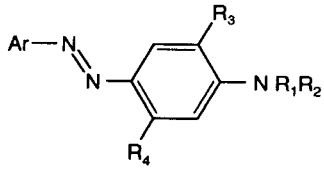

2

The ^{1}H chemical shifts of the side-chain protons of these compounds are listed in Tables 2–4. The data are taken from the review by Foris,[5] which covers NMR data on azo dyestuffs published before 1977; newer papers are collected in the article by Fedorov.[6] Fedorov *et al.*[7] recently published an extensive set of ^{1}H NMR data on compounds **3–40** in DMSO-d_6 with the aim of studying the electronic effects of substituents, rotational isomerism and hydrogen bonding. The values in Table 5 are typical of azo dyes and are complementary to those of side-chain protons (Tables 2–4).

Table 2. ^{1}H Chemical shifts of side-chain protons in 4-R_1- and 4-R_1-4′-R_2-azobenzenes (**1**).

Side-chains		Chemical shifts	
R_1	R_2	R_1	R_2
Me	H	2.38	—
SMe	H	2.47	—
NHMe	H	4.13, 2.48	—
NMe_2	H	3.02	—
N(Me)COMe	H	3.17, 1.88	—
OMe	H	3.77	—
Me	Me	2.43	2.43
OMe	NH_2	3.74	3.47
OMe	N(Me)Ac	3.84	3.26, 1.90
OMe	NHMe	3.80	—, 2.82
OMe	NMe_2	3.80	2.99
OMe	OH	3.80	8.90
OMe	OCOMe	3.90	2.33
OMe	OMe	3.96	3.96
NMe_2	NH_2	3.06	~ 3.06
NMe_2	NHAc	3.56	—, 2.51
NMe_2	N(Me)Ac	3.06	3.67, 1.92
NMe_2	NHMe	2.98	—, 2.83
NMe_2	NMe_2	3.60	3.60
NO_2	NH_2	—	5.84
NO_2	NHAc	—	—, 2.50
NO_2	N(Me)Ac	—	3.30, 1.96
NO_2	NHMe	—	—, 3.45
NO_2	NMe_2	—	3.69
NO_2	OH	—	9.65
NO_2	OCOMe	—	2.35
NO_2	OMe	—	3.96
OH	OH	10.1	10.1

From Ref. 5.

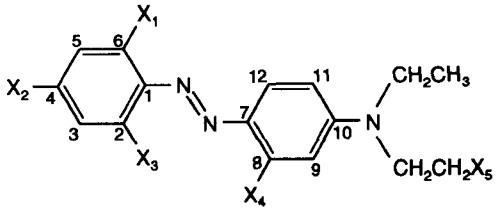

3–40

^{1}H Chemical shifts of azobenzene-like compounds,[8–26] *ortho*-, *ortho*′-dihydroxyazopyrazole[27] and diazonium salts coupling products with guaiacol,[28] 5-aminopyrazole,[29] 2-phenyl-5-oxazolone,[30] 3-(4-methoxyphenyl)-1-oxo-1H,5H-pyrido[1,2-a]benzimidazole,[31] 2-(*ortho*, *meta*, *para*-aminophenyl)oxazolo-

Table 3. ^{1}H Chemical shifts of side-chain protons in azo dyes of type **2**.

R_1 and/or R_2	Chemical shifts (left to right)				
CH_2CH_2	3.3–3.7	1.1–1.3			
$(H)CH_2CH_3$	6.95	3.33	1.24		
CH_2CH_2Cl	~3.8	~3.8			
CH_2CH_2OH	3.6–3.9	3.6–3.9	4.7–5.0		
CH_2CH_2CN	3.7–4.0	2.5–3.0			
CH_2Ph	4.7–4.9	7.3–7.7			
CH_2CH_2Ph	3.63	2.57	7.27		
$CHMe_2$	4.2–4.3	1.3			
$CH_2CH_2CONH_2$	~3.8	2.53	6.96		
$CH_2CH_2CH_2CH_3$	3.56	1.61	1.37	0.95	
CH_2CH_2OCOMe	3.6–3.9	4.2–4.4	2.0–2.1		
CH_2CH_2COOMe	3.89	2.73	3.73		
$CH_2CH_2OCOOMe$	3.9	4.42	3.78		
$CH_2CH_2NHCOMe$	~3.4	~3.4	~ 7.9	1.85	
CH_2CH_2OCOPh	4.0	4.6			
$(H)CH_2CH_2COOCH_2CH_3$	6.3	3.7	2.8	4.2	1.3
$CH_2CH_2COOCH_2CH_3$	3.7–3.8	2.6–2.7	4.0–4.1	1.1–1.2	
$CH_2CH_2OCOCH_2CH_2CH_3$	3.89	4.36	3.26	1.61	0.91

From Ref. 5.

[4,5-b]pyridine,[32] 4-hydroxycoumarin,[33] salicylaldehyde,[34] aminophenyloxazolopyridines,[35] aminophenylthiazoles,[36] aminophenyl-X-azolopyridines,[37] γ-carbolines,[38] pyridones[39,40] and 3-amino-7-nitro-2H-1,2-benzothiazine-1,1-dioxide[41] have been reported. Many compounds mentioned in these papers contain the same $(X_1, X_2, X_3)C_6H_2N{=}N$-parts as the dyes shown in Table 5.

While the ^{1}H NMR signals in the azobenzene type of compounds can be assigned easily, in most cases the assignment in azonaphthalene derivatives is more complicated and the application of two-dimensional (2D) NMR spectroscopy[3,4,42–44] is strongly recommended. We used 500-MHz ^{1}H NMR (Fig. 1) and H,H-COSY (Fig. 2) spectra of compound **43** and succeeded in assigning all the proton signals (Table 6).

Table 4. ^{1}H Chemical shifts of side-chain protons in azo dyes of type **2**.

R_3	R_4	Chemical shifts (left to right)			
H	Me	—	2.4–2.8		
H	NHAc	—	9–13	2.1–1.3	
H	$NHCOCH_2CH_2Cl$	—	~11–12	3.0–3.1	3.8–3.9
Me	NHAc	2.11	9.85	2.18	
OMe	H	3.95			
OMe	NHAc	3.7–3.9	8.7–9.3	2.1–2.3	
OCH_2CH_3	NHAc	3.8–4.1	1.3–1.5	7.6–9.1	2.1–2.4

From Ref. 5.

Table 5. ^{1}H NMR Chemical shifts of disperse dyes **3–40** in DMSO-d_8.

	X_1	X_2	X_3	X_4	X_5	H_2	H_3	H_4	H_5	H_6	H_8	H_9	H_{11}	H_{12}
3		CN				7.96	7.87		7.87	7.96	7.82	6.82	6.82	7.82
4		NO_2				7.93	8.36		8.36	7.93	7.85	6.86	6.86	7.85
5	NO_2					~7.74	7.75	7.60	7.99		7.74	6.84	6.84	7.74
6	Cl					7.64	~7.43	~7.43	~7.64		7.82	6.83	6.83	7.82
7	Br					7.62	7.47	7.34	7.80		7.82	6.83	6.83	7.82
8	Cl		Cl				7.56	7.32	7.56		7.78	6.83	6.83	7.78
9	NO_2	OCH_3				7.76	7.31		7.59		7.69	6.80	6.80	7.69
10	Br	NO_2	Cl				8.46		8.54		7.82	6.88	6.88	7.82
11					OH	7.78	7.53	7.44	7.53	7.78	7.78	6.84	6.84	7.78
12	CN				OH	7.96	7.86		7.86	7.96	7.81	6.86	6.86	7.81
13		NO_2			OH	7.91	8.34		8.34	7.91	7.83	6.87	6.87	7.83
14	NO_2				OH	~7.74	7.75	7.66	7.99		7.74	6.87	6.87	7.74
15	NO_2	NO_2			OH	7.91	8.50		8.80		7.78	6.93	6.93	7.78
16					CN	7.81	7.55	7.47	7.55	7.81	7.82	6.92	6.92	7.82
17		OCH_3			CN	7.80	7.09		7.09	7.80	7.77	6.89	6.89	7.77
18		CN			CN	7.98	7.89		7.89	7.98	7.84	6.94	6.94	7.84
19		NO_2			CN	7.96	8.38		8.38	7.96	7.88	6.97	6.97	7.88
20	NO_2				CN	~7.33	~7.75	7.63	8.02		7.77	6.96	6.96	7.77
21	Cl				CN	~7.64	~7.45	~7.45	~7.64		7.84	6.94	6.94	7.84
22	Br				CN	7.62	7.48	7.39	7.81		7.84	6.95	6.95	7.84
23	CN	NO_2			CN	7.91	8.50		8.79		7.86	7.01	7.01	7.86
24	Cl		Cl		CN		7.59	7.35	7.59		7.81	6.96	6.96	7.81
25	Cl	NO_2	Cl		CN		8.44		8.44		7.85	6.99	6.99	7.85
26		CN		CH_3	CN	7.96	7.83		7.87	7.96		6.76	6.74	7.69
27	Br			CH_3	CN	7.60	7.47	7.34	7.80			6.75	6.75	7.71
28	Cl	NO_2	Cl	CH_3	CN		8.43		8.43			6.80	~6.81	7.71
29	Br	NO_2	Br	CH_3	CN		8.57		8.57			~6.81	~6.82	7.73
30	Br	NO_2	Cl	CH_3	CN		8.41		8.50			6.80	6.80	7.71
31		CN		$NHCOCH_3$		7.99	7.95		7.95	7.99		7.86	6.58	7.73

(*continued*)

Table 5. (*Continued*)

	X_1	X_2	X_3	X_4	X_5	H_2	H_3	H_4	H_5	H_6	H_8	H_9	H_{11}	H_{12}
32		NO_2		$NHCOCH_3$		8.03	7.34		8.34	8.03		7.90	~6.63	~7.79
33	NO_2			$NHCOCH_3$		7.95	7.76	7.56	7.98			7.92	6.62	7.64
34	NO_2	OCH_3		$NHCOCH_3$		7.96	7.33		7.57			7.90	6.59	7.57
35	Cl		Cl	$NHCOCH_3$			7.58	7.32	7.58			7.93	6.61	7.69
36	CN			$NHCOCH_3$		7.98	7.81	7.53	7.93			7.94	6.62	7.75
37	Br	NO_2	Cl	$NHCOCH_3$			8.44		8.52			7.93	6.68	7.72
38	NO_2	OCH_3		NH_2		7.88	7.28		7.51			5.95	6.25	7.42
39	CN			CH_3		7.83	7.79	7.53	7.95			6.65	6.68	7.76
40	CN			CH_3		7.94	7.84		7.84	7.94		6.65	6.63	7.70

The ^{1}H chemical shifts of compounds **41–77** were assigned in a similar way. High-field ^{1}H NMR, H,H-COSY, NOESY (or 1D NOE difference spectra) were measured. NOESY spectra were used for deciding the diazo coupling positions of 4-nitrobenzenediazonium and benzenediazonium chloride with 2-amino-5-naphthol-7-sulphonic acid[50] and 4,5-dihydroxy-2,7-naphthalenedisulphonic acid,[52] respectively. In *ortho*-to-hydroxy group coupling products **65** and **70**, off-diagonal peaks in the NOESY spectrum correlate spins which share a dipolar coupling, i.e. appropriate protons must be in the *peri* position (Fig. 3). In the *para* coupling product (**66**) such off-diagonal peaks cannot exist.[50] NOESY data corrected the conclusions based on a wrong analysis of 1D ^{1}H NMR spectra.[55]

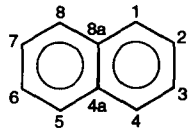

41–77

(Only prevailing tautomeric forms shown)
41 1: $N{=}NC_6H_5$
42 2: $N{=}NC_6H_5$
43 1: N=N(1-naphthyl)
44 2: N=N(2-naphthyl)
45 1: OH; 4: $N_\beta{=}N_\alpha C_6H_5$
46 1: =O; 2: $-N_\beta N_\alpha HC_6H_5$
47 1: =O; 2: $=NN_\alpha HC_6H_5$; 4: $N{=}NC_6H_5$
48 1: $=N_\beta N_\alpha HC_6H_5$, 2: =O
49 1: $=NNHC_6H_5$; 2: =O; 7: OH
50 1 = 8: $N{=}NC_6H_5$; 2 = 7: OH
51 1: $=NN_\alpha HC_6H_5$; 2: =O; 3: COOH
52 1: $=NN_\alpha HC_6H_5$; 2: =O; 3: $CONHC_6H_5$
53 1: $=NN_\alpha HC_6H_5$; 2: =O; 3: $COOCH_3$
54 1: $N_\beta{=}N_\alpha C_6H_5$; 2: NH_2
55 1: NH_2, 2: $N_\beta{=}N_\alpha C_6H_5$
56 1: NH_2, 4: $N_\beta{=}N_\alpha C_6H_5$
57 1: NH_2, 2 = 4: $N{=}NC_6H_5$
58 1: $N_\beta{=}N_\alpha C_6H_5$, 2: $NHCOCH_3$
59 1: $NHCOCH_3$; 2: $N_\beta{=}N_\alpha C_6H_5$
60 1: $NHCOCH_3$; 4: $N_\beta{=}N_\alpha C_6H_5$
61 1: $NHCOCH_3$; 2 = 4: $N{=}NC_6H_5$
62 2: SO_3^-; 3: $=NN_\alpha HC_6H_5$; 4: =O; 7: NH_2
63 2 = 7: SO_3^-; 3: $=NN_\alpha HC_6H_5$; 4: =O; 5: NH_2
64 2: SO_3^-; 3: $=NN_\alpha HC_6H_5$; 4: =O; 6: NH_2
65 2: SO_3^-; 3: $=NN_\alpha HC_6H_4(4\text{-}NO_2)$; 4: =O; 7: NH_2
66 1: $=NN_\alpha HC_6H_4(4\text{-}NO_2)$; 2: SO_3^-; 4: =O; 7: NH_2
67 2: SO_3^-; 4: OH; 7: NH_2; 8: $N{=}NC_6H_4(4\text{-}NO_2)$
68 1: =O; 2: $=NN_\alpha HC_6H_5$; 5: SO_3Na; 8: NH_2

69 1: =O; 2: $=NN_\alpha HC_6H_5$; 5: SO_3NH_4; 7: $N=NC_6H_5$; 8: NH_2
70 1: =O; 2: $=NN_\alpha HC_6H_5$; 3 = 6: SO_3^-; 8: OH
71 1: $=NNHC_6H_4(2'\text{-}NO_2)$; 2: =O; 3: $OCOCH=CH_2$
72 1: $=NNHC_6H_3(2'\text{-}NO_2\text{-}4'\text{-}OCH_3)$; 2: =O; 3: $OCOCH=CH_2$
73 1: $=NNHC_6H_3(2'\text{-}NO_2\text{-}4'\text{-}Cl)$; 2: =O; 3: $OCOCH=CH_2$
74 1: $=NNHC_6H_4(2'\text{-}NO_2)$; 2: =O; 7: $OCOCH=CH_2$
75 1: $=NNHC_6H_3(2'\text{-}NO_2\text{-}4'\text{-}OCH_3)$; 2: =O; 7: $OCOCH=CH_2$
76 1: $=NNHC_6H_3(2'\text{-}NO_2\text{-}4'\text{-}Cl)$; 2: =O; 7: $OCOCH=CH_2$
77 2: $CONHC_6H_5$; 3: =O; 4: $=NNHC_6H_2(2'\text{-}OH\text{-}3', 5'\text{-}diNO_2)$

3.2. Azo–hydrazone tautomerism

There are two basic types of azo–hydrazone tautomerism:

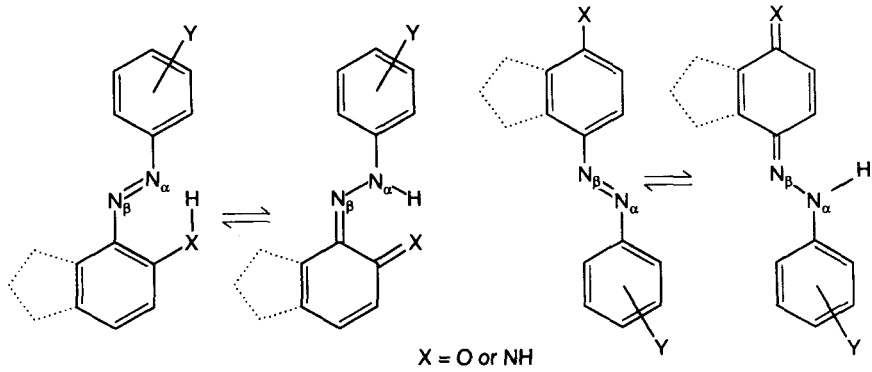

Many methods have been proposed for the determination of azo–hydrazone contents[56–59] but none of them is the "absolute" one. They are based on a better or worse choice of model compounds having either completely azo or completely hydrazone forms. NMR spectroscopy seems to give the most reliable results.[59]

The proton exchange between $=N_\alpha-$ and X groups is fast on the NMR time-scale in practically all cases and, hence, only one set of NMR signals is observed. Azo–hydrazone content is calculated as a weighted average of two contributing forms.

Bekárek *et al.*[60,61] proposed the use of $^1J(^{15}N_\alpha, H)_{exp}$ coupling constants for estimation of azo–hydrazone contents. This coupling constant is taken to be 0 Hz for pure azo compounds[60,61] and 89.8–96 Hz for pure hydrazone forms ($^1J(^{15}N_\alpha, H)_H$ = 89.8–93 Hz for compounds without[61,68] intramolecular hydrogen bonds or with two intramolecular hydrogen bonds;[66] ^1J = 96 Hz for compounds with one intramolecular hydrogen bond).[63] The hydrazone

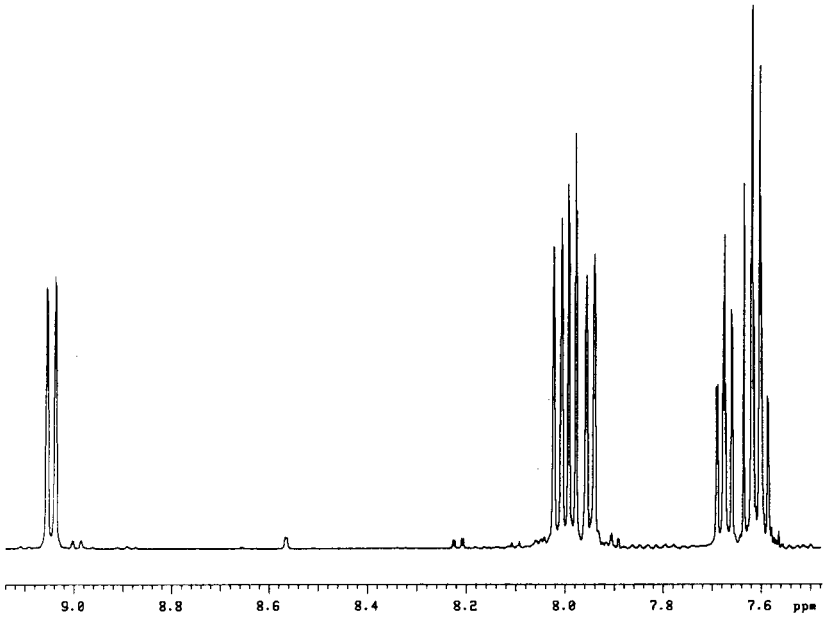

Fig. 1. 500-MHz ^{1}H NMR spectrum of 1, 1′-azonaphthalene (**43**) in $CDCl_3$.

content is calculated according to:

$$\% \text{ hydrazone form} = \frac{^1J(^{15}N_\alpha, H)_{exp}}{^1J(^{15}N_\alpha, H)_H} \times 100 \quad (1)$$

Most data were obtained by measurements of ^{1}H NMR spectra of $^{15}N_\alpha$-labelled compounds.[30,49–52,60–68] In some cases (sufficiently high value of $^1J(^{15}N_\alpha, H)_{exp}$ and relatively narrow signal of exchanging proton), it is possible to observe 0.18% natural abundance ^{15}N satellites in the ^{1}H NMR spectrum of non-labelled compounds.[46] Figure 4 shows ^{15}N INEPT spectrum of compound **48** measured at the natural abundance level of ^{15}N from which $^1J(^{15}N_\alpha, H)_{exp}$ can be read.

Further possibility consists in heteronuclear multiple-quantum coherence spectra measurements.[46]

Haessner *et al.*[67] measured $^1J(^{15}N_\alpha, H)_{exp}$ of compound **48** in various solvents and calculated azo–hydrazone content (values of ^1J from 42.2 Hz in diethylether to 65.0 Hz in $CHCl_3$).

Temperature dependences of $^1J(^{15}N_\alpha, H)$ in compounds **46**,[68] **47**,[68], **48**,[63] **51–53**[66] and **68–70**[49] have been determined.

The application of $^1J(^{15}N_\alpha, H)$ measurement fails when there is an interaction of acidic proton with solvents (e.g. pyridine, DMSO).[62] In this case ^{13}C and ^{15}N NMR spectra measurements were recommended.[69]

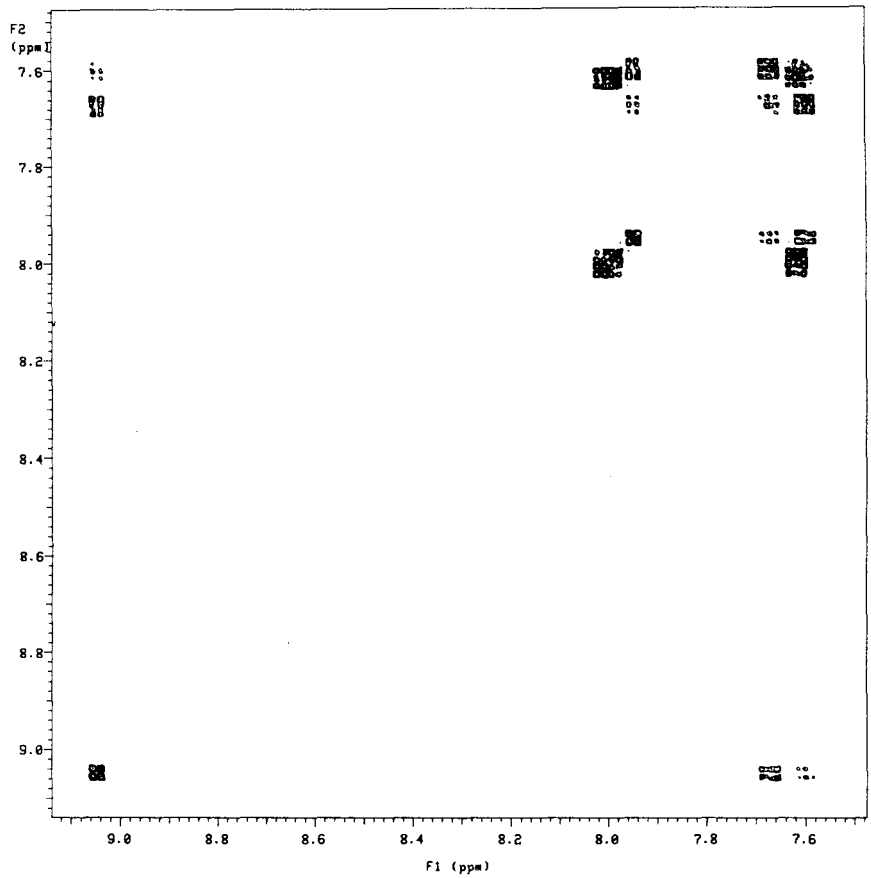

Fig. 2. H,H-COSY spectrum of 1, 1′-azonaphthalene (**43**) in $CDCl_3$.

In 1-(substituted phenylazo)-2-naphthols both δH_3 and δH_8 of the naphthalene ring were used independently to determine the azo–hydrazone equilibrium constants.[70]

A common mistake is to attempt to use δ^1H of $C_6H_5N{=}N/C_6H_5NHN{=}$ protons for the estimation of azo–hydrazone equilibrium. This does not work because the protons are on the periphery of dye molecules and thus accessible to various other effects.[47]

4. ^{13}C NMR SPECTROSCOPY

4.1. ^{13}C NMR data

Carbon-13 NMR spectroscopy allows the direct observation of carbon skeletons of dyestuffs including functional groups containing carbon atoms (e.g.

Table 6. ^{1}H Chemical shifts of compounds **41–77**.

	H_1	H_2	H_3	H_4	H_5	H_6	H_7	H_8	Ref.
41[a]	—	7.85	7.60	8.00	7.94	7.60	7.60	8.96	45
41[b]	—	7.83	7.70	8.18	8.08	7.70	7.70	8.90	45
42[a]	8.45	—	8.01	8.01	8.01	7.55	7.55	8.01	45
42[b]	8.61	—	7.98	8.05	8.02	7.65	7.65	8.19	45
43[a]	—	7.98	7.62	8.01	7.95	7.60	7.67	9.05	46
44[a]	8.51	—	8.13	7.94	7.90	7.58	7.55	8.03	46
45[b]		7.02	7.99	—	8.89	7.75	7.63	8.27	47
46[a]	—	—	7.19	6.98	7.53	7.57	7.44	8.40	47
47[a]	—	—	7.74	—	8.71	7.78	7.58	8.51	47
48[b]	—	—	6.96	7.99	7.82	7.50	7.65	8.58	47
48[a]	—	—	6.81	7.63	7.53	7.33	7.51	8.49	47
49[a]	—	—	6.70	7.62	7.49	6.91	—	7.92	47
50[a]	—	—	6.93	7.64	7.64	6.93	—	—	47
51[a]	—	—	—	8.88	7.75	7.48	7.69	8.46	47
52[a]	—	—	—	8.97	7.73	7.43	7.62	8.43	47
53[a]	—	—	—	8.34	7.57	7.32	7.53	8.37	47
54[a]	—	—	6.75	7.57	7.26	7.28	7.51	8.85	48
54[b]	—	—	7.23	7.81	7.78	7.36	7.58	8.80	48
55[a]	—	—	7.88	7.13	7.65	7.42	7.30	7.77	48
55[b]	—	—	8.14	7.28	7.87	7.65	7.65	8.73	48
56[a]	—	6.63	7.86	—	9.01	7.56	7.41	7.63	48
56[b]	—	7.03	8.14	—	9.13	7.76	7.61	8.43	48
57[b]	—	—	8.42	—	9.00	7.84	7.70	8.70	48
58[a]	—	—	8.83	7.81	7.73	7.44	7.55	8.81	48
58[b]	—	—	8.72	8.16	8.03	7.62	7.73	8.89	48
59[b]	—	—	7.94	8.01	8.07	7.71	7.70	8.22	[d]
60[b]	—	8.09	7.92	—	9.02	7.81	7.76	8.35	48
61[b]	—	—	8.17	—	9.02	7.92	7.86	8.38	48
62[b]	7.40	—	—	—	8.07	6.95	—	7.01	49
63[b]	7.32	—	—	—	—	7.08	—	6.91	49
64[b]	7.52	—	—	—	7.49	—	7.07	7.46	49
65[b]	7.35	—	—	—	7.95	6.73	—	6.71	50
66[b]	—	—	7.01	—	7.86	7.04	—	7.96	50
67[b]	8.48	—	7.13	—	8.06	7.11	—	—	50
68[b]	—	—	6.95	8.01	—	7.87	6.70	—	51
69[b]	—	—	7.22	8.14	—	8.52	—	—	51
70[b]	—	—	—	7.61	7.51	—	7.21	—	52
71[c]	—	—	—	6.95	7.40	7.40	7.40	?	53
72[c]	—	—	—	7.25	7.40	7.40	7.40	?	53
73[c]	—	—	—	6.65	7.4	7.4	7.4	?	53
74[c]	—	—	6.5	7.8	7.6	7.0	—	7.85	53
75[c]	—	—	6.60	7.80	7.60	7.10	—	7.85	53
76[c]	—	—	6.40	7.75	7.5	7.0	—	7.80	53
77[b]	8.78	—	—	—	8.40	7.74	7.49	7.95	54

[a] $CdCl_3$.
[b] DMSO-d_6.
[c] Acetone-d_6.
[d] Correction of values from Ref. 48.

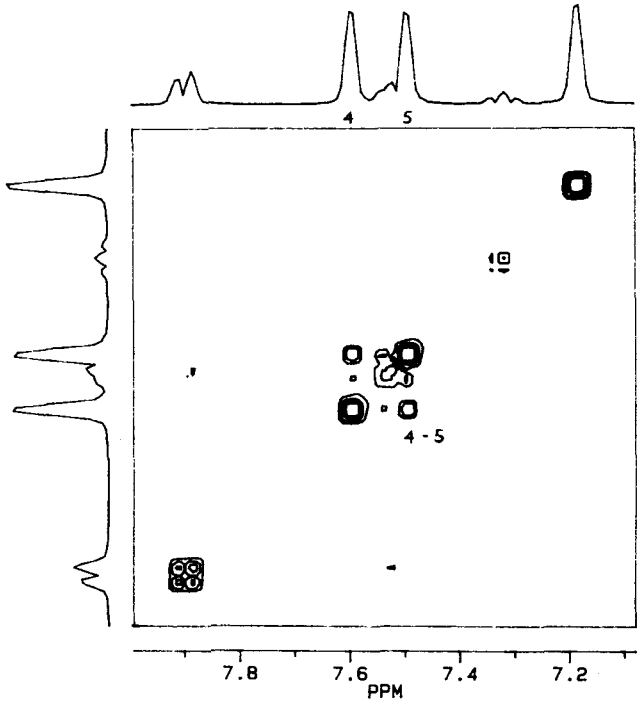

Fig. 3. NOESY spectrum of compound **70** in DMSO-d_6.

–COOR, –COR, $CONR^1R^2$, –CN). Since 1977 when Foris's review[5] dealing with NMR spectroscopy of dyes was published, in which only a very small number of ^{13}C chemical shifts was mentioned, ^{13}C NMR spectroscopy has became the routine method of measurement due to the progress in NMR instrumentation. A wide range of ^{13}C chemical shifts in azo dyestuffs, the assignments of which are based mostly on 1D NMR spectra, has been published by Federov.[71]

Similarly as in ^1H NMR spectra, ^{13}C chemical shifts in substituted azobenzenes can be assigned easily.[72–76] ^{13}C Chemical shifts in 4- and 4,4′-disubstituted azobenzenes are shown in Tables 7 and 8 respectively.

Table 9 gives the ^{13}C chemical shifts of the compounds[77] (**3–40**) listed in Table 5. Depending on the nature and orientation of the substituents in the dyes, different conformers, resultant from inner rotation around the C–N bonds, could be identified. The ^{13}C chemical shifts of azobenzene-like compounds and diazonium salts coupling products with heterocycles are reported in Refs. 9, 18, 25, 26, 36, 39, 48, 78–87. The ^{13}C chemical shifts of dyes derived from 3-methyl-1-phenylpyrazol-5-one (of type **78**; Table 10),[88] pyridone (**81**),[39] and acetoacetanilide (**82**)[65] existing completely in hydrazone forms were assigned.

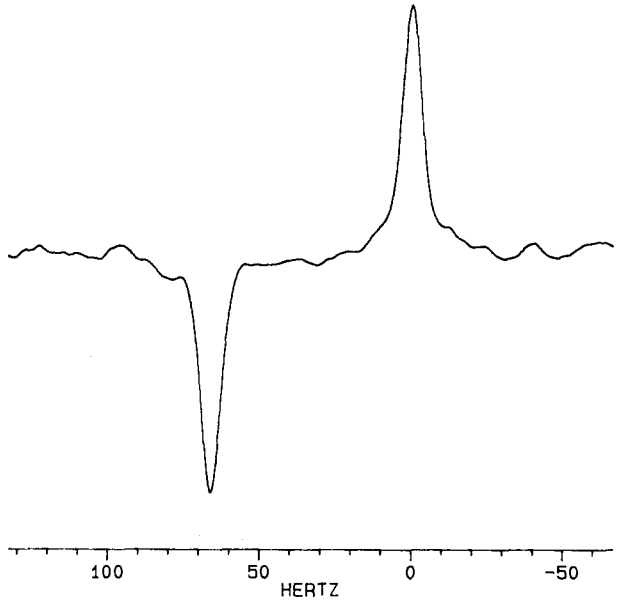

Fig. 4. Natural abundance 40.56-MHz ^{15}N INEPT spectrum of compound **48** (0.4 g of **48** in 2.5 ml $CDCl_3$, 200 pulses).

Allen *et al.*[90] reported on the ^{13}C chemical shifts of diarylazophosphonium salts **83** (Table 11).

Several partially different ^{13}C chemical shift assignments of compound **48** have been published[91–93] based on 1D spectra measured at a low field in some cases. The assignment of the chemical shifts of tautomeric compounds, even with a relatively simple structure like **48**, is difficult because of a lack of precise reference data, and because a perturbation due to substitution may lead to a shift in the equilibrium, thus preventing the use of traditional assignment techniques. Final assignment of ^{13}C chemical shifts of compound **48** (and similarly **46**) was achieved after the application of 1D SEMINA-1 technique[94] based on $J(^{13}C,^{13}C)$ coupling constants (Table 12) and it was checked by means of 2D INADEQUATE.[4] The use of carbon–carbon connectivities obtained from one-bond or long-range carbon–carbon coupling constants is therefore an ideal assignment tool.[94] Table 13 contains a selection of carbon–carbon coupling constants in *cis*- and *trans*-azobenzene and compounds **48** and **78**. Unfortunately, these techniques require the use of concentrated solutions of compounds and, even in these cases, they are very time-consuming. That is why some alternative 2D techniques, especially H,C-COSY (optimized both for one-bond and three-bond $J(^{13}C,H)$ coupling constants), COLOC, H,C-RELAY, etc. have been used. The data for substituted naphthalene derivatives, the assignments of which are based on 2D NMR spectra, are listed in Table 12.

Table 7. ^{13}C Chemical shifts in *trans* azobenzenes (4-X)-C_6H_4-N_α=N_β-C_6H_4-(4′-Y).

X	Y	C_1	C_2	C_3	C_4	$C_{1'}$	$C_{2'}$	$C_{3'}$	$C_{4'}$	X; Y
H[a]	H	152.5	122.8	129.0	130.9	152.5	122.8	129.0	130.9	
		(1.8)[d]	(4.0)	(1.8)	(0.6)	(5.2)	(4.0)	(0.5)	(0.6)	
H[b]	H	151.9	122.5	129.4	131.4	151.9	122.5	129.4	131.4	
H[c]	H	152.7	122.9	128.4	130.2	152.7	122.9	128.4	130.2	
$N(CH_3)_2$ [a]	H	143.4	124.8	111.3	152.2	153.0	122.0	128.8	129.2	40.6
NH_2 [a]	H	145.3	125.0	114.5	149.5	152.8	122.2	128.9	129.7	
NH_2 [b]	H	143.3	125.5	113.8	152.9	152.7	122.1	129.4	129.6	
OH[b]	H	145.5	125.1	116.1	161.0	152.3	122.3	129.5	130.8	
OCH_3 [a]	H	146.8	124.6	114.1	161.9	152.6	122.5	128.9	130.2	55.4
CH_3 [a]	H	150.7	122.8	129.8	141.4	152.6	122.7	129.0	130.6	21.4
Br[a]	H	151.2	124.3	132.2	125.3	152.4	122.9	129.1	131.2	
NO_2 [a]	H	155.5	123.3	124.6	148.5	152.2	123.3	129.2	132.3	
OH[b]	NO_2	145.3	125.5	116.1	162.4	155.5	122.6	124.5	147.5	
NH_2 [b]	OH	143.2	123.9[e]	113.7	151.9	145.8	124.7[d]	115.9	159.2	
$N(CH_3)_2$ [a]	CH_3	143.5	124.7	111.4	152.1	151.1	122.1	129.5	139.5	40.2; 21.4
$N(CH_3)_2$ [a]	NO_2	144.1	126.1	111.7	153.6	157.0	122.6	124.6	147.7	40.2
F[f]	H	149.1	124.8	116.0	164.3	152.4	122.8	129.1	131.0	
		(252.7)[g]	(23.0)	(9.2)	(3.0)					

From Ref. 72.

[a] $CDCl_3$.

[b] DMSO-d_6.

[c] Hexane.

[d] $^nJ(^{15}N,^{13}C)$ in C_1-^{15}N monolabelled compound.

[e] The assignment may be opposite.

[f] Ref. 75.

[g] $^nJ(^{19}F,^{13}C)$.

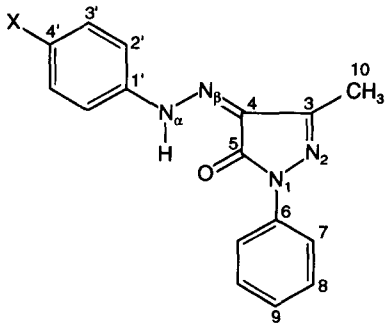

78(X=H); **79**(X=F); **80**(X=CF_3)

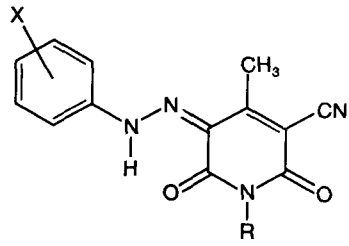

81

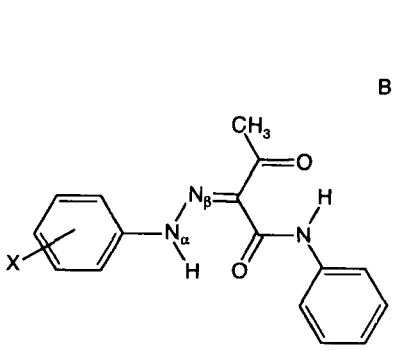

82

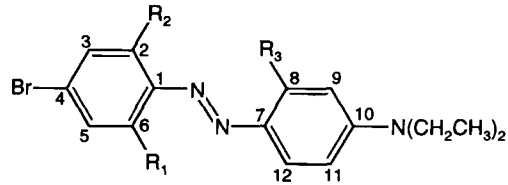

83

Azo dyestuffs derived from sulphonated 1- and 2-naphthols have been studied by means of ^{13}C NMR spectroscopy.[95–100] In azo dyes containing fluorine and phosphorus and in ^{15}N-labelled compounds the appropriate $^{n}J(X,^{13}C)$ coupling constants have been found. Typical values of these constants are shown in Tables 7, 10, 11 and 14.

Table 8. ^{13}C Chemical shifts in *cis* azobenzenes (4-X)-C_6H_4-N_α=N_β-C_6H_4-(4′-Y).

X	Y	C_1	C_2	C_3	C_4	$C_{1'}$	$C_{2'}$	$C_{3'}$	$C_{4'}$	Reference
H[a]	H	153.3	120.5	128.6	127.3	153.3	120.5	128.6	127.3	72
H[b]	H	153.8	120.1	129.1	127.5	153.8	120.1	129.1	127.5	72
H[c]	H	154.1	120.2	128.0	126.2	154.1	120.2	128.0	126.2	72
Cl[a]	Cl		121.9		133.5		121.9		133.5	74
I[a]	I		122.2	138.1	93.1		122.2	138.1	93.1	74

[a] $CDCl_3$.
[b] DMSO-d_6.
[c] Hexane.

Table 9. ^{13}C Chemical shifts of compounds **3–40** in DMSO-d_6.

Compound	C_1	C_2	C_3	C_4	C_5	C_6	C_7	C_8	C_9	C_{10}	C_{11}	C_{12}	C_{13}	C_{14}	C_{15}	C_{16}
3	154.70	122.40	133.57	110.81	133.57	122.40	142.30	126.13	111.21	151.12	111.21	126.13	44.27	12.57	44.27	12.57
4	156.33	122.27	124.78	146.71	124.78	122.27	142.50	126.15	111.26	151.31	111.26	126.15	44.17	12.41	44.17	12.41
5	146.95	118.35	133.01	129.26	123.72	144.66	142.33	126.14	111.23	151.16	111.23	126.14	44.25	12.50	44.25	12.50
6	148.53	117.37	127.85	130.33	130.33	132.55	142.59	125.77	111.11	150.67	111.11	125.77	44.16	12.52	44.16	12.52
7	149.40	117.57	128.47	130.64	133.46	123.44	142.48	125.81	111.15	150.67	111.15	125.81	44.19	12.55	44.19	12.55
8	148.48	126.08	129.21	128.24	129.21	126.08	142.01	125.64	110.98	151.18	110.98	125.64	44.25	12.49	44.25	12.49
9	137.81	119.13	118.91	159.78	108.02	148.64	142.20	125.61	111.18	150.68	111.18	125.61	44.19	12.52	44.19	12.52
10	154.31	126.15	127.33	145.57	126.41	116.11	141.97	125.17	111.31	152.00	111.31	125.17	44.47	12.57	44.47	12.57
11	152.56	121.82	129.24	129.47	129.24	121.82	142.23	125.08	111.16	150.65	111.16	125.08	45.15	12.08	52.20	58.41
12	154.98	122.40	133.70	110.84	133.70	122.40	142.40	125.98	111.41	151.67	111.41	125.98	45.31	12.08	52.23	58.44
13	156.33	122.42	124.95	146.74	124.95	122.42	142.61	126.20	111.50	151.91	111.50	126.20	45.34	12.07	52.25	58.44
14	146.97	118.40	133.09	129.34	123.80	144.68	142.44	126.05	111.45	151.80	111.45	126.05	45.34	12.07	52.25	58.46
15	148.12	119.92	127.31	146.09	119.24	145.48	143.14	127.65	112.07	153.16	112.07	127.65	45.65	12.10	52.38	58.52
16	152.48	121.96	129.33	129.81	129.33	121.96	142.91	125.04	111.73	149.73	111.73	125.04	44.58	12.18	45.52	15.86
17	146.61	123.62	114.44	160.72	114.44	123.62	142.91	124.51	111.70	149.11	111.70	124.51	44.51	12.15	45.52	15.83
18	154.82	122.51	133.61	111.24	133.61	122.51	143.01	125.84	111.86	150.71	111.86	125.84	44.64	12.15	45.49	15.83
19	156.15	122.63	125.03	147.07	125.03	122.63	143.17	126.08	111.94	150.97	111.94	126.08	44.68	12.16	45.49	15.83
20	146.92	118.44	133.20	129.73	123.86	144.61	143.06	125.92	111.91	150.84	111.91	125.92	44.69	12.15	45.50	15.81
21	148.41	117.47	127.95	130.78	130.54	132.76	143.32	125.60	111.81	150.26	111.81	125.60	44.64	12.16	45.50	15.83

22	149.34	117.65	128.55	131.04	133.54	123.63	143.22	125.60	111.83	150.26	111.83	125.60	44.64	12.16	45.50	15.83
23	156.84	117.57	129.54	146.25	129.05	110.90	143.50	127.20	112.41	152.38	112.41	127.20	44.95	12.21	45.55	15.83
24	148.38	125.98	129.28	128.50	129.28	125.98	142.74	125.45	111.70	150.84	111.70	125.45	44.66	12.11	45.49	15.79
25	153.09	126.75	124.59	145.48	124.59	126.75	142.80	126.13	111.87	151.62	111.87	126.13	44.72	12.16	45.42	15.77
26	155.22	122.53	133.56	110.84	133.56	122.53	142.54	141.31	112.54	150.71	110.35	117.23	44.53	12.28	45.34	15.88
27	149.73	117.84	128.50	130.67	133.44	123.49	141.54	141.54	112.56	150.16	110.34	117.78	44.51	12.24	45.36	15.86
28	152.95	127.01	124.65	145.20	124.65	127.01	143.43	141.57	112.44	151.74	110.56	117.50	44.68	12.24	45.37	15.88
29	155.04	115.41	127.99	145.65	127.99	115.41	143.24	141.12	112.25	151.63	110.57	117.62	44.68	12.26	45.35	15.85
30	154.31	126.57	127.70	145.75	125.53	116.53	143.66	141.63	112.75	152.00	110.85	117.86	44.97	12.57	45.67	16.17
31	154.96	122.53	133.40	110.29	133.40	122.53	131.13	139.48	101.04	151.06	107.60	122.53	44.56	12.60	44.56	12.60
32	156.36	122.21	124.57	146.30	124.57	122.21	131.35	139.30	100.96	152.32	107.68	123.39	44.42	12.41	44.42	12.41
33	146.37	118.80	133.02	128.79	123.78	144.44	130.95	138.62	100.72	152.27	107.68	125.81	44.66	12.60	44.66	12.60
34	138.19	119.95	119.14	159.47	107.98	147.67	130.67	137.90	100.88	151.57	107.42	124.75	44.53	12.58	44.53	12.58
35	146.92	126.63	129.24	128.01	129.24	126.63	130.05	138.55	100.07	151.98	106.95	123.49	44.30	12.26	44.30	12.26
36	153.96	119.60	134.21	128.87	134.09	107.19	130.72	139.28	100.67	152.55	107.94	124.61	44.79	12.71	44.79	12.71
37	153.68	127.17	127.65	145.14	125.45	116.87	130.90	139.85	100.55	153.00	108.33	124.17	45.03	12.70	45.03	12.70
38	139.14	119.69	118.44	157.98	107.95	146.37	129.78	146.37	94.14	151.23	103.83	119.69	44.11	12.89	44.11	12.89
39	154.28	117.96	133.95	128.94	133.82	109.30	142.90	140.66	111.78	151.36	110.14	117.60	44.17	12.65	44.17	12.65
40	155.43	122.35	133.48	110.37	133.48	122.35	142.67	140.68	111.76	151.15	109.90	117.41	44.11	12.63	44.11	12.63

From Ref. 77.

Table 10. ^{13}C Chemical shifts in 3-methyl-1-phenylpyrazole-4,5-dione (4-X)hydrazones in $CDCl_3$.

Carbon no.	**78**	**79**	**80**[c]
3	148.3 (2.90)[a] (8.64)[b]	148.2	148.5
4	128.3 (0.60) (5.13)	128.3	129.9
5	157.6 (1.68)	157.5	157.5
6	137.9	137.9	137.7
7	118.3	118.2	118.2
8	128.8	128.7	128.8
9	124.9	124.9	125.2
10	11.7	11.6	11.6
1′	140.9 (18.77) (5.71)	137.3 (2.4)[d]	143.7
2′	115.6 (1.83) (2.34)	117.0 (8.5)	115.4
3′	129.5 (2.44)	116.4 (23.2)	126.8 (3.7)[d]
4′	125.6	160.3 (246.6)	126.9 (33.0)

From Ref. 88.
[a] $^nJ(^{15}N_\alpha, ^{13}C)$.
[b] $^nJ(^{15}N_\beta, ^{13}C)$.
[c] $\delta(CF_3) = 123.9$; $^1J(^{19}F, ^{13}C) = 271.6$.
[d] $^nJ(^{19}F, ^{13}C)$.

Negrebetskii *et al.*[101] studied temperature dependence of $^nJ(^{15}N, ^{13}C)$ coupling constants in compounds **84**. Considerable differences were found in these values for compounds **84a, b** at 30°C and −8°C and −120°C respectively (Table 14). At lower temperatures, rotation about $C_4-N=$ does not take place and carbons C_3/C_5 C_2/C_6 are not equivalent. The assignment of these signals is based on the stereospecific behaviour of $^2J(^{15}N, ^{13}C)$ coupling constants. At laboratory temperatures, average values are observed (Tables 7, 10 and 14).

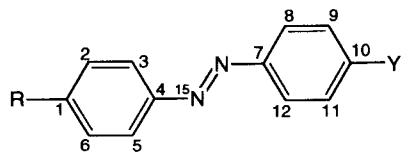

84

4.2. Azo–hydrazone tautomerism

Jacques *et al.*[9] recognized for the first time the considerable differences in ^{13}C chemical shifts of azo and hydrazone forms. They studied compounds **85** and **86**. The ^{13}C chemical shifts of $N=NC_6H_5$ in **85** were 152.7 (C_i); 122.6 (C_o); 129.1 (C_m); 130.5

Table 11. ^{13}C Chemical shifts, coupling constants $^{n}J(^{13}P,^{13}C)$ (values in parentheses) and ^{31}P chemical shifts of compounds **83**.

R_1	R_2	R_3	C_1	C_2	C_3	C_4	C_5	C_6	C_7	C_8	C_9	C_{10}	C_{11}	C_{12}	$\delta^{31}P$
H	PPh_3^+	H	154.4 (3)	117.6 (90)	137.7 (12)	122.8 (17)	139.9 (2)	118.8 (8)	142.2	127.4	111.2	152.3			23.1
	PPh_3^+	$NHCOCH_3$	153.6 (3)	118.0 (92)	137.4 (10)	122.0 (17)	140.7 (2)	119.9 (8)	131.6	142.0	100.8	154.0	108.1	118.3	22.9
	PBu_3^+	H	154.2 (2)	117.7 (74)	134.9 (8)	122.8 (14)	138.2 (1)	118.4 (8)	142.6	127.3	111.8	152.2			32.4
	PBu_3^+	$NHCOCH_3$	154.5 (2)	117.1 (84)	134.9 (7)	122.0 (14)	138.6 (1)	118.3 (9)	142.2	142.1	100.6	154.1	109.2	131.3	32.2
CH_3	PPh_3^+	H	151.6 (2)	111.6 (93)	137.1 (12)	122.0 (19)	142.2 (2)	138.3 (8)	141.0	126.0	111.0	152.0			25.0
	PPh_3^+	$NHCOCH_3$	152.1 (2)	114.6	136.7 (12)	120.9 (19)	142.8 (2)		131.1	140.2	100.5	153.7	107.8	120.6	24.0
	PBu_3^+	H	153.8 (3)	116.5 (76)	138.3 (8)	120.8 (15)	141.3 (1)	133.3 (6)	142.3	126.4	111.6	152.1			32.3
	PBu_3^+	$NHCOCH_3$	153.8 (3)	117.6 (75)	133.2 (7)	120.2 (15)	141.6 (1)	131.4 (7)	141.6	141.6	100.2	154.1	109.0	131.0	32.1
H	$P(2\text{-Furyl})_3^+$	H	154.3 (4)	113.5 (107)	136.6 (14)	122.5 (20)	140.7 (3)	120.2 (9)	142.0	127.6	111.8	152.7			−18.8
	$P(2\text{-Th})_3^+$	H	153.4 (4)	120.7 (102)	136.1 (12)	122.5 (19)	140.1 (3)	118.6 (9)	142.5	128.2	111.6	152.6			2.0
H	$PPh_2(CH_2Ph)^+$	H	154.0 (3)	117.8 (85)	137.7 (10)	122.7 (16)	139.4 (2)	118.6 (8)	142.9	127.4	111.7	152.4			22.8

From Ref. 90.

Table 12. ^{13}C Chemical shifts of compounds **43–77**.

Compound	C_1	C_2	C_3	C_4	C_{4a}	C_5	C_6	C_7	C_8	C_{8a}	$C_{1'}$	$C_{2'}$	$C_{3'}$	$C_{4'}$	Reference
43[a]	148.3	112.3	125.7	131.4	131.5	128.0	126.5	126.9	123.6	134.4					46
44[a]	127.9	150.3	117.1	129.1	134.8	127.9	127.5	126.7	129.4	133.0					46
45[b]	157.8	108.5	113.9	139.6	132.8	122.6	127.9	125.6	122.6	124.5	152.8	122.6	129.5	129.5	68
46[a]	174.0	132.6	128.1	120.8	136.9	127.4	132.0	126.0	126.5	130.1	143.0	117.4	129.3	126.5	94
47[a]	174.5	[d]	114.0	141.8	135.4	123.9	132.5	126.8	126.8	[d]	143.1	118.1	129.6	127.6	68
48[a]	129.7	171.6	124.5	139.6	127.7	128.3	125.4	128.5	121.4	133.3	144.4	118.3	129.2	127.0	94
54[a]	127.0	138.4	119.5	133.6	127.4	128.0	123.2	127.6	122.1	134.8	153.7	121.9	129.1	128.9	48
54[b]	125.3	140.2	120.1	133.8	126.5	128.1	122.8	127.6	121.0	134.3	153.3	121.4	129.3	128.7	48
55[a]	141.6	132.5	121.5	117.8	135.6	128.6	128.1	125.3	121.9	124.1	153.4	122.1	129.0	129.5	48
55[b]	144.2	131.3	120.4	116.4	135.6	128.3	128.5	125.2	124.1	124.2	153.1	122.1	129.1	129.3	48
56[a]	146.2	109.0	113.9	140.3	133.1	124.0	127.0	125.2	120.5	122.3	153.6	122.6	129.0	129.7	48
56[b]	150.4	107.6	112.5	137.2	133.5	122.9	127.5	124.4	122.8	121.5	153.4	122.0	129.2	129.1	48
57[b]	148.3	129.9	104.2	137.0	133.8	123.3	129.6	125.8	124.2	123.5	[e]	[e]	[e]	[e]	48
58[a]	130.4	129.5	120.0	133.3	130.0	128.0	125.5	128.1	123.0	131.2	152.0	122.4	129.6	131.5	48
58[b]	129.6	129.4	119.4	133.8	130.2	127.8	125.2	127.5	123.3	133.2	152.3	122.2	129.3	130.9	48
59[b]	134.9	143.8	114.3	127.4	134.9	128.1	126.9	128.0	124.7	130.6	152.6	122.6	129.4	131.4	[h]

60[b]	137.6	120.0	111.9	143.5	131.5	123.1	127.3	126.4	122.9	127.2	152.7	122.8	129.5	131.3	48
62[b]	121.2	143.4	128.5	176.2	122.4	129.1	116.6	149.8	113.7	137.6	143.0	117.0	129.6	125.5	49
63[b]	122.8	142.7	129.0	181.5	112.3	[f]	112.1	[f]	113.5	136.5	142.8	116.7	129.6	124.9	49
64[b]	122.4	137.7	129.4	176.2	132.3	109.6	149.3	121.4	130.6	125.6	143.6	118.0	130.0	126.5	49
65[b]	124.3	143.5	131.1	178.3	119.2	130.1	114.2	155.3	111.2	138.2	148.7	116.1	125.5	142.7	50
66[b]	128.7	145.8	127.7	182.2	122.9	127.1	117.7	147.0	111.3	139.4	149.0	113.8	126.0	141.2	50
67[b]	109.3	147.9	105.4	153.8	117.3	130.1	118.9	142.5	127.5	135.1	157.4	121.9	125.3	146.2	50
68[b]	181.6	132.7	126.8	122.4	134.5	132.1	134.0	112.5	154.0	112.7	142.1	115.9	129.8	124.9	51
69[b]	180.3	132.8	129.8	121.5	138.4	[g]	124.6	[g]	150.7	115.1	141.7	116.9	129.8	126.1	51
70[b]	180.2	127.9	143.3	121.1	136.6	116.9	154.4	111.9	162.6	115.8					52
71[c]	135.8	175.0	148.0	118.5	131.0	128.0	123.6	127.0	129.0	129.5					53
72[c]	135.0	173.0	148.5	119.5	131.5	127.8	124.5	127.3	129.0	129.2					53
73[c]	135.5	174.5	148.5	119.0	131.5	128.2	123.8	127.0	129.3	129.5					53
74[c]	135.8	177.5	123.2	132.2	133.0	132.0	117.0	161.0	109.0	122.8					53
75[c]	136.0	177.5	123.6	132.5	132.0	132.0	117.5	161.0	109.0	123.0					53
76[c]	136.0	182.0	123.8	133.0	130.0	132.5	117.5	161.0	110.0	122.8					53
77[b]	144.6	126.0	175.8	134.5	126.6	121.1	131.2	126.5	131.0	128.0					54

[a] $CDCl_3$.
[b] DMSO-d_6.
[c] Acetone-d_6.
[d] 131.9 or 130.1.
[e] 153.0 or 152.6; 122.5 or 122.3; 129.0 or 129.2; 130.0 or 129.9.
[f] 153.2 or 153.1.
[g] 132.5 or 132.3.
[h] Correction of values from Ref. 48.

Table 13. Coupling constants $^{n}J(^{13}C,^{13}C)$ in *cis*- and *trans*-azobenzenes and compounds **78** and **48**.

trans-Azobenzene[a]	*cis*-Azobenzene[a]	**78**[b]	**48**[c]
$^{1}J(1,2) = 67$	$^{1}J(1,2) = 64$	$^{1}J(3,4) = 63.7$	$^{1}J(1,2) = 60.0$
$^{1}J(3,4) = 56$	$^{1}J(3,4) = 52$	$^{1}J(4,5) = 66.9$	$^{1}J(2,3) = 57.7$
$^{2}J(2,4) = 2$	$^{2}J(2,4) = 2$	$^{1}J(6,7) = 64.4$	$^{1}J(3,4) = 61.1$
$^{3}J(1,4) = 9$		$^{1}J(7,8) = 57.8$	$^{1}J(4,4a) = 52.8$
$^{4}J(1,2') = 4$	$^{4}J(1,2') = 3$	$^{1}J(8,9) = 55.9$	$^{1}J(5,6) = 58.4$
		$^{1}J(3,10) = 52.6$	$^{1}J(6,7) = 54.4$
		$^{1}J(1',2') = 65.2$	$^{1}J(7,8) = 58.8$
		$^{1}J(2',3') = 59.0$	$^{1}J(8,8a) = 58.7$
		$^{1}J(3',4') = 56.0$	$^{1}J(1',2') = 65.1$
			$^{1}J(2',3') = 58.2$
			$^{1}J(3',4') = 55.9$

[a] From Ref. 74.
[b] From Ref. 88.
[c] From Ref. 94.

(C_p); 138.3 (C–OH) and those of $=NNHC_6H_5$ in **86** were 142.6 (C_i); 115.5 (C_o); 129.6 (C_m); 124.5 (C_p); 186.1 (C=O). A similar approach was used[91] for azo dyes with intramolecular hydrogen bonds. 2-Hydroxy-5-*tert*-butylazobenzene **87** (model azo compound) and 3-methyl-1-phenylpyrazole-4,5-dione 4-phenylhydrazone **78** (hydrazone model) and compound **48**, as a representative of classical tautomeric system, were studied. The ^{13}C chemical shifts of the phenyl groups enable an estimation of hydrazone content from chemical shifts of C_i, C_o and C_p to be 66%, 61% and 66%, respectively.

Table 14. Temperature dependence of coupling constants $^{n}J(^{15}N,^{13}C)$ of compounds **84** in $CDCl_3$.

Compound R(Y)	$J(^{15}N^{13}C)$				
	$^{1}J_{NC(4)}$	$^{2}J_{NC(5)}$	$^{2}J_{NC(7)}$	$^{3}J_{NC(2,6)}$	$^{3}J_{2NC(8,12)}$
84a NEt_2 (NO_2)	4.7[a] (126.55)	4.7 (126.55)	5.8	2.1	4.0
	≤ 1.5[b] (117.0)	10 ± 1 (136.1)	5.5 ± 0.5		
84b NEt_2 (H)	4.4[a] (125.43)	4.4 (125.43)	4.8	2.2	4.0
	≤ 2[c] (116.9)	11 ± 1 (134.9)	5.0 ± 0.5		
84c H (NEt_2)	3.7[a]	3.7	5.2	1.9	4.0

From Ref. 101.
[a] 30°C.
[b] −8°C.
[c] −120°C.

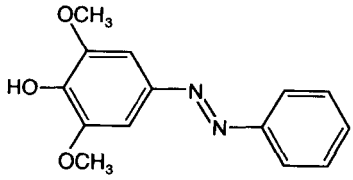

85

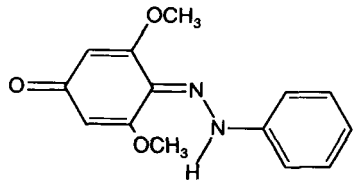

86

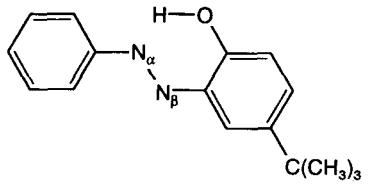

87

Kelemen *et al.*[102] proposed the use of $\delta^{13}C{=}O/^{13}C{-}OH$ or $\delta^{13}C{=}NR/^{13}C{-}NHR$ of carbons directly engaged in the azo–hydrazone tautomeric system. For 1-(4-X-phenyl)azo-2-naphthols **88**, $\delta^{13}C_2$ are substituent-dependent (e.g. X = NO_2: δ = 180.0; X = OCH_3: δ = 160.8) while practically no differences in $\delta^{13}C_2$ were found in 1-(4-X-phenyl)azo-2-naphthylamines **89** (X = NO_2: δ = 139.9; X = OCH_3: δ = 138.1).

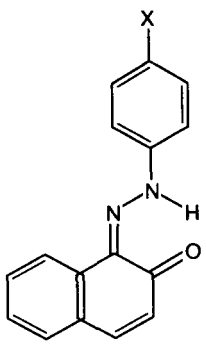

88

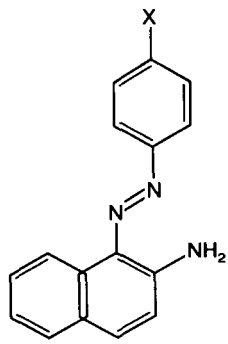

89

The above-mentioned two basic principles, i.e. ^{13}C chemical shift measurements of phenyl group (with respect to substituted phenyl groups after taking the substituent effects into account) and C=O/C–OH compared with C=NR/C–NHR carbons have often been used for azo–hydrazone content determination including temperature and solvent effects.[9,39,49–54,65,68,69,71,78,80–88,91,95–100,102,103] This is because the measurements are fast and no labelling is necessary.

5. ^{14}N NMR SPECTROSCOPY

Berrie *et al.* determined[104] ^{14}N chemical shifts of nitrogen in α position to the phenyl ring in 1-(substituted phenyl)azo-2-naphthols **88** using the nitrogen-14 double irradiation technique. The data are given in Table 15. By comparing ^{14}N chemical shifts for the nitrogen atom α to the phenyl ring in the pure azo and hydrazone forms of azobenzene and 10-(4-methoxyphenylazo)-9-phenanthrol, respectively, they calculated the hydrazone constants. The values found are higher than those obtained from ^{1}H and ^{13}C NMR data.[103] This is because a more suitable standard for pure azo compound is necessary (see Section 6.2).

6. ^{15}N NMR SPECTROSCOPY

6.1. ^{15}N NMR data

Azo dyes of common formula X–N=N–Y contain at least two nitrogen atoms in the azo bond but also, in many cases, have other groups containing nitrogen atoms (NR^1R^2, $CONR^1R^2$, NO_2, CN, nitrogen atoms in heterocycles, etc.). Nitrogen NMR spectroscopy provides a sensitive method for the study of chemical structure and bonding of azo dyes. Despite its low natural abundance and receptivity (Table 1) the ^{15}N isotope is preferred because, in contrast to ^{14}N NMR spectra, very narrow signals are observed in ^{15}N NMR spectra, enabling very subtle changes in ^{15}N chemical shifts and $^{n}J(^{15}N, X)$ coupling constants to be detected. The sensitivity of ^{15}N NMR measurements may be enhanced by the application of high magnetic field wide-bore magnets, by the application of polarization transfer technique (INEPT, DEPT), by multiple-quantum coherence experiments and by ^{15}N enrichment.[105–107]

Table 15. ^{14}N chemical shifts of the nitrogen α to the phenyl ring in 1-(X-phenyl)azo-2-naphthols in $CDCl_3$.

X	$\delta^{14}N^a$	Hydrazone content (%)	X	$\delta^{14}N^a$	Hydrazone content (%)[b]
4-CN	-166 ± 15	97	H	-111 ± 3	79
3-CN	-150 ± 10	91	4-Cl	-108 ± 4	78
3-Cl	-119 ± 4	81	4-CH_3	-81 ± 3	69
3-OCH_3	-117 ± 3	81	4-OCH_3	-31 ± 8	52
3-CH_3	-115 ± 3	80	H	14 ± 12^b	38

From Ref. 104.

[a] Reference compound: nitrate nitrogen of 4.5 M NH_4NO_3 in aqueous 3 N HCl.

[b] Measured in hexane.

The ^{15}N chemical shifts in asymmetrically substituted azobenzenes differ only slightly and their assignment was confirmed by measurements of selectively ^{15}N-labelled compounds (Table 16).

The ^{15}N chemical shifts of heavily substituted azobenzenes of type **90**[108] are shown in Table 17, including $\delta^{15}N$ of nitro and acetamido groups.

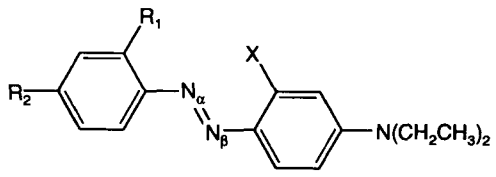

90

The differentiation between the ^{15}N chemical shifts in dyes existing practically completely in their hydrazone forms is easy because $-N_\alpha H-$ signals are shifted upfield and they are detected as strong negative signals because of the negative nuclear Overhauser effect (Table 18).[88]

The temperature dependence of ^{15}N chemical shifts of naphthalene compounds of **54**, **56**, **58**, **60**[109] were measured and relatively small changes were observed (Table 19) in contrast to analogous data for aryldiazonium salts coupling products with substituted naphthols.[49,50,68,110] The temperature (in)dependences of ^{15}N chemical shifts have been used for azo–hydrazone content determination.

The protonation positions of 4-aminoazobenzene in weak (HCl) and strong (H_2SO_4) acid solutions seem to be different.[111]

Yamamoto *et al.*[112] measured the ^{15}N NMR spectra of some water-soluble dyes and their intermediates in natural abundance and the structural dependency of azo–hydrazone tautomerism was determined.

A ^{15}N NMR investigation of azo–hydrazone acid–base equilibria of tartrazine and its two analogues[113] has been published. The ^{15}N chemical shifts in neutral, basic and strongly basic solutions were given.

One-bond coupling constants $^1J(^{15}N,^{15}N)$ were found in ^{15}N double-labelled azo dyes. Typical values are 15.3 ± 0.7 Hz in pure azo forms and 11 ± 0.7 in pure hydrazone forms.[63,65,69,109]

Kuroda *et al.*[114] reported on the determination of the sign of the one-bond $^1J(^{15}N,^{15}N)$ coupling constant in ^{15}N-labelled 4-acetylaminoazobenzene by selective ^{15}N decoupling experiments in ^{13}C NMR spectra. The sign was found to be negative in contrast to the theoretical prediction. This is attributed to the large negative contribution from the orbital-dipole mechanism of an N=N double bond.

Table 16. ^{15}N Chemical shifts in *trans*-azobenzenes (4-X)$-C_6H_4-N_\alpha=N_\beta-C_6H_4-$(4-Y).

X	Y	$\delta^{15}N_\alpha$ [a]			$\delta^{15}N_\beta$ [a]	
		A	B	C	A	C
H	H	129.0[b]	127.6	127.5	129.0	127.5
		130.1[c]	128.7	128.4	130.1	128.4
		129.1[d]			129.1	
$N(CH_3)_2$ [e]	H	119.2[b]	116.5	117.7		96.2
NH_2 [g]	H			118.9[b]		101.7
				118.2[c]		91.4
OH	H	124.2[c]			110.2	
OCH_3	H			121.8[b]		113.7
CH_3	H			126.1[b]	123.6	122.2
Br	H			122.1[b]	130.7	128.6
NO_2	H			120.9[b]		144.0
OH	NO_2 [g]	138.7[c]	137.2	138.0		101.2
NH_2	OH			103.6[c]	91.8	91.1
$N(CH_3)_2$	CH_3			113.1[b]		96.2
$N(CH_3)_2$	NO_2	132.1[b]				
F[h]	H			123.8[b]		126.1
H[i]	H	146.5[b]			146.5	
H[i]	H	150.6[c]			150.6	

Data taken from Ref. 72.
Reference compound $CH_3{}^{15}NO_2$.
[a] A: ^{15}N-Monolabelled compound; B: ^{15}N-monolabelled compound with $Cr(acac)_3$ added; C: measured at ^{15}N natural abundance level, $Cr(acac)_3$ added.
[b] Deuteriochloroform.
[c] Hexadeuteriodimethyl sulphoxide.
[d] *n*-Hexane.
[e] $\delta N(CH_3)_2 = -325.5$.
[f] $\delta NH_2 = -318.4$ (natural abundance), -314.0 (method C).
[g] $\delta NO_2 = -10.3$ (C).
[h] Data taken from Ref. 75.
[i] *cis*-Azobenzene.

6.2. Azo–hydrazone tautomerism

Nitrogen atoms of the azo bond are directly engaged in the azo–hydrazone tautomeric system and it can be expected that $^{14/15}$N chemical shifts should reflect the changes in equilibrium. This basic idea was proposed by Berrie *et al.*,[104] who used ^{14}N chemical shifts of NH_α/N_α atoms and calculated hydrazone contents (Table 15). They obtained naturally only one set of data measurable by double irradiation technique. The intramolecular hydrogen bond has a marked effect on δN, as can be seen after comparison of $^{15}N_\alpha$ chemical shifts in *trans*-azobenzene ($\delta = 128$), and compounds **87** and 4-hydroxyazobenzene (**91**)[110] (Table 20). From these data it follows that the proper model compounds for tautomeric systems with intramolecular

Table 17. ^{15}N Chemical shifts in *trans*-azobenzenes **90** in deuteriochloroform.

R_1	R_2	X	δN_α [a]	δN_β	δNEt_2	δX
H	H	H	93.12	116.62	−295.91	
Br	CH_3	H	90.63	115.89	−295.16	
H	CH_3	H	92.99	112.28	−296.81	
CH_3	CH_3	H	96.02	109.65	−297.69	
NO_2	NO_2	H	127.60	54.09	−282.67	−13.87, −16.92
H	H	$NHCOCH_3$	63.80	103.64	−289.28	−253.40
Br	H	$NHCOCH_3$	51.39	114.61	−286.10	−251.50
Br	CH_3	$NHCOCH_3$	53.90	112.26	−287.84	−251.86
H	H	OH	−23.72	81.31	−285.44	
H	CH_3	OH	−11.73	84.22	−286.86	
CH_3	CH_3	OH		71.18	−285.97	

From Ref. 108.

[a] Reference compound: external $CH_3{}^{15}NO_2$, $Cr(acac)_3$ added.

Table 18. ^{15}N Chemical shifts of 3-methyl-1-phenylpyrazole-4,5-dione 4-X-phenylhydrazones of type **78** in deuteriochloroform.

X	$\delta^{15}N_\alpha$	$\delta^{15}N_\alpha$ [f]	$\delta^{15}N_\beta$ [f]	$\delta^{15}N_1$ [f]	$\delta^{15}N_2$ [f]
NH_2	−199.9		−17.4	−191.3	−80.4
OCH_3	−203.6	−204.4	−19.0	−192.4	−79.2
CH_3	−204.5	−205.8	−19.8	−192.9	−78.1
H	−205.6	−206.4	−18.9	−192.4	−76.1
H[a,b]	−202.8		−18.6		
H[a–c]	−202.2		−16.5		
H[a,d]	−208.3		−21.8		
H[a–e]	−206.4		−19.4		
F	−207.6	−208.6	−19.8	−192.1	−75.8
Cl	−208.7	−209.4	−20.8	−192.3	−74.2
Br	−208.2	−209.3	−20.8	−192.5	−74.7
I	−208.6	−209.2	−21.3	−192.1	−73.9
CH_3COO	−209.8	−210.8	−22.7	−192.9	−72.3
CF_3	−210.9	−212.1	−22.2	−192.8	−72.1
NO_2	−212.9		−22.4		
CH_3CONH		−213.2	−22.7	−191.9	−67.4

Data taken from Ref. 88.

Reference: external neat $CH_3{}^{15}NO_2$.

[a] Data taken from Ref. 69.

[b] DMSO-d_6.

[c] 330 K.

[d] Pyridine-d_5.

[e] 350 K.

[f] $Cr(acac)_3$ added.

Table 19. Temperature dependence of ^{15}N chemical shifts of compounds **54**, **56**, **58**, **60**[a] in various solvents.

Compound	Solvent	Temperature (K)	$\delta^{15}N_{\alpha}$ [b]	$\delta^{15}N_{\beta}$ [b]
54	$CDCl_3$	230	115.8	69.0
	$CDCl_3$	300	118.9	72.9
	DMSO-d_6	300	114.8	65.9
	DMSO-d_6	370		70.8
	Acetone-d_6	200	112.8	63.9
	Acetone-d_6	300	116.1	67.6
56	$CDCl_3$	300	117.8	101.3
	DMSO-d_6	300	112.8	86.4
	DMSO-d_6	370		92.5
	Acetone-d_6	230	114.2	95.5
	Acetone-d_6	300	114.5	93.1
58	$CDCl_3$	230	125.8	89.1
	$CDCl_3$	300	129.3	94.1
	$CDCl_3$	330	130.3	95.9
60	DMSO-d_6	300	123.2	123.4
	DMSO-d_6	370	126.4	126.6

[a] From Ref. 109.
[b] Reference: external neat $CH_3{}^{15}NO_2$.

hydrogen bonds must have intramolecular hydrogen bonds, too. The difference in $\delta^{15}N_{\alpha}$ caused the hydrazone content obtained by Berrie *et al.*[104] (Table 15) to be systematically higher[103] due to the incorrect choice of a model compound which exists completely in the azo form.

For the study of azo–hydrazone tautomerism direct measurement of ^{15}N chemical shifts has been recommended.[110] Such measurements make it possible to obtain two independent sets of data for the calculation of tautomer abundances (from N_{α} and N_{β}), so that an intrinsic check is possible. The compounds **78** and **87** were chosen as standard hydrazo and azo compounds. Strong intramolecular hydrogen bonds exist in both model compounds as

Table 20. ^{15}N Chemical shifts of compounds **78**, **87**, **91**[a] in $CDCl_3$.

Temperature (K)	**78**		**91**		**87**	
	$\delta^{15}N_{\alpha}$	$\delta^{15}N_{\beta}$	$\delta^{15}N_{\alpha}$	$\delta^{15}N_{\beta}$	$\delta^{15}N_{\alpha}$	$\delta^{15}N_{\beta}$
360			112.7	126.4		
330	−205.7	−17.0	111.5	125.2	70.9	128.1
300	−205.2	−17.3	110.2	124.2	69.4	126.9
270	−205.4	−17.6			68.1	125.3
240	−204.6	−17.9			67.0	123.7

Reference: external neat $CH_3{}^{15}NO_2$.
[a] From Ref. 110.

Table 21. Temperature dependence of ^{15}N chemical shifts and hydrazone content of compound **48** in $CDCl_3$.

Temperature (K) (K)	$\delta^{15}N_\alpha$ [a]	Hydrazone content (%)	$\delta^{15}N_\alpha$ [a]	Hydrazone content (%)
330	−108.0	64.7	32.7	65.7
310	−116.9	67.8	28.0	68.7
290	−126.2	71.2	22.8	72.0
270	−137.4	75.3	17.0	75.8
250	−148.5	79.3	10.6	80.0
230	−158.2	82.9	4.7	83.9

From Ref. 110.

[a] Reference: external neat $CH_3{}^{15}NO_2$.

well as in the tautomeric compound **48**. The temperature dependence of ^{15}N chemical shifts and the calculated hydrazone content for compound **48** from equation (2) is given in Table 21.[110]

$$\% \text{ hydrazone} = \frac{\delta^{15}N(\mathbf{87}) - \delta^{15}N(\mathbf{48})}{\delta^{15}N(\mathbf{87}) - \delta^{15}N(\mathbf{78})} \times 100 \qquad (2)$$

The contents of the hydrazone form calculated from two (N_α and N_β) sets of data are in very good agreement. In other cases,[49,50,68] the differences between N_α and N_β were less than 10%.

Small variations of ^{15}N chemical shifts with temperature in amino azo dyes (Table 19) are hardly any indication of the presence of a significant amount of hydrazone forms. In compound **54**, measured in acetone at 200 and 300 K, the differences in $\delta^{15}N$ are less than 3.8 ppm, contrary to the values found in the hydroxy analogue **48**, for which the difference for N_α is 50.2 ppm within the same temperature interval (230 and 330 K in $CDCl_3$). ^{15}N Chemical shifts lead to the conclusion that aminoazo compounds exist in azo forms in a broad temperature range, in agreement with the ^{13}C NMR results.[102]

Table 22. ^{19}F Chemical shifts of 4-fluoro-(3′ or 4′-substituted) azobenzenes in deuteriochloroform.

X	$\delta^{19}F^a$	X	$\delta^{19}F^a$
4′-$N(CH_3)_2$	−33.37	4′-Br	−29.87
4′-OCH_3	−31.70	3′-$COCH_3$	−29.65
4′-CH_3	−31.16	3′-Cl	−29.60
3′-CH_3	−30.86	4′-$COOCH_3$	−29.24
H	−30.66	4′-$COCH_3$	−29.06
4′-F	−30.49	3′-NO_2	−28.41
4′-I	−29.83	4′-NO_2	−27.82
4′-Cl	−30.00		

From Ref. 75.

[a] Reference: external neat trifluoroacetic acid.

Table 23. Temperature dependence of the ^{19}F chemical shifts and hydrazone contents in compounds **79**, **92–94** in deuteriochloroform.

Temperature (K)	**79**	**92**	**93**		**94**	
	$\delta^{19}F$	$\delta^{19}F$	$\delta^{19}F$	Hydrazone content (%)	$\delta^{19}F$	Hydrazone content (%)
330	−116.76	−109.77	−113.00	46.2	−114.11	62.1
310	−116.60	−109.56	−113.03	49.3	−114.13	64.9
290	−116.47	−109.39	−113.03	51.4	−114.17	67.5
270	−116.38	−109.27	−113.07	53.4	−114.24	69.9
250	−116.24	−109.10	−113.18	57.1	−114.35	73.5
230	−116.10	−108.88	−113.38	62.3	−114.54	78.4

From Ref. 118.
Reference compound: internal $CFCl_3$.

On the other hand, a considerable contribution of hydrazone forms can be expected in the last three compounds in Table 17 as a result of the substituent effects of alkylamino groups.

Deuteration[115] of the acidic proton in *ortho*-hydroxyazo dyes leads to a small shift in the azo–hydrazone equilibrium.

7. ^{17}O NMR SPECTROSCOPY

Oxygen-17 NMR spectroscopy would also be attractive for azo compounds derived from oxygen-containing starting components but it suffers from poor receptivity because of the very low natural abundance level of the ^{17}O isotope (Table 1) and the quadrupolar character of this nucleus. The oxygen atom is, like the nitrogen atom, directly engaged in tautomeric systems and ^{17}O NMR spectroscopy clearly reflects the character of carbon–oxygen bonds (C–O vs.

Table 24. ^{19}F Chemical shifts and linewidths of the CF_3 group of compound **95** in aqueous solutions.

Temperature (K)	Concentration (mol/dm^3)		
	5.0×10^{-2}	5.0×10^{-3}	5.0×10^{-5}
295	13.10 (94)		
299	13.12 (110)		
303	12.95 (165)	13.16 (4)	13.31 (3)
313	12.49 (133)	13.14 (5)	
323	12.51 (35)	13.15 (7)	
327	12.57 (19)	13.16 (4)	13.28 (3)
343	12.79 (3)		

From Ref. 119.
Reference: CF_3COOD.

C=O). Reuben and Samuel[116] observed ^{17}O chemical shift in compound **48** ($\delta = 315$). Lippert *et al.*[117] reported on ^{17}O chemical shifts in compound **46** ($\delta = 340$). Having compared $\delta^{17}O$ in 2-naphthol ($\delta = 73$), β-tetralone ($\delta = 556$) and the above-mentioned values we have additional evidence for the prevailing double bond character of carbon–oxygen bond in compounds **46** and **48**.

8. ^{19}F NMR SPECTROSCOPY

The sensitivity of ^{19}F NMR spectroscopy is very high (Table 1) and ^{19}F NMR spectra have been used for the characterization of fluorine-containing azo dyes. The ^{19}F chemical shifts of fifteen 4-fluoro-(3′- or 4′-substituted)azobenzenes[75] are shown in Table 22. The $\delta^{19}F$ values correlate with the corresponding $\sigma_{m,p}$ constants ($\delta^{19}F = 3.60\sigma_{m,p} - 30.78$). The resonances of the aromatic CF_3 groups *meta* or *ortho* to the azo linkage were observed in the -61 to -57 region (DMSO-d_6, internal CCl_3F).[5]

From the view point of azo–hydrazone tautomerism, it is important to have an NMR method that enables comparisons to be made between azo–hydrazone content data obtained by means of electronic absorption spectra under similar concentration conditions. The application of fluorine as a "spy nucleus" has been proposed for this purpose.[118] Table 23 summarizes the ^{19}F chemical shifts in **79**, 4-fluoro-2′-hydroxy-5′-*tert*-butylazobenzene (**92**), 1-(4-fluorophenylazo)-2-naphthol (**93**) and 2-(4-fluorophenylazo)-1-naphthol (**94**) and the calculated hydrazone contents.

A similar procedure was used for 2-fluorophenyl derivatives.[118] High-field NMR instruments allow the use of very diluted solutions for ^{19}F NMR studies. The ^{19}F NMR spectra of 1×10^{-4} M solution of a dye in chloroform can be obtained within *ca.* 10 min of accumulation in a 5-mm tube at 376.5 MHz. Practically no changes of ^{19}F chemical shifts were obtained within the concentration range 1×10^{-2} to 1×10^{-4} mol/litre, in contrast to the following case.

Skrabal *et al.*[119] reported on the temperature and concentration dependence of monoazo dye **95** in aqueous solutions. A selection of data ($\delta^{19}F$ and $\omega_{1/2}$) are given in Table 24. Aggregation constants K were determined.

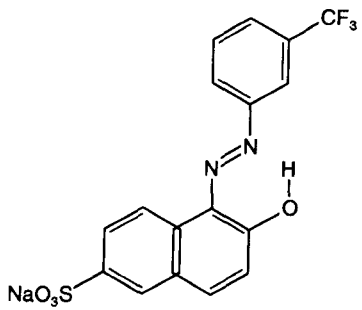

95

9. ^{31}P NMR SPECTROSCOPY

The ^{31}P chemical shifts[90] were determined for compounds **83**. The data are reported in Table 11.

ACKNOWLEDGEMENT

I thank Mrs Věra Stará for her excellent technical assistance.

REFERENCES

1. H. Zollinger, *Colour Chemistry*. Verlag Chemie, Weinheim, 1987.
2. R.K. Harris, in *NMR and the Periodic Table* (ed. R.K. Harris and B.E. Mann), p. 5. Academic Press, London, 1978.
3. G.A. Morris, *Magn. Reson. Chem.*, 1986, **24,** 371.
4. A. Lyčka and J. Jirman, in *Colour Chemistry* (ed. A.T. Peters and H.S. Freeman), Chap. 10. Elsevier Applied Science, London, 1991.
5. A. Foris, in *The Analytical Chemistry of Synthetic Dyes* (ed. K. Venkataraman), Chap. 8. Wiley, New York, 1977.
6. L.A. Fedorov, *Usp. Khim.*, 1988, **57,** 1643.
7. L.A. Fedorov, P. Savarino, V.I. Dostovalova, G. Viscardi, R. Carpignano and E. Barni, *Magn. Reson. Chem.*, 1991, **29,** 747.
8. N.R. Ayyangar, R.J. Lahoti, V. Parameswaran and D.R. Wagle, *Indian J. Chem.*, 1978, **16B,** 551.
9. P. Jacques, H. Strub, J. See and J.-P. Fleury, *Tetrahedron*, 1979, **35,** 2071.
10. E. Barni, P. Savarino, G. DiModica and R. Carpignano, *Dyes Pigm.*, 1984, **5,** 15.
11. L. Skulski and S. Smialek-Kazmierowska, *Pol. J. Chem.*, 1985, **59,** 17.
12. H.S. Freeman, C.S. Williard and W.N. Hsu, *Dyes Pigm.*, 1986, **7,** 397.
13. H.S. Freeman and C.S. Williard, *Dyes Pigm.*, 1986, **7,** 397.
14. Jia-zhen Hu, P. Skrabal and H. Zollinger, *Dyes Pigm.*, 1987, **8,** 189.
15. H.S. Freeman, L.S. Moser and W.H. Whaley, *Dyes Pigm.*, 1988, **9,** 57.
16. M.G. Hutchings and I. Matthews, *Dyes Pigm.*, 1988, **9,** 385.
17. J. Sokolowska-Gajda and J. Kraska, *Dyes Pigm.*, 1989, **10,** 285.
18. H.S. Freeman, J. Sokolowska-Gajda and Z. Hao, *Text. Chem. Color*, 1989, **21,** 24.
19. N. Hocaoglu, T. Uyar and L. Tuerker, *Dyes Pigm.*, 1990, **12,** 187.
20. H.S. Freeman, Z. Hao, S.A. McIntosh, J.C. Posey and W.N. Hsu, *Dyes Pigm.*, 1990, **12,** 233.
21. R. Rajagopal and S. Seshadri, *Dyes Pigm.*, 1990, **13,** 29.
22. H.S. Freeman, J.F. Esancy and L.D. Claxton, *Dyes Pigm.*, 1990, **13,** 55.
23. T. Hatta, S. Mataka and M. Tashiro, *Dyes Pigm.*, 1990, **13,** 107.
24. M.G. Hutchings, *Dyes Pigm.*, 1991, **17,** 227.
25. J. Jirman, *Collect. Czech. Chem. Commun.*, 1991, **56,** 2160.
26. W.P. Neumann and C. Wicenec, *Chem. Ber.*, 1991, **124,** 2297.
27. H. Balli and H. Ritter, *Dyes Pigm.*, 1981, **2,** 93.
28. J.W. Ronaldson, *Austr. J. Chem.*, 1981, **34,** 1935.
29. R.J. Lahoti, *Indian J. Chem.*, 1981, **20B,** 490.
30. A.S. Shawali, A.O. Abdelhamid, N.F. Ahmad and C. Parkanyi, *Heterocycles*, 1982, **19,** 2331.
31. D.V. Dikshit and K.D. Deodhar, *Dyes Pigm.*, 1985, **6,** 99.

32. E. Barni, S. Pasquino, P. Savarino and G. DiModena, *Dyes Pigm.*, 1985, **6,** 1.
33. A.S. Shawali, N.M.S. Harb and K.O. Badahdah, *J. Heterocycl. Chem.*, 1985, **22,** 1397.
34. R.M. Issa, M.M. El Kersh, M.M. Gaber and I.A. Abd-El Salam, *Egypt J. Chem.*, 1988, **30,** 1.
35. P. Savarino, G. Viscardi, R. Carpignano and E. Barni, *J. Heterocycl. Chem.*, 1989, **26,** 77.
36. P. Savarino, G. Viscardi, R. Carpignano, E. Barni, G. Alberti and A. Loi, *Dyes Pigm.*, 1989, **10,** 269.
37. P. Savarino, G. Viscardi, R. Carpignano, E. Barni and G. Ferrero, *Dyes Pigm.*, 1989, **11,** 163.
38. H.S. Freeman, S.-D. Kim, R.D. Gilbert and R. McGregor, *Dyes Pigm.*, 1991, **17,** 83.
39. A. Cee, B. Horáková and A. Lyčka, *Dyes Pigm.*, 1988, **9,** 357.
40. C.C. Chien and I.J. Wang, *Dyes Pigm.*, 1991, **15,** 69.
41. R. Rajagopal and S. Seshadri, *Dyes Pigm.*, 1990, **13,** 93.
42. R.R. Ernst, G. Bodenhausen and A. Wokaun, *Principles of Nuclear Magnetic Resonance in One and Two Dimensions.* Clarendon Press, Oxford, 1987.
43. J.K.M. Sanders and B.K. Hunter, *Modern NMR Spectroscopy.* Oxford University Press, Oxford, 1987.
44. H. Kessler, H. Gehrke and C. Griesinger, *Angew. Chem. Int. Ed. Engl.*, 1988, **27,** 490.
45. H.S. Freeman, W.N. Hsu, J.F. Esancy and M.K. Esancy, *Dyes Pigm.*, 1988, **9,** 67.
46. A. Lyčka and J. Pelnař, unpublished results.
47. A. Lyčka, J. Jirman and M. Nečas, *Dyes Pigm.*, 1991, **15,** 23.
48. A. Lyčka, J. Jirman and P.E. Hansen, *Dyes Pigm.*, 1989, **10,** 259.
49. A. Lyčka and J. Jirman, *Dyes Pigm.*, 1987, **8,** 315.
50. A. Lyčka, J. Jirman and J. Podstata, *Dyes Pigm.*, 1987, **8,** 465.
51. J. Jirman and A. Lyčka, *Dyes Pigm.*, 1988, **9,** 453.
52. L.A. Fedorov, A. Lyčka and J. Jirman, *Izv. Acad. Nauk SSSR, Ser. Khim.*, 1989, 2530.
53. K.F. Shuhaibar and H. Pasch, *Dyes Pigm.*, 1991, **15,** 57.
54. B.R. Hsieh, R.K. Crandall and B.A. Weinstein, *Dyes Pigm.*, 1991, **17,** 141.
55. H.S. Freeman, W.M. Whaley, M.K. Esancy and J.F. Esancy, *Dyes Pigm.*, 1986, **7,** 215.
56. I.Y. Berhstein and O.F. Ginsburg, *Usp. Khim.*, 1972, **41,** 177.
57. R.A. Cox and E. Buncel, in *The Chemistry of the Hydrazo, Azo and Azoxy Groups* (ed. S. Patai), p. 838. Wiley, London, 1975.
58. P. Ball and C.H. Nicholls, *Dyes Pigm.*, 1982, **3,** 5.
59. H. Mustroph, *Z. Chem.*, 1987, **27,** 281.
60. V. Bekárek, K. Rothschein, P. Vetešník and M. Večeřa, *Tetrahedron Lett.*, 1968, 3711.
61. V. Bekárek, J. Dobáš, J. Socha, P. Vetešník and M. Večeřa, *Collect. Czech. Chem. Commun.*, 1970, **35,** 1406.
62. G.J. Lestina and T.H. Regan, *J. Org. Chem.*, 1969, **34,** 1685.
63. A. Lyčka and D. Šnobl, *Collect. Czech. Chem. Commun.*, 1980, **46,** 892.
64. F.A. Snavely and S. Un, *J. Org. Chem.*, 1981, **46,** 2764.
65. J. Jirman and A. Lyčka, *Dyes Pigm.*, 1987, **8,** 55.
66. A. Lyčka, M. Nečas, J. Jirman, J. Straka and B. Schneider, *Collect. Czech. Chem. Commun.*, 1990, **55,** 193.
67. R. Haessner, H. Mustroph and R. Borsdorf, *Dyes Pigm.*, 1985, **6,** 277.
68. A. Lyčka and V. Macháček, *Dyes Pigm.*, 1986, **7,** 171.
69. A. Lyčka and H. Mustroph, *J. Prakt. Chem.*, 1989, **331,** 11.
70. R. Haessner, H. Mustroph and R. Borsdorf, *J. Prakt. Chem.*, 1985, **327,** 555.
71. L.A. Fedorov, *NMR Spectroscopy of Organic Analytical Reagents and Their Complexes with Metal Ions*, Chap. 1. Nauka, Moscow, 1987 (in Russian).
72. A. Lyčka, *Collect. Czech. Chem. Commun.*, 1982, **47,** 1112.
73. D. Christoforou and D.A.R. Happer, *Austr. J. Chem.*, 1983, **36,** 2083.
74. H.J. Shine and W. Subotkowski, *Magn. Reson. Chem.*, 1991, **29,** 964.

75. A. Lyčka and J. Kaválek, *Collect. Czech. Chem. Commun.*, 1984, **49,** 58.
76. S. Simova, E. Fanghaenel and R. Radeglia, *Org. Magn. Reson.*, 1983, **21,** 163.
77. P. Savarino, G. Viscardi, E. Barni, R. Carpignano and L.A. Fedorov, *Dyes Pigm.*, 1990, **13,** 71.
78. G. Hinsche, E. Uhlemann, D. Zeigan and G. Engelhardt, *Z. Chem.*, 1981, **21,** 414.
79. C.E. Holloway and C.D. Hubbard, *Inorg. Chim. Acta*, 1985, **98,** 131.
80. L.A. Fedorov, M.S. Zhukov and A.N. Ermakov, *Izv. Acad. Nauk SSSR, Ser. Khim.*, 1984, 1185.
81. L.A. Fedorov, *Zh. Anal. Chem.*, 1985, **40,** 29.
82. L.A. Fedorov, *Zh. Anal. Chem.*, 1985, **40,** 1771.
83. L.A. Fedorov, A.N. Ermakov, N.N. Basargin and Yu.G. Rozovskii, *Zh. Org. Khim.*, 1985, **21,** 2182.
84. L.A. Fedorov, S.A. Sokolovskii and A.N. Ermakov, *Zh. Strukt. Khim.*, 1987, **28,** 50.
85. L.A. Fedorov and S.A. Sokolovskii, *Zh. Anal. Khim.*, 1987, **43,** 1753.
86. L.A. Fedorov, S.A. Sokolovskii, S.I. Dvoskin, T. Drakenberg and A.N. Ermakov, *Izv. Akad. Nauk SSSR, Ser. Khim.*, 1988, 325.
87. L.A. Fedorov, S.A. Sokolovskii and A.V. Sultanov, *Zh. Anal. Chem.*, 1988, **43,** 798.
88. A. Lyčka, T. Liptaj and J. Jirman, *Collect. Czech. Chem. Commun.*, 1987, **52,** 727.
89. L.A. Fedorov, N.I. Grebenchikov, T.G. Akimova and A.N. Ermakov, *Izv. Akad. Nauk SSSR, Ser. Khim.*, 1983, 927.
90. D.W. Allen, I.W. Nowell, L.A. March and B.F. Taylor, *J. Chem. Soc., Perkin Trans I*, 1984, 2523.
91. A. Lyčka, D. Šnobl, V. Macháček and M. Večeřa, *Org. Magn. Reson.*, 1981, **15,** 390.
92. M. Miyahara, *Eisei Shikensho Hokoku*, 1982, **100,** 135. *Chem. Abstr.*, 1984, **100,** 5716f.
93. L.A. Fedorov, M.S. Zhukov, I.V. Korsakov, Yu.M. Dedkov and A.I. Ermakov, *Izv. Akad. Nauk SSSR, Ser. Khim.*, 1984, 1763.
94. P.E. Hansen and A. Lyčka, *Magn. Reson. Chem.*, 1986, **24,** 772.
95. L.A. Fedorov, T.G. Akimova, E.M. Sanayeva and A.N. Ermakov, *Izv. Akad. Nauk SSSR, Ser. Khim.*, 1983, 324.
96. L.A. Fedorov, M.S. Zhukov, T.V. Petrova and S.B. Savvin, *Zh. Anal. Khim.*, 1984, **39,** 1754.
97. L.A. Fedorov, *Zh. Anal. Khim.*, 1984, **39,** 1754.
98. L.A. Fedorov, M.S. Zhukov, A.V. Sultanov and S.B. Savvin, *Zh. Anal. Khim.*, 1985, **40,** 1949.
99. L.A. Fedorov, S.A. Sokolovskii and C.I. Dvoskin, *Zh. Anal. Khim.*, 1987, **43,** 1987.
100. L.A. Fedorov, S.I. Dvoskin and S.A. Sokolovskii, *Izv. Akad. Nauk SSSR, Ser. Khim.*, 1989, 2721.
101. V.V. Negrebetskii, A.I. Bokanov and B.I. Stepanov, *Zh. Strukt. Khim.*, 1981, **22,** 88.
102. J. Kelemen, S. Moss, H. Sauter and T. Winkler, *Dyes Pigm.*, 1982, **3,** 27.
103. M.V. Gorelik, V.I. Rybinov and T.X. Gladysheva, *Zh. Obsch. Khim.*, 1988, **58,** 2360.
104. A.H. Berrie, P. Hampson, S.W. Longworth and A. Matias, *J. Chem. Soc. B*, 1968, 1308.
105. M. Witanowski, L. Stefaniak and G.A. Webb, *Annual Reports on NMR Spectroscopy*, Vols 7, 11B and 18. Academic Press, New York, 1977, 1981 and 1986.
106. W. von Philipsborn and R. Mueller, *Angew. Chem., Int. Ed. Engl.*, 1986, **25,** 383.
107. G.W. Buchanan, *Tetrahedron*, 1989, **45,** 581.
108. J.A. Connor, R.J. Kennedy, H.M. Dawes, M.B. Hursthouse and N.P.C. Walker, *J. Chem. Soc., Perkin Trans. II*, 1990, 203.
109. A. Lyčka, *Collect. Czech. Chem. Commun.*, 1983, **48,** 3104.
110. A. Lyčka, D. Šnobl, V. Macháček and M. Večeřa, *Org. Magn. Reson.*, 1981, **16,** 17.
111. Y. Kuroda, H. Lee and A. Kuwae, *J. Phys. Chem.*, 1980, **84,** 3417.
112. K. Yamamoto, K. Nakai and T. Kawaguchi, *Dyes Pigm.*, 1989, **11,** 173.
113. S.J. Bell, E.P. Mazzola and B. Coxon, *Dyes Pigm.*, 1989, **11,** 93.

114. Y. Kuroda, Y. Fujiwara, A. Kuwae and K. Matsushita, *J. Chem. Soc. Perkin Trans. II*, 1986, 675.
115. A. Lyčka and P.E. Hansen, *Magn. Reson. Chem.*, 1984, **22,** 569.
116. J. Reuben and D. Samuel, *Israel J. Chem.*, 1963, **1,** 279.
117. E. Lippert, D. Samuel and E. Fischer, *Ber. Bunsenges. Physik. Chem.*, 1965, **65,** 155.
118. A. Lyčka, *Dyes Pigm.*, 1990, **12,** 179.
119. P. Skrabal, F. Bangerter, K. Hamada and T. Iijima, *Dyes Pigm.*, 1987, **8,** 371.

Index